JOURNAL OF THE AERONAUTICAL SCIENCES

VOLUME 24 JULY, 1957 NUMBER 7

ST. LOUIS
JUL 8 1957
PUBLIC LIBRARY

CONTENTS

The Prediction of Nonlinear Pitching and Yawing Motion of Symmetric Missiles..... CHARLES H. MURPHY, JR. 473

On Transition Experiments at Moderate Supersonic Speeds.... MARK V. MORKOVIN 480

On the Frequency Spectrum Generated by a Maneuvering Aircraft.... A. P. BROGLIE 487

Remarks on the Equilibrium Turbulent Boundary Layer..... DONALD COLES 495

A Theoretical and Experimental Study of Airplane Dynamics in Large-Disturbance Maneuvers..... DONALD W. RHOADS AND JOHN M. SCHULER 507

Optimum Nose Shapes for Missiles in the Superaerodynamic Region.. W. J. CARTER 527

Nonlinear Deflections of Shallow Spherical Shells..... EDWARD L. REISS, HERBERT J. GREENBERG, AND HERBERT B. KELLER 533

Readers' Forum..... 544

Published by
INSTITUTE OF THE AERONAUTICAL SCIENCES, INC.

JOURNAL OF THE AERONAUTICAL SCIENCES

Editor: W. R. SEARS

Director, Graduate School of Aeronautical Engineering, Cornell University

Associate Editor: ROBERT R. DEXTER *Managing Editor:* RITA J. TURINO

Editorial Assistant: CAROLINE TAYLOR

Editorial Committee

Aerodynamics and Fluid Mechanics

Holt Ashley
H. Julian Allen
Dean R. Chapman
Francis H. Clauser
Hugh L. Dryden
John C. Evvard
Antonio Ferri
Alexander Flax
Wallace D. Hayes
R. T. Jones
Carl Kaplan
H. W. Liepmann
C. C. Lin
H. F. Ludloff
Harold Luskin
Clark B. Millikan
H. J. E. Reid
George S. Schairer
G. B. Schubauer
John Stack
Theodore Theodorsen
Arthur N. Tifford
Th. von Kármán

Flight Testing

R. R. Gilruth
Melvin N. Gough
W. L. Howland
W. F. Milliken, Jr.

Rotating Wing Aircraft

F. B. Gustafson
K. H. Hohenemser
Bartram Kelley
R. B. Maloy
Ralph McClarren
R. H. Miller
R. H. Prewitt
Igor I. Sikorsky

Structures

John E. Duberg
R. R. Heldenfels
N. J. Hoff
Samuel Levy
J. F. McBrearty
W. Ramberg
E. E. Sechler
F. R. Shanley
C. R. Strang
S. Timoshenko

Meteorology

C. F. Brooks
D. M. Little
F. W. Reichelderfer
K. C. Spengler

Vibration and Flutter

Lee Arnold
M. A. Biot
R. L. Bisplinghoff
Harold A. Cheilek
I. E. Garrick
Martin Goland

Aircraft Design

W. E. Beall
E. H. Heinemann
Hall L. Hibbard
Richard Hutton
C. L. Johnson
A. A. Kartveli
F. K. Teichmann

Electronics

K. C. Black
M. V. Kiebert, Jr.
David S. Little
Paul Rosenberg
Giles J. Strickroth

Physiologic Problems

H. G. Armstrong
Louis H. Bauer
Robert J. Benford
W. Randolph Lovelace, II
Ross A. MacFarland

Flight Propulsion

William Bollay
George W. Brady
R. P. Kroon
Frank E. Marble
Abe Silverstein
E. S. Taylor

Instruments

Alan G. Binnie
Charles H. Colvin
Frank R. Cook
C. S. Draper
S. G. Eskin
C. F. Savage
R. C. Sylvander

SUBSCRIPTION RATES

JOURNAL OF THE AERONAUTICAL SCIENCES, Published Monthly. United States and Possessions: 1 Year, $15.00; Single Copies, $1.50. Foreign Countries Including Canada (American Currency Rates): 1 Year, $16.00; Single Copies, $1.50.

AERONAUTICAL ENGINEERING REVIEW, Published Monthly. United States and Possessions: 1 Year, $3.00; Single Copies, $0.50. Foreign Countries Including Canada (American Currency Rates): 1 Year, $3.50; Single Copies, $0.50.

Notices of change of address should be sent to the Institute at least 30 days prior to actual change of address.

Manuscripts for publication, proofs, and all correspondence should be addressed to the Editorial Office of the JOURNAL.

Publication Office, 20th and Northampton Sts., Easton, Pa. Correspondence regarding subscriptions may be addressed to the Editorial Office of the JOURNAL OF THE AERONAUTICAL SCIENCES, 2 East 64th Street, New York 21, N.Y.

© *Copyright, 1957, by the Institute of the Aeronautical Sciences, Inc.*

Entered as Second-Class Matter at the Post Office, Easton, Pa., May 1, 1937. Acceptance for mailing at a special rate of Postage provided for in the Act of August 24, 1912. Authorized April 29, 1937.

JOURNAL OF THE AERONAUTICAL SCIENCES

VOLUME 24 JULY, 1957 NUMBER 7

The Prediction of Nonlinear Pitching and Yawing Motion of Symmetric Missiles†

CHARLES H. MURPHY, JR.*

Ballistic Research Laboratories, Aberdeen Proving Ground

SUMMARY

The problem of predicting the combined pitching and yawing motion of an aerodynamic configuration which is acted on by nonlinear moments has been considered too difficult for a general solution. When the problem is restricted to symmetric missiles, which may be spinning, relations for the amplitudes and frequencies of the actual motion can be derived by an equivalent linearization technique. For cubic nonlinearities and relatively short trajectories, these relations have been checked by free-flight tests on the Ballistic Research Laboratories' spark ranges.

By the use of an "amplitude plane" the dependence of the character of the motion on initial conditions is simply displayed. As examples of this technique, amplitude planes are constructed for missiles whose moments are cubic functions of the total angle of attack.

The ability of the theory to specify possible limit motions is described. Theoretical predictions of these limit motions are compared with exact numerical integrations, and the predictions are shown to be very accurate.

SYMBOLS‡

C_j	=	aerodynamic coefficients [see Eqs. (1)–(4)]
H	=	$(\rho Sl/2m)\ [C_{N_\alpha} - 2C_D - k_t^{-2}\ (C_{M_q} + \gamma C_{M_{\dot\alpha}})]$
I_x, I_y, I_z	=	moments of inertia
K_j	=	amplitude of j-mode
k_a	=	dimensionless axial radius of gyration
k_t	=	dimensionless transverse radius of gyration
L, M, N	=	aerodynamic moments about missile-fixed X, Y, Z axes, respectively
l	=	reference length
M	=	$(\rho Sl/2m)\ \gamma k_t^{-2}\ C_{M_\alpha}$
m	=	mass
P	=	$(I_x/I_y)\ (pl/V)$ (gyroscopic spin)
p, q, r	=	components of the angular velocity of the missile in space along the X, Y, Z axes
S	=	reference area
s	=	$\int_0^t (V/l)dt$ = dimensionless distance along trajectory
T	=	$(\rho Sl/2m)\ [C_{N_\alpha} - C_D + k_a^{-2}\ \gamma C_{M_{\dot p\alpha}}]$
u, v, w	=	components of the linear velocity of the missile along the X, Y, Z axes
V	=	magnitude of missile's velocity
X, Y, Z	=	components of aerodynamic force along the missile-fixed X, Y, Z axes
α	=	angle of attack
β	=	angle of sideslip
γ	=	cosine of angle between missile's axis and trajectory
η	=	sine of angle between missile's axis and trajectory
λ_j	=	exponential damping of the j-mode
ξ	=	$(v + iw)/V$
ρ	=	air density
ϕ_j	=	phase of the j-mode
ϕ	=	$\hat\phi_2 + \psi_2 - \hat\phi_1 - \psi_1$
ψ_j	=	perturbation of phase of the j-mode [Eq. (10)]

Superscripts

$\dot{}$	indicates derivatives with respect to time t
$'$	indicates derivatives with respect to distance s
$\sim$	indicates quantities in nonrotating coordinate system—i.e., $\tilde\xi = \xi e^{i\int p\,dt}$
$\wedge$	indicates parameters of basic epicycle without damping

INTRODUCTION

AN IMPORTANT CURRENT aerodynamic problem is the prediction of missile motion for configurations acted on by nonlinear aerodynamic moments. Although linearized theory has proved very successful in most cases, there remain important exceptions for which the nonlinear terms must be considered. Examples of these would include sideward fire of rockets from moving ships, sideward fire of bullets or missiles from high-speed aircraft, and roll-pitch interactions of high-speed aircraft.

Unfortunately, most of the results which have been obtained in the field of nonlinear mechanics have been restricted to second-order systems and, therefore, are not directly applicable to the general sixth-order systems which describe missile motion. In this paper we

Presented at the Aerodynamics—II Session, Twenty-Fifth Annual Meeting, IAS, New York, January 28–31, 1957.

† This paper is an abridgement of a dissertation submitted to the Faculty of Philosophy of the Johns Hopkins University in conformity with the requirements for the degree of Doctor of Philosophy.

* Deputy Chief, Free Flight Aerodynamics Branch.

‡ Wherever it is possible these symbols are those defined in reference 6.

will not consider this general case but will restrict ourselves to the intermediate case of a special fourth-order system. This intermediate case is based on the assumption of constant drag coefficient and constant spin-to-velocity ratio. We will further restrict ourselves to missiles with a plane of mirror symmetry and an angle of rotational symmetry less than or equal to 120°. (These restrictions exclude the important case of a high-speed airplane.)

Under these conditions special types of nonlinear pitching and yawing motion have been studied in references 1–4. By an extension of the Kryloff-Bogoliuboff equivalent linearization technique[5] the most general motion will be considered in this paper. The results of this technique can be presented in the simple, graphic form of an amplitude plane. The accuracy of the theory has been verified by actual free-flight tests and by numerical integration of the exact equations of motion. Some of these comparisons will be presented later in the paper.

Equations of Motion

Although the linear expansion of the aerodynamic force and moment in terms of the dynamic variables $\alpha, \beta, \dot{\alpha}, \dot{\beta}, p, q, r, \dot{p}, \dot{q}, \dot{r}$ requires the use of 60 stability derivatives, the assumed symmetry reduces this number to eleven different nonzero derivatives. Since a symmetric missile is frequently given a high spin rate, quadratic terms containing p are usually considered. These terms are called Magnus terms. For the assumed symmetry there are only eight different terms of this type. This total of 19 distinct coefficients can be reduced to seven if only those quantities which usually have a measurable effect on the motion are retained.

Under these assumptions the expressions for drag and axial spin are*

$$\text{Drag} = (1/2)\rho V^2 S C_D \tag{1}$$

$$L = (1/2)\rho V^2 S l C_{l_p} (pl/V) \tag{2}$$

As a result of the rotational symmetry the transverse components of the aerodynamic force and moment can be conveniently expanded in terms of complex variables:

$$Y + iZ = -(1/2)\rho V^2 S C_{N_\alpha} (\beta + i\alpha) \tag{3}$$

$$M + iN = (1/2)\rho V^2 S l \left\{ [(pl/V) C_{M_{p\alpha}} - iC_{M_\alpha}] \times [\beta + i\alpha] + C_{M_q} \left[\frac{(q + ir)l}{V} \right] - iC_{M_{\dot{\alpha}}} \left[\frac{(\dot{\beta} + i\dot{\alpha})l}{V} + \frac{ipl(\beta + i\alpha)}{V} \right] \right\} \tag{4}$$

where

$$\begin{aligned} C_{N_\alpha} &= -C_{Y_\beta} = -C_{Z_\alpha} \\ C_{M_\alpha} &= C_{m_\alpha} = -C_{n_\beta} \\ C_{Mp_\alpha} &= C_{mp_\beta} = C_{np_\alpha} \\ C_{M_q} &= C_{m_q} = C_{n_r} \\ C_{M_{\dot{\alpha}}} &= C_{m_{\dot{\alpha}}} = -C_{n_{\dot{\beta}}} \end{aligned}$$

(The expression following $C_{M_{\dot{\alpha}}}$ is the derivative of $\beta + i\alpha$ in a nonrolling coordinate system. As has been pointed out by Sacks,[7] this derivative is more convenient than a derivative in missile-fixed coordinates.) It should be noted that, if the aerodynamic force and moment in Eqs. (3) and (4) are nonlinear functions, the coefficients are defined by Eqs. (3) and (4) and not by differentiation. When these coefficients are functions of only α and β, this definition is unique. This distinction is important for the nonlinear case.

When large angles are considered, the exact definition of $\beta + i\alpha$ becomes awkward, and the use of transverse components of the velocity seems to be more convenient. We will therefore replace $\beta + i\alpha$ in the above equations by a complex quantity ξ which reduces to it for small angles and is defined by the equation

$$\xi = (v + iw)/V \tag{5}$$

According to the above definition, ξ is measured in a missile-fixed coordinate system. Since nonrolling coordinates have certain attractive features, we will make use of a ξ which is determined by velocity components in a nonrolling coordinate system ($\bar{\xi} = \xi e^{i\int p\,dt}$). If the effect of gravity is neglected, the aerodynamic force is assumed to be linear, and the mass distribution is assumed to be symmetric ($I_y = I_z$), the following differential equation for $\bar{\xi}$ can be derived:[8]

$$\bar{\xi}'' + [H - (\gamma'/\gamma) - iP]\bar{\xi}' - (M + iPT)\bar{\xi} = 0 \tag{6}$$

where

$$\begin{aligned} H &= (\rho Sl/2m)\,[C_{N_\alpha} - 2C_D - k_t^{-2}(C_{M_q} + \gamma C_{M_{\dot{\alpha}}})] \\ M &= (\rho Sl/2m)\,[\gamma k_t^{-2} C_{M_\alpha} + (\rho Sl/2m) \times (C_{N_\alpha} - C_D)(k_t^{-2} C_{M_q} + C_D)] \doteq (\rho Sl/2m)\gamma k_t^{-2} C_{M_\alpha} \\ T &= (\rho Sl/2m)\,[C_{N_\alpha} - C_D + \gamma k_a^{-2} C_{Mp_\alpha}] \\ P &= (pl/V)(I_x/I_y) \\ \gamma &= u/V \text{ (cosine of angle between missile's axis and trajectory)} \\ k_t &= \sqrt{I_y/ml^2} = \sqrt{I_z/ml^2} = \text{transverse radius of gyration} \\ k_a &= \sqrt{I_x/ml^2} = \text{axial radius of gyration} \end{aligned}$$

and primes denote derivatives with respect to the dimensionless arclength $s = \int (V/l)dt$.

For small angles ($\gamma' = 0$, $\gamma = 1$), constant spin-to-velocity ratio ($P' = 0$), and constant moment coefficients, Eq. (6) can be easily solved:

$$\bar{\xi} = K_1 e^{i\phi_1} + K_2 e^{i\phi_2} \tag{7}$$

where

$$\begin{aligned} \phi_j &= \phi_{j0} + \phi'_j s \\ K_j &= K_{j0} e^{\lambda_j s} \\ \lambda_j + i\phi_j' &= (1/2)\left[-H + iP \pm \sqrt{4M + H^2 - P^2 + 2Pi(2T - H)}\right] \end{aligned}$$

* If the symmetry conditions are relaxed so that a roll moment due to deflected control surfaces can be added to Eq. (2), the results of the paper will still apply.

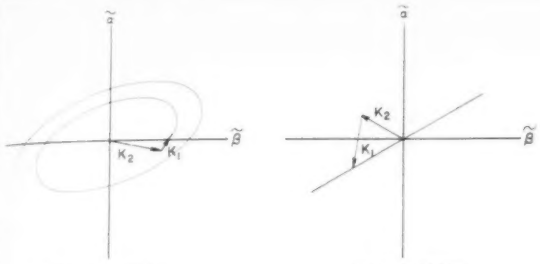

FIG. 1a FIG. 1b

FIG. 1. Nonrolling statically stable symmetric missile.

The pitching and yawing motion is, therefore, described in a complex plane by the sum of two exponentially damped complex vectors which are rotating with angular velocities ϕ_j'. For a statically stable missile with zero spin ($M < 0$, $P = 0$) the motion is described by a damped ellipse (see Fig. 1). For special initial conditions ($K_1 = K_2$), the motion goes through the origin, the ellipse degenerates into a line, and the axis of the missile is confined to a plane (planar motion). If the missile is allowed to spin, the ellipse will precess and become an epicycle (see Fig. 2). A statically unstable missile which is spin stabilized has an epicyclic motion with the nodes on the inside.

Solution of Nonlinear Equation

The most common nonlinearity associated with a symmetric missile is a dependence of the aerodynamic coefficients on the sine of the total angle of attack. Symmetry requires that they be even functions of this quantity. It is, therefore, assumed that the aerodynamic moment coefficients in Eq. (6) are functions of $\eta^2 = |\xi|^2$.

At this point we impose the reasonable condition that for "small" nonlinearities the solution of the nonlinear equations can be approximated by an epicycle without damping. The approximate solution is then improved by a perturbation method. If Eq. (6) is written in the form

$$\xi'' - iP\,\xi' - M(0)\,\xi = -[H(\eta^2) - (\gamma'/\gamma)]\xi' + [M(\eta^2) - M(0) + iPT(\eta^2)]\xi \quad (8)$$

the solution of the left side set equal to zero is an epicycle without damping.

$$\xi = K_{10}e^{i\hat{\phi}_1} + K_{20}e^{i\hat{\phi}_2} \quad (9)$$

where
$$\hat{\phi}_j = \phi_{j0} + \phi_j'\,s$$
$$\phi_j' = (1/2)\,[P \pm \sqrt{P^2 - 4M(0)}]$$
$$P^2 - 4M(0) > 0$$

The inequality, $P^2 - 4M(0) > 0$, is always satisfied for statically stable missiles. For a statically unstable missile it is the criterion for proper spin stabilization.

The perturbation procedure which will be used is a generalization of the Kryloff-Bogoliuboff method and is quite similar to the method of variation of parameters for the solution of inhomogeneous linear equations.

We assume a solution of the form

$$\xi = K\,e^{i(\hat{\phi}_1+\psi_1)} + K_2e^{i(\hat{\phi}_2+\psi_2)} \quad (10)$$

where $K_1(s)$ and $\psi_j(s)$ are unknown functions of s. Differentiating Eq. (10),

$$\xi' = i\phi_1'\,K_1e^{i(\hat{\phi}_1+\psi_1)} + i\phi_2'K_2e^{i(\hat{\phi}_2+\psi_2)} + (K_1' + i\,\psi_1'K_1)\,e^{i(\hat{\phi}_1+\psi_1)} + (K_2' + i\psi_2'K_2)\,e^{i(\hat{\phi}_2+\psi_2)} \quad (11)$$

The sum of the last two terms is set equal to zero, and ξ' is differentiated.

$$(K_1' + i\psi_1'K_1)e^{i(\hat{\phi}_1+\psi_1)} + (K_2' + i\psi_2'K_2)\,e^{i(\hat{\phi}_2+\psi_2)} = 0 \quad (12)$$

$$\xi'' = -\phi_1'^2K_1e^{i(\hat{\phi}_1+\psi_1)} - \phi_2'^2K_2e^{i(\hat{\phi}_2+\psi_2)} + i\phi_1'(K_1' + i\psi_1'K_1)e^{i(\hat{\phi}_1+\psi_1)} + i\phi_2'(K_2' + i\psi_2'K_2)e^{i(\hat{\phi}_2+\psi_2)} \quad (13)$$

If Eqs. (10), (11), and (13) are substituted in Eq. (8), then

$$i\phi_1'\,(K_1' + i\psi_1'K_1)e^{i(\hat{\phi}_1+\psi_1)} + i\phi_2'(K_2' + i\psi_2'K_2)e^{i(\hat{\phi}_2+\psi_2)} = -[H(\eta^2) - (\gamma'/\gamma)]\,\xi' + [M(\eta^2) - M(0) + iPT\,(\eta^2)]\xi \quad (14)$$

where

$$\eta^2 = |\xi|^2 = K_1^2 + K_2^2 + 2K_1K_2\cos\phi$$
$$\gamma = \sqrt{1 - \eta^2}$$
$$\phi = \hat{\phi}_2 + \psi_2 - \hat{\phi}_1' - \psi_1$$

and ξ is given by Eq. (10). $K_2' + i\psi_2'K_2$ can be eliminated between Eqs. (12) and (14) to yield the following equation for the functions K_1 and ψ_1:

$$(K_1'/K_1) + i\psi_1' = f\,(K_1, K_2, \phi) \quad (15)$$

where

$$f(K_1, K_2, \phi) = -(\phi_1' - \phi_2')^{-1}\,([H(\eta^2) - (\gamma'/\gamma)]\,[\phi_1' + \phi_2'\,(K_2/K_1)e^{i\phi}] + \tfrac{1}{2}PT(\eta^2) - i[M(\eta^2) - M(0)]\,[1 + (K_2/K_1)e^{i\phi}])$$

Eq. (15) is very difficult to solve because of the explicit presence of the independent variable in ϕ. Our basic assumption that the motion can be approximated by an epicycle without damping implies that the derivatives in Eq. (15) are such that the character of the motion changes little over a cycle of ϕ. This equation must describe changes in phase and amplitude over a number of cycles. We therefore average Eq. (15) over a cycle of ϕ and separate into real and imaginary parts.

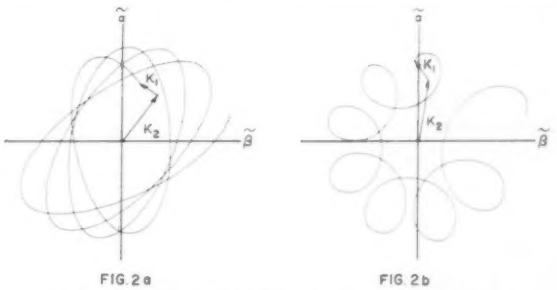

FIG. 2a FIG. 2b

FIG. 2. Rolling statically stable symmetric missile.

$$K_1'/K_1 = \lambda_1(K_1, K_2) = \frac{-1}{2\pi(\hat{\phi}_1' - \hat{\phi}_2')}\int_0^{2\pi}\left\{H(\eta^2)\,[\hat{\phi}_1' + \hat{\phi}_2'(K_2/K_1)\cos\phi] - PT(\eta^2)\times[1 + (K_2/K_1)\cos\phi]\right\}d\phi \quad (16)$$

$$\psi_1' = \frac{-1}{2\pi(\hat{\phi}_1' - \hat{\phi}_2')}\int_0^{2\pi}\left\{[M(\eta^2) - M(0)]\times[1 + (K_2/K_1)\cos\phi] + (\gamma'/\gamma)\times\hat{\phi}_2'(K_2/K_1)\sin\phi\right\}d\phi \quad (17)$$

Similar equations for K_2 and ψ_2 can be obtained by interchanging the subscripts 1 and 2 in the above equations.

Application of Theory to Short Trajectories

If we consider short trajectories over which the modal amplitudes (K_j's) do not change very much, the solution obtained in the preceding section can be easily described. The motion is a damped epicycle with frequencies $\phi_j' = \hat{\phi}_j' + \psi_j'$ and damping exponents λ_j. Both the frequencies and the damping exponents are, however, functions of K_1 and K_2.

An interesting application of the theory has been made in the data analysis of test firings on the Ballistic Research Laboratories' aerodynamics ranges. For cubic static moment and small angles,

$$M = M_0 + M_2\eta^2 \quad (18)$$

$$\gamma \doteq 1 - (1/2)\eta^2 \quad (19)$$

Substituting these equations in the equations for the frequencies, we have the following equations:

$$\phi_1' \doteq \hat{\phi}_1' - [M_2(K_1^2 + 2K_2^2)/(\hat{\phi}_1' - \hat{\phi}_2')] - (\hat{\phi}_2'K_2^2/2)$$
$$\phi_2' \doteq \hat{\phi}_2' - [M_2(K_2^2 + 2K_1^2)/(\hat{\phi}_2' - \hat{\phi}_1')] - (\hat{\phi}_1'K_1^2/2) \quad (20)$$

where $\hat{\phi}_j' = (1/2)\,[P \pm \sqrt{P^2 - 4M_0}]$

If these equations are multiplied and the K_j^4 terms are neglected,

$$\phi_1'\cdot\phi_2'\{1 + [(K_1^2 + K_2^2)/2]\} = M_0 + M_2\eta_e^2 \quad (21)$$

where

$$\eta_e^2 = K_1^2 + K_2^2 + [(\phi_1'K_1^2 - \phi_2'K_2^2)/(\phi_1' - \phi_2')]$$

From a group of flight tests of the same configuration at the same Mach Number, values of K_j and ϕ_j' can be obtained. These values can be fitted by Eq. (21) to yield M_0 and M_2. This has been done for a number of programs.[8] The results possessed excellent internal consistency and compared well with direct wind-tunnel measurements. Similar relations have been used to measure cubic Magnus moments.

The Amplitude Plane

Although the case of short trajectories is of some importance, the primary interest of a designer is in the behavior of the missile over long trajectories. As long as the motion predicted by the linearized equation is gyroscopically stable [$P^2 - 4M(0) > 0$], it can be seen from Eqs. (16) and (17) that the only effect of a mildly nonlinear static moment M is to change the frequency of the motion. Unfortunately, strong nonlinearities in M would invalidate the perturbation process and, hence, are not considered in this paper. Strong nonlinearities in the other moments affect the damping and can be considered if the predicted damping over a cycle is reasonably small. It is this damping or undamping of the motion over a large number of cycles which we will consider in detail.

In order to do this we will study the following first-order nonlinear equations:

$$(K_1^2)'/K_1^2 = 2\lambda_1(K_1^2, K_2^2) \quad (22)$$

$$(K_2^2)'/K_2^2 = 2\lambda_2(K_1^2, K_2^2) \quad (23)$$

where the $\lambda_j(K_1^2, K_2^2)$ are given by Eq. (16) and the corresponding equation for the 2-mode. These equations are now divided to eliminate the independent variable.

$$d(K_2^2)/d(K_1^2) = K_2^2\lambda_2(K_1^2, K_2^2)/K_1^2\lambda_1(K_1^2, K_2^2) \quad (24)$$

Eq. (24) has been extensively studied by Poincaré.[9] Its essential behavior is determined by its properties in the vicinity of points for which the numerator and denominator both vanish (singular points).

Solution curves of Eq. (24) are trajectories in the K_1^2-K_2^2 plane. This plane, which will be called the amplitude plane, is of fundamental importance for stability studies of missiles acted on by nonlinear moments.

For the linear case, the λ_j's are constants, and the origin is the only singular point. If the spin is zero, $\lambda_1 = \lambda_2$, and all the trajectories go either toward or away from the origin (see Fig. 3a). The particular curve which describes a given motion is specified by the initial values of K_j and direction of motion along the curve by the sign of λ_j. For positive λ_j's the motion undamps away from the origin. The damping exponents of spinning missiles are not necessarily equal and may differ in sign. The origin can, therefore, be either a nodal point (Fig. 4a) or a saddle point (Fig. 4b). All of these figures display an important characteristic of linear systems—i.e., the type of motion is independent of initial conditions.

Amplitude planes will now be constructed for two simple nonlinearities. In the first example, the effect of a nonlinear damping on the motion of a nonspinning missile will be considered while, in the second, the effect of a nonlinear Magnus moment on the motion of a spinning missile is described. In both cases the angles will be assumed small so that the geometric nonlinearities can be neglected ($\gamma' = 0$, $\gamma = 1$).

Example 1:

$$P = 0; \quad C_{M_q} + C_{M_{\dot{\alpha}}} = a_0 + a_2\eta^2$$

For zero spin, $\hat{\phi}_1' = -\hat{\phi}_2'$; and the equations for the damping exponent λ_j take on the form

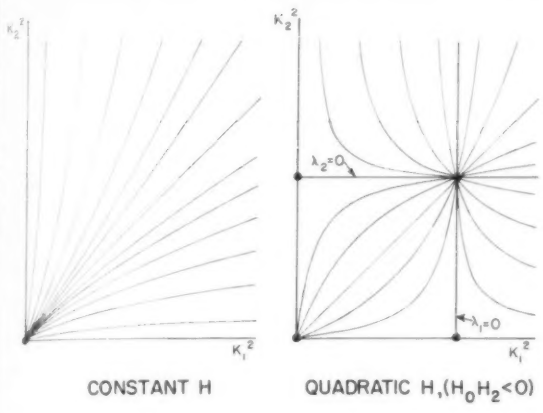

FIG. 3. Nonrolling statically stable missiles.

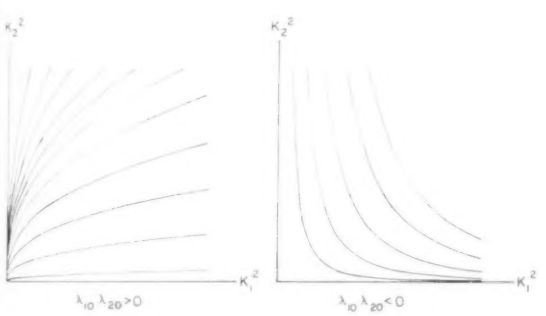

FIG. 4. Amplitude plane for linear equation ($p \neq 0$).

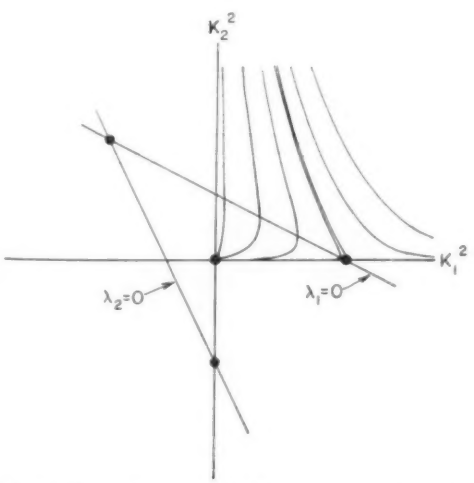

FIG. 5. Amplitude plane for cubic Magnus moment ($\lambda_{10}\lambda_{20} > 0$).

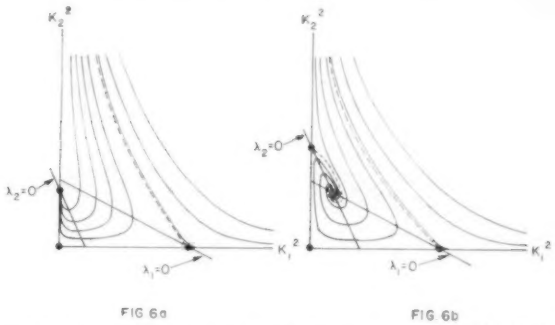

FIG. 6. Amplitude plane for cubic Magnus moment ($\lambda_{10}\lambda_{20} < 0$).

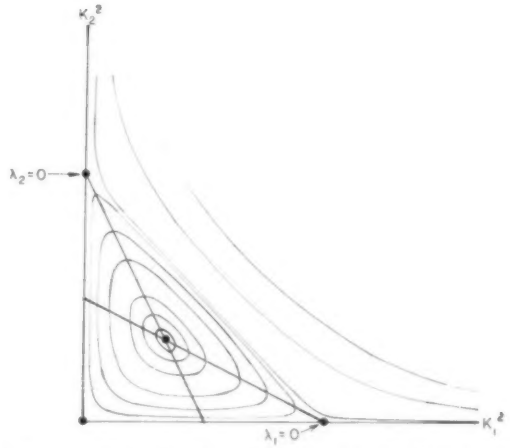

FIG. 7. Amplitude plane for cubic Magnus moment ($\lambda_{10} = -\lambda_{20}$)

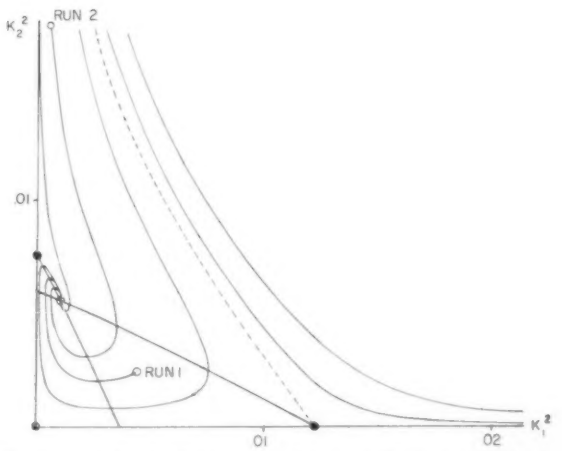

FIG. 8. Amplitude plane for Naval Proving Ground calculations.

$$\lambda_1 (K_1^2, K_2^2) = -(1/4\pi) \int_0^{2\pi} H(\eta^2) \times [1 + (K_2/K_1) \cos \phi] \, d\phi \quad (25)$$

$$\lambda_2 (K_1^2, K_2^2) = -(1/4\pi) \int_0^{2\pi} H(\eta^2) \times [1 + (K_1/K_2) \cos \phi] \, d\phi \quad (26)$$

where $\eta^2 = K_1^2 + K_2^2 + 2K_1K_2 \cos \phi$

If the damping derivatives are linear functions of η^2, $H(\eta^2)$ has the simple form

$$H(\eta^2) = H_0 + H_2 \eta^2 \quad (27)$$

where

$$H_0 = (\rho Sl/2m) [C_{N\alpha} - 2C_D - k_t^{-2} a_0]$$
$$H = -(\rho Sl/2m) k_t^{-2} a_2$$

$$\therefore \quad \lambda_1(K_1^2, K_2^2) = -(1/2) [H_0 + H_2K_1^2] \quad (28)$$

$$\lambda_2 (K_1^2, K_2^2) = -(1/2) [H_0 + H_2K_2^2] \quad (29)$$

The amplitude plane for the interesting case for which the damping changes sign ($H_0H_2 < 0$) is shown in Fig. 3b. The lines of zero damping are given by Eqs. (28) and (29) set equal to zero and are shown in the Figure together with the four singular points at [0, 0], [0, $-(H_0/H_2)$], [$-(H_0/H_2)$, 0], and [$-(H_0/H_2)$, $-(H_0/H_2)$].

If the origin is first assumed to be a stable node, this Figure shows the characteristic nonlinear dependence of the type of motion on initial conditions. For initial amplitudes which are inside the square formed by the axes and the zero damping lines, the motion will damp to the origin; for amplitudes outside, the motion will grow.

Under the reverse assumption that the origin is an unstable node, the other node becomes a stable one, and all trajectories lead to this limiting value. This existence of a limit motion is another characteristic of nonlinear systems. It is interesting to note that, if we had restricted ourselves to planar motion, Eq. (6) would have reduced to the well-known van der Pol equation, and the singularity at [$-(H_0/H_2)$, $-(H_0 \div H_2)$] is the limit cycle predicted for that equation.

Example 2:

$$P, H \text{ constant}; \quad C_{M_{p\alpha}} = b_0 + b_2 \eta^2$$

The equations for the damping exponents reduce to

$$\lambda_1 = \lambda_{10} + \lambda_{12} (K_1^2 + 2K_2^2)$$
$$\lambda_2 = \lambda_{20} + \lambda_{22} (K_2^2 + 2K_1^2)$$

where

$$\lambda_{10} = (H \dot{\phi}_1' - PT_0)/(\dot{\phi}_1' - \dot{\phi}_2')$$
$$\lambda_{20} = (H \dot{\phi}_2' - PT_0)/(\dot{\phi}_2' - \dot{\phi}_1')$$
$$\lambda_{12} = -\lambda_{22} = -PT_2/(\dot{\phi}_1' - \dot{\phi}_2')$$
$$T_0 = (\rho Sl/2m) [C_{N\alpha} - C_D + k_a^{-2} b_0]$$
$$T_2 = (\rho Sl/2m) k_a^{-2} b_2$$

The quadratic Magnus moment coefficient which corresponds to a cubic Magnus moment can give rise to several interesting amplitude planes (see Figs. 5–7).

In Fig. 5, the origin is a node, and the dependence of the type of motion on initial conditions is once more shown. Figs. 6 and 7, which illustrate amplitude planes for which the origin is a saddle, show limit motions. In Fig. 6a, the nodal singularity on the K_2^2 axis predicts a limit circular motion of the missile's axis about the trajectory. In Fig. 6b, the spiral singularity predicts a limit epicycle. Fig. 7 shows the transition case where the spiral point becomes a center and the limit epicycle passes through the origin of the ξ plane.

In summary, the important problem of stability for nonlinear motion can be reduced to the construction of the appropriate amplitude plane. The initial conditions for which the motion will remain bounded can then be easily identified.

Numerical Check of the Theory

The examples in the preceding section show that a rapid calculation of the dependence of the motion on initial conditions can be made by the use of an amplitude plane. These examples also indicate that, for rather simple nonlinearities in the moments, the flight characteristics may change quite radically with initial conditions. Such characteristics have been observed in actual missile flights. It remains, however, to determine the quantitative accuracy of the theory.

This has been done by means of exact numerical integrations of Eq. (6) at the Naval Proving Ground.[1] For this check, linear static and damping moments were assumed. The Magnus moment was selected to be a quintic function of η such that a limit epicyclic motion would be predicted by the theory. The amplitude plane for this case is shown in Fig. 8.

First, the predicted location of the separatrix was checked by fixing K_2^2 and varying K_1^2 across the predicted curve. This was done for two values of K_2^2. The exact equations were then integrated for five periods of η^2, and the runs for which the angles increased were denoted by "U" (unstable), those for which they decreased by "S" (stable), and those for which no decision could be made by "N" (neutral). Since the modal amplitudes do not completely determine the initial conditions (ξ_0', ξ_0), the initial conditions were selected for both an initial maximum and an initial minimum of ξ. The theory makes no distinction between these cases. As can be seen from Table 1, the predictions of the theory are quite good.

Next, the existence of the predicted limit motion was investigated. This was done by selecting initial conditions corresponding to amplitudes which lie to the left of the separatrix and integrating for 30 periods of η^2. The motion near the end of each run was analyzed and found in all cases to be epicyclic with zero damping. The values of the amplitudes checked to four decimal places with the predicted values of $K_1 = 0.0268$, $K_2 = 0.0784$. Two of these runs are shown in Fig. 8, and the time history of Run 1 is shown in Fig. 9. The curves in Fig. 9 were obtained from Eqs. (22) and (23) while the circled points came from integration of Eq. (6).

TABLE 1

$10^2K_2^2$	$10^2K_1^2$	Initial Maximum	Initial Minimum
0.600	0.800	S	S
0.600	0.825	S	S
0.600	0.850	S	S
0.600	0.875	S	S
0.600	0.900	N	U
0.600	0.925	U	U
	Predicted $10^2K_1^2$: 0.895		
1.200	0.450	S	S
1.200	0.475	S	S
1.200	0.500	S	S
1.200	0.525	S	S
1.200	0.550	S	U
1.200	0.575	U	U
1.200	0.600	U	U
	Predicted $10^2K_1^2$: 0.555		

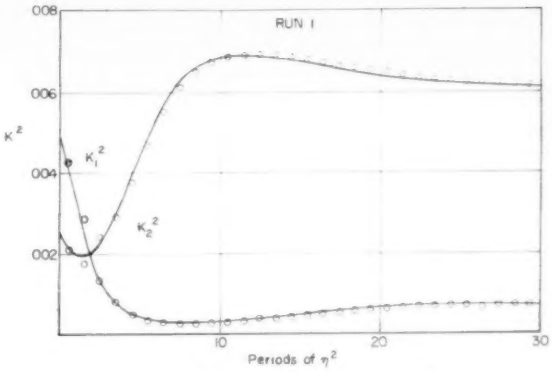

FIG. 9. K_1^2 and K_2^2 vs. periods of η^2.

CONCLUSIONS

An approximate solution of the nonlinear angular motion of a symmetric missile has been obtained. The concept of an amplitude plane which is associated with this solution has been introduced and shown to be very valuable in the determination of the dependence of the type of motion on initial conditions. The results of the theory have been checked with free-flight measurements and exact numerical calculations.

REFERENCES

[1] Highberg, I., N.O.T.S. T.N. 5036-94 July, 1951 (Confidential).

[2] Zaroodny, S., *Special Yawing Motions of 81-mm M56 Shell—A Study in Non-Linear Theory*, BRL Memorandum Report 682, May, 1953.

[3] Davis, L., Follin, J. W., and Blitzer, L., *Exterior Ballistics of Rockets*, Office of Naval Research P-1002, July, 1953 (Confidential).

[4] Lietmann, G., *Non-Linear Equations of Motion of Spin-Stabilized Missile Solved by a Perturbation Method*, NAVORD 3364, August, 1954.

[5] Kryloff, N., and Bogoliuboff, N. B., *Introduction to Non-Linear Mechanics* (translated by S. Lefschetz); Princeton University Press, 1947.

[6] *American Standard Letter Symbols for Aeronautical Sciences*, ASA Y10.7-1954, American Society of Mechanical Engineers, October, 1954.

[7] Sacks, A. H., *Aerodynamic Forces, Moments and Stability Derivatives for Slender Bodies of General Cross Section*, NACA TN 3283, November, 1954.

[8] Murphy, C. H., *The Measurement of Non-Linear Forces and Moments by Means of Free Flight Tests*, BRL Report 974, February, 1956.

[9] Poincaré, H., *Sur Les Courbes Definies par une Equation Differentielle, Oeuvres*, Vol. 1; Gauthier-Villon, Paris, 1892.

[10] Murphy, C. H., *Prediction of the Motion of Missiles Acted on by Non-Linear Forces and Moments*, BRL Report 995, October, 1956.

[11] Cohen, C. J., and Hubbard, E. D., Unpublished NORC Computations, U.S. Naval Proving Ground, September, 1956.

IAS Twenty-Sixth Annual Meeting

Hotel Sheraton-Astor, New York City, January 27–30, 1958

The Meetings Committee plans to schedule sessions on Aerodynamics, Aeroelasticity, Design, Electronics, Flight Propulsion, Instruments, Rotating Wing Aircraft, Safety in Flight, Structures, Air Transportation, etc.

Members or organizations wishing to have papers considered for presentation at this meeting should submit outlines or short abstracts to the Meetings Committee, 2 East 64th St., New York 21, N.Y., no later than August 1, 1957.

On Transition Experiments at Moderate Supersonic Speeds†

MARK V. MORKOVIN*
The Johns Hopkins University

SUMMARY

Studies of transition over a flat plate at Mach Number 1.76 were carried out using a hot-wire anemometer as one of the principal tools. The nature and measurements of free-stream disturbances at supersonic speeds are analyzed. The experimental results are interpreted in the light of present overall information on transition at supersonic speeds and conclusions as to further fruitful experiments are drawn.

SYMBOLS

db = decibel level of sound intensity with the pressure of 2×10^{-4} dynes/cm.^{2} as reference level = $20 \log_{10} (\Delta p') + 74$
M = Mach Number
p = pressure, dynes/cm.^{2}
Re = Reynolds Number, based on free-stream conditions and length indicated by subscript
T = mean absolute temperature
u = perturbation in axial velocity component
U = mean axial velocity
v = vertical velocity component
x = axial distance from leading edge of plate, in.
y = vertical distance from plate, in.
z = lateral distance from centerline of plate, in.
δ = boundary-layer thickness
δ^* = displacement thickness of boundary layer
Δ = perturbation of the quantity which follows
θ = momentum thickness of boundary layer

Subscripts

0 = free-stream value in settling chamber
1 = free-stream supersonic value

Superscripts

′ = root mean square value of fluctuation
″ = inches

INTRODUCTION

DURING 1952 and 1953 a series of experiments on transition on a flat plate were performed in The Johns Hopkins University continuous supersonic wind tunnel at the free-stream Mach Number of 1.76. The distinctive feature of the program was the usage of a supersonic hot-wire anemometer. It was concluded at the time that, with the available equipment, the individual measurement and control of the many causes of transition and the measurement of the corresponding disturbances in the boundary layer fell short of that needed for a fundamental study. It has been suggested that a brief account of these results would be useful to other investigators in the light of our present understanding of the problem, at least in a qualitative manner. In particular, it should throw some light on the possible influence of free-stream "turbulence" and other tunnel disturbances on the differences in transition Reynolds Numbers observed in different tunnels. For flat plates in streams near Mach Number 2, reported transition Reynolds Numbers range from approximately one million[25, 34] to more than three millions.[9, 13]

Received October 22, 1956.

† This research was supported jointly by the Office of Naval Research, U.S. Navy, and by the Air Office of Scientific Research, U.S. Air Force. The author is greatly indebted for many-sided help and cooperation on the part of his colleagues and assistants, in particular Dr. F. Clauser, Dr. L. S. G. Kovasznay, Mr. L. T. Miller, Mrs. F. Baake Chenoweth, and Mrs. P. Clarken McIlroy.

* Research Scientist, Department of Aeronautics.

EXPERIMENTAL CONDITIONS

The test section of the tunnel expands slowly to compensate for the growth of the wall boundary layer. It is 7.27 in. wide and 10.93 in. high at the leading edge of the flat plate, where the thickness δ and the displacement thickness δ^* of the turbulent sidewall boundary layer were approximately 0.6 and 0.12 in. In order to minimize the interaction with the sidewall boundary layer the plate extended only about halfway into the layer at the leading edge, where it was 6.75 in. wide, and was attached to the wall 15 in. downstream. The plate was 0.25 in. thick with a leading-edge angle of 11.2° (see Fig. 1). The higher pressure from the slanted lower surface "leaked" through the sidewall boundary layer over a distance of 1.26 in. and was followed by an expansion wave of approximately the same strength and length. The adverse pressure gradient on the top surface was thus kept within two oblique strips ($\varphi \sim 35°$) from the

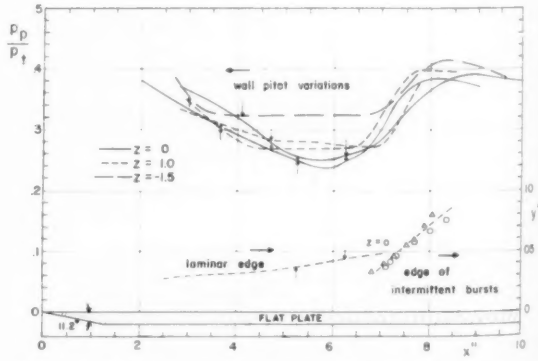

FIG. 1. Edge of boundary layer and wall pitot traverses in transition region. p_p = pitot pressure with probe pressed against plate; p_t = free-stream total pressure; z = distance from centerline; ↑ = beginning of mild adverse pressure gradient from corner of plate; ↓ = beginning of compensating favorable pressure gradient; Reynolds Number per in. $\sim .37 \times 10^6$.

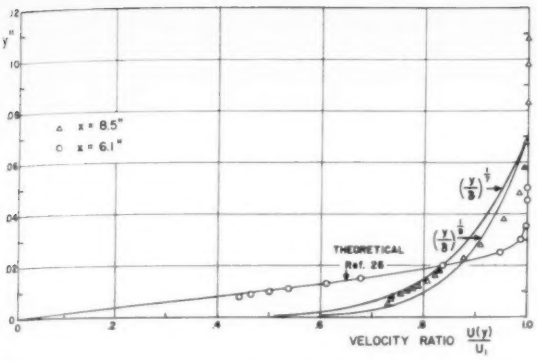

FIG. 2. Mean velocity profiles ahead and near end of transition region.

corners and corresponded to a maximum (gradual) Mach Number change from the unaffected forward value of 1.72 at $x = 5.0$ to 1.69 at $x = 6.25$ on the centerline $z = 0$. For most of the tests the plate was kept at a small negative angle of attack in order to decrease the chance of a disturbing separated bubble on the top surface.[33] Since there was some variation of the settling chamber turbulence level over the available range of stagnation pressures (±10 per cent of atmospheric), the tests were run at an essentially fixed Reynolds Number per inch—namely, 0.37×10^6. Continuous (but not simultaneous) vertical and horizontal traverses with standard JHU (Johns Hopkins University) hot wires[1] and conventional circular Pitot tubes (0.016 in. OD, 0.010 ID) provided the observed variations of boundary layer characteristics.

Transition Patterns

It does not appear to be generally appreciated that (except in the regions where Tollmien-Schlichting waves dominate) the traces from a hot wire inside a laminar boundary layer differ primarily in amplitude but not in character from those in a turbulent layer (see, for example, Fig. 13 of reference 2 and Fig. 11 of reference 17). A clear distinction and, therefore, a simple positive identification of the transition region can, however, be made from the character of the entry into the boundary layer from the free stream during vertical traversing with the hot wire, especially at high speeds. Entry into the laminar layer was characterized by pronounced low-frequency (90–120 c.p.s.) undulations of the trace corresponding to small natural vibrations of the probe-supporting mechanism; vertical motion of the wire on the order of 0.001 in. across the "edge" of the very thin layer corresponded to effective velocity signals of 3 ft./sec. and higher.† The outer edge of the turbulent layer is detected from the unmistakable high-intensity short-duration spikes corresponding to the difference of fluctuations in the free stream and in the turbulent crests of the layer (see Fig. 16 of reference 1). Sample outlines of the edges of the layers so obtained are seen in Fig. 1.

Fig. 1 suggests that the initial turbulent bursts originate well within the laminar layer but that they grow very rapidly outward, at lateral speeds of 30 to 60 ft./sec. Limitations on spatial and frequency resolution due to the high speeds[1] prevented more detailed study of the structure and of the statistical distribution of these spots, which could well correspond to those of Emmons.[3, 4] From continuity considerations, the upstream edge of the turbulent fluid should radiate a local narrow rarefaction wave. However, the occurrence of the high lateral speeds of the turbulent crests above the extrapolated edge of the laminar layer suggests that actual motion of mass is involved and not merely a wave propagation of velocity in an unstable layer. Hence strong compressive sound waves should be generated whether the relative horizontal speed of the turbulent lumps with respect to the free stream is subsonic or supersonic. Horizontal traverses with the hot wire well above the boundary layer indeed picked up the radiated sound as a substantial but gradual rise in a.c. signal downstream of the Mach line originating near $x = 6.5$. Analysis[5] of the incremental signal indicated that the wave fronts of the sound pulses do not exhibit any dominant direction, even though as a whole they move outward along free-stream Mach lines. Intensities on the order of 140 db. or more (based on 2×10^{-4} dynes/cm.^{2} as zero pressure level), that is, r.m.s. pressures of 0.9 per cent of local free-stream pressure were inferred. The fine structure of the field (which at higher speeds includes discontinuities observable on shadowgrams)[6, 7] should contribute substantially to the total sound energy but was obscured and partially suppressed by the frequency limitations.

Comparison of Transition Reynolds Numbers

Repeated hot-wire breakage close to the plate (especially in the violent region between $x = 6.5$ and 7.5) and local flow separation[8] when the probe approached the wall farther upstream prevented exploration of the edge of bursts ahead of the $x = 6.8$ station. Reasonable extrapolation of the hot-wire measurements from Fig. 1 would lead to the following Reynolds Numbers for the start‡ of the transition region:

† Similar generation of signal by lateral motion across a shear gradient was employed to determine the natural frequency of vibration of the flat plate—another potential transition promoter. A low-speed jet in the otherwise quiescent tunnel created a shear layer over the plate. When the plate was struck sharply, its vibrations moved the layer across a hot wire, giving rise to regular waves between 180 and 220 cps, of no consequence to supersonic transition.

‡ Since one could not reliably distinguish between signals from small laminar lacunae imbedded in turbulent regions and signals from the variation in turbulent velocities themselves at these high speeds the hot wire gave a poor indication of the end of the transition region. In particular, the criterion of maximum wall pitot pressure indicated an ending at $Re_x \sim 3.2 \times 10^6$ while the a.c. hot-wire traverse of the layer at the point showed little resemblance to the structure of the developed turbulent layers at the wall (reference 1, Figs. 16 and 17), and the mean velocity profile could not be fitted into the customary power-law shapes (see Fig. 2).

$$Re_x \sim 2.3 \times 10^6, \quad Re_\delta \sim 1.6 \times 10^4,$$
$$Re_{\delta^*} \sim 7.6 \times 10^3, \quad Re_\theta \sim 1.7 \times 10^3$$

Comparison should be made with the highest reported transition Reynolds Number on flat surfaces at the same Reynolds Number per inch and comparably "low" supersonic Mach Numbers. Coles' data[9] (see Fig. 18, Re/in. $\sim .37 \times 10^6$ at $M = 1.97$) give $Re_x \sim 3.3 \times 10^6$ when judged by the rise in wall static pressure and $Re_x \sim 2.6 \times 10^6$ when judged by the minimum of shearing stress,** while Shoulberg et al. (Fig. 4 of reference 13,†† Re/in. ~ 0.3 to 0.46×10^6, $M \sim 1.98$) indicate $Re_x \sim 3.3 \times 10^6$ based on the minimum of the temperature recovery factor. The minimum shearing stress criterion should correspond to that of minimum wall pitot pressure (see Fig. 1) which on the centerline gave $Re_x \sim 2.1 \times 10^6$. In view of the known trends[9, 10] of transition Re with Mach Number, the JHU transition would appear to occur somewhat early.

The fundamental fact which obscures our understanding of transition lies in the existence of large number of its causes[10, 15] (promoters) whose effect cumulates and varies with local boundary-layer velocity and temperature distribution, Reynolds Number, Mach Number, etc. Often enough one or two causes dominate and mask the effect of the others until they are sufficiently reduced in strength so that other dominant causes may emerge. It is therefore not surprising that different testing facilities indicate contradictory trends as a given parameter is varied. For experimental clarification it seems essential to be able both to characterize or measure the causes and to control the corresponding nondimensional parameters individually within wide limits. Furthermore, studies§ of the cumulating response (prior to transition) of the laminar layer to the controlled promoters should furnish clues as to the mechanism(s) of transition itself. The background of even partial theories[11, 12] is of course an invaluable help for the design of the experiment and the correlation of the data.

The Effect of Variations of Disturbances

The specific difficulties with supersonic experiments center around the problems of the detailed control of model and wind-tunnel conditions and of the spatial and timewise resolution of the measuring instruments (which include probe interference, vibrations, noise, etc.).

Gross changes in those promoters which were likely to affect the laminar layer and the transition pattern as described were tried in order to bracket the effects. The distributed roughness of the plate increased gradually through the experiments and was diminished abruptly by careful repolishing without any palpable effects. Trippers near the leading edge, especially those that provided a length of separated boundary layer (such as two bands of tape 0.014 in. thick with a gap of 0.35 in.) did move the transition pattern forward—i.e., it became dominant at this relatively low Mach Number.† The actual location of the transition occurred 0.5 to 3 in. downstream‡ of the reattachment but seemed to depend rather strongly on free-stream disturbances (cf. page 6 of reference 21). The uniformity and sharpness (approximately 0.001 in. in diameter) of the leading edge deteriorated with time and was restored without appreciable shift in transition. This lack of sensitivity does not contradict our present knowledge[16] of a range of influence of leading-edge thickness because of the relatively small Mach Number and small thickness changes in the experiment. Spanwise nonuniformities of the leading edge have been known to promote earlier transition on wedges presumably by generating streamwise vortices but apparently did not constitute strong enough disturbances in the present case.

Furthermore, no measurable shift of transition resulted when the axial component of the settling chamber turbulence‡‡ was raised from 0.74 per cent to 4.6 per cent of the mean velocity (10.2 ft./sec.) by installing a special grid (0.75 in. square bars, 4 in. on center) 57 in. upstream of the beginning of the nozzle. Temperature fluctuations in the settling chamber were on the order of the noise of the equipment—negligible. The settling chamber turbulence was also raised by placing a horizontal cylindrical bar, 1 in. in diameter, 12 in. upstream of the beginning of the nozzle and in line with the leading edge of the plate. The turbulent pattern downstream of such rods, including the probability distribution and spectrum of u', was known from Roshko's studies.[20] The turbulent fields observable in the settling chamber are, of course, strongly modified during the passage through the nozzle. These changes can be estimated to some extent by relying on linear theories of Ribner and Tucker[26] and on their comparison with Uberoi's experiments.[27] Some limited measurements of turbulence in the supersonic test section are also available as will be discussed in the section on free-stream disturbances in supersonic tunnels in general.

** Need for caution when interpreting experiments only in terms of location of transition is underlined by the fact that, in the same tunnel, with essentially the same plate as Coles worked in 1952, reference 25, p. 7, reports in 1956 the beginning of transition as sensed by a hot wire at $Re_x \sim 0.9 \times 10^6$, whereas Coles' data interpolated to the corresponding Mach Number and Re/in. would indicate Re_x of 1.7 to 2.1×10^6.

†† Reference 13 exhibits a trend of transition Re with Re/in. at variance with that generally reported[10, 15] for models without pressure gradients, especially with reference 9.

§ Such as attempted at low speeds by Schubauer and Skramstad,[17] Schubauer and Klebanoff,[3] Bennett,[2] Liepmann[33] and others and at high speeds by Laufer and Vrebalovich [24]

† Trippers become less effective as Mach Number increases,[8] and it is probably more than coincidence that there is a corresponding very large increase in the stability of free boundary layers as seen in Fig. 8 of reference 19 and predicted in reference 35.

‡ As in reference 18 ($M_1 = 5.8$) lateral contamination angles were narrower than at low speeds,[3] namely 5° to 7°, increasing slowly downstream.

‡‡ These and the simultaneous supersonic measurements were performed by P. Clarken and L. S. G. Kovasznay.

The circular bar (Reynolds Number $\sim$ 5,400, Strouhal Number[20] $\sim$ 0.21) was shoved in and out of the settling chamber as the heated wire monitored the supersonic laminar layer on the plate. The comparison established beyond doubt that, with the rod in, turbulent spots, "lasting" less than a millisecond, originated somewhere upstream of $x = 3''$ with an average frequency of approximately one in twenty seconds—i.e., not often enough to influence the mean location of transition. Presumably, these spots were brought about by the high tail end of the distribution function of the velocity fluctuations (reference 20, Fig. 19) not unlike the spots of Schubauer and Klebanoff[3] were generated by high velocity disturbances associated with discharge of sparks.

Otherwise, the lack of sensitivity of the transition region on the plate to changes in stream turbulence in the settling chamber contrasts with the effects reported for 10° cones by Evvard et al.[14] at $M_1 = 3.12$, and for 5° cones by Laufer and Marte[10] at Mach Numbers below 2.2. However, Laufer and Marte found no effect of settling chamber turbulence on transition in the test section at $M_1 = 2.55$ and higher. It is possible that (1) slender cones are more sensitive to free-stream turbulence with high energy slow eddies being equivalent to changes in angle of attack [this might be inferred from the observed rapid forward shift of transition when the angle of attack changes (see Witt,[7] Fig. 9, and Jedlicka, et al.[6]), presumably because of lower stability of three-dimensional boundary-layer flows[22]]; (2) the transition on the JHU plate was dominated by some other cause than free-stream fluctuations; (3) the actual maximum disturbance level in the supersonic section was lower in the JHU tunnel because of the high speed ratio across the nozzle (150) and remained below the threshold observed in reference 10 at higher Mach Numbers, $M_1 > 2.55$.

A number of measurements were made of the free-stream disturbances at the time of the experiments and in 1955 but these must be interpreted in terms of our present understanding of hot-wire response at high speeds.[5] To appreciate the situation let us consider free-stream disturbances in supersonic wind tunnels in some detail, especially since many other discrepancies in reported measurements have been "explained" as probably due to differences in free-stream "turbulence." (See also reference 39.)

Free-Stream Disturbances in Supersonic Tunnels

At any given point fluctuations in a gas can be viewed[1, 5] in the first approximation as a superposition of three modes of covarying physical properties: (1) "sound" mode (variation of pressure, density, and temperature at constant entropy and of the coupled irrotational velocity field); (2) "entropy" mode (variation of entropy, density, and temperature at constant pressure), and (3) "vorticity" mode (variation of the solenoidal component of the velocity field which is known as "turbulence" at incompressible speeds). The entropy and vorticity modes are essentially convected

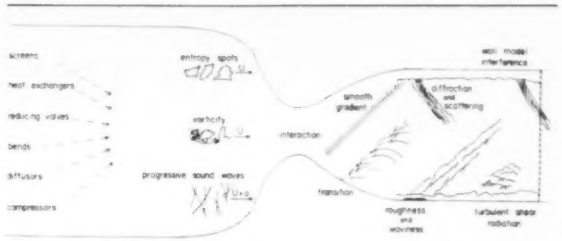

FIG. 3. Free-stream disturbances in supersonic wind tunnels.

along streamlines (see Fig. 3) so that in a supersonic tunnel they must be traceable (with distortion) to conditions in the settling chamber (or be generated during the acceleration through the nozzle, a second-order effect according to present beliefs). The sound disturbances can travel across streamlines so that they may come from the settling chamber† and from the boundaries of the test section.‡ Disturbance levels that are high enough in any of the three modes may promote transition, although the actual coupling mechanisms are not known.

For convenience, sound fluctuations originating at the wall (see Fig. 3) can be classified into four types: (a) radiation from nascent turbulence as described earlier, (b) radiation from developed turbulent boundary layers [see references 23, 24], (c) diffraction and scattering of otherwise steady pressure gradients and shock waves (as generated by nozzle contours, unintended waviness or roughness, models, supports, etc.) through the turbulent boundary layer, and (d) radiation from unsteady wall vibrations caused by pressure fluctuations in the boundary layer or by the loads on the diffusor, associated with the unsteadiness of the terminal shock wave.** While the hot-wire anemometer is

† In low-speed tunnels sounds from the various parts of the system are critical for low-turbulence operations.[17, 37] In supersonic tunnels the noise level has to exceed 120 db or more to be of consequence relative to the high free-stream speeds—i.e., 1,500 ft./sec. in the present case. The amplification of the sound due to the contraction could not exceed 6 db. Sound levels on the order of 114 db were definitely not reached in the settling chamber as the author can testify from personal experience. As the wind tunnel was going up in speed, the noise in the settling chamber did rise to very uncomfortable heights until the speed of sound was reached in the nozzle and cut off the sound sources in the diffusor. Thereafter, a pleasant though breezy atmosphere prevailed with the noise level estimated at no more than 70–80 db—of no consequence for disturbances in the supersonic test section.

‡ There may be substantial generation of sound when high-intensity entropy spots are swept through the nozzle, as in jet engines and rockets.

** Assessment of the magnitude of sound of category (d) along the lines of Ribner[38] and Corcos-Liepmann[37] indicates that it is unlikely to reach the intensity of the sound of category (c)—i.e., 120–130 decibels. A similar conclusion follows from the comparison of the wall sound radiated into the tunnel with its counterpart, sensed in the room around the tunnel. Since the tunnel walls (in contrast to the skin of aircraft) are designed to minimal deflections, this conclusion is not surprising. Other factors which limit the inward wall radiation are (1) the very low air density near the wall, (2) the relatively high density of the wall material, and (3) the relative thinness of the boundary layer which governs the scale of the pressure fluctuations.

sensitive to all of the fluctuation modes and categories of sound, the combined electrical signal cannot be satisfactorily decomposed into the separate contributions unless the sound mode has a preferred wave-front orientation.[5] That happens to be the case for progressive waves from isolated sources and for the diffracted pressure gradients but not for the other categories of sound where more random orientation prevails. Consequently, there will remain some uncertainty as to the composition and intensity of free-stream disturbances in the tunnel when measured by a single hot wire no matter how accurate the electrical measurements may be.

Actually, measurements of free-stream fluctuations in good supersonic tunnels are of the threshold type, plagued by problems of calibration, noise, frequency resolution, and unsteady strain-gage effect,[5] so that the decomposition of the signal into the constituent flow disturbances is further complicated and uncertain. Depending then on the assumptions of specific orientation of sound wave and the presence or absence of correlation between the entropy and the vorticity modes, the free-stream data indicated the vorticity-mode measure u'/U_1 from 0.0003 to 0.0007 and the entropy-mode measure $\Delta T'/T_1$ from 0.0003 to 0.0008—i.e., r.m.s. (solenoidal) velocity fluctuations u' from 0.5 to 1.05 ft./sec. and r.m.s. (nonisentropic) temperature fluctuations from 0.1 to 0.26°F. In view of the presence of extraneous electrical signals these results are believed to be high by a factor up to 3.

Before turning to the corresponding indications of sound intensity, it is instructive to compare these results with the prediction of Ribner-Tucker linear theory.[26] For the quoted u'/U_0 of 0.0074 in the settling chamber (assumed isotropic) the theory would lead to the longitudinal component u'/U_1 of 0.00023 and the lateral component v'/U_1 of 0.00028. From Uberoi's measurements at low speeds (see Figs. 8 and 9 of reference 27) one can infer that the nonlinear effects and the viscous decay, which were neglected in the theory would tend to equalize the lateral and the longitudinal components and reduce the total energy. Thus measurements and theory, with proper interpretation, indicate that the vorticity level in the supersonic test section was indeed very low. As to the entropy fluctuations, one would expect these to be preserved in the passage through the nozzle except for some decay due to heat conduction. Indeed, temperature fluctuations on the order of 0.16 to 0.42°F. were consistent with the measurements in the settling chamber (the low-speed temperature sensitivity being relatively poorer). The level of temperature (entropy) fluctuations in the supersonic test section was then also very low since fluctuations of 0.2°F., for instance, need to be compared with the total change of static temperature of 172°F. across the laminar layer.

In view of the low absolute level of vorticity and entropy fluctuations in the supersonic section, the lack of shift in transition when the settling chamber turbulence was raised sixfold appears now less surprising. Originally it was inferred from the supersonic hot-wire data that the corresponding rise in vorticity could not have exceeded 15 per cent. It now appears likely that the assumptions of the absence of sound of categories (a) and (b) and of the absence of an extraneous electrical signal, which led to the 15 per cent estimate, were unjustified. Since uncorrelated signals are added in the square, the low vorticity in the supersonic section may have risen four to sixfold and caused only a small increase in the r.m.s. electrical signal in presence of the other larger disturbances.

In absence of strain-gage signals the inferred sound intensity in the free stream ranged from 125 to 131 db, i.e., r.m.s. pressure fluctuations were from 0.2 to 0.4 per cent of free-stream pressure. The corresponding values of the r.m.s. longitudinal component of the irrotational velocity fluctuations u' would be from 0.7 to 1.4 ft./sec. if the dominant sound were of category (c)—shivering Mach waves. When estimates of possible extraneous signals are taken into account, the sound level may be lowered by as much as 10 db. and the velocity and pressure fluctuation decreased by a factor up to 3.

The most accurate sound measurements were those of "incremental" sound—i.e., from the rise in signal between two points on the same streamline which is due to a localized increase in sound generation at the wall (such as that due to an element of roughness, diffracted by the turbulent boundary layer or due to transition on the plate). Because the background contributions are subtracted it is not necessary to assume specific orientations for the analysis—most often the near Mach line orientation is deducible from the data.[5] In the same way one can analyze their spectra. A 1955 experiment by the author[5] traced a very weak shock ($M_1 = 1.76$, steady $\Delta p/p_1 = 0.049$; unsteady pressure signal = 145 db., $\Delta p'/p_1 = 0.02$; total unsteady horizontal spread sensed by the imperfectly resolving hot wire = 0.004 in.) as it impinged upon the turbulent wall boundary layer (0.6 in. thick) and reflected outward. The reflected unsteady wave exceeded 125 db. level over a horizontal distance of 0.4 in. and reached a maximum† of 134 db. (r.m.s. $\Delta p' = 0.7$ per cent of local static pressure). Its normalized energy spectrum as well as the vorticity and entropy spectra at a representative point in the reflecting boundary layer ($y/\delta = 0.2$) are shown in Fig. 4.

It would therefore appear that imperfections in nozzle contours and wall giving rise to narrow d.c. pressure changes are accompanied by a.c. pressure waves which spread appreciably upon each reflection from the turbulent boundary layer. Experience, as well as calculations (based on data of reference 38), indicates that most Mach waves discernible by sensitive schlieren apparatus have an a.c. content on the order of 120 to 130 db. even if they appear steady to the eye. Many tunnels are then dense with shivering sound waves. One can

† The sharp shocklet was followed by a gradual Prandtl-Meyer expansion wave to $M = 1.96$ which may have reduced the intensity of the reflected wave somewhat.

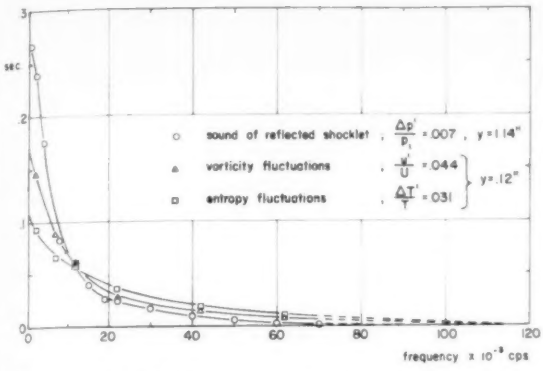
sec
sound of reflected shocklet , $\frac{\Delta p'}{p_1}$ = .007 , y = 1.14"
vorticity fluctuations , $\frac{u'}{U}$ = .044
entropy fluctuations , $\frac{\Delta T'}{T}$ = .031
y = .12"
frequency x 10⁻³ cps

FIG. 4. Normalized spectra of vorticity and entropy fluctuations in a turbulent boundary layer at $M_1 = 1.76$ and of the sound reflected from the layer.

speculate that their strength varies with $\delta\partial(\log p)/\partial x$, where $p(x)$ would be the pressure field generated by the obstacle in an inviscid fluid, and with the intensity of the local Mach Number fluctuations. Lower frequency fluctuations would cause larger spatial excursions of wave fronts and would increase the sound strength. Furthermore, the various parameters governing upstream influence in supersonic boundary layers as analyzed by Lighthill[31] should also affect the present phenomenon. Thus, for a given wall geometry this sound of category (c) is likely to decrease with Mach Number [while that of category (b) may possibly increase].

In some tunnels stronger waves (even when weak enough to be missed during tunnel calibration[29]) were shown to be the direct cause of early transition (see reference 14, p. 8, and reference 30, p. 5). One must keep in mind that lateral Mach waves from sidewalls of tunnels are more likely to be missed because they are not visible with schlieren apparatus‡ and are sensed by hot wires only if mounted vertically. Transition may be hastened by such pressure waves through (1) local steady or unsteady separation of the boundary layer, (2) inducement of steady three-dimensional boundary-layer flow which is less stable[22] (on bodies of revolution generally and on flat plates in presence of lateral pressure waves), and (3) feeding of disturbance energy into two- or three-dimensional Tollmien-Schlichting waves. For the JHU boundary layer the dangerous frequency band was estimated to fall between 12 and 30 kc. per sec., and a glance at Fig. 4 shows that the relative contribution to that band from the sound of category (c) is on the same order as the contributions from free-stream turbulence at low speeds.[2, 12] By contrast, free-stream vorticity and temperature fluctuations which were generated in the low-speed parts of the supersonic tunnel system by grids and rods[20, 27] were estimated to have no appreciable energy above 4–8 kc. and were therefore less likely to feed the T-S waves in the supersonic boundary layer.

Actually one of the many reasons for discontinuing the experiment was that no regular frequencies of the signals were discernible in 1952 and 1953 (when no suitable harmonic analyzer was available) and it was surmised that a different mechanism dominated the transition pattern. Recently, Laufer and Vrebalovich[25] discovered that Tollmien-Schlichting waves do build up at supersonic speeds as well, but that their amplification rate is very much smaller than at low speeds (as predicted by recent advances in the stability theory), a fact that explains the need of a harmonic analyzer for their detection. The mechanism and the final criterion for the breakdown of T-S waves into a turbulent pattern—i.e., the actual occurrence of transition—remains unclear at any speeds.[3, 12, 33]

One clue as to the presence of a potentially strong transition promoter came from the early flattening of the surface-tube traverses off centerline on the flat plate (see Fig. 1). The measured static pressure or Mach number gradients, quoted earlier, did not appear more serious than those for other tunnels—for instance, for reference 13 where higher transition Reynolds Numbers were reached. In particular, they were weak enough not to cause steady local two-dimensional boundary-layer separation. However, an axial traverse with the hot-wire vertical just outside of the boundary layer along $z = 0.82$ in. disclosed a strong peak in the sound signal at $x = 4.4$ in. Superposed on the gradual mean pressure field from the corner of the flat plate was a relatively narrow sound wave of maximum intensity of 136 db. ($\Delta p'/p_1 = 0.0073$, $u' = 2.6$ ft./sec.). It is conceivable that this oblique wave occasionally reached instantaneous values sufficient to separate the layer locally and cause the time-averaged flat variation of pitot wall pressure seen in Fig. 1. The unsteady character was impressed upon the pressure wave by the sidewall boundary layer so that its spectrum probably resembled that of the reflected sound in Fig. 4. The corner waves then could also feed energy into the unstable Tollmien-Schlichting waves.

An attempt was made to compare the hot-wire traces upstream and downstream of this oblique corner wave but no differences were discernible with the equipment then available. This was indeed disappointing in view of the overall indications that there was some cause dominating the transition pattern in the JHU tunnel and that the corner and side-wall interference formed the strongest disturbance measured. This inability to trace the direct effect of such disturbances on the boundary layer was the final reason leading to the conclusion that a more versatile tunnel (allowing higher Mach Numbers and a wide variation in stagnation pressure) as well as improved equipment and techniques were needed for a basic experimental program on supersonic transition.

CONCLUSION

Partial description of the transition pattern on a plate and of free-stream disturbances in supersonic wind tunnels as sensed by a hot-wire anemometer has been presented. The specific case was used as an illustration of existing limitations on our knowledge of the set of conditions under which a given pattern of transi-

‡ Their reflection from cylindrical models or probes is visible.[32]

tion occurs on a given model in a given testing facility. A particular supersonic transition experiment must indeed be evaluated with care and all inferences drawn with caution. Still, the cumulative experience from different facilities has led (despite many contradictions) to valuable empirical conjectures and to substantiation of some trends of transition predicted by linearized stability theory. However, for more basic understanding of the transition phenomenon, broader studies (including features of efforts such as in references 2, 3, 17, 25, and 33) in the best of available facilities with substantially improved instrumentation remain essential.

References

[1] Kovasznay, L. S. G., *Turbulence in Supersonic Flow*, Journal of the Aeronautical Sciences, Vol. 20, No. 10, pp. 657–675, October, 1953.

[2] Bennett, H. W., *An Experimental Study of Boundary Layer Transition*, Kimberly-Clark Corp., Neenah, Wisconsin, September, 1953.

[3] Schubauer, G. B., and Klebanoff, P. S., *Contributions on the Mechanics of Boundary-Layer Transition*, NACA TN 3489, September, 1955.

[4] Emmons, H. W., *The Laminar-Turbulent Transition in a Boundary Layer*, Part I, Journal of the Aeronautical Sciences, Vol. 18, No. 7, pp. 490–498, July, 1951.

[5] Morkovin, M. V., *Fluctuations and Hot-Wire Anemometry in Compressible Fluids*, AGARDograph No. 24, NATO, June, 1956.

[6] Jedlicka, J. R., Wilkins, M. E., and Seiff, A., *Experimental Determination of Boundary-Layer Transition on a Body of Revolution at M = 3.5*, NACA TN 3342, October, 1954.

[7] Witt, W. R., Jr., *Free-Flight Boundary Layer Transition Studies on Cones*, Proc. Midwestern Conference on Fluid and Solid Mechanics, September, 1955.

[8] Morkovin, M. V., and Bradfield, W., *Probe Interference in Measurements in Supersonic Laminar Boundary Layers*, Journal of the Aeronautical Sciences, Vol. 21, No. 11, pp. 785–787, November, 1954.

[9] Coles, D., *Measurements of Turbulent Friction on a Smooth Flat Plate in Supersonic Flow*, Journal of the Aeronautical Sciences, Vol. 21, No. 7, pp. 433–448, July, 1954.

[10] Laufer, J., and Marte, J. E., *Results and Critical Disussion of Transition-Reynolds-Number Measurements on Insulated Cones and Flat Plates in Supersonic Wind Tunnels*, Jet Propulsion Laboratory Report No. 20–96, California Institute of Technology, November, 1955.

[11] Dunn, D. W., and Lin, C. C., *On the Stability of the Laminar Boundary Layer in a Compressible Fluid*, Journal of the Aeronautical Sciences, Vol. 22, No. 7, pp. 455–477, July, 1955.

[12] Lees, L., *Instability of Laminar Flows and Transition to Turbulence*, Consolidated Vultee Aircraft Report No. ZA-7-006, February, 1952.

[13] Shoulberg, R. H., Hill, J. A. F., and Rivas, M. A., Jr., *An Experimental Determination of Flat Plate Recovery Factors for Mach Numbers Between 1.90 and 3.14*, Journal of the Aeronautical Sciences, Vol. 21, No. 11, pp. 763–771, November, 1954.

[14] Evvard, J. C., Tucker, M., and Burgess, W. C., Jr., *Transition-Point Fluctuations in Supersonic Flow*, Journal of the Aeronautical Sciences, Vol. 21, No. 11, pp. 731–738, November, 1954; also NACA TN 3100.

[15] Dryden, H. L., *Recent Investigations of the Problem of Transition*, Zeit. f. Flügwissen., Vol. 4, No. 3–4, pp. 89–95, March, 1956.

[16] Brinich, P. F., *Effect of Leading-Edge Geometry on Boundary Layer Transition at Mach 3.1*, NACA TN 3659, March, 1956.

[17] Schubauer, G. B., and Skramstad, H. K., *Laminar Boundary Layer Oscillations and Transitions on a Flat Plate*, NACA TR 909, 1948.

[18] Korkegi, R. H., *Transition Studies and Skin-Friction Measurements on an Insulated Flat Plate at a Mach Number of 5.8*, Journal of the Aeronautical Sciences, Vol. 23, No. 2, pp. 97–108, February, 1956.

[19] Chapman, D. R., Kuehn, D. M., and Larson, H. K., *Preliminary Report on a Study of Separated Flows in Supersonic and Subsonic Streams*, NACA RM A55L14, June, 1956.

[20] Roshko, A., *On the Development of Turbulent Wakes from Vortex Streets*, NACA TN 2913, March, 1953, also NACA TR 1191.

[21] Sinclair, A. R., and Czarnecki, K. R., *Investigation of Boundary-Layer Transition on 10° Cone in Langley 4-by-4-Foot Supersonic Pressure Tunnel at Mach Numbers 1.41, 1.61, and 2.01*, NACA TN 3648, May, 1956.

[22] Gregory N., Walker, W. S., and Stuart, J. J., *On the Stability of Three-Dimensional Boundary-Layer with Application to the Flow Due to a Rotating Disc*, Phil. Trans. Roy. Soc. London, Series A, Vol. 248, No. 943, pp. 155–199, July, 1955.

[23] Curle, N., *The Influence of Solid-Boundaries Upon Aerodynamic Sound*, Proc. Roy. Soc. A, Vol. 231, pp. 505–514, 1955.

[24] Liepmann, H. W., *On the Acoustic Radiation from Boundary Layers and Jets*, Paper presented at the 23rd Annual Meeting of the Institute of the Aeronautical Sciences, January 24–28, 1955.

[25] Laufer, J., and Vrebalovich, T., *Experiments on the Instability of a Supersonic Boundary Layer*, Jet Propulsion Laboratory, California Institute of Technology, Publ. No. 350, August, 1956.

[26] Ribner, H. S., and Tucker, M., *Spectrum of Turbulence in a Contracting Stream*, NACA TN 2606, January, 1952; also NACA TR 1113.

[27] Uberoi, M. S., *Effect of Wind-Tunnel Contraction on Free-Stream Turbulence*, Journal of the Aeronautical Sciences, Vol. 23, No. 8, pp. 754–764, August, 1956.

[28] Chapman, D. R., and Rubesin, M. W., *Temperature and Velocity Profiles in the Compressible Laminar Boundary Layer with Arbitrary Distribution of Surface Temperature*, Journal of the Aeronautical Sciences, Vol. 16, No. 9, p. 547, September, 1949.

[29] Abbott, I. H., *Some Factors Contributing to Scale Effect at Supersonic Speeds*, AGARD Memo. AG 8/M4, September, 1953.

[30] Ross, A. E., *Determination of Boundary-Layer Transition Reynolds Numbers by Surface-Temperature Measurement of a 10° Cone in Various Supersonic Wind Tunnels*, NACA TN 3020, October, 1953.

[31] Lighthill, M. J., *On Boundary Layers and Upstream Influence II: Supersonic Flows Without Separation*, Proc. Roy. Soc. A, Vol. 217, p. 478, 1953.

[32] Morkovin, M. V., Migotsky, E., Bailey, H. E., and Phinney, R. E., *Experiments on Interaction of Shock Waves and Cylindrical Bodies at Supersonic Speeds*, Journal of the Aeronautical Sciences, Vol. 19, No. 4, pp. 237–248, April, 1952.

[33] Liepmann, H. W., *Investigations on Laminar Boundary Layer Stability and Transition on Curved Boundaries*, NACA Wartime Report No. W-107, August, 1943.

[34] Ladenburg, R., and Bershader, D., *Optical Studies of Boundary-Layer Phenomena on a Flat Plate at a Mach Number 2.35*, Palmer Physical Laboratory, Princeton, N. J., December, 1952.

[35] Lin, C. C., *On the Stability of the Laminar Mixing Region Between Two Parallel Streams in a Gas*, NACA TN 2887, January, 1953.

[36] Ribner, H. S., *Boundary-Layer-Induced Noise in the Interior of Aircraft*, Report No. 37, University of Toronto, Institute of Aerophysics, April, 1956.

[37] Corcos, G. M., and Liepmann, H. W., *On the Contribution of Turbulent Boundary Layers to the Noise inside a Fuselage*, NACA TM 1420, December, 1956.

[38] Mair, W. A., *The Sensitivity and Range Required in a Toepler Schlieren Apparatus for Photography of High-Speed Air Flow*, Aero. Quarterly, Vol. 4, No. 1, August, 1952.

[39] Morkovin, M. V., *Thoughts on Supersonic Wind Tunnels with Low Free-Stream Disturbances*, Johns Hopkins Univ. Rept., November, 1956, AFOSR Tech. Note TN-56-540, ASTIA Document No. AD-110-359.

On the Frequency Spectrum Generated by a Maneuvering Aircraft†

A. P. BROGLE*

U.S. Army Signal Engineering Laboratories

SUMMARY

In this paper, an upper limit in amplitude for the frequency spectrum of aircraft motion is found. The existence of a bound on the absolute value of acceleration—i.e., a finite centripetal acceleration capability of aircraft—is the underlying phenomenon which determines the limit on the transformed position motion. In determining this bound, only periodic motions of the aircraft are considered, and the only aircraft characteristic taken into account is maximum acceleration. It is shown that the derived maximum may be applied to the determination of the bandwidth characteristics for a communication-control fire direction or interception system. A simple relationship is found to exist between the value of the amplitude limit at any frequency and the maximum error in position, without regard to time delay and noise, which occurs in a communication-control system of specified bandwidth. Since a dominant criterion of these systems appears to be to obtain adequate performance during maneuvers of the aircraft, the general result applies to an important operational problem. Several examples of the usefulness of the result in the determination of such system characteristics as bandwidth, sampling interval, or transfer function for a specified accuracy are illustrated.

INTRODUCTION

COMMUNICATION and control systems in which the position of a moving aircraft is the applied information variable are receiving considerable attention today. Like other communications systems, these communication - fire-control systems depend upon the ability of a limited band of frequencies to convey to the ultimate receiver an up-to-date reproduction of the flight information, even though the information itself is not spectrum limited. This condition is, in general, basic to all of these systems and specifies that fine structure of the information is inevitably lost during measurement, transmission, or computation. Since a limited time is prescribed in which to recover flight information in the communication - fire-control system, this loss of detail always results in distortion at the system output. An important problem of these systems is to assess the magnitude of this error in terms of the characteristics of the applied information and for given bandwidth conditions.

With the ever-increasing problem of reduced channel capacity for communication-control systems, a further question arises concerning the optimum balance between signal and noise to achieve best performance within the confined bandwidth. For example, if the available channel bandwidth is weighed too heavily in favor of noise, signal bandwidth is reduced, and the dynamic errors may become excessive. On the other hand, noise cannot be ignored to obtain rapid following since the fine detail obtained may be mostly noise.

In the presence of distortion and noise then, optimization of a system results only from the use of as much a priori knowledge of the nature of the applied information as can be obtained. For systems of the type of interest here, the information variable is any one of an infinite number of possible flight paths.‡ Since this statement alone is not a sufficient description, it is desirable to find some common characteristic of the input variable that is meaningful in terms of the operational problem to be solved by the system. For example, if it is the average behavior of the system that is important, a flight path can be described, by statistical means, that is representative of the class of input functions to be handled. This method is often a convenient one since noise is also best described in statistical terms, and techniques are then available which can specify the average response for a given transfer function or, alternatively, a system transfer function that yields best average response, usually in the mean square sense. However, it is believed that this and similar averaging methods do not, in general, satisfy an important operational requirement which is placed upon communication - fire-control systems.

In examining the usual application of these systems—namely, to air defense and to air navigation and control—it becomes apparent that, irrespective of noise conditions, a primary condition sought is adequate performance during the times when evasive actions or turning motions of the aircraft are occurring. This is so because of the severe operational consequences usually attached to the loss of a target. Since it is at just the times of maneuver that the system has most difficulty in following the target, the probability of losing or of missing the target is also greatest during this same period. Thus, if aircraft maneuver is an event which may well defeat the purpose for which a system is designed and if that event is a likely occurrence, an essential requirement of the system is established. It immediately follows, therefore, that a dominant criterion of these systems must be to keep the posi-

Received January 9, 1956.

† The author is indebted to M. M. Brenner who provided the original incentive for this work and to his other associates at U.S. Army Signal Engineering Laboratories for their interest and cooperation. Acknowledgment is also made to W. D. White of Airborne Instruments Laboratory who offered stimulating criticism during an early phase of the work.

* Electronics Engineer, Countermeasures Division.

‡ The term "flight path" is used to denote the continuous line in space that is generated by a moving aircraft.

tion error during anticipated maneuvers of the aircraft within the resolution capability of the system. Resolution capability as used here is a rather general term and applies to the ability of the system to perform acceptably any or all of the functions of initial tracking of the aircraft at the system input, of transmitting this information over the communication channel, and of aiming the guns or directing the interceptor or missile to the target at the output.

Although the foregoing is a principal argument supporting the maneuver criterion, it is well to point out that many factors other than those indicated are important in specifying the detailed performance required for any real application. Nevertheless, the significant point here is that aircraft maneuver appears to be a most important input form to be considered for these systems and that adequate protection against this event probably has to be obtained at the expense of a higher level of average performance than would be required by a less stringent, but more unrealistic, criterion.

If position error during maneuver is to serve as a useful measure of system performance, it is evidently desirable to find the relationship which exists between the position error at the system output and both the characteristic of the system input variable which specifies maneuver capability and the characteristics of the system itself. In this paper, such a relationship is found which appears to be useful in a number of important cases.

Although several approaches to the problem of defining the behavior of the applied information variable are undoubtedly available, a method which has possible advantages is a study of the transformed motion—i.e., the frequency spectrum of a maneuvering aircraft. An immediate advantage is that such a description permits consistent usage of the well-known frequency domain language in which the communication or control system is usually described. Recalling that an infinite number of flight paths is possible, it is seen that this spectrum may take on an infinite variety of shapes. A possible limitation of the frequency domain technique in expressing a priori information in concise form therefore becomes apparent, especially since statistical techniques which lead to average results do not appear to best match the physical situation here. However, it will be shown that a particular spectrum can be found which defines the upper limit in amplitude under which all spectra of moving aircraft of specified acceleration capability are constrained to fall. Furthermore, this spectrum is obtained for a maneuver that appears to be a highly probable form of evasive action. Thus, a common characteristic of the input variable which specifies maneuver capability is determined. It will also be shown that the amplitude limit at any frequency is related simply to the maximum "bandwidth" error of the communication or control system which attempts to follow the continuously changing position of a moving aircraft. A powerful link is therefore established between a fundamental characteristic of aircraft motion and communication-control system performance.

Amplitude Limit

In general, the Fourier series furnishes a method of obtaining an analytical expression for a function between any two arbitrary values of the independent variable. The series is used in this paper to represent the path of a moving aircraft over any arbitrary duration of time.* In this manner, the position in space of a moving aircraft at any time t is represented by

$$r(t) = ix(t) + jy(t) + kz(t) = i\sum_{n=-\infty}^{\infty} X(n\omega_0)e^{jn\omega_0 t} + j\sum_{n=-\infty}^{\infty} Y(n\omega_0)e^{jn\omega_0 t} + k\sum_{n=-\infty}^{\infty} Z(n\omega_0)e^{jn\omega_0 t} \quad (1)$$

where i, j, k are the unit direction vectors in Cartesian coordinates. $X(n\omega_0)$, $Y(n\omega_0)$, $Z(n\omega_0)$ in this expression are the coordinate frequency spectra of the moving aircraft and are related to the original flight path $r(t)$ by

$$\left.\begin{aligned} X(n\omega_0) &= (1/T)\int_0^T x(t)e^{-jn\omega_0 t}\,dt \\ Y(n\omega_0) &= (1/T)\int_0^T y(t)e^{-jn\omega_0 t}\,dt \\ Z(n\omega_0) &= (1/T)\int_0^T z(t)e^{-jn\omega_0 t}\,dt \end{aligned}\right\} \quad (2)$$

* Although the Fourier integral permits a more convenient representation in some respects, the infinitesimal amplitudes of the transformed motion in this method present certain difficulties in interpretation not encountered in the series representation where amplitude is preserved.

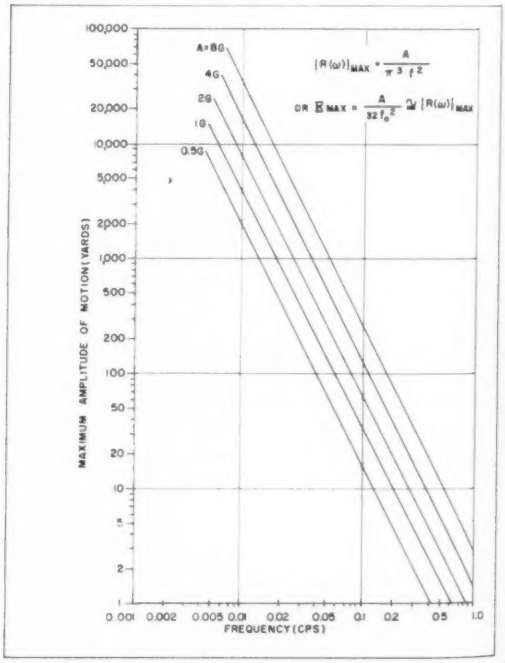

FIG. 1. Upper bound of the frequency spectrum of aircraft motion.

where $T = 2\pi/\omega_0$ is the arbitrary expansion interval over which the aircraft motion is of interest and outside of which the motion is assumed to be repeated. Differentiation of Eq. (1) gives the velocity and acceleration of the aircraft as

$$\dot{r}(t) = i\dot{x}(t) + j\dot{y}(t) + k\dot{z}(t) =$$
$$i \sum_{-\infty}^{\infty} (jn\omega_0)\, X\,(n\omega_0)e^{jn\omega_0 t} + j \sum_{-\infty}^{\infty} (jn\omega_0)\, Y(n\omega_0)e^{jn\omega_0 t} +$$
$$k \sum_{-\infty}^{\infty} (jn\omega_0) Z(n\omega_0)e^{jn\omega_0 t} \quad (3)$$

$$\ddot{r}(t) = i\ddot{x}(t) + j\ddot{y}(t) + k\ddot{z}(t) =$$
$$i \sum_{-\infty}^{\infty} -(n\omega_0)^2\, X\,(n\omega_0)e^{jn\omega_0 t} + j \sum_{-\infty}^{\infty} -$$
$$(n\omega_0)^2 Y(n\omega_0)e^{jn\omega_0 t} + k \sum_{-\infty}^{\infty} -(n\omega_0)^2 Z(n\omega_0)e^{jn\omega_0 t} \quad (4)$$

The coordinate transforms of Eq. (4) are

$$\left.\begin{aligned} X_a(n\omega_0) &= -(n\omega_0)^2\, X\,(n\omega_0) = \\ &\quad (1/T)\int_0^T \ddot{x}(t)e^{-jn\omega_0 t}\,dt \\ Y_a(n\omega_0) &= -(n\omega_0)^2 Y(n\omega_0) = \\ &\quad (1/T)\int_0^T \ddot{y}(t)e^{-jn\omega_0 t}\,dt \\ Z_a(n\omega_0) &= -(n\omega_0)^2 Z(n\omega_0) = \\ &\quad (1/T)\int_0^T \ddot{z}(t)e^{-jn\omega_0 t}\,dt \end{aligned}\right\} \quad (5)$$

By revising Eq. (5) slightly, the spectrum of $r(t)$ may now be written as

$$\left.\begin{aligned} X(n\omega_0) &= -[1/(n\omega_0)^2 T]\int_0^T \ddot{x}(t)e^{-jn\omega_0 t}\,dt \\ Y(n\omega_0) &= -[1/(n\omega_0)^2 T]\int_0^T \ddot{y}(t)e^{-jn\omega_0 t}\,dt \\ Z(n\omega_0) &= -[1/(n\omega_0)^2 T]\int_0^T \ddot{z}(t)e^{-jn\omega_0 t}\,dt \end{aligned}\right\} \quad (6)$$

These equations express the frequency spectrum generated by a moving aircraft as a function of the coordinate accelerations $\ddot{x}(t)$, $\ddot{y}(t)$, and $\ddot{z}(t)$. These components are referenced to the coordinate system from which the motion of the aircraft is observed, rather than the coordinates of the aircraft where the accelerations causing maneuver are actually applied, and it is desirable to relate the spectra of Eq. (6) to the vector acceleration $\ddot{r}(t)$. This is done quite simply by noting that the vector acceleration at any instant of time is defined by its projections on the fixed coordinate axes:

$$\left.\begin{aligned} \ddot{x}(t) &= \ddot{r}(t)\cos\alpha \\ \ddot{y}(t) &= \ddot{r}(t)\cos\beta \\ \ddot{z}(t) &= \ddot{r}(t)\cos\gamma \end{aligned}\right\} \quad (7)$$

where α, β, and γ are the angles formed between the vector acceleration and the x, y, and z axes, respectively. Thus, if Eq. (6) is considered as defining a vector spectrum

$$R(n\omega_0) = iX(n\omega_0) + jY(n\omega_0) + kZ(n\omega_0) \quad (8)$$

the transformed motion, as a result of Eq. (7), becomes

$$R(n\omega_0) = -[1/(n\omega_0)^2 T] \times$$
$$\left[i\int_0^T \ddot{r}(t)\cos\alpha e^{-jn\omega_0 t}\,dt + j\int_0^T \ddot{r}(t)\cos\beta e^{-jn\omega_0 t}\,dt + k\int_0^T \ddot{r}\cos\gamma e^{-jn\omega_0 t}\,dt \right] \quad (9)$$

The frequency spectrum $R(n\omega_0)$ is now stated in terms of the acceleration resulting directly from the forces produced on the aircraft. For convenience of terminology, this acceleration will hereafter be called the "applied" acceleration.

For aircraft, however, a fundamental statement concerning $\ddot{r}(t)$ is that its values are bounded—namely,

$$|\ddot{r}(t)| \leq A \quad (10)$$

where A is the maximum acceleration capability of the aircraft. It is important to note that this condition specifies only a maximum value for $\ddot{r}(t)$ and does not restrict the variation of vector acceleration in any way within this range.* The main problem here is to determine the manner in which the restriction on the range of $\ddot{r}(t)$ affects the magnitude of the position spectrum of Eq. (9).

The result of $R(n\omega_0)$ because of the existence of a finite bound on the magnitude of the vector acceleration can be shown to be

$$R(n\omega_0)_{max} = \left| -4A/\pi(n\omega_0)^2 \right| \times$$
$$[i\cos\alpha + j\cos\beta + k\cos\gamma] \quad (11)$$

where n now takes on only positive values. It can also be shown that maximum $R(n\omega_0)$ is achieved only when $\ddot{r}(t)$ is an applied square wave of acceleration of amplitude A and period $2\pi/(n\omega_0)$. In practice, this maneuver is obtained in an aircraft by the repeated application of maximum acceleration first in one direction for a time $\pi/n\omega_0$ and then in the opposite direction for the same length of time. The resulting motion is a more or less weaving or serpentine path consisting of a series of equal left and right turns of the aircraft or a prolonged climbing and diving path (as illustrated by the curves of Fig. 3). This square wave of acceleration both satisfies the condition for complete variation within $\pm A$ set down previously and appears to approximate a real case of evasive maneuver. The range of Eq. (11), therefore, not only is a theoretical maximum but can serve as a practical maximum as well.

In order to visualize the conditions of Eq. (11), it is helpful to observe that the terms within the square brackets define a direction vector of unit magnitude corresponding to the instantaneous direction of the applied acceleration. These terms relate the orientation of the coordinates of the aircraft to the fixed coordinates described by i, j, and k. The term out-

* The rate of change of acceleration is also limited because of aerodynamic considerations. The corrections to the basic analysis due to the finite rate of an aircraft's response to the controls are indicated in the Appendix.

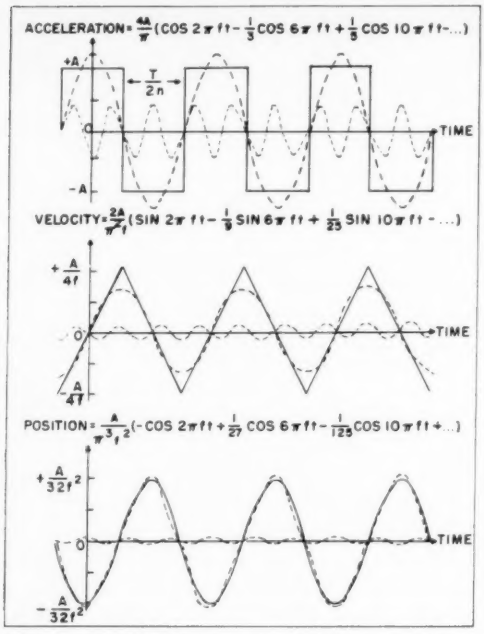
ACCELERATION = $\frac{4A}{\pi}(\cos 2\pi ft - \frac{1}{3}\cos 6\pi ft + \frac{1}{5}\cos 10\pi ft - \ldots)$
+A
-A
$\frac{T}{2n}$
TIME
VELOCITY = $\frac{2A}{\pi^2 f}(\sin 2\pi ft - \frac{1}{9}\sin 6\pi ft + \frac{1}{25}\sin 10\pi ft - \ldots)$
$+\frac{A}{4f}$
$-\frac{A}{4f}$
TIME
POSITION = $\frac{A}{\pi^3 f^2}(-\cos 2\pi ft + \frac{1}{27}\cos 6\pi ft - \frac{1}{125}\cos 10\pi ft + \ldots)$
$+\frac{A}{32f^2}$
$-\frac{A}{32f^2}$
TIME

FIG. 2. Applied maneuver to attain bound of Fig. 1.

side the square brackets represents the maximum amplitude that can be achieved by any sinusoidal frequency during a maximum maneuver by the aircraft. Taken together, these two terms define a vector frequency spectrum whose maximum value in any of the fixed coordinate directions is continuously modified by the projection of the acceleration-direction vector on that coordinate. However, a simpler interpretation is possible when only the magnitude of the position spectrum is considered.

Since the absolute value of the bracketed terms of Eq. (11) is by definition unity, the magnitude of $R(n\omega_0)$ becomes

$$|R(n\omega_0)|_{max} = 4A/\pi(n\omega_0)^2 \qquad (12)$$

Therefore, with reference to Eq. (9), the maximum amplitude of any frequency component of the position variable $r(t)$ can never exceed the value expressed by Eq. (12). Although this amplitude limit can be treated as a scalar quantity, it is important to remember that the limit at any frequency is actually free to occur in any direction. The spectrum of Eq. (12) is thus a spatial representation of the upper bound of the frequency spectrum generated by a maneuvering aircraft.

The importance of Eq. (12) in limiting the frequency spectrum of aircraft motion is demonstrated by the curves of Fig. 1. In the Figure, it can be observed that frequency components that are in the vicinity of 0.1 cps, for example, are permitted a maximum amplitude of approximately 65 yards for a $2g$ acceleration, whereas frequency components near 1.0 cps are allowed an amplitude of but 0.65 yard for the same limitation on the acceleration. Therefore, the component amplitudes of motion in space are significant only over a rather small range of the frequency variable $(n\omega_0)$. The extent of this band which must be preserved in order to meet given system error requirements will be the subject matter of the remainder of this paper.

Relation of Frequency Spectrum to Position Error

In the previous section it was stated that an applied square wave of acceleration is the only form of motion which produces amplitudes equal to the bound of Fig. 1. Fig. 2 shows the essential characteristics of the applied acceleration motion and the corresponding velocity and position variations resulting from this disturbance. As before, the square wave of acceleration is taken only with respect to the motion of the aircraft. The solid curves represent the total motion while the dashed curves indicate, for illustration purposes, the fundamental and third harmonic components. Also shown are the corresponding analytical expressions for the motion. Integration of the applied acceleration produces a linear variation of velocity, and integration of the velocity yields the resultant parabolic position variation. Since the main interest here is in the motion due to maneuver, the constants of the integrations are not included. The frequency components produced by the successive integrations occur with the amplitudes and phases shown in order that their sum always produces the total motion. With reference to the resultant position variation, it is important to note that, because of the rapid convergence of the position series, the fundamental component, of amplitude $A/\pi^3 f^2$,* is not significantly different per-

* For the remainder of this paper the continuous variable f can replace the discrete variable $(n\omega_0)$ without loss of generality.

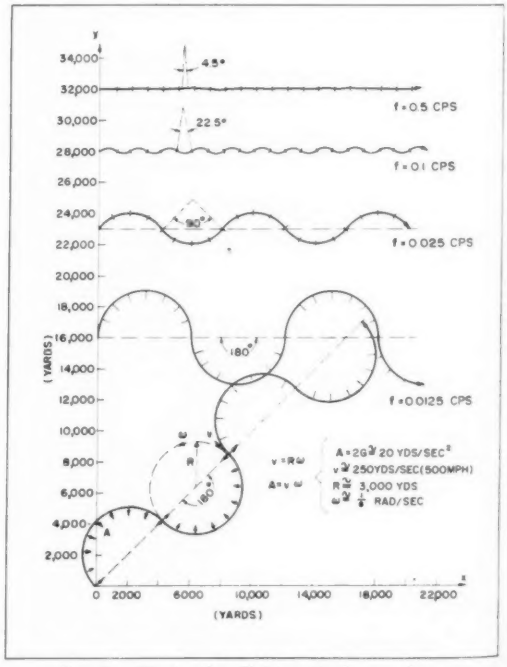

FIG. 3. Illustrative flight paths in x-y plane.

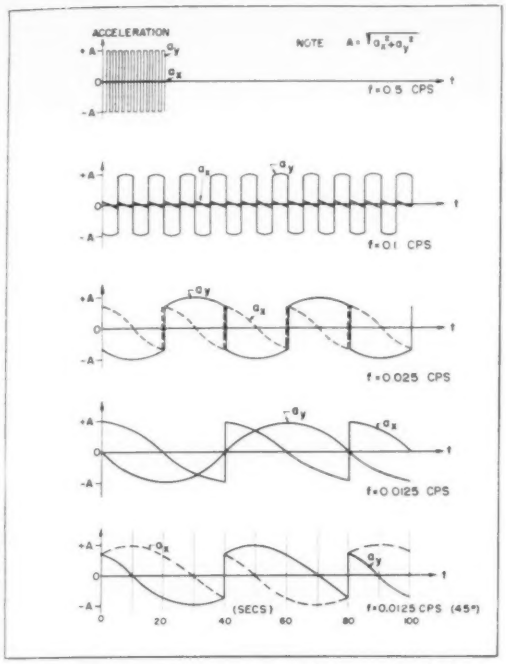

FIG. 4. Coordinate accelerations of flight paths of Fig. 3.

centagewise from the total motion of amplitude $A/32f^2$. In fact, it is only at rather low frequencies that the difference in terms of the absolute distance becomes appreciable.

In order to illustrate the foregoing statements and to demonstrate by example the validity of the spatial representation of the previous section, a two-dimensional case of aircraft motion is considered. Fig. 3 shows a number of possible flight paths occurring in a horizontal (x-y) plane for various values of the frequency of the applied square wave of acceleration of Fig. 2. The uppermost four curves represent flight in the general direction of the x coordinate at different frequencies of maneuver, while the lowest curve is an example of a flight path with an average direction 45° to the x and y axes and for the same frequency as the flight path immediately above it. A maximum acceleration of $A = 2g$ and a velocity of 500 m.p.h. have been chosen for the illustration. Since the motion in the x-y plane will be circular, the corresponding values of turn radius and turn rate for the paths are $R \cong 3{,}000$ yards and $\omega \cong 1/8$ rad./sec., respectively. Time is shown by the dots which are placed at 5-sec. intervals along the curves. Similarly, the vector acceleration is shown for a portion of the lowest curve by the arrows, all of which are of magnitude A. Figs. 4 and 5 show the resulting coordinate acceleration and position variations as functions of time. If a careful examination is made of the curves, it is seen that, even though the motion is relatively complicated in its details, the amplitude of the motion about the mean position is almost exactly equal to the corresponding amplitude given by Fig. 1 for all frequencies above approximately 0.025 cps.* For frequencies below 0.025 cps and with reference to any particular coordinate, the amplitudes of Fig. 1 appear to be high by a factor of approximately 4/3. This condition is as expected, however, since the applied coordinate acceleration at these frequencies is nearer sinusoidal than square wave in shape, and Fig. 2 shows that the resulting position motion for a purely sinusoidal acceleration will have an amplitude $\pi/4$ as large as the amplitude for the square-wave case. Since this apparent difference occurs well within the pass-band in most applications and therefore lies outside the range of interest here, and because it does not affect the spatial representation, it is not included as a refinement to the curves of Fig. 1.

Examination of the possible conditions existing at a particular frequency f of Fig. 1 also permits a valuable observation to be made. At the outset, it is evident that a component can occur at f due either to the presence of a fundamental component resulting from the application of the square wave of acceleration at that frequency or to the presence of a harmonic of an equivalent motion whose fundamental is at some lower frequency. If the fundamental is present at f, its maximum amplitude can be $A/\pi^3 f^2$. On the other hand, the maximum amplitude that a third harmonic can have at this frequency is, from Fig. 2, just $A/27\pi^3(f/3)^2$ or $A/3\pi^3 f^2$. Similarly, the maximum amplitude of a fifth harmonic is $A/5\pi^3 f^2$, and further harmonics take the approximate form $A/n\pi^3 f^2$. Since the foregoing argument holds at every frequency, it is seen that the fundamental component of the motion alone determines the bound of Fig. 1.

* This frequency will differ slightly for different velocities. However, it can be verified that velocity is not a significant factor in the analysis.

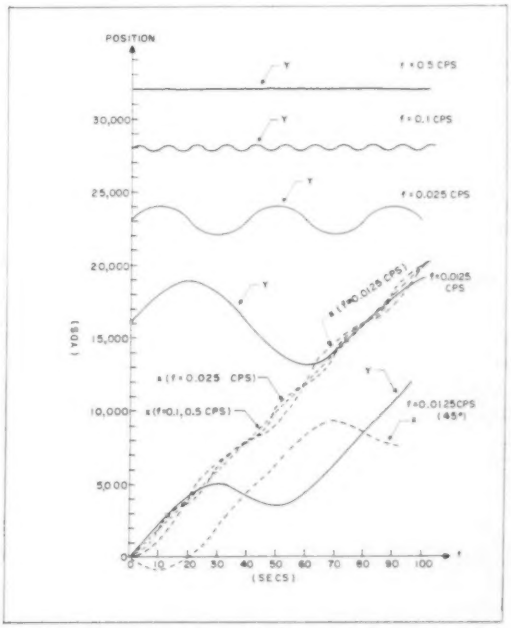

FIG. 5. Coordinate position variations of flight paths of Fig. 3.

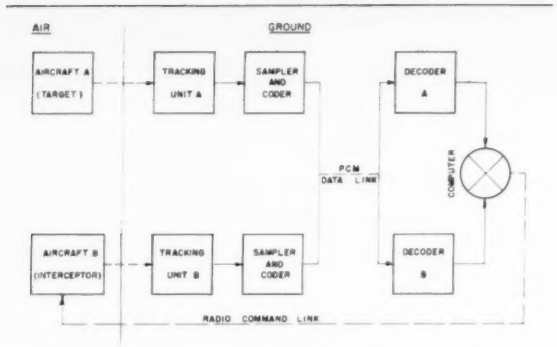

FIG. 6. A possible communication-control interception system.

It is now appropriate to pursue the main problem of relating the special properties of the frequency spectrum of a maneuvering aircraft found by the previous analysis to the performance of a communication or control system. Stated simply, the basic operations performed by such a system are usually (1) to measure and track the path generated by a moving aircraft, (2) to recover the path at a remote location or to perform some other operation on the information, and (3) to carry out these operations accurately, in real time, and without undue time delay. A fundamental characteristic of any of these systems is the availability of a limited band of frequencies in which to measure, compute, or convey flight information.

Consider Fig. 6 which is an elementary block diagram of a system incorporating features of both communication and automatic control. This Figure represents one of a number of ways in which aircraft "B" might be automatically controlled from the ground to intercept a target, aircraft "A." It is assumed that the computing facilities are located at some distance from the tracking site, that high precision is required, and that the interconnecting link may be noisy. The use of coded transmission is therefore probably called for, and sampling makes it possible to time-share the position coordinates of both aircraft over the same narrow-band channel. The computer compares the positions of target and interceptor aircraft and calculates a command signal for the interceptor. This signal is then transmitted by radio to the intercepting aircraft in such a form that the automatic pilot completely takes over the flight.

The response of a linear system, such as Fig. 6, to a position input $r(t)$ will be the product of the frequency spectrum generated by the moving aircraft and the transfer-function spectrum of the system. Since there will always be some frequency f_c beyond which the system does not sensibly respond to the input, a portion of the frequency spectrum $R(n\omega_0)$ of Eq. (8) can be lost. In particular, if $R(n\omega_0)$ occurs entirely above f_c, essentially no motion is observed by the system. Again, it is the frequency components of the maneuver that are important. It is reasonable then to postulate that the maximum error of the system, exclusive of noise and time delay considerations, in describing the position of the moving aircraft occurs when the applied maneuver of Fig. 2 takes place just outside f_c.* In this case, the maximum error in position is equal to the total motion of f_c. From Fig. 2, the resultant spatial error for this condition is

$$E_{max} = A/32f_c^2 \tag{13}$$

Since this error is not essentially different from the maximum amplitude of the fundamental component of the motion at f_0, Fig. 1 can now serve not only as the upper bound of the frequency spectrum generated by the aircraft but also as the error vs. bandwidth measure of the system that accepts the position variation of this aircraft as input.

Eq. (13), although derived heuristically and from essentially a steady-state analysis, nevertheless provides a fundamental relationship between the physical behavior of a moving aircraft and a basic characteristic of the associated communication or control system. Since the motions which determine the bound of Fig. 1 also seem to be highly probable maneuvers of the aircraft at the time when the system is called upon to perform most accurately, a realistic figure of merit in evaluating system performance is introduced. In addition, it appears that the techniques which lead to this result can be extended to take account of time delay and noise and can be applied to the solution of

* It has been verified by calculation that this error is greater than the error which can occur in a typical low-pass system when the fundamental component of the motion of Fig. 2 occurs below f_c and only harmonics of the motion are eliminated by the system.

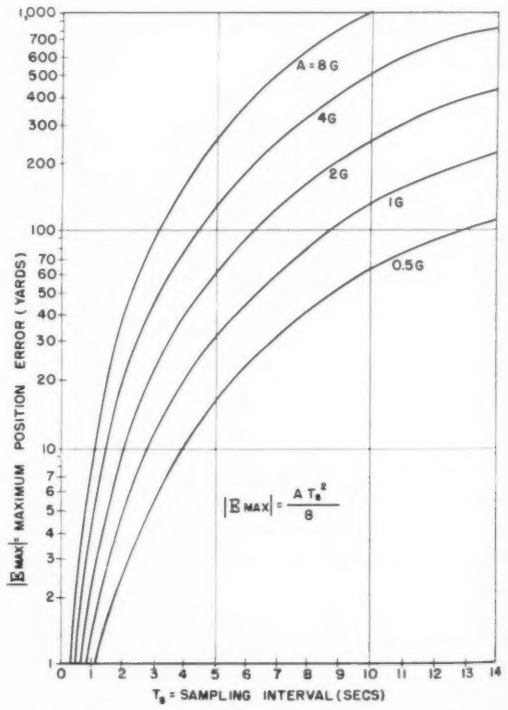

FIG. 7. Maximum position error vs. sampling interval.

other problems involving aircraft maneuvers. The final section will be devoted to two examples of the usefulness of the results in the determination of important communication or control system characteristics.

Determination of System Characteristics

The system transfer function of Fig. 6 is a rather complicated expression consisting of the closed-loop relationship of the individual transfer functions of the tracking units, the sampling and coding processes, the decoding processes, the computer operation, the transmission links, and the autopilot-interceptor combination. On a system basis, the design of each of these parts must be related intimately to the performance of the others and to the characteristics of the applied information. In general, only one of these components will be instrumental to specifying the cutoff frequency f_c for the system. Application of Eq. (13) will then determine the maximum position error in space expected for the cutoff frequency f_c and the maximum acceleration capability assigned for the aircraft. On the other hand, when more freedom of design is permitted, f_c can be adjusted in order to meet the error limit set for the system. Thus, Eq. (13) can be used directly to predict overall system performance. A specific example is the calculation of the performance of the samplers of Fig. 6.

The operation of sampling is usually employed in a communication or control system when the data are inherently obtained in this form or when it is desired to time-share signals from two or more separate sources over the same channel or to use a digital computer in the system. In order to preserve the information, it is well known that samples of the time-varying input must be taken at a rate that is at least twice the highest significant frequency of the input or

$$f_s \geq 2f_c \tag{14}$$

In terms of a uniform sampling interval T_s, Eq. (14) becomes

$$T_s \leq 1/2f_c \tag{15}$$

It is evident immediately that the highest significant frequency f_c in the case of a moving aircraft is just the cutoff frequency defined previously. Therefore, from Eqs. (13) and (15), the maximum error associated with a particular sampling interval T_s is

$$\mathrm{E}_{max} = A T_s^2/8 \tag{16}$$

This equation is plotted in Fig. 7 for several values of the acceleration capability A. When the sampling operation is the bandwidth determining factor, the curves of this Figure express directly the inherent penalty attached to the choice of a particular sampling interval in the system. Note that an added penalty exists for the use of longer intervals because of the squared nature of the variation. In cases, such as Fig. 6, where the sampling operation is probably not the bandwidth determining factor but is included as a component transfer function of the system, the same general technique applies. Here, however, the sampling interval is chosen by Eq. (16) or Fig. 7 so that undue error is not contributed by the operation. In systems where the information is encoded into digital form either for transmission or for computation, these relations are also helpful in balancing the quantizing error (noise) against the error or position uncertainty due to maneuver. Since quantizing error decreases with longer sampling intervals because of the inherent smoothing obtained whereas maneuver error increases rather rapidly, the choice of a compromise interval is often quite important.

Another example of the usefulness of the concepts presented in this paper is the calculation of the shape of the system transfer function which provides best protection against noise without degrading the accuracy for maneuvers beyond the limit set by E_{max}. It was pointed out earlier that maximum position error occurs only for a motion of Fig. 2 whose fundamental variation is located at the cutoff f_c. Furthermore, the errors for other conditions of motion below f_c are quite small compared to the maximum motion. This is largely due to the fact that the fundamental, and often several harmonics, are contained within the transmission band of the system for motion below f_c. If now the maximum error can be tolerated for any frequency of maneuver of the aircraft, it is possible to minimize the magnitude of the transfer function of the system everywhere within the transmission band to a value compatible with this error. By providing minimum gain for the system, the transfer function is, in an intuitive sense, automatically adjusted to furnish best protection against noise.

Let E_{max} be the maximum error in distance that can be tolerated for a particular system and $\mathrm{E}(f)$ the percentage error at any frequency f. In order to apportion the error over the transmission range, the percentage error must be

$$\mathrm{E}(f) = \mathrm{E}_{max}/|R(f)|_{max} = (A/32f_c^2)/(A/\pi^3 f^2) \cong (f/f_c)^2 \tag{17}*$$

where $|R(f)|_{max}$ is, as before, the maximum amplitude of motion at f—i.e., the upper bound of Fig. 1 at that frequency. If

$$H(f) = V_0(f)/V_i(f) \tag{18}$$

is the voltage transfer function of the system, the percentage error at any frequency is related to this quantity by

$$\mathrm{E}(f) = [V_i(f) - V_0(f)]/V_i(f) = 1 - H(f) \tag{19}$$

Substitution of Eq. (17) in Eq. (19) immediately gives

$$H(f) = 1 - \mathrm{E}_{max}/|R(f)|_{max} \cong 1 - (f/f_c)^2 \tag{20}$$

This equation then is the desired system transfer function to allow E_{max} anywhere in the transmission range and hence to achieve noise protection. Fig. 8 shows the

* This equation neglects the small error already existing at $f < f_c$.

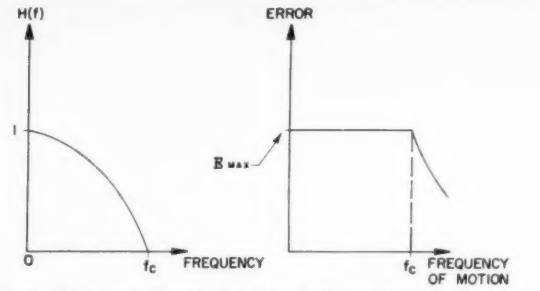

FIG. 8. Optimum transfer function and resulting error curve to achieve maximum noise protection in system.

resulting system characteristics in graphical form. Although the transfer function of the Figure is not realizable exactly, it can be approximated satisfactorily by a few network components. It can also be observed that the effective attenuation of noise is greatest for higher frequencies in the band. In fact, at $0.9f$, it is 14 db. and increases theoretically to infinity at f_c.

APPENDIX

Another factor limiting the upper bound of the frequency spectrum of aircraft motion is the restriction of a finite rate of change of acceleration corresponding to the existence of control surfaces and aerodynamics. Thus, it is seen that the square wave of acceleration of Fig. 2 is not a completely accurate representation of the physical situation. Although the transfer function expressing the rate of the aircraft's response to the controls is complicated, involving many time delay factors, this expression can be approximated for illustration purposes* by the single time constant term

$$G(S) = (\theta p/\delta)(S) = 1/(1 + TS) \qquad (21)$$

where

θp = direction of motion of the aircraft
δ = control-surface deflection†
T = lumped time constant of the aircraft response
S = complex frequency variable

Since θp, the change in direction of motion or amount of turn of the aircraft, is proportional to the magnitude of the centripetal acceleration causing turn, Eq. (21) also expresses the rate of change of acceleration in response to control-surface deflection. This then is the form of the factor which must be applied to the amplitudes of Fig. 1 of the text.

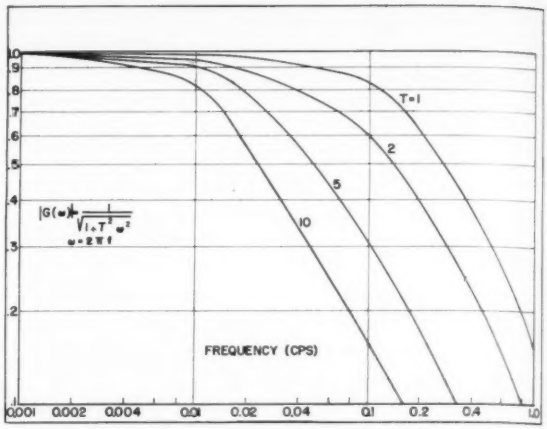

FIG. 9. Correction factor to Fig. 1 to take account of aerodynamic considerations.

Combining this factor with Eq. (12), the resultant expression for the maximum amplitude is

$$|R(\omega)|_{max} = [4A/\pi(\omega)^2] \cdot (1/\sqrt{1 + T^2\omega^2}) \qquad (22)$$

For aircraft, T appears to take on a fairly wide range of values depending on the characteristics of the particular aircraft, including the peak acceleration capability. Fig. 9 is a plot of the correction factor term of Eq. (22) for values of the response time constant of 1, 2, 5, and 10 sec. From the Figure, it can be noted that the effect of aerodynamic lag is, as expected, most pronounced at the higher frequencies and produces a significant reduction in amplitude for frequencies in the range of 0.1 to 1 cps and for the higher values of T. Thus, an adjustment may have to be made in the curves of Figs. 1 and 7, but not in the basic method of the report, in applications where this difference will cause a marked change in the results and when the aerodynamic response characteristics of the aircraft are known.

* Over restricted ranges of frequency, representation of the acceleration spectrum as related to the characteristics of the aircraft by a second-order transfer function is possible but literally never by the first-order function chosen here.

† The time lag introduced by the controls themselves are assumed to be negligible compared to the lags of the aircraft response.

REFERENCES

[1] Bollay, W., *Aerodynamic Stability and Automatic Control*, Journal of the Aeronautical Sciences, Vol. 18, No. 9, pp. 569–617, September, 1951.

[2] Guillemin, E. A., *The Mathematics of Circuit Analysis;* John Wiley & Sons, Inc., New York, 1949.

[3] James, H. F., Nichols, N. B., and Phillips, R. S., *Theory of Servomechanisms*, M.I.T. Radiation Laboratory Series, Vol. 25; McGraw-Hill Book Company, Inc., New York, 1947.

[4] Laning, J. H., and Battin, R. H., *Random Processes in Automatic Control;* McGraw-Hill Book Company, Inc., New York, 1956.

Remarks on the Equilibrium Turbulent Boundary Layer

DONALD COLES*

California Institute of Technology

SUMMARY

Two similarity laws are known for the mean-velocity profile in a turbulent boundary layer with constant pressure. These are Prandtl's law of the wall and Kármán's momentum-defect law. The first law has recently been generalized empirically to flows with arbitrary pressure gradient by Ludwieg and Tillmann, and the second law to a certain class of equilibrium flows by F. Clauser.

In the present paper it is shown that the pressure distribution corresponding to a given equilibrium flow can be computed by assuming that a certain parameter $D = (\tau_w/q)dq/d\tau_w$ is constant, where q and τ_w are the dynamic pressure in the free stream and the shearing stress at the wall, respectively. The hypothesis D = constant is suggested by a study of the integrated continuity equation and is supported by a rigorous analogy between the class of equilibrium flows defined by Clauser and the class of laminar flows studied by Falkner and Skan. The hypothesis D = constant is also verified using experimental data for several equilibrium turbulent flows and is interpreted physically from a kinematic point of view.

Two hypothetical limiting cases of equilibrium flow are described. At one extreme is the boundary layer in a sink flow, with a completely logarithmic mean-velocity profile outside the sublayer. At the other extreme is a continuously separating boundary layer in a dimensionless pressure gradient $(x/q)dq/dx$ approximately twice that for the corresponding laminar flow. Typical shearing-stress profiles are computed for several equilibrium turbulent flows, including the two limiting cases.

SYMBOLS

D	= parameter defined by Eq. (5)
n	= exponent in $u_1 x^{-n}$ = constant
p	= static pressure
P	= parameter defined by Eq. (6)
q	= $\rho u_1^2/2$ = dynamic pressure
s	= velocity defined by Eq. (47)
u, v	= mean velocities tangential and normal to wall
u_τ	= $\sqrt{\tau_w/\rho}$ = friction velocity
x, y	= coordinates tangential and normal to wall
z	= $\kappa u_1/u_\tau$, except following Eq. (1)
δ	= boundary-layer thickness
δ^*	= displacement thickness defined by Eq. (22)
ζ	= $\kappa u/u_\tau$ or y/δ according to context
θ	= momentum thickness defined by Eq. (23)
κ	= Kármán's constant in Eq. (1)
λ	= $-u_\tau dx/du_\tau$
μ	= viscosity
ν	= kinematic viscosity
π	= profile parameter in Eq. (1)
ρ	= density
τ	= shearing stress
Ω_1, Ω_2	= functions of π defined by Eqs. (24) and (25)
ω_1, ω_2	= functions of π and y/δ defined in reference 4

Received June 28, 1956. Revised and received February 14, 1957.

* Assistant Professor of Aeronautics, Guggenheim Aeronautical Laboratory.

Subscripts

0	= conditions at reference station $x = x_0$
1	= conditions at edge of boundary layer
w	= conditions at wall

(1) STATEMENT OF THE PROBLEM

(a) *Introduction*

FOR FIFTY YEARS the problem of turbulent shear flow has occupied a prominent place in the literature of fluid mechanics. During this time, the principle of physical similarity has always been an important tool in the study of easily observable quantities, such as the mean-velocity distribution. For the turbulent boundary layer, in particular, appreciable progress has been made in dealing with what I will call the direct problem—that of describing empirically the mean-velocity profile in flows which have been observed experimentally. However, no really satisfactory solution has yet been found for what I will call the inverse problem—that of predicting the behavior of turbulent flows which have not necessarily been observed but which develop in a specified environment.

From the beginning, most attempts to solve the inverse problem for the turbulent boundary layer have relied on approximate methods which are known to be successful in the corresponding laminar problem or in the problem of free turbulence. These methods assume that the mean motion can be realistically described by one or more local similarity laws involving certain characteristic parameters. The nature and number of the laws and parameters in any particular case depend on the data of the problem. For example, in a turbulent free shear flow the mean motion is usually assumed to be independent of the fluid viscosity, in which case the width of the shear flow and the velocities at the boundaries or at points of symmetry are the natural parameters of the flow. Similarity laws for mean velocity and turbulent shearing stress may first be derived by an elementary dimensional analysis. The laws governing the development of the profile parameters with distance then follow from the equations of mean motion in differential or in integral form. A summary of the main conclusions of this method for several free turbulent flows has been given by Squire.[1]

If these same methods are applied to a shear flow bounded by a wall, however, a difficulty arises immediately. The influence of viscosity in the sublayer introduces a new characteristic length, say ν/u_1, and the finite shearing stress at the wall introduces a new

characteristic velocity, say u_τ. But with three lengths y, δ, and ν/u_τ and three velocities u, u_1, and u_τ to be accounted for, the most that can be said a priori is that u/u_1 expressed as a function of y/δ may depend also on u_1/u_τ and $\delta u_\tau/\nu$. Thus it is necessary to solve the direct problem—i.e., to describe the velocity profile in much more specific language than that of dimensional analysis—before integral laws for the conservation of mass, momentum, or energy can be applied with confidence.

If the flow is laminar, the methods of dimensional analysis can often be replaced by a genuine similarity argument based on the equations of motion. In particular, similarity laws for velocity and shearing stress need not be formulated separately, as either determines the other through the Newtonian stress law $\tau = \mu \partial u/\partial y$. The real justification for the assumption of similarity in laminar flow, however, is not often emphasized. It is the empirical fact that similar flows are apparently the ones which tend to occur in nature whenever the physical conditions are appropriate. Obvious examples, in addition to various free shear flows, are the Blasius flow, the plane stagnation-point flow, the laminar free-convection layer on a vertical wall, the asymptotic case of large suction, and so on. Hence the common assumption that laminar boundary-layer profiles in general form a single-parameter family, in which u/u_1 as a function of y/δ depends only on the ratio of τ_w to $\mu u_1/\delta$, or in the present notation of u_1/u_τ to $\delta u_\tau/\nu$. Not only is this assumption a natural one but its limitations are intuitively clear once the physical processes involved in the generation, transport, and diffusion of vorticity are understood.

Any discussion of turbulent flow, on the other hand, must proceed in the vacuum created by lack of understanding of turbulent transport processes in even the simplest turbulent motions. In these circumstances there is usually little choice except to abandon any formal analogy with laminar flow and to rely openly on empirical similarity laws. The similarity laws in question have evolved very slowly, and the efforts of many investigators have been required to reach even the present imperfect state of the art. I think it is important to remember, however, that the similarity laws to be cited here were originally discovered by a study of turbulent flows which also occur, so to speak, in nature—namely, the fully developed pipe and channel flows and the turbulent boundary layer with constant pressure.

Unfortunately, it is usually found in practice that a solution of the direct problem for the turbulent boundary layer, although necessary for the application of integral methods, is not sufficient to allow a solution of the inverse problem. In fact, the only analytical solution worthy of the name which has so far been found is Kármán's analysis of flow at constant pressure. The difficulty is simply that any more complicated flow than the one treated by Kármán must involve at least one additional parameter in the mean-velocity profile. At whatever level a solution is attempted, some theoretical or phenomenological argument has to be found to connect this parameter with other quantities describing the flow. The search for such a principle has been carried out in many directions, and accounts for a large part of the extensive literature in this field, including the present paper.

No attempt will be made here to solve the inverse problem for an arbitrary turbulent boundary layer. I propose instead to study certain turbulent flows which are analogous to the laminar flows of Falkner and Skan in the same sense that the turbulent boundary layer with constant pressure is analogous to the laminar flow of Blasius. The main element in the analogy is a new concept of kinematic similarity—i.e., of similarity based on the continuity equation. This concept will be introduced following a brief but explicit statement of the inverse problem.

(*b*) *The Direct Problem*

Various theoretical and experimental investigations have led long ago to the recognition of two similarity laws for the mean-velocity profile in the turbulent boundary layer. These are Prandtl's law of the wall and Kármán's momentum-defect law. Recently both concepts have been extended empirically, the law of the wall to flows with arbitrary pressure gradient by Ludwieg and Tillmann,[2] and the defect law to a special class of equilibrium flows by F. Clauser.[3]

Taking the work of Clauser as a point of departure, I have proposed in another paper[4] a formulation of the mean-velocity profile which incorporates the similarity laws in their extended form but which is not restricted to equilibrium flow. To be specific, consider turbulent flow of an incompressible fluid past a smooth plane surface, at which the velocity vanishes and the friction is Newtonian. For flows which are steady and two-dimensional in the mean, it is found that the mean-velocity profile $u(x, y)$ may be quite generally represented by a formula

$$\frac{u(x, y)}{u_\tau(x)} = f\left[\frac{y u_\tau(x)}{\nu}\right] + \frac{\pi(x)}{\kappa} w\left[\frac{y}{\delta(x)}\right] \qquad (1)$$

where $u_\tau(x) = \sqrt{\tau_w(x)/\rho}$. The quantity $\tau_w(x)$ is the wall shearing stress; $\delta(x)$ is a boundary-layer thickness which is uniquely defined; and κ is Kármán's universal constant, taken here as 0.400. The function $f(yu_\tau/\nu)$, called the law of the wall, has the properties that $f(z) \to z$ for $z \to 0$ ($z < 1$, say), and $f(z) \to (1/\kappa) \ln z + c$, where c is a second constant taken here as 5.10, for $z \to \infty$ ($z > 50$, say). The function $w(y/\delta)$, which I have called the law of the wake, has by definition the properties that $w(0) = w'(0) = 0$, $w(1) = 2$, and $\int_0^2 (y/\delta) dw = 1$. The parameter $\pi(x)$ is then a measure of the relative magnitude of the wake and wall components of the flow.

I want to emphasize that the two functions called the law of the wall and the law of the wake are to be regarded as completely empirical functions established by direct observation of the mean-velocity profile. No attempt is made here to discuss the problem of turbu-

lence per se, and this omission is both the greatest strength and the greatest weakness of the present development. At the same time, the analogy which is implied by the term "law of the wake" is meant to be taken seriously, in that a knowledge of turbulent mixing processes in free shear flows should have direct application to the more complicated problem of the turbulent boundary layer.

According to the experimental evidence,[4] the conditions under which the two-parameter formula (1) is valid are nearly equivalent to the conditions under which the boundary-layer approximation itself might be expected to apply. The formula will certainly fail in the vicinity of strong anomalies in either the surface geometry or the boundary conditions—for example, close to a spoiler. On the other hand, there is no reason as yet to suppose that the formula must necessarily fail in flows which are actually separated from the adjacent wall. The important point is that Eq. (1) provides a quite accurate analytical representation of the mean-velocity profile for a large class of flows as a linear combination of two universal functions $f(yu_\tau/\nu)$ and $w(y/\delta)$. Eq. (1) therefore constitutes a useful if tentative solution of the direct problem for a general turbulent boundary layer.

(c) *Equilibrium Flow*

A local friction law for the turbulent boundary layer is obtained from Eq. (1) by putting $y = \delta$,

$$u_1/u_\tau = (1/\kappa) \ln (\delta u_\tau/\nu) + c + (2\pi/\kappa) \qquad (2)$$

and the defect law is then obtained by forming the difference

$$(u_1 - u)/u_\tau = -(1/\kappa) \ln (y/\delta) + (\pi/\kappa)[2 - w(y/\delta)] \quad (3)$$

or, more generally,

$$(u_1 - u)/u_\tau = F(\pi, y/\delta) \qquad (4)$$

If π is constant in Eq. (4)—i.e., independent of x—the momentum defect $(u_1 - u)/u_\tau$ depends only on y/δ outside the sublayer. This property defines a turbulent equilibrium boundary layer for the purposes of the present paper. It may sometimes be convenient to exhibit the fact that the defect law (4) varies from one equilibrium flow to another by retaining the notation of Eqs. (1) to (3), in which the parameter π is defined explicitly, without, however, assuming that the wake function $w(y/\delta)$ has any universal validity. In any event, the defect law will be found to be an essential element in the later discussion, while the law of the wake will not.

(d) *The Inverse Problem*

If the similarity laws of the previous sections are valid, the dimensionless mean-velocity profiles form a two-parameter family whenever the flow is bounded by a wall. This property supposedly expresses the simultaneous importance of turbulent and laminar transport processes in different regions of the flow. As pointed out in the Introduction, problems in free turbulence can be viewed as a special case for which the parameter u_τ and also the kinematic viscosity ν may be omitted. The number of dimensionless parameters is then reduced, the integral conservation laws are easily applied, and various well-known properties of free turbulent shear flows—e.g., the linear rate of growth of a turbulent jet—are easily inferred.

The development of a general turbulent boundary layer, however, can only be completely described in terms of two constants μ and ρ characterizing the fluid and four parameters u_1, u_τ, δ, and π characterizing the state of the flow, the latter quantities being considered as functions of a single variable x. Knowledge of these four parameters in any region determines not only the surface friction and the rate of boundary-layer growth, but the complete mean-velocity profile and, therefore, at least within the limitations of the similarity laws and of the usual boundary-layer approximation, the shearing-stress field and the rate of energy transfer from the mean motion to the turbulent secondary motion.

Four independent relationships among the four parameters u_1, u_τ, δ, and π are obviously required in any general formulation of the inverse problem founded on Eq. (1). Two of these relationships are provided by the local friction law (2) and by the Kármán momentum-integral equation which will be introduced in its proper place. A third relationship is ordinarily included in specified conditions for a particular flow—e.g., π = constant for an equilibrium flow, or $u_1 = u_1(x)$ for a prescribed external flow.

The assumption that a fourth equation can be found is not essentially different from the traditional single-parameter hypothesis of the turbulent boundary-layer literature. Both express the hope that the turbulent mixing process can somehow be represented by a single empirical relationship describing the response of the boundary layer to its environment. Numerous relationships, sometimes supported by physical arguments and sometimes not, have been proposed to serve this need in various engineering applications. However, the law of the wake and especially the concept of equilibrium flow are new elements in the problem which suggest that the office of fourth equation cannot usefully be filled until these elements have been accounted for.

(2) Kinematic Similarity

(a) *The Continuity Equation*

In spite of the difficulties mentioned in the Introduction, there is one important area of study in which the inverse problem for laminar flow can serve as a model for turbulent flow. This area involves the idea of equilibrium flow, an idea which is not confined to the turbulent boundary layer if the term "equilibrium" is interpreted to mean invariance of the similarity laws for the mean-velocity profile. A restricted class of two-dimensional laminar boundary-layer flows with

this property was first studied by Falkner and Skan,[5] and later investigations have included certain effects of compressibility, of axial symmetry, and of suction or blowing at the wall. Briefly stated, the purpose of the present paper is to point out and to exploit an analogy between the laminar equilibrium flows of Falkner and Skan and the turbulent equilibrium flows of Clauser. The substance of the analogy will be found to consist largely of consequences, inferences, or conjectures drawn from the continuity equation and from the information about equilibrium turbulent flows which is available in the law of the wall and the momentum-defect law.

The first of these consequences has already been recorded elsewhere;[6] it is that the continuity equation $\partial u/\partial x + \partial v/\partial y = 0$ and the law of the wall $u/u_\tau = f(yu_\tau/\nu)$ together require the mean streamline slope v/u for fixed x to increase linearly with y in some neighborhood of the wall.

A second consequence of the continuity equation follows on making a weak and universally accepted approximation of boundary-layer type for the external flow. If the velocity u is taken as sensibly independent of y outside the boundary layer and denoted by $u_1(x)$, then $\partial v/\partial y$ in this region is a function only of x, and the streamline slope $v/u = v/u_1$ for fixed x is once again a linear function of y.

These observations mean physically that the divergence or convergence of the streamlines outside a boundary layer is determined entirely by the distribution of surface pressure. At the same time, the divergence or convergence of the mean streamlines within the boundary layer, at least sufficiently close to the wall, is determined entirely by the distribution of surface shearing stress. These results will be combined for the sake of both generality and brevity in the form of a theorem, which follows almost automatically on introducing appropriate nondimensional variables.

THEOREM: Consider a shear flow with mean-velocity components $u(x, y, t)$ and $v(x, y, t)$ such that $\partial u/\partial x + \partial v/\partial y = 0$. Assume $u = v = 0$ at $y = 0$ and $\lim_{y\to 0} \mu\partial u/\partial y = \tau_w(x, t)$ where μ is a constant. Suppose that u is independent of y for y larger than some value $\delta(x, t)$. Define $u_\tau(x, t) = \sqrt{\tau_w/\rho}$ where ρ is a constant; $u_1(x, t) = u(x, \delta, t)$; $\delta^*(x, t) = \int_0^\delta (1 - u/u_1)dy$; $1/\lambda = -(1/u_\tau)\partial u_\tau/\partial x$; $\nu = \mu/\rho$; and

$$D(x, t) = \frac{\partial \ln u_1/\partial x}{\partial \ln u_\tau/\partial x} \tag{5}$$

$$P(x, t) = \frac{\delta^*}{\delta}\,\frac{\partial \ln (\delta^* u_1/\nu)/\partial x}{\partial \ln (u_1/u_\tau)/\partial x} \tag{6}$$

Then the curve obtained by plotting $\lambda v/P\delta u$ against $y/P\delta$ for fixed x and t must leave the origin with slope unity and must coincide for $y > \delta$ with the straight line passing with slope D through the point (1, 1).

To prove the theorem stated above, note first that the formula $u/u_\tau = f(yu_\tau/\nu)$ for the velocity profile is equivalent[6] to the relationship $v/u = y/\lambda$. The assumption of Newtonian friction at the wall, because it requires $u/u_\tau = yu_\tau/\nu$ + higher order terms in y, is therefore sufficient to establish the result of the theorem at the surface.

Outside the shear flow, on the other hand, $u(x, y, t) = u_1(x, t)$, and $\partial v/\partial y = -\partial u_1(x, t)/\partial x$, so that $v(x, y, t) - v(x, \delta, t) = -(y - \delta)\partial u_1/\partial x$, and, therefore,

$$\lambda v/\delta u = (\lambda v_1/\delta u_1) + (u_\tau/u_1)[(\partial u_1/\partial x)/(\partial u_\tau/\partial x)] \times [(y/\delta) - 1] \tag{7}$$

where $v_1 = v_1(x, t) = v(x, \delta, t)$. Now in the coordinate system $(\lambda v/\delta u, y/\delta)$, the straight line defined by the last equation intersects the straight line $\lambda v/\delta u = y/\delta$ at the point (P, P), where

$$P = [(\lambda v_1/\delta u_1) - D]/(1 - D) \tag{8}$$

and D is defined by Eq. (5). Eliminating $\lambda v_1/\delta u_1$ between Eqs. (7) and (8), the integral of the continuity equation outside the shear flow becomes

$$(1/P)(\lambda v/\delta u) - 1 = D[(1/P)(y/\delta) - 1]$$

Finally, from the usual definition of displacement thickness δ^* it can be shown that

$$(1/u_1)(\partial u_1\delta^*/\partial x) = (v_1/u_1) + (\delta/u_1)(\partial u_1/\partial x)$$

Substitution for v_1/u_1 in Eq. (8) yields Eq. (6) for P, and the result stated in the theorem follows. Note that the flow has not been specified to be either laminar or turbulent, the mean continuity equation in two dimensions being the same for both, and that the mean flow has not been required to be independent of time.

(*b*) *Laminar Equilibrium Flow*

The two parameters D and P have so far been defined by completely kinematic considerations. I now propose to show that these two parameters are separately constant—i.e., independent of x—in any one of the laminar flows studied by Falkner and Skan, and that at least the parameter P is independent of x in an equilibrium turbulent flow as defined by Clauser.

Consider first the case of laminar flow, for which the statement of equilibrium—i.e., of similarity in the velocity profile—takes the form

$$u/u_1 = \varphi(y/\delta) \quad \text{or} \quad (u_1 - u)/u_1 = \phi(y/\delta) \tag{9}$$

Noting that the shearing stress at the wall is $\tau_w = (\mu\partial u/\partial y)_w = \rho u_\tau^2$ by definition, it follows from Eq. (9) that $\delta u_\tau^2/u_1 =$ constant. Furthermore, the displacement thickness δ^* is evidently proportional to the boundary-layer thickness δ. Thus,

$$(\delta^* u_1/\nu)(u_\tau^2/u_1^2) = \text{constant} \tag{10}$$

Substituting for $\delta^* u_1/\nu$ in the definition (6) for P, it is found immediately that

$$P = \frac{\delta^*}{\delta}\,\frac{d \ln (\delta^* u_1/\nu)}{d \ln (u_1/u_\tau)} = 2\,\frac{\delta^*}{\delta} = \text{constant} \tag{11}$$

Turning now to the parameter D, note first that the momentum equation evaluated at the wall implies

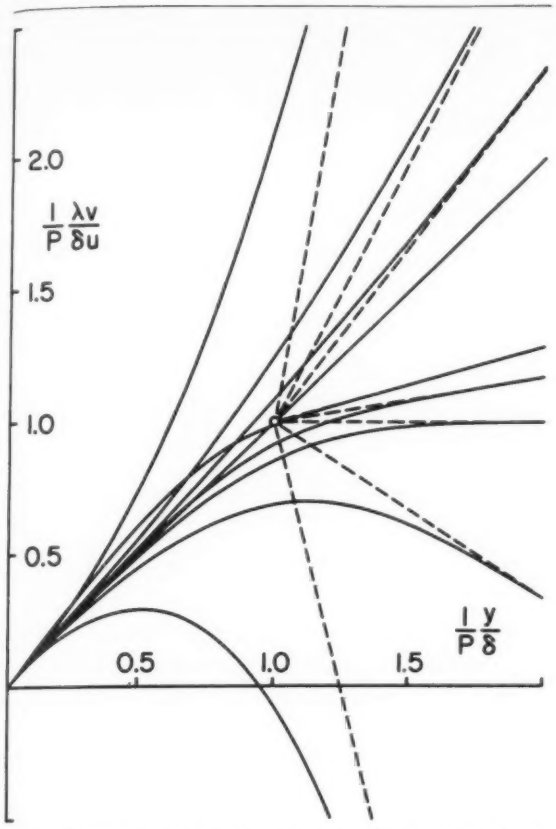

FIG. 1. Kinematic similarity for the laminar Falkner-Skan flows.

$\mu(\partial^2 u/\partial y^2)_w = dp/dx = -\rho u_1 du_1/dx$. Using Eq. (9) for $u(y)$, then

$$(\delta^2/\nu)(du_1/dx) = \text{constant} \tag{12}$$

The two conditions (10) and (12) may be combined with the two specifications for the variation of u_1 with x which are found by more elaborate analyses to be appropriate for the Falkner-Skan flows. Suppose first that

$$u_1 = K_1 x^n$$

Then $\delta = K_2 x^{(1-n)/2}$, $u_\tau = K_3 x^{(3n-1)/4}$, and

$$D = \frac{d \ln u_1}{d \ln u_\tau} = \frac{4n}{3n-1} = \text{constant} \tag{13}$$

Alternatively, suppose that

$$u_1 = C_1 e^{\alpha x}$$

Then $\delta = C_2 e^{-\alpha x/2}$, $u_\tau = C_3 e^{3\alpha x/4}$, and

$$D = \frac{d \ln u_1}{d \ln u_\tau} = \frac{4}{3} = \text{constant} \tag{14}$$

The exponential velocity variation thus replaces the power-law variation when $n = \pm\infty$.

Having identified the parameters D and P and the associated coordinates $\lambda v/P\delta u$ and $y/P\delta$, it can be shown that each of the equilibrium laminar flows of Falkner and Skan is represented in these coordinates by a single curve independent of Reynolds Number. Several typical curves, computed from Smith's tables[7] for various values of the parameter n in $u_1 x^{-n} =$ constant, are shown in Fig. 1. Noting that $P\delta = 2\delta^*$ for these flows, it is clear that the curves in the Figure do not depend on the definition adopted for the boundary-layer thickness δ.

Finally, the fact that the parameters D and P are constant for the Falkner-Skan flows implies a relationship $D(P)$ between these two parameters. This relationship, however, does depend on the definition of δ. If δ is arbitrarily taken as the value of y for which $u/u_1 = 0.99$, the curve plotted in Fig. 2 is obtained from the numerical solutions tabulated by Smith.

(c) *Turbulent Equilibrium Flow*

The results just derived for laminar flow are somewhat academic, as a great variety of constant parameters can be found to identify the various Falkner-Skan solutions. However, consider now the case of equilibrium turbulent flow, for which the mean-velocity profile obeys the defect law

$$(u_1 - u)/u_\tau = F(y/\delta) \tag{15}$$

outside the sublayer, whereas the local friction law has the form

$$\kappa(u_1/u_\tau) = \ln(\delta u_\tau/\nu) + \text{constant} \tag{16}$$

A calculation of the displacement thickness δ^*, neglecting the failure of the defect law in the sublayer,† gives

$$\delta^* u_1/\delta u_\tau = \int_0^1 F(y/\delta)\, d(y/\delta) = \text{constant} \tag{17}$$

Consequently,

† If the true profile given by the law of the wall had been used instead of the logarithmic approximation in the sublayer, there would have been obtained instead of Eq. (17) the relationship

$$\delta^* u_1/\delta u_\tau = \text{constant} + [\epsilon/(\delta u_\tau/\nu)]$$

where the constant ϵ is small (of the order of 75) compared to $\delta^* u_1/\nu$ for flow at large Reynolds Numbers. The conclusion that the parameter P is constant and equal to $1 + \pi$ for turbulent equilibrium flow is unchanged when this more accurate expression is substituted for Eq. (17) of the text.

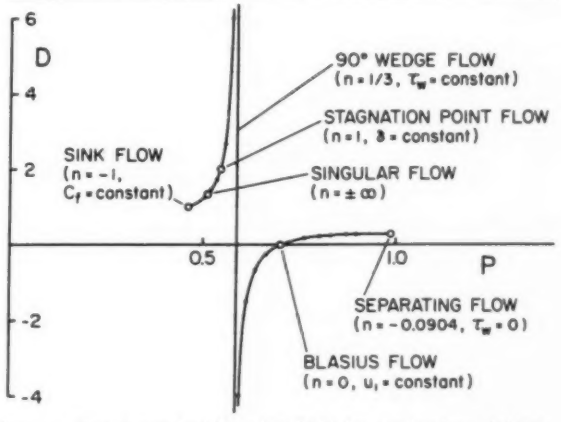

FIG. 2. The theoretical function $D(P)$ for the laminar Falkner-Skan flows.

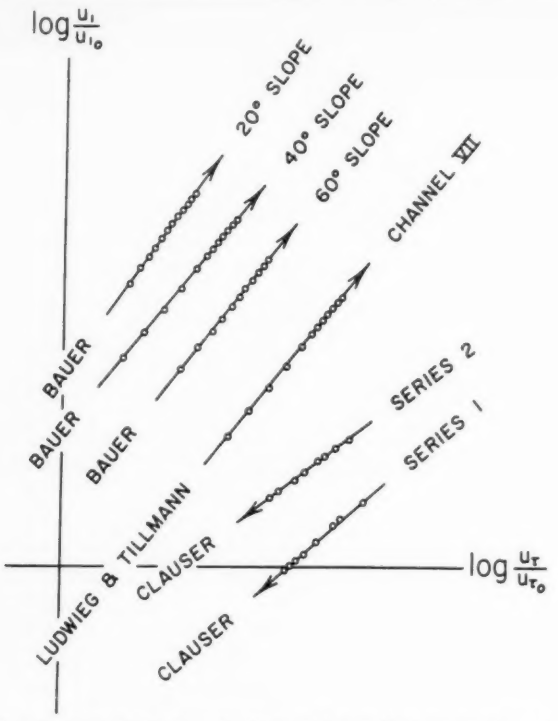

FIG 3. Test of the hypothesis $D = d \ln u_1/d \ln u_\tau = \text{constant}$ for equilibrium turbulent flow.

$$\frac{d \ln (\delta^* u_1/\nu)}{d \ln (u_1/u_\tau)} = \frac{u_1}{u_\tau} \frac{d \ln (\delta u_\tau/\nu)}{d(u_1/u_\tau)} = \kappa \frac{u_1}{u_\tau}$$

and

$$P = \frac{\delta^*}{\delta} \frac{d \ln (\delta^* u_1/\nu)}{d \ln (u_1/u_\tau)} = \kappa \frac{\delta^* u_1}{\delta u_\tau} = \text{constant} \quad (18)$$

This expression should be compared to the corresponding Eq. (11) for laminar flow. For the particular defect law given by Eq. (3), moreover, the constant in Eq. (18) can be written explicitly as

$$P = 1 + \pi \quad (19)$$

This last result, first obtained in October, 1954, provides almost the entire motivation for the present analysis. For note that the parameters D and P were originally defined and connected by one of the most general kinematic relationships which might be developed for flows of boundary-layer type without being so general as to be useless. The relationships (15) and (16), on the other hand, are of the essence of contemporary empirical knowledge of phenomena in turbulent boundary layers. The emphasis is on the word "empirical." That these apparently unrelated lines of investigation are found to converge in the simple Eq. (19) must be either a remarkable coincidence or a spontaneous manifestation of a fundamental order in the problem being studied here.

(*d*) *Kinematic Similarity*

I have shown that the two parameters D and P occur naturally together in the integrated continuity equation; that D and P are separately constant for any one of the laminar Falkner-Skan flows; and that P is constant for an equilibrium turbulent flow. These observations inevitably suggest the particular hypothesis

$$D = (d \ln u_1)/(d \ln u_\tau) = \text{constant}$$

for the equilibrium turbulent boundary layer. From the definition it is seen that the parameter D depends on the relative magnitude and rate of change of u_1 and u_τ, or alternatively of the free-stream dynamic pressure q and the surface shearing stress τ_w. The situation is therefore a happy one, in that the hypothesis D = constant can be tested a priori by an examination of experimental data.

Six equilibrium or near-equilibrium flows, omitting the case u_1 = constant, are included in an extensive survey of the experimental literature reported elsewhere.[4] For these six flows, Fig. 3 shows a plot in logarithmic coordinates of u_1/u_{1_0} against u_τ/u_{τ_0}, where u_τ is inferred from the law of the wall and u_{1_0} and u_{τ_0} are arbitrary constant reference velocities. The supposition that the data might define a straight line is borne out in each case, and the corresponding values of D and P are listed in Table 1 and plotted in Fig. 4.

Hereafter, the term *kinematic similarity* will be used to refer to the property which is implied for an equilibrium flow by the statement D = constant. The analogy mentioned in the Introduction is seen to emerge

TABLE 1
Summary of Experimental Data on D and P in Turbulent Equilibrium Flow

Reference or Remarks	$P = 1 + \pi$	$D = \frac{d \ln u_1}{d \ln u_\tau}$	D (revised)
Pure wall flow	1	1	
Ludwieg and Tillmann,[2] Channel VII	1.20 ± 0.02	1.22 ± 0.03	
Bauer,[8] 20° slope	1.22 ± 0.02	1.42 ± 0.03	
40° slope	1.24 ± 0.02	1.33 ± 0.03	
60° slope	1.23 ± 0.02	1.30 ± 0.03	
Wieghardt,[9] constant pressure	1.55 ± 0.01	0	
Clauser,[3] Series 1	2.54 ± 0.05	0.86 ± 0.05	0.795 ± 0.012
Series 2	4.93 ± 0.10	0.75 ± 0.05	0.863 ± 0.002
Pure wake flow	∞	1	

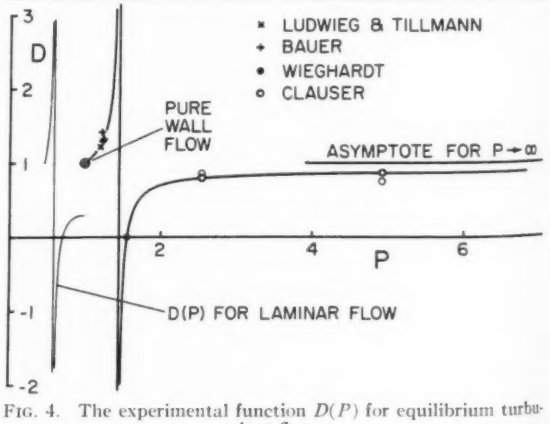

FIG. 4. The experimental function $D(P)$ for equilibrium turbulent flow.

from this property, inasmuch as the turbulent equilibrium flows of Clauser, like the laminar equilibrium flows of Falkner and Skan, are then characterized by a power-law relationship between the two parameters u_1 and u_τ. This laminar-turbulent analogy will be discussed at some length in Section (4), following a demonstration that the assumption of kinematic similarity leads to a solution of the inverse problem for the equilibrium turbulent boundary layer.

(3) Solution of the Inverse Problem

(a) *The Kármán Momentum-Integral Equation*

Clauser's main purpose in reference 3 was to show experimentally the existence and properties of equilibrium turbulent boundary-layer flows with non-vanishing pressure gradient. The appropriate pressure distribution was determined in each case by repeated trials, working in the direction of the flow. I will now show that the assumption D = constant allows Clauser's ad hoc determination of pressure distribution to be replaced, at least in principle, by an analytical calculation.

Three of the four equations needed in the formulation of the inverse problem for equilibrium turbulent flow are the stipulation

$$\pi = \text{constant} \tag{20}$$

together with the local friction law (2),

$$\kappa(u_1/u_\tau) = \ln(\delta u_\tau/\nu) + \kappa c + 2\pi$$

and the momentum-integral equation of Kármán,

$$\tau_w/\rho = u_\tau^2 = (d/dx)u_1^2\theta + u_1\delta^*(du_1/dx) \tag{21}$$

For the present, only these three equations will be considered, with the four quantities u_1, u_τ, δ, and π taken as dependent variables and x as independent variable. As a preliminary operation it is necessary to express the displacement thickness δ^* and the momentum thickness θ in Eq. (21) in terms of the primary variables of the problem. For this purpose, as remarked earlier, the concept of a defect law is sufficient. In what follows, however, I will retain the notation of Eq. (1) in order to show explicitly the dependence of various quantities on the single parameter—e.g., π—which characterizes an equilibrium flow.

Substituting the defect law given by Eq. (3) in the definitions

$$\delta^* = \int_0^\delta [1 - (u/u_1)]dy \tag{22}$$

$$\theta = \int_0^\delta (u/u_1)[1 - (u/u_1)]dy \tag{23}$$

and neglecting the small error in the sublayer, the two relationships are obtained.†

† Clauser[3] uses the notation Δ/δ for the quantity called here $\Omega_1(\pi)/\kappa$, and the notation $G\Delta/\delta$ for the quantity $2\Omega_2(\pi)/\kappa^2$. Rotta[10] uses $\delta^* u_1/\delta u_\tau$ and $I_1\delta^* u_1/\delta u_\tau$, respectively.

$$\kappa\frac{\delta^* u_1}{\delta u_\tau} = 1 + \pi\int_0^2 \frac{y}{\delta}\,dw = \Omega_1(\pi) \tag{24}$$

$$\frac{\kappa^2}{2}\left(\frac{\delta^* - \theta}{\delta}\right)\frac{u_1^2}{u_\tau^2} = \Omega_1 + \pi\int_0^2 \frac{y}{\delta}\ln\frac{y}{\delta}\,dw + \pi^2\int_0^2 \frac{y}{\delta}(2 - w)dw = \Omega_2(\pi) \tag{25}$$

In applying these relationships, a convenient first step is the use of Eqs. (25) and (24) successively in Eq. (21) to eliminate θ and δ^* in favor of u_1, u_τ, and δ. Remembering that π is constant, the result is

$$\kappa^2 = \frac{\delta}{u_1}\frac{du_1}{dx}\left(\kappa\frac{u_1}{u_\tau}\right)^2 - \frac{\delta}{u_\tau}\frac{du_\tau}{dx}\left[\left(\kappa\frac{u_1}{u_\tau}\right)^2 - \left(\kappa\frac{u_1}{u_\tau}\right)(3\Omega_1 - 1) + 2(2\Omega_2 - \Omega_1)\right] + \frac{d\delta}{dx}\left[\left(\kappa\frac{u_1}{u_\tau}\right)(\Omega_1 - 1) - 2(\Omega_2 - \Omega_1)\right]$$

A second step is the suppression of one of the three derivatives in the last equation with the aid of the local friction law (2) in differentiated form. The natural choice for elimination is $d\delta/dx$, yielding

$$\kappa^2 = \frac{\delta}{u_1}\frac{du_1}{dx}\left[\left(\kappa\frac{u_1}{u_\tau}\right)^2\Omega_1 - 2\left(\kappa\frac{u_1}{u_\tau}\right)(\Omega_2 - \Omega_1)\right] - \frac{\delta}{u_\tau}\frac{du_\tau}{dx}\left[\left(\kappa\frac{u_1}{u_\tau}\right)^2\Omega_1 - 2\left(\kappa\frac{u_1}{u_\tau}\right)\Omega_2 + 2\Omega_2\right] \tag{26}$$

A third step, suggested by Eq. (26) as well as by experience with the special case u_1 = constant, is the recognition of the quantity

$$z = \kappa(u_1/u_\tau)$$

as a fundamental variable. Differentiating the last expression, then

$$(1/z)(dz/dx) = [(D - 1)/D](1/u_1)(du_1/dx) = (D - 1)(1/u_\tau)(du_\tau/dx)$$

where $D = d\ln u_1/d\ln u_\tau$ by definition. Eq. (26) becomes finally

$$\kappa^2\frac{dx}{\delta} = \frac{dz}{z}\left[z^2\Omega_1 - 2z\Omega_2 - 2z\Omega_1\left(\frac{D}{1 - D}\right) + 2\Omega_2\left(\frac{1}{1 - D}\right)\right] \tag{27}$$

To recapitulate, Eq. (27) is the momentum-integral Eq. (21) evaluated for the special mean-velocity profile (1) with constant π. The defect law (3) has been taken to apply throughout the flow, including the sublayer. Because no assumption has yet been made concerning the parameter D, the effect of the manipulation just carried out has been to change the nature but not the number of the variables in the problem. It is even conceivable that the form of Eq. (27) would eventually suggest the assumption D = constant as a heuristic measure, if attention had not been attracted to this hypothesis by consideration of the continuity equation.

Note that the flow with $D = 0$ or $u_1 =$ constant appears as a special case of Eq. (27) for which an integral may be obtained immediately, using Eq. (2) to eliminate δ in favor of z. The integral in question was first obtained by Kármán and is the one cited in the introduction as the only previously known solution of the inverse problem for the turbulent boundary layer.

(*b*) *Integration of the Kármán Equation*

I will now assume that an equilibrium turbulent boundary layer has the property of kinematic similarity;

$$D = (u_\tau/u_1)(du_1/du_\tau) = \text{constant} \tag{28}$$

Eq. (28) evidently provides the fourth relationship needed in the formulation of the inverse problem, and is to be considered jointly with the momentum-integral Eq. (27), the local friction law (2), and the equilibrium condition (20). Now Eq. (28) is itself a differential equation which may be integrated immediately, with the result

$$u_1/u_{1_0} = (u_\tau/u_{\tau_0})^D \tag{29}$$

where $u_{1_0} = u_1(x_0)$, $u_{\tau_0} = u_\tau(x_0)$, and x_0 is any convenient reference point. Returning to Eq. (27), the factor δ on the left-hand side can be eliminated by observing, in view of Eqs. (2) and (29), that

$$\delta/\delta_0 = (z/z_0)^{1/(1-D)} e^{z-z_0}$$

where $\delta_0 = \delta(x_0)$ and $z_0 = z(x_0)$. Substituting for δ in Eq. (27) there is obtained finally

$$\frac{\kappa^2 z_0^{1/(1-D)}\, e^{z_0}}{\delta_0}\, dx = z^{[1/(1-D)]-1}\, e^z\, dz \left[z^2\Omega_1 - 2z\Omega_2 - 2z\Omega_1\left(\frac{D}{1-D}\right) + 2\Omega_2\left(\frac{1}{1-D}\right)\right] \tag{30}$$

This equation may be integrated in closed form if $1/(1-D)$ is an integer or half-integer. For example, if $D = 4/3$,

$$\kappa^2\left(\frac{x-x_0}{\delta}\right) = (5\Omega_1 - 2\Omega_2) z_0^3 e^{-z_0}[Ei(z) - Ei(z_0)] - (5\Omega_1 - 2\Omega_2) z_0^2 \left[\frac{\delta}{\delta_0}\left(\frac{z}{z_0}\right)^2 - 1\right] - (4\Omega_1 - 2\Omega_2)\, z_0 \left[\frac{\delta}{\delta_0}\left(\frac{z}{z_0}\right) - 1\right] + 2\Omega_2\left[\frac{\delta}{\delta_0} - 1\right] \tag{31}$$

where $$Ei(z) = \int_{-\infty}^{z} \frac{e^t}{t}\, dt$$

and $$\delta/\delta_0 = (z/z_0)^{-3} e^{z-z_0} \tag{32}$$

The quantities (x, δ, z) and (x_0, δ_0, z_0) in these expressions may be considered as variables and parameters, respectively, or vice versa, depending on the application. Note that two independent constants of integration, δ_0 and z_0, are encountered in integrating the system (27) and (28). Because $z = \kappa u_1/u_\tau$ determines $\delta u_\tau/\nu$ for an equilibrium flow by virtue of the local friction law (2), this means that the two physical scales δ and ν/u_τ may be specified independently at any one station.

I have evaluated Eqs. (31) and (32) for $D = 4/3$ numerically, taking $\pi = 0.24$. These values are intended to represent the spillway flow with 40° slope studied by Bauer[8] (see Fig. 8 of reference 4). The functions $\Omega_1(\pi)$ and $\Omega_2(\pi)$ have been given the form $\Omega_1 = 1 + \pi$ and $\Omega_2 = 1 + 1.600\pi + 0.761\pi^2$ required by the particular wake function $w(y/\delta)$ tabulated in reference 4; the experimental values are not significantly different. Similar calculations have been made for $\pi = 0.55$ and $D = 0$, corresponding to the flow with a constant external velocity of 33.0 meters per sec. studied by Wieghardt[9] (see Fig. 4 of reference 4), and for $\pi = 1.54$ and $D = 4/5$, corresponding to the flow with moderately rising pressure† studied by Clauser[3] (see Fig. 15 of reference 4). Taking the constants δ_0 and z_0 in each case from the experimental data at a point well downstream, the calculated and measured values for $\delta^*(x)$, $u_1(x)$, and $z(x)$ are compared in Fig. 5.

(*c*) *Uniqueness*

One important consequence of the hypothesis $D =$ constant for an equilibrium turbulent boundary layer is an explicit statement of uniqueness for such flows. Given a constant value for D, consider first an integral of Eq. (30) in the form $(x - x_0)/\delta_0 = E(z, z_0, \pi, D)$. On eliminating the thickness δ_0 in favor of δ, z, and z_0 this integral can be written $(x - x_0)/\delta = F(z, z_0, \pi, D)$. Next, note that if P (or π) and D are separately constant for an equilibrium flow, these quantities must be related by some function $D(P)$ like the one for laminar flow shown in Fig. 2. This being so, the dependence of the flow on the parameter D need not be stated ex-

† The value $D = 4/5$ (actually 0.795) attributed here to Clauser's flow is different from the experimental value $D = 0.86$ listed in Table 1. The need for some revision in the original value of D can be argued from the momentum-integral equation in the differentiated form (26). Let this equation be rewritten as

$$\kappa^2(\lambda/\delta) = z^2\Omega_1(1 - D) - 2z[\Omega_1 D + \Omega_2(1 - D)] + 2\Omega_2$$

Now the quantity $\kappa^2\lambda/\delta$ can also be evaluated by differentiating the local friction law (2) to obtain

$$\kappa^2(\lambda/\delta) = [\kappa^2/(d\delta/dx)][z(1 - D) + 1]$$

Elimination of λ/δ allows any one of the three quantities z, D, and $d\delta/dx$ to be computed if π and the other two quantities are known. The first equation assumes two-dimensional momentum balance as well as similarity in the mean-velocity profile in the sense required by the law of the wall and the defect law. The second equation assumes similarity only. Taking $\pi = 1.54$ and $D = 0.86$ from Table 1 for Clauser's first series of experiments, together with a typical value $z = 13$, it is found that the computed value of $d\delta/dx$ is negative. I have therefore reversed the calculation, estimating $d\delta/dx$ from the experiments and calculating D instead. The revised values for D are listed in Table 1, together with an estimate of probable error corresponding to an uncertainty of ±20 per cent in $d\delta/dx$. That the revisions should be in opposite directions for Clauser's two flows is suggested by slight discrepancies in momentum balance noted elsewhere [cf. the functions $\Phi(x)$ in Figs. 15 and 16 of reference 4].

plicitly; thus $(x - x_0)/\delta = G(z, z_0, \pi)$. Finally, suppose that a convention can be found for specifying the origin or initial point x_0, δ_0, z_0, etc. in such a way that z_0 depends on π alone. For example, require the momentum thickness θ to vanish for $x = x_0 = 0$, and note that Eqs. (24) and (25) then imply $\kappa u_1/u_\tau = z = z_0 = 2\Omega_2(\pi)/\Omega_1(\pi)$. The integral of Eq. (30) under these conditions can thus be expressed ultimately in the form $x/\delta = H(z, \pi)$. But if $\delta u_\tau/\nu$ and δ/x for constant π are functions of $z = \kappa u_1/u_\tau$ alone, then so are $u_\tau x/\nu$ and $u_1 x/\nu$. So also are $\delta^* x/\delta^*$, $\theta/u_1\theta/\nu$, and similar quantities, by virtue of various relationships already derived from the momentum-defect law.

Given the property D = constant, therefore, the conclusion is that quantities like δ^*/θ, $C_f = 2u_\tau^2/u_1^2$, and $R_\theta = u_1\theta/\nu$ can be expressed as one-parameter functions of a uniquely defined streamwise Reynolds Number $R = u_1 x/\nu$ for the class of equilibrium turbulent flows even when u_1 depends on x. This conclusion does not require the assumption that the wake function $w(y/\delta)$ in Eq. (1) is universal, because the mean-velocity profile in an equilibrium flow is adequately expressed for the purpose of this argument by the defect law (4). Neither would the conclusion stated here be changed if the exact mean-velocity profile in the sublayer had been considered in Eqs. (24) and (25), as the quantities $\Omega_1(\pi)$ and $\Omega_2(\pi)$ could then be replaced by $\Omega_1(\pi, z)$ and $\Omega_2(\pi, z)$.

(d) *The Shearing-Stress Profile*

The distribution of shearing stress within an equilibrium turbulent boundary layer may be found by integrating the boundary-layer equations

$$(\partial u/\partial x) + (\partial v/\partial y) = 0 \tag{33}$$

$$u(\partial u/\partial x) + v(\partial u/\partial y) = u_1(du_1/dx) + (1/\rho)(\partial\tau/\partial y) \tag{34}$$

for the profile of Eq. (1) with constant π. This calculation, which amounts to inferring the forces applied to the fluid from the observed accelerations, should be equivalent within the boundary-layer approximation to a direct measurement of the shearing stress. Noting that $\tau_w = \rho u_\tau^2$ by definition, the result of a tedious lot of algebra is

$$\kappa^2(\lambda/\delta)[1 - (\tau/\tau_w)] = (y/\delta)[\zeta^2 - Dz^2 + (1 - D)\zeta z \times (\omega_1 - 1) - 2(1 - D)z(\omega_2 - \omega_1) - 2\zeta\omega_1 + 2\omega_2] \tag{35}$$

where $z = \kappa u_1/u_\tau$, $\zeta = \kappa u/u_\tau$, and ω_1 and ω_2 are incomplete integrals corresponding to Ω_1 and Ω_2 in Eqs. (24) and (25). The functions $\omega_1(\pi, y/\delta)$ and $\omega_2(\pi, y/\delta)$ are defined and tabulated in reference 4.

Taking $\delta u_\tau/\nu = 5{,}000$ for four equilibrium flows which have been observed experimentally—first, $P = 1.24$, $D = 1.33$; second, $P = 1.55$, $D = 0$; third, $P = 2.54$, $D = 0.80$; and fourth, $P = 4.93$, $D = 0.86$—the mean-velocity profile according to Eq. (1) and the total shearing-stress profile according to Eq. (35) are shown in Fig. 6. Also shown as a crosshatched region is the velocity defect in the equivalent wake.[4]

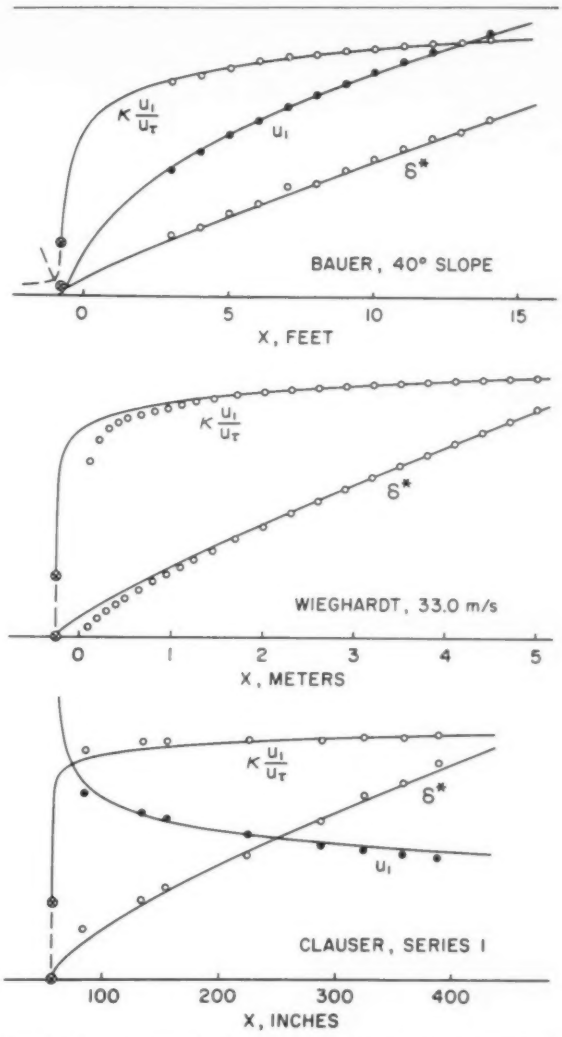

FIG. 5. Comparison of calculated and observed development of three equilibrium turbulent flows.

(4) THE FUNCTION $D(P)$

(a) *The Pure Wake Flow*

Earlier, an analogy between laminar and turbulent equilibrium flow was suggested on the ground that

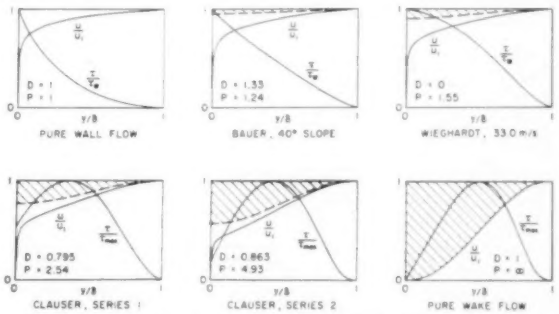

FIG. 6. Typical mean-velocity and total shearing-stress profiles in several equilibrium turbulent flows at the same local Reynolds Number $\delta u_\tau/\nu = 5{,}000$.

either class of flows can be represented by a certain function $D(P)$. To study this analogy more closely, the flows in question may be arranged according to increasing values of the parameter P, as in Figs. 2 and 4. Noting that the present analysis of turbulent flow is based on a defect law with four characteristic parameters u_1, u_τ, δ, and P, two points of coincidence appear at $D = 0$ and $D = \infty$, corresponding to the cases $u_1 =$ constant and $u_\tau =$ constant, respectively. The case $\delta =$ constant, which in the laminar Falkner-Skan family is the plane stagnation-point flow, apparently does not appear among the turbulent equilibrium flows.

Two other special cases will be investigated here as possible points of coincidence in the laminar-turbulent analogy. The first is the case $u_\tau = 0$, and the second is the case $u_1/u_\tau =$ constant. Both will be treated by slight extrapolations of the ideas in Sections (1) and (2), and the arguments given here may be accepted or rejected on their merits without seriously prejudicing any of the earlier discussion.

The profile parameter π in Eqs. (1) and (2) is a measure of the relative magnitude of the wake and wall components in the mean-velocity profile. According to Eq. (2), π must become indefinitely large if u_τ approaches zero while δ and u_1 remain finite. At the same time the product $2\pi u_\tau/\kappa u_1$ approaches unity, so that the mean-velocity profile for $\tau_w = 0$ is locally

$$u/u_1 = (1/2)w(y/\delta) \tag{36}$$

where $w = 2$ when $y = \delta$ by definition.

I will now define a pure wake flow as an equilibrium turbulent boundary layer for which the surface shearing stress is zero everywhere. The profile is then given by Eq. (36), the parameter $P = 1 + \pi$ is infinite, and the quantities δ^*/δ, θ/δ, and δ^*/θ are constants. As might be expected, the laminar equilibrium boundary layer with $\tau_w = 0$ is one of the Falkner-Skan family—namely, the flow for which P has its largest value in Fig. 2. The velocity profile for this laminar flow can also be represented by Eq. (36), although with a different function $w(y/\delta)$.

Consider therefore the momentum-integral equation of Kármán, Eq. (21), when $\theta/\delta =$ constant and $\tau_w = 0$; thus,

$$\frac{1}{\delta}\frac{d\delta}{dx} + \left(2 + \frac{\delta^*}{\theta}\right)\left(\frac{1}{u_1}\right)\frac{du_1}{dx} = 0 \tag{37}$$

It follows that

$$\delta u_1^{2+\delta^*/\theta} = \text{constant} \tag{38}$$

The shearing-stress profile is readily obtained by integrating the boundary-layer Eqs. (33) and (34) directly for the velocity distribution (36). The result can be written

$$\frac{v/u}{d\delta/dx} = \frac{y}{\delta} - \left(\frac{1 + \delta^*/\theta}{2 + \delta^*/\theta}\right)\frac{1}{w}\int_0^{y/\delta} w d\zeta \tag{39}$$

$$\frac{\tau/\rho u_1^2}{d\delta/dx} = \left(\frac{1}{2 + \delta^*/\theta}\right)\frac{y}{\delta} - \left(\frac{1 + \delta^*/\theta}{2 + \delta^*/\theta}\right)\frac{w}{4}\int_0^{y/\delta} w d\zeta + \left(\frac{\delta^*/\theta}{2 + \delta^*/\theta}\right)\frac{1}{4}\int_0^{y/\delta} w^2 d\zeta \tag{40}$$

If the flow is laminar, the shearing stress τ in Eq. (40) must be related to the velocity by the Newtonian law $\tau = \mu\partial u/\partial y = (\mu u_1/2\delta)w'(y/\delta)$. Substituting in Eq. (40) and noting that the left side, like the right, must be a function of y/δ only, it follows for the continuously separating laminar equilibrium flow that

$$(\delta u_1/\nu)(d\delta/dx) = \text{constant}$$

Combining this condition with Eq. (38), it is seen that

$$u_1 x^{1/(3+2\delta^*/\theta)} = \text{constant} \tag{41}$$

where it has been assumed that $u_1 = \infty$ at $x = 0$. This expression has the proper form $u_1 x^{-n} =$ constant, and the value of the exponent n is known[7] to be very nearly $n = -0.0904$ for the flow in question. In the present context, however, it is instructive to form an independent estimate of this exponent by taking $\delta^*/\theta = 4$, a value consistent with the expected antisymmetry of the velocity profile. Then $n = -1/(3 + 2\delta^*/\theta) = -1/11 = -0.0909$.

Next consider turbulent flow, for which the Newtonian stress law $\tau = \mu\partial u/\partial y$ is no longer valid and has to be replaced by some other assumption. Taking into account the condition $\tau_w = 0$, it is reasonable to require the mean motion to be independent of the viscosity, as in the case of free shear flow. If so, then only two lengths δ and x can appear in the problem, and these two lengths must be proportional. But if $d\delta/dx$ is a constant, it follows from Eqs. (39) and (40) that v/u and τ/q are functions of y/δ only; and the converse is also true. Finally, replacing δ in Eq. (38) by x, there is obtained

$$u_1 x^{1/(2+\delta^*/\theta)} = \text{constant} \tag{42}$$

If δ^*/θ is again taken as 4, the exponent is $1/6$, while the supposedly more accurate value $\delta^*/\theta = 4.18$ from reference 4 gives 0.162. In any event, the difference between the exponents in Eqs. (41) and (42) for laminar and turbulent flow is consistent with the empirical observation that turbulent flow will in general support a more rapid pressure rise.

Finally, it can be shown that the parameter D must be equal to unity for the turbulent pure wake flow. Eliminating $d\delta/dx$ between Eqs. (37) and (39) with the latter evaluated at $y = \delta$, substituting for v_1/u_1 in Eq. (8) for P, and noting that $D = -(\lambda/u_1)du_1/dx$, then

$$P = \frac{1}{2}\left(\frac{D}{1 - D}\right)\left(1 + \frac{\delta^*}{\theta}\right) \tag{43}$$

If the flow is laminar, then $P = 2\delta^*/\delta$ must be nearly unity and δ^*/θ must be nearly 4, so that $(1 - D)/D = 5/2$ and $D = 2/7$. The exponent n obtained from Eq. (13) of Section (2) is again $-1/11$. If the flow is turbulent, on the other hand, the parameter $P = 1 + \pi$ is infinite in Eq. (43), and therefore $D = 1$.

The mean-velocity distribution (36) and the shearing-stress distribution (40) are plotted in Fig. 6 for the particular wake function $w(y/\delta)$ of reference 4. The shearing stress being computed as τ/τ_{max}, it is not

necessary to specify a value of $d\delta/dx$ for the flow in question.

(b) *The Pure Wall Flow*

A second special case of considerable interest is pure wall flow, obtained from Eq. (1) by putting $\pi = 0$—i.e., $P = 1$. The mean-velocity profile is then given by the law of the wall, $u/u_\tau = f(yu_\tau/\nu)$, from which it follows[6] that u/u_τ and yu_τ/ν are constant on mean streamlines and that

$$\lambda v/\delta u = y/\delta \tag{44}$$

where $1/\lambda = -(1/u_\tau)du_\tau/dx$ as before. The shearing-stress profile is most readily obtained by putting $\omega_1 = \omega_2 = 1$ in Eq. (35):

$$\kappa^2\frac{\lambda}{\delta}\left(1 - \frac{\tau}{\tau_w}\right) = \frac{y}{\delta}\left[-D\left(\kappa\frac{u_1}{u_\tau}\right)^2 + \left(\kappa\frac{u}{u_\tau}\right) - 2\left(\kappa\frac{u}{u_\tau}\right) + 2\right] \tag{45}$$

At $y = \delta$, therefore, where $u = u_1$ and $\tau = 0$,

$$\kappa^2\frac{\lambda}{\delta} = \left(\kappa\frac{u_1}{u_\tau}\right)^2(1 - D) - 2\left(\kappa\frac{u_1}{u_\tau}\right) + 2 \tag{46}$$

A number of arguments can be found, all of them unfortunately somewhat porous, for supposing that if the parameter D is constant for the pure wall flow it ought to have the value unity. Certainly the point $P = D = 1$ is favorably located in Fig. 4 with respect to the experimentally determined points in accelerating flow, if the hypothetical function $D(P)$ for equilibrium turbulent flow is to resemble the one in Fig. 2 for laminar flow. The statement $D = 1$ can also be argued on dimensional grounds; the first of the two characteristic lengths δ and ν/u_τ does not enter the problem explicitly, and the two lengths in question should therefore be proportional to each other. Finally, the statement $D = 1$ follows if v/u and τ/τ_w in Eqs. (44) and (45) are required to be functions of y/δ alone, and conversely.

If $D = 1$ for the pure wall flow, then $\delta u_\tau/\nu$, u_1/u_τ, and δ/λ are constants, and, therefore, u_1x/ν = constant. The external flow is either a source or a sink flow, and only the latter is permitted by the conditions $\lambda/\delta < 0$ and $v_1/u_1 < 0$ which are obtained from Eqs. (46) and (44) when u_1 and u_τ are taken as positive quantities. The corresponding laminar sink flow is readily identified as the one for which P takes on its smallest value in Fig. 2. This flow may be studied (1) directly;[11] (2) by making a boundary-layer approximation in the known exact solution of the Navier-Stokes equations for radial sink flow; or (3) by a suitable limiting process in the Falkner-Skan equation, letting the exponent n in u_1x^{-n} = constant approach -1 from below so that the Falkner-Skan parameter $\beta = 2n/(n + 1)$ approaches $+\infty$. Because $v/u = y/x$ for this laminar flow by assumption, the friction coefficient must be independent of x and the velocity profile must be expressible[6] in the form $u/u_\tau = \varphi(yu_\tau/\nu)$ with u_1/u_τ as parameter. For a given laminar flow there is only one function $\varphi(yu_\tau/\nu)$ such that the boundary-layer equations are satisfied at the same time that $\tau = \mu\partial u/\partial y$. For turbulent flow, on the other hand, the function $\varphi(yu_\tau/\nu)$ has to be identified with the function $f(yu_\tau/\nu)$ in the law of the wall, and the momentum equation is automatically satisfied because $u(x, y)$ is given and $\tau(x, y)$ is computed therefrom. In either case the friction coefficient is constant but its value can apparently be chosen arbitrarily.

The logarithmic mean-velocity profile and the corresponding shearing-stress profile in the pure wall flow are shown in Fig. 6 for $\delta u_\tau/\nu = 5{,}000$ and $D = 1$. I have also computed the function τ/τ_w for values of $\delta u_\tau/\nu$ ranging from 10^3 to 10^9, and have found that the various curves can scarcely be distinguished in the Figure. That is, τ/τ_w as a function of y/δ is for practical purposes independent of the Reynolds Number $\delta u_\tau/\nu$ for the pure wall flow. These calculations refer to physically different boundary layers, not to different stations in the same boundary layer.

Finally, if the conjecture $D = 1$ is in fact correct for the pure wall flow, then the edge of the boundary layer is a mean streamline and the net velocity of propagation of the laminar-turbulent interface into the nonturbulent fluid is zero.

(c) *An Interpolation Scheme*

In any practical application of the concept of kinematic similarity—for example, to diffuser design—some interpolation method is needed to supplement the experimental values of $D(P)$ listed in Table 1. The method proposed here is far from unique, and depends on the development of two quantities which, unlike the parameters D and P, remain finite as π increases from zero to infinity. One such quantity is the strength of the equivalent wake, $2\pi u_\tau/\kappa u_1 = 2\pi/z$. Another is the rate of mass entrainment in the boundary layer. Defining

$$(s/u_1) = (d\delta/dx) - (v_1/u_1) = (1/\rho u_1)(d/dx)[\rho u_1(\delta - \delta^*)] \tag{47}$$

then the quantity s is seen to be the net velocity of propagation of the boundary $y = \delta$ with respect to the free stream. Now the ratio s/u_1 may be expressed in terms of the local friction coefficient and the parameter π with the aid of Eqs. (2) and (18):

$$s/u_1 = (\delta/z)(dz/dx)(z - \pi)$$

where $z = \kappa u_1/u_\tau$. But $(\delta/z)dz/dx$ is a known function of z, π, and D from Eq. (27); thus,

$$\frac{1}{\kappa^2}\frac{s}{u_1} = \frac{(z - \pi)(1 - D)}{(1 - D)(z^2\Omega_1 - 2z\Omega_2) - 2Dz\Omega_1 + 2\Omega_2} \tag{48}$$

The case of pure wake flow is most conveniently treated separately to obtain $2\pi/z = 1$, and, from Eqs. (47) and (39),

$$\frac{1}{\kappa^2}\frac{s}{u_1} = \frac{1}{2\kappa^2}\frac{d\delta}{dx}\left(\frac{1 + \delta^*/\theta}{2 + \delta^*/\theta}\right)$$

For given values of π and D and for a specified value of $\delta u_\tau/\nu$, the quantities z, $2\pi/z$, and $s/\kappa^2 u_1$ may be computed from Eqs. (2) and (48). Plotting $s/\kappa^2 u_1$ against $2\pi/z$ for the six flows of Fig. 6, estimating $d\delta/dx = 0.252$ for the pure wake flow from reference 4, and using essentially straight line interpolation except near $\pi = 0$, the inverse calculation† for $D(P)$ leads for $\delta u_\tau/\nu = 5{,}000$ to the curve shown in Fig. 4. This calculation, as might be expected, is not at all sensitive to the value chosen for $\delta u_\tau/\nu$.

(*d*) *The Hypothetical Function D(P)*

Perhaps the most instructive physical interpretation of the new parameter D comes from the fact that the mean streamlines in a shear flow intersect at a common origin for any region in which v/u for fixed x is a linear function of y. For a boundary layer one such region is the one near the wall, including the sublayer in the case of turbulent flow; here $v/u = y/\lambda$. In the absence of viscosity there is a corresponding relationship $v/u = Dy/\lambda$ for the ambient flow. Thus the parameter D is a measure of the extent to which any divergence or convergence of the streamlines in the external flow, which is to say any pressure gradient, affects the streamlines in the neighborhood of the wall. This interpretation applies equally for laminar and turbulent flow under quite general conditions, and like the defect law itself does not involve the viscosity of the fluid explicitly.

At the beginning of this paper the inverse problem was defined as the determination of the surface shearing-stress distribution $\tau_w(x)$, given the ambient pressure distribution $p(x)$ and suitable initial and boundary conditions. For a general flow a direct solution other than an experimental one is not yet possible for this problem. However, a knowledge of $p(x)$ is sufficient to determine the streamline pattern outside the boundary layer, while a knowledge of $\tau_w(x)$ is sufficient to determine the streamline pattern near the wall. For equilibrium flow the assumption of kinematic similarity connects these two observations directly, thus providing a detour as it were around the obstacle represented by the turbulent transport mechanism. The connection may be viewed either as a relationship between streamline patterns in two regions of the flow or simply as a power-law relationship between q and τ_w.

The second of these two interpretations shows more clearly the role which is played by the concept of kinematic similarity in the solution of the inverse problem. For an equilibrium turbulent boundary layer it is evident from Eqs. (2) and (26) that the Kármán momentum-integral Eq. (21) can be reduced to the form $dx = G_1(u_1, u_\tau, P)du_1 + G_2(u_1, u_\tau, P)du_\tau$. The assumption D = constant or $u_1 u_\tau^{-D}$ = constant then leads to a separation of variables, and the only further information required for a full solution is the empirical function $D(P)$.

What is ultimately needed, of course, is not a physical interpretation but a physical principle, from which might be deduced not only the existence of a function $D(P)$ for equilibrium turbulent flow but the form of this function. Granted that Fig. 3 justifies the assumption D = constant as an interpolation device for the data of the Figure, other reasons must be found for making the same assumption for a general equilibrium flow. The theorem presented earlier, in which the two parameters D and P first occur, amounts at best only to circumstantial evidence. So does the analogy proposed here for laminar and turbulent equilibrium flows. In the absence of a physical principle, therefore, any discussion of kinematic similarity requires an act of faith in that neither of the two statements D = constant or P = constant can be said to imply the other. The problem having been stated in these terms, it follows from experience with the special but by no means trivial case u_1 = constant or $D = 0$ that a further attempt must be made to account directly and specifically for the concept of a defect law.

† For Clauser's second flow it appears that the parameter D ought to be taken as 0.866 if a smooth curve is to be obtained in the coordinates $(2\pi/z, s/\kappa^2 u_1)$.

References

[1] Squire, H., *Reconsideration of the Theory of Free Turbulence* Phil. Mag., 7th Series, Vol. 39, No. 288, pp. 1–20, 1948.

[2] Ludwieg, H., and Tillmann, W., *Untersuchungen über die Wandschubspannung in turbulenten Reibungsschichten*, Ing.-Arch., Vol. 17, No. 4, pp. 288–299, 1949; translated as *Investigations of the Wall Shearing Stress in Turbulent Boundary Layers*, NACA TM 1285, 1950.

[3] Clauser, F., *Turbulent Boundary Layers in Adverse Pressure Gradients*, Journal of the Aeronautical Sciences, Vol. 21, No 2, pp. 91–108, 1954.

[4] Coles, D., *The Law of the Wake in the Turbulent Boundary Layer*, J. Fluid Mech., Vol. I, Part 2, pp. 191–226, 1956.

[5] Falkner, V., and Skan, S., *Some Approximate Solutions of the Boundary Layer Equations*, ARC R&M 1314, 1930.

[6] Coles, D., *The Law of the Wall in Turbulent Shear Flow*, 50 Jahre Grenzschichtforschung, pp. 153–163, F. Vieweg & Sohn, Braunschweig, Germany, 1955.

[7] Smith, A. M. O., *Improved Solutions of the Falkner and Skan Boundary-Layer Equations*, IAS Fairchild Fund Paper No. FF-10, 1955.

[8] Bauer, W., *The Development of the Turbulent Boundary Layer on Steep Slopes*, State Univ. of Iowa, Thesis, 1951; abridged in Proc. ASCE, Separate No. 281, 1953.

[9] Wieghardt, K., *Über die Wandschubspannung in turbulenten Reibungsschichten bei veränderlichem Aussendruck*, Göttingen, U&M 6603, 1943; see also Wieghardt, K., and Tillmann, W., *Zur turbulenten Reibungsschicht bei Druckanstieg*, Göttingen, U&M 6617, 1944; translated as *On the Turbulent Friction Layer for Rising Pressure*, NACA TM 1314, 1951.

[10] Rotta, J., *Über die Theorie der turbulenten Grenzschichten*, Mitt. Max-Planck-Inst. für Strömungsforschung, No. 1, Göttingen, 1950; translated as *On the Theory of the Turbulent Boundary Layer*, NACA TM 1344, 1953.

[11] Schlichting, H., *Boundary Layer Theory*, Chap. IX; McGraw-Hill Book Company, Inc., New York, 1955.

A Theoretical and Experimental Study of Airplane Dynamics in Large-Disturbance Maneuvers

DONALD W. RHOADS* AND JOHN M. SCHULER**

Cornell Aeronautical Laboratory, Inc.

SUMMARY

This paper reviews an effort to solve some problems of large-disturbance maneuvering flight. The period covered is from 1949 to the present, and results of both theoretical and flight test investigations are presented.

The rolling pull-out, a critical maneuver for vertical tail loads, was chosen for study. Equations of motion were developed, and solutions were compared with responses obtained from flight tests. The equations, validated by this comparison, were then applied to critical present-day airplane configurations, and a general study of large-disturbance motion was made including variation of pertinent parameters.

This paper represents a first step in the study of nonlinear aspects of airplane dynamics and control in large-disturbance maneuvers. Results show that inertial and aerodynamic nonlinearities introduce destabilizing tendencies not predicted by linear theory. Although complex equations are required to predict motions accurately, the characteristics of the motion may be described using simple mathematical techniques.

SYMBOLS AND DEFINITIONS

The orientation of the airplane body axes with respect to earth axes or inertial space, defined by rotations ψ, θ, and ϕ, is shown in Fig. 1. The orientation of wind axes, stability axes, and body axes and the conventions for linear velocities, angular velocities, forces, moments, and control surface deflections are shown in Fig. 2. The symbols and definitions used in this paper agree substantially with those recommended in reference 13.

x_s, y_s, z_s = stability axes
x, y, z = body axes

The body axes (unless otherwise noted) are oriented so as to coincide with the stability axes for straight and level flight in the reference flight condition.

ψ, θ, ϕ = orientation angles of earth to body axes (see Fig. 1)
β = angle of sideslip (see Fig. 2)
α = angle of attack (see Fig. 2)
δ = control surface deflection
η = angle of attack of the x principal axis
u, v, w = components of linear velocity
p, q, r = components of angular velocity
n_z = component of acceleration along z axis, g's
X, Y, Z = components of force
L, M, N = components of moment
N_V = load on the vertical tail
N_H = load on the horizontal tail
m = mass
t = time
W = weight
I_x, I_y, I_z = moments of inertia
I_{xz} = product of inertia
ρ = air density
h = altitude
M = Mach Number
V = total airplane velocity $= \sqrt{u^2 + v^2 + w^2}$
U_1 = reference forward velocity along the x axis
q = dynamic pressure, $(1/2)\rho V^2$
c = wing mean aerodynamic chord
b = wing span
g = acceleration of gravity, 32.2 ft./sec.^{2}
AR = aspect ratio
Λ = sweep angle, sweep of quarter chord line
C_x, C_y, C_z = $X/(1/2)\rho V^2 S$, $Y/(1/2)\rho V^2 S$, $Z/(1/2)\rho V^2 S$
C_l, C_m, C_n = $L/(1/2)\rho V^2 Sb$, $M/(1/2)\rho V^2 Sc$, $N/(1/2)\rho V^2 Sb$
C_L = Lift$/(1/2)\rho V^2 S$
C_D = Drag$/(1/2)\rho V^2 S$
C_{K_p} = $\partial C_K/\partial(pb/2V)$; $K = x, y, z, l, m, n$
C_{K_q} = $\partial C_K/\partial(qc/2V)$; "
C_{K_r} = $\partial C_K/\partial(rb/2V)$; "
$C_{K_{\dot\alpha}}$ = $\partial C_K/\partial(\dot\alpha c/2V)$; "
C_{K_α} = $\partial C_K/\partial\alpha$; "

Derivatives with respect to β, δ_a, δ_r, and δ_t are defined similarly to those with respect to α

$C_{L_{\delta_a{}^2}}$ = $\partial C_L/\partial\delta_a{}^2$
$C_{m_{\delta_a{}^2}}$ = $\partial C_m/\partial\delta_a{}^2$
$\Delta C_{y_{FF}}$ = $\Delta\,\partial C_y/\partial(pb/2V)_F$ = side force due to rolling velocity—dihedral contribution.
C_{l_r}/α = $[\partial C_l/\partial(rb/2V)]/\alpha$ = variation of rolling moment coefficient due to yawing velocity with angle of attack—untwisted wing contribution
ΔC_{l_r} = $\Delta[\partial C_l/\partial(rb/2V)]$ = C_{l_r} due to wing twist
C_{n_p}/α = $[\partial C_n/\partial(pb/2V)]/\alpha$ = variation of yawing moment coefficient due to rolling velocity with angle of attack—wing contribution
ΔC_{n_p} = $\Delta[\partial C_n/\partial(pb/2V)]$ = C_{n_p} due to wing twist
C_{n_r}/α^2 = $[\partial C_{n_r}/\partial(rb/2V)]/\alpha^2$ = variation of yawing moment coefficient due to yawing velocity with angle of attack
ΔC_{n_r} = $\Delta[\partial C_{n_r}/\partial(rb/2V)]$ = C_{n_r} due to profile drag
$N(\delta_{aR}) - N(\delta_{aL})$ = $\partial C_n/\partial\delta_a$ = $f(\alpha)$ = yawing moment due to aileron as a function of angle of attack
l_V, l_H = distances from the c.g. to the center of pressures of the vertical tail and horizontal tail, respectively

Presented at the Stability and Control Problems During Large Maneuvers Session, Twenty-Fifth Annual Meeting, IAS, New York, January 28–31, 1957.

* Research Aeronautical Engineer, Flight Research Department.

** Associate Research Aeronautical Engineer, Flight Research Department.

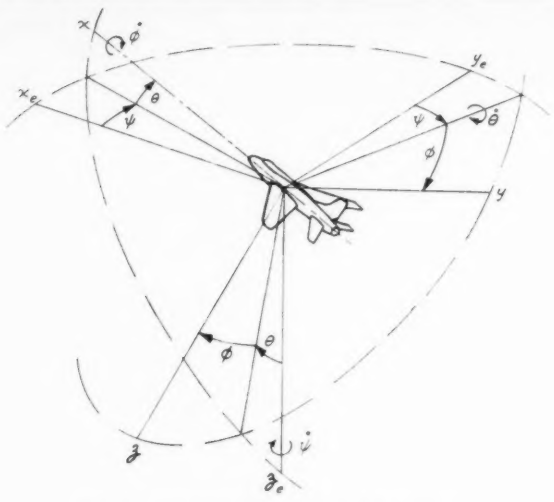

FIG. 1. Orientation of earth and body axes.

z_V = distance from x body axis to center of pressure of vertical tail

α_{A_1} = angle between the zero lift line and the x body axis in reference condition

α_{ref} = angle of attack for a given δ_e in a steady pull-up, index of α in a rolling pull-out

p_{ref} = roll rate measured at $\phi = 90°$, index of p in a rolling pull-out

p_{crit} = critical roll rate

$a, c, f, h, k, F, G, H, K, L, \bar{B}, \bar{C}, \bar{F}, \bar{G}, \bar{H}, J, \bar{K}, L, P, Q, R, \bar{S}, \bar{T}, \bar{V}, \bar{W}, \bar{X}$ = Mach Number and airplane geometric constants used in this paper

Dimensions

time, sec.
distance, ft
angle, rad. (unless otherwise noted)
force, lb.
moment, ft.-lb.
mass, slugs

Subscripts

e = earth, component or axis
w = wind, component or axis
s = stability, component or axis
e = elevator
a = aileron
r = rudder

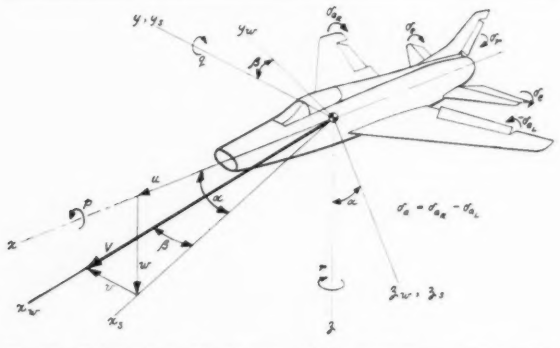

FIG. 2. Orientation of body and stability axes, linear and angular velocities, and control deflections.

FRL = fuselage reference line
1 = reference conditions
W = wing
$W + F$ = wing plus fuselage
H = horizontal tail
V = vertical tail
0 = incompressible—e. g., $C_{l_{\beta_{W+F_0}}}$
, s = derivatives in which all components refer to stability axes—e. g., $C_{n_{p,s}} = \partial C n_s / \partial (p_s b/2V)$

INTRODUCTION

DURING WORLD WAR II, investigations by the NACA established that certain vertical tail failures were caused by maneuvers combining a roll and pull-up, simultaneously. Large sideslip angles, resulting from the yawing moments, were responsible. Thus, a need was established for designing structurally for such a maneuver, which was named a rolling pull-out.

Simplified equations developed for these early tail failures were found to be inadequate for a later airplane. Theory did not agree with flight test, so more complete equations were developed. Further experiments and efforts by aircraft manufacturers to design for this phenomena led to considerable confusion. A number of different equations were developed and proposed for use in design.

In 1949, the Structures Branch of the Aircraft Laboratory, WADC, contracted with Cornell Aeronautical Laboratory to perform studies and flight tests as suggested by Joseph Kelly, Jr., of WADC. First, as complete a set of equations as possible (limited only by the available data and practical details of computation) was to be written for the rolling pull-out maneuver; a typical problem was to be programed using these equations; and simplifications were to be determined which caused no significant loss in accuracy. Next, work was to start on the measurement of tail loads and airplane motions in flight tests of the rolling pull-out maneuver. Finally, the equations previously developed were to be used to calculate motions and tail loads for the purpose of comparing theory and experiment. The actual control inputs measured in flight were to be used. Solutions for the initial theoretical study were obtained by the Institute for Numerical Analysis of the National Bureau of Standards.[14] Most of the computations for the final stage were performed on analog equipment at the Aeronautical Research Laboratory, WADC. This work, using an F-80A airplane as a test vehicle, was successfully completed after several years. The resulting five degree of freedom equations found considerable use.

However, by this time, many investigators were finding that certain trends in airplane design resulted in rolling pull-outs which were so extreme as to be intolerable both structurally and to the pilot. Therefore, in 1953, under the administration of Philip Parmley and Walter Boccius of the Structures Branch, Aircraft Laboratory, WADC, the Cornell Aeronautical Laboratory was placed under contract to study this maneuver as it applied to modern fighter aircraft. The effects of

changes in airplane configuration, flight conditions, and control motions were to be studied. Though the calculation of tail loads remained the primary objective, emphasis was placed on obtaining a fuller understanding of the dynamics, since once the motions are satisfactorily defined, the loads can be predicted with confidence.

A digest of the results of this series of investigations is presented in this paper.

Initial Theoretical Studies

Initial theoretical studies of the rolling pull-out maneuver proceeded with the thought that the equations of motion should represent large-disturbance maneuvers as completely as possible. This immediately implies that coupling between the lateral and longitudinal modes must be included, since, by definition, separation based on small-disturbance linearized theory is no longer valid.

This concept of "complete" coupled equations of motion requires important inclusions—namely: (1) Inclusion of an expression for the summation of forces along the x axis, or "forward speed change" equation, in the equation system. This has an additional note of complexity in that to be consistent, changes in Mach Number throughout the equations must be taken into account. (2) Inclusion of products of disturbances (such as wp, vr, and qr). (3) Inclusion of variations in the stability derivatives due to angle of attack (also Mach Number) and other aerodynamic coupling.

Because of the practical limitations, several restricting assumptions had to be made.

(1) The effects of nonstationary flow are omitted. Previous work had shown that this omission will not cause significant errors. (2) Additional degrees of freedom due to aeroelastic effects are neglected. The aircraft to which these equations were applied (F-80A) has sufficient structural stiffness so that structural vibration frequencies are far removed from those of airplane motion as a rigid body. The systems may be considered independent, and only quasi-static effects need be included if required. (3) Engine gyroscopic effects were felt to be small for the configuration under study and were not included.

The system of equations thus derived represents a set of six simultaneous nonlinear equations with variable coefficients, describing motion along and about all three axes of the aircraft.

An important step toward the practical application of the equations of motion to the prediction of motions and loads for a new aircraft design was that of simplification. It was obvious from the initial considerations of the problem that the derived equations would require considerable effort to solve, even if use was made of available machine techniques. Thus, a plan of simplification was devised with the purpose of arriving at a set of equations, more adaptable to solution, but without undue sacrifice of accuracy. This was considered a "broad" plan with the thought that the simplified system selected might warrant further study along these lines.

Since the primary unknown effect was that of speed change, the obvious procedure was to eliminate this equation from the set, and compare the solution with that of the complete system. This promised to be a rather far-reaching simplification, since Mach Number functions, which were included for essentially all the derivatives, would be eliminated. A second simplification (which also included the first) was to decouple the aerodynamic terms. This was thought to be indeed drastic, since even cursory examination of the rolling pull-out maneuver reveals a dependency of yawing moment on angle of attack. A third simplification, somewhat academic, was to (including the above two simplifications) uncouple the inertia terms. This latter step would resolve the motion to that of an aileron roll, and while not thought to be critical, would provide an interesting comparison.

The complete equations of motion, derived on the basis of the assumptions noted at the beginning of this section are found below. The inputs are elevator and aileron; a rudder locked condition is assumed.

$$m[\dot{u} - vr + wq] = -W\sin\theta + C_{L_{\alpha_0}}\left(\frac{AR+2}{AR\sqrt{1-M^2}+2}\right)\alpha qS\sin\alpha - \left\{a + k\left[C_{L_{\alpha_0}}\left(\frac{AR+2}{AR\sqrt{1-M^2}+2}\right)(\alpha_{A_1}+\alpha)\right] + f\beta^b\right\} qS\cos\alpha + C_{D_1}\frac{\rho}{2}U_1^2S + W\sin\alpha \quad (1a)$$

$$m[\dot{v} - wp + r(U_1+u)] = \left[C_{y_{\beta_{W+F}}} - C_{L_{\alpha_{V_0}}}\left(\frac{AR_V+2}{AR_V\sqrt{1-M^2}+2}\right)\frac{S_V}{S}\right]\beta qS - C_{L_{\alpha_{V_0}}}\left(\frac{AR_V+2}{AR_V\sqrt{1-M^2}}\right)\frac{pz_V}{U_1+u}qS_V + \left\{\left[\Delta C_{y_{p_\Gamma}}\frac{F}{G\sqrt{1-M^2}+H}\right] + \left[\frac{1}{AR}C_{L_{\alpha_0}}\left(\frac{AR+2}{AR\sqrt{1-M^2}+2}\right)(\alpha_{A_1}+\alpha)\right]\right\}\frac{pb}{2(U_1+u)}qS + W\cos\theta\sin\phi \quad (1b)$$

$$m[\dot{w} - (U_1+u)q + vp] = W\cos\theta\cos\phi - C_{L_{\alpha_0}}\left(\frac{AR+2}{AR\sqrt{1-M^2}}\right)\alpha qS\cos\alpha - \left\{a + k\left[C_{L_{\alpha_0}}\left(\frac{AR+2}{AR\sqrt{1-M^2}}\right)(\alpha_{A_1}+\alpha)\right]^c + f\beta^b\right\} qS\sin\alpha + C_{m_{\delta_e}}qS\frac{c}{l_H}\delta_e\cos\alpha - W\cos\alpha \quad (1c)$$

$$I_x\dot{p} - I_{xz}pq + (I_z - I_y)qr - I_{xz}\dot{r} = \left[C_{l_{p_{W_0}}}\left(\frac{F}{G\sqrt{1-M^2}+H}\right) + C_{l_{p_{H_0}}}\left(\frac{\mathcal{R}_H+2}{\mathcal{R}_H\sqrt{1-M^2}+2}\right)\frac{b_H{}^2S_H}{b^2S^2}\right]\times$$
$$\frac{pb^2}{2(U_1+u)}qS + C_{l_{\beta_{W+F_0}}}\left(\frac{F}{G\sqrt{1-M^2}+H}\right)\beta qSb - C_{L_{\alpha V_0}}\left(\frac{\mathcal{R}_V+2}{\mathcal{R}_V\sqrt{1-M^2}+2}\right)\beta qS_Vz_V +$$
$$\left[\frac{C_{l_r}}{\alpha}(\alpha_{A_1}+\alpha) + \Delta C_{l_{r_0}}\left(\frac{J}{K\sqrt{1-M^2}}\right)\right]\frac{rb^2}{2(U_1+u)}qS + C_{L_{\alpha V_0}}\left(\frac{\mathcal{R}_V+2}{\mathcal{R}_V\sqrt{1-M^2}+2}\right)\times$$
$$l_Vz_VS_Vq\frac{r}{U_1+u} + C_{l_{\delta_{a_0}}}\left(\frac{F}{G\sqrt{1-M^2}+H}\right)\delta_aqSb \quad (1d)$$

$$I_y\dot{q} + (I_x - I_z)pr + I_{xz}p^2 - I_{xz}r^2 = \left\{\bar{B}C_{L_{\alpha_0}}\left(\frac{\mathcal{R}+2}{\mathcal{R}\sqrt{1-M^2}+2}\right)\alpha + \bar{C}\left[C_{L_{\alpha_0}{}^2}\left(\frac{\mathcal{R}+2}{\mathcal{R}\sqrt{1-M^2}+2}\right)^2\times\right.\right.$$
$$\left.\left.(2\alpha_{A_1}\alpha + \alpha^2)\right]\right\}qSc - C_{L_{\alpha H_0}}\left(\frac{\mathcal{R}_H+2}{\mathcal{R}_H\sqrt{1-M^2}+2}\right)\frac{ql_t{}^2}{U_1+u}qS_H - C_{L_{\alpha H_0}}\left(\frac{\mathcal{R}_H+2}{\mathcal{R}_H\sqrt{1-M^2}+2}\right)\times$$
$$(\bar{F}+\bar{G}M+\bar{H}M^2)\left[\frac{(U_1+u)\dot{w}-w\dot{u}}{(U_1+u)^2}\right]\frac{l_t{}^2S_H}{U_1+u}q + C_{m_{\delta_e}}\delta_eqSc \quad (1e)$$

$$I_z\dot{r} + (I_y - I_x)pq - I_{xz}\dot{p} + I_{xz}rq = \left[C_{n_{\beta_{W+F}}} + C_{L_{\alpha V_0}}\left(\frac{\mathcal{R}_V+2}{\mathcal{R}_V\sqrt{1-M^2}+2}\right)\frac{S_Vl_V}{Sb}\right]\beta qSb +$$
$$\left[\frac{C_{n_p}}{\alpha}(\alpha_{A_1}+\alpha)\frac{\bar{P}}{(\bar{R}\sqrt{1-M^2}+\bar{S})(\bar{Q}\sqrt{1-M^2}+\bar{T})} + \Delta C_{n_p}\right]\frac{pb}{2(U_1+u)}qS +$$
$$\left[\frac{C_{n_r}}{\alpha^2}(\alpha_{A_1}+\alpha)^2 + \Delta C_{n_r} - 2C_{L_{\alpha V_0}}\left(\frac{\mathcal{R}_V+2}{\mathcal{R}_V\sqrt{1-M^2}+2}\right)\frac{l_V{}^2S_V}{b^2S}\right]\frac{rb^2}{2(U_1+u)}qS +$$
$$[N(\delta_{a_R}) - N(\delta_{a_L})]\frac{\bar{P}}{(\bar{R}\sqrt{1-M^2}+\bar{S})(\bar{Q}\sqrt{1-M^2}+\bar{T})}C_{L_{\alpha_0}}\left(\frac{\mathcal{R}+2}{\mathcal{R}\sqrt{1-M^2}+2}\right)(\alpha_{A_1}+\alpha)qSb \quad (1f)$$

In addition to these equations, others were needed to describe the motion, and further point to the complexity of the system. An equation used to express total normal acceleration in gravity units was

$$n_z = \left\{[\dot{w} - (U_1+u)q + vp]/g\right\} - \cos\theta\cos\phi \quad (2)$$

The following trigonometric functions were used for the angle of attack and sideslip:

$$\alpha = \tan^{-1}[w/(U_1+u)] \qquad \beta = \tan^{-1}[v/(U_1+u)]$$

The orientation angles, ϕ, θ, and ψ were expressed as

$$\phi = \int(p + q\sin\phi\tan\theta + r\cos\phi\tan\theta)dt \quad (3a)$$

$$\theta = \int(q\cos\phi - r\sin\phi)dt \quad (3b)$$

$$\psi = \int[(q\sin\phi + r\cos\phi)/\cos\theta]dt \quad (3c)$$

The tail load equations, which are based simply on the motions obtained from the above, were defined as

$$N_V = C_{L_{\alpha V_0}}\left(\frac{\mathcal{R}_V+2}{\mathcal{R}_V\sqrt{1-M^2}+2}\right)\times$$
$$\left[-\beta - \tan^{-1}\frac{pz_V}{U_1+u} + \tan^{-1}\frac{rl_V}{U_1+u}\right]qS_V \quad (4a)$$

$$N_H = -C_{L_{\alpha H_0}}\left(\frac{\mathcal{R}_H+2}{\mathcal{R}_H\sqrt{1-M^2}+2}\right)\times$$
$$\left\{\alpha\left(1-\frac{d\epsilon}{d\alpha}\right) + \frac{d\epsilon}{d\alpha}\left[\frac{(U_1+u)\dot{w}-w\dot{u}}{(U_1+u)^2}\right]\times\right.$$
$$\left.\frac{l_H}{U_1+u} + \frac{ql_H}{U_1+u} + \frac{d\alpha}{d\delta_e}\delta_e\right\}qS_H \quad (4b)$$

u as used in the equations in this section refers to incremental forward velocity, and the dynamic pressure $q = (\rho/2)[(U_1+u)^2 + v^2 + w^2]$.

No attempt will be made here to describe in detail the derivation of the various terms in the equations of motion; this may be found in reference 1. The acceleration terms (left-hand side) are shown in well known form; the aerodynamic terms (right-hand sides), though general in overall concept, are based in detail on the aerodynamic data available at the time for the F-80A airplane under the initial flight conditions of level flight of Mach Number 0.60 and 20,000 ft. altitude. It is important to note the aerodynamic nonlinear and coupling functions included. The drag component is partially a function of sideslip angle (the term $f\beta^b$); the pitching moment is represented as a nonlinear function of angle of attack; and the lateral derivatives C_{n_p}, C_{n_r}, and $C_{n_{\delta_a}}$ are functions of α. It is obvious that these particular variations pertain to the configuration under study, and that the nonlinearities must be considered separately for each configuration.

It is obvious from examination of these equations that one of the major contributions to their complexity is forward speed change, particularly as applied to Mach Number variation. Due to complexity, it was necessary to employ the slower but larger capacity digital computer rather than the faster analog type. Solutions for this initial study were made using the digital facilities of the National Bureau of Standards Institute for Numerical Analysis at Los Angeles.

Comparisons of the solution of the complete equations of motion with those employing the aforementioned simplifications are shown in Fig. 3. As analysis of the solution for the complete equations proceeded, it became obvious that on the basis of the resulting motions, additional "local" simplifications could be made. Thus, the first simplification (speed change neglected) could be extended to include the following:

$$\sin\theta = \tan\theta = \theta \qquad \cos\theta = 1$$

$$\beta = v/U_1, \quad \alpha = w/U_1 \qquad \cos\alpha = 1$$

z direction force due to drag $\times \sin\alpha = 0$—i.e.,

$$\left\{a + k\left[\frac{dC_L}{d\alpha}\,\frac{AR+2}{AR\sqrt{1-M^2}+2}\,(\alpha_{i_1}+\alpha)\right]^c + f\beta^n\right\}\times \sin\alpha = 0$$

$$q = (\rho/2)U_1^2$$

It must be reiterated that such simplifications are based on the initial conditions and resulting motions; each case must be considered separately.

There are two interesting conclusions which may be drawn from this initial study comparison. They are: (1) For the case where derivatives do not change rapidly with Mach Number, the forward speed change equation (and Mach Number functions) may be neglected. For flight conditions where the above is not so, the effect of speed change should be further investigated. (2) Uncoupling of the aerodynamic terms results in unconservative values of sideslip angle and vertical tail loads of such magnitude as to render this simplification invalid.

Flight Test Program

As part of the overall initial rolling pull-out study program, a flight test phase was instigated, the purpose of which was twofold: (1) to provide a wealth of actual rolling pull-out flight test data, which although, because of practical considerations, remained within the safe structural limits of the airplane, could be used as a basis for further research on vertical tail loads. Through extrapolation or more severe flight tests, the critical rolling pull-out maneuvers for vertical tail design for structural integrity might be determined. (2) to use such flight test data in an effort to validate the equations of motion. The obvious importance of this is that accurate predesign prediction would be possible. This plus the determination of the critical rolling pull-out maneuvers noted above would greatly aid in the development of vertical tail design criteria.

An F-80A airplane was instrumented to provide motion and load data under various flight conditions. These conditions may best be described with aid of Chart 1. The branches represent changes to the basic condition. (Condition 5 was unobtainable and is therefore omitted).

A number of variables were recorded on an oscillograph. They were:

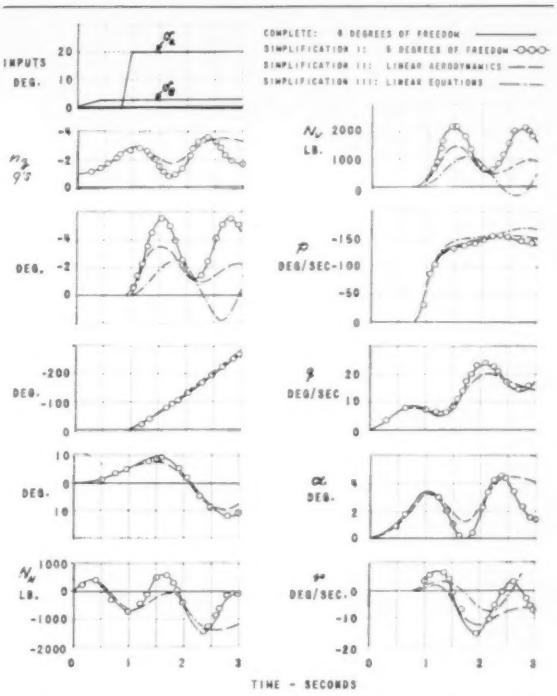

Fig. 3. Calculated rolling pull-out responses; effect of simplifications.

(1) Aileron position
(2) Elevator position
(3) Rudder position
(4) Normal acceleration
(5) Fin shear
(6) Fin bending moment
(7) Sideslip angle
(8) Rolling velocity
(9) Yawing velocity
(10) Right stabilizer shear
(11) Right stabilizer bending moment
(12) Left stabilizer shear
(13) Left stabilizer bending moment

In addition, the following items were recorded on the photo-observer by a 35-mm. movie camera:

(1) Airspeed (ship's system)
(2) Altitude
(3) Outside air temperature
(4) Fuel quantity remaining
(5) Airspeed (Prandtl tube)
(6) Run number
(7) Frame number
(8) Bank angle
(9) Time

It is not proposed to describe the instrumentation details here. For the interested reader, references 2 and 15 describe recording instrumentation design procedures and the methods used to measure tail loads.

The flight test program resulted in satisfactory data for 58 pertinent rolling pull-out maneuvers which are presented in reference 2. These maneuvers are: six of

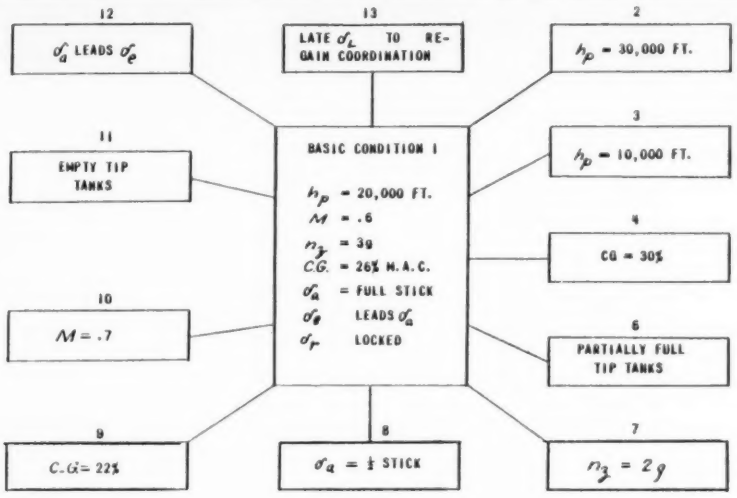

CHART 1.

the basic maneuver, four of each of the alternatives, and eight with unusual characteristics. The latter were obtained during the "build-up" portion of the program, a procedure necessary since solutions to the complete equations of motion were not available at the time the flight program was scheduled to begin. In order to assure pilot-airplane safety, it was necessary to predict the loads to be sustained on an approximate basis, then fly several "build-up" maneuvers (increasing g and roll rate) until the values specified in the flight program were attained.

At the conclusion of the flight test program, sufficient data were at hand to enter what was considered to be the most important phase, that of comparing flight test with theory.

Comparison of Theory and Experiment

Having derived a set of motion equations thought to describe the rolling pull-out maneuver adequately, and having performed a number of actual rolling pull-out flight tests, the next step in the program was to attempt to validate the equations of motion through comparison. In addition, the shortcomings of equations, at least in terms of those quantities which could be readily varied, would become evident and could be investigated.

The set of equations used was essentially that of the first simplification of the theoretical part of the program. Due to the fact that during flight, rudder motion was inadvertently applied (and recorded), such rudder input terms had to be added to the basic rudder-locked equations. These were $C_{y_{\delta_r}}\delta_r$ in the ΣY equation, $C_{l_{\delta_r}}\delta_r$ in the ΣL equation, and $C_{n_{\delta_r}}\delta_r$ in the ΣN equation. To further the exactness of the comparison, aerodynamic and mass parameters, substituted in the equations of motion, were, where appropriate, based on the exact conditions of flight test. This was done for the initial straight and level lift coefficient, C_L, absolute angle of attack, α_{A_1}, altitude, moments of inertia, and tail length. The derivative C_{m_α} was calculated for the flight c.g. position. For the case where tip tanks were installed during the maneuvers, the expressions which describe the derivatives C_{y_β}, C_{l_β}, C_{n_β}, C_{l_p}, C_{n_p}, C_{l_r}, $C_{l_{\delta_a}}$, and $C_{n_{\delta_a}}$ were recalculated to include the "body" contribution of the tanks.

Inputs to the equations of motion were those recorded for each flight test maneuver selected for comparison. The conditions selected included all those previously noted as test flown, with the exception of conditions 7 and 11, which appeared to be the least critical.

On the basis of preliminary comparisons, a further adjustment was made to the derivatives $C_{l_{\delta_a}}$ and $C_{n_{\delta_a}}$ to account for aeroelastic effects, data for which was unavailable at the time of the initial theoretical studies. This essentially amounted to matching the roll rates, and adjusting $C_{l_{\delta_a}}$, and matching the initial yaw rates, and adjusting $C_{n_{\delta_a}}$. All further comparisons and parameter variations were made from this reference.

As in the case of the initial theoretical calculations, preliminary comparison calculations were made using digital facilities. The majority of the calculations were made using the analog facilities at WADC, which were quite adequate for the simplified five degree of freedom equations.

The results of these calculations permitted comparisons, under the flight condition variations previously noted, of calculated and measured normal acceleration, sideslip angle, vertical and horizontal tail loads, roll rate, and yaw rate. Although the intent was not to vary any of the parameters, a limited additional series of calculations was carried out in the interest of improving agreement between flight test and theory. The parameters varied included C_{m_α}, $C_{m_{\delta_e}}$, C_{n_β}, $C_{n_{\delta_a}}$, I_{zz}, and I_{zz}.

This paper presents some of the more interesting results of these investigations. The entire comparison phase has been reported in reference 3.

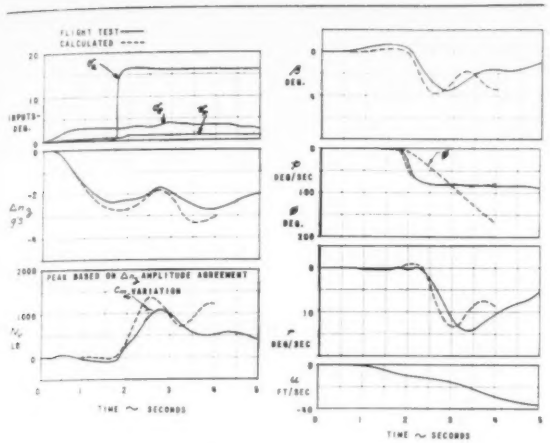

FIG. 4. Comparison of flight test and calculation; condition 1.

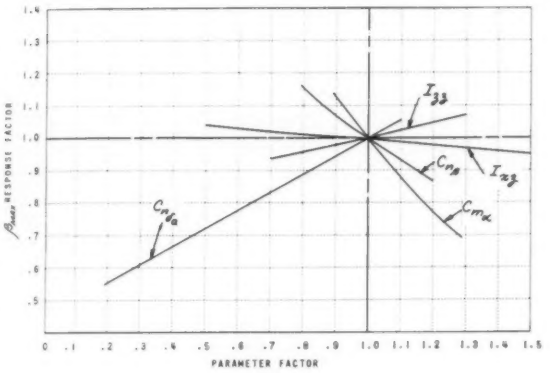

FIG. 5. Relative effect of parameters varied on maximum sideslip angle; condition 1.

Fig. 4 shows the comparison between calculation and flight condition 1. Except for the differences already noted, this is the basic condition used in the initial theoretical study and the basic condition of the flight program. It may be noted that the calculated incremental normal acceleration is somewhat higher than flight test. Both β and the vertical tail load are also somewhat higher. If normal acceleration agreement is obtained (in this case it was done by changing C_{m_α}), then β and N_V amplitudes show reasonable agreement. The second peak in the N_V response is much larger, suggesting that the rudder effectiveness might be too large. No attempt was made to validate this. The extent of parameter variation attempted is illustrated in Fig. 5, where the effects are presented in terms of the change in maximum sideslip angle, as a function of the change in parameter value. A strong coupling effect is evidenced by the large variation of maximum sideslip angle with C_{m_α}. The obvious effect of C_{n_β} is noticed as is the extreme importance of $C_{n_{\delta_a}}$. Thus, two of the derivatives, (C_{m_α} and $C_{n_{\delta_a}}$), which exhibit nonlinearities and which were comparatively difficult to estimate, show a very strong effect on the motion.

Fig. 6 shows the comparison for condition 12; similar to condition 1 except that instead of the elevator leading the aileron, the two control inputs occur somewhat simultaneously. Generally good agreement was obtained for this condition, although adjustment of Δn_z for agreement at the first peak would result in a slightly greater unconservative sideslip response than shown here. No parameter changes were investigated for this case.

Condition 13, again similar to condition 1 except for the control inputs, which in this case includes rudder application in an attempt to regain coordination, is compared to calculation in Fig. 7. Agreement again is reasonable except in the case of yawing velocity where, perhaps because of too large a $C_{n_{\delta_a}}$, the calculated r is much larger than flight. Reduction of $C_{n_{\delta_a}}$ would undoubtedly reduce the maximum sideslip angle and vertical tail loads, thus producing slightly unconservative values for these variables.

In all cases the flight test forward speed change is shown alone, since this was neglected in these calculations.

As was previously implied, no attempt was made in this study to investigate the effects of all important derivatives and mass parameters separately or in all

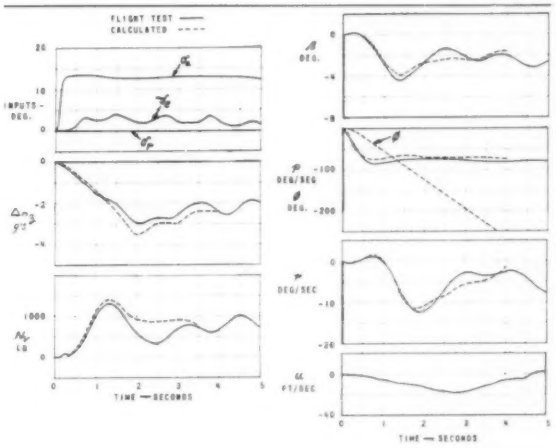

FIG. 6. Comparison of flight test and calculation; condition 12.

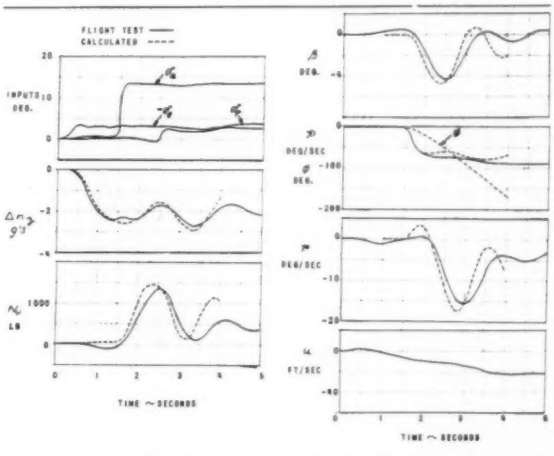

FIG. 7. Comparison of flight test and calculation; condition 13.

reasonable combinations which may have produced near perfect agreement with flight test. Such effort as was directed along these lines was done so on the basis of those variables which were thought to be least accurately estimated.

Important results were obtained from this comparison and limited parameter variation study. The discrepancies noted between flight test and calculation were similar to those encountered in small disturbance maneuver comparisons (basically attributed to inadequate aerodynamic data), thus lending credence to the five degree of freedom method of calculation proposed, but indicating that, because of the importance of aerodynamic coupling, it might be necessary to estimate aerodynamic data with greater accuracy and precision. The initial theoretical study pointed to the need of five degrees of freedom to describe large disturbance motion. This was further emphasized in the parameter study by the strong effect of longitudinal parameters on lateral motion.

The promising results of the overall initial investigation were to provide a firm background for an extended program designed to investigate the "less conventional" airframe, where the effects of more complex aerodynamic coupling and, in particular, the effects of more extreme inertia coupling could be studied.

A Simple Approximation

While work was proceeding on the comparison phase of the program, some thought was being given to the derivation of a relatively simple expression for maximum sideslip angle which would include the essential parameters, yet would dispense with the arduous computation associated with the five degree of freedom set of equations.

Basically, it was felt that several coupling terms could be included without undue complexity. Most important was the coupling term $(I_y - I_z)pq$, appearing in the yawing moment equation. This term includes three important rolling pull-out parameters, one of which, of particular interest, is the moment of inertia difference. Emphasis was placed on this difference, since the trend in modern fighter design indicated larger and larger values for it.

The approximation should be defined in terms of basic parameters which could be readily assumed for preliminary prediction of maximum sideslip angle. Load factor, roll rate, and basic flight condition appeared to be most promising.

The yawing moment equation was reduced to the following:

$$(I_y - I_z)pq = qSbC_{n_\beta}\beta + qSbC_{n_p}(\alpha)(pb/2U) + qSbC_{n_{\delta_a}}(\alpha)\delta_a$$

Letting the yawing moments due to p and δ_a (and α) be represented by $\Delta C_n(\alpha)$,

$$(I_y - I_z)pq/qSb = C_{n_\beta}\beta + \Delta C_n(\alpha)$$

q is approximated in the following manner. The normal force equation in terms of load factor may be approximated as

$$-q + \beta p = (g/U)\Delta n_z = -(g/U)(n - 1)$$

or

$$q = \beta p + (g/U)(n - 1)$$

Substituting in the yawing moment equation,

$$\frac{(I_y - I_z)p[\beta p + (g/U)(n - 1)]}{qSb} = C_{n_\beta}\beta + \Delta C_n(\alpha)$$

$$\frac{(I_y - I_z)\beta p^2 + (I_y - I_z)(g/U)(n - 1)p}{qSb} = C_{n_\beta}\beta + \Delta C_n(\alpha)$$

$$\frac{(I_y - I_z)\beta p^2}{qSb} - C_{n_\beta}\beta = \Delta C_n(\alpha) - \frac{(I_y - I_z)(g/U)(n - 1)p}{qSb}$$

$$\beta = \frac{\Delta C_n(\alpha) - [(I_y - I_z)(g/U)(n - 1)p/qSb]}{[(I_y - I_z)/qSb]p^2 - C_{n_\beta}}$$

If steady-state values for n and p are assumed, along with a dynamic overshoot factor of 2 (assumption of zero damping), the maximum sideslip angle becomes

$$\beta_{max} = 2\left[\frac{\Delta C_n(\alpha) - \dfrac{(I_y - I_z)(g/U)(n_{ss} - 1)p_{ss}}{qSb}}{[(I_y - I_z)/qSb]p_{ss}^2 - C_{n_\beta}}\right] \quad (5)$$

A word must be said about the $\Delta C_n(\alpha)$ term. As previously noted,

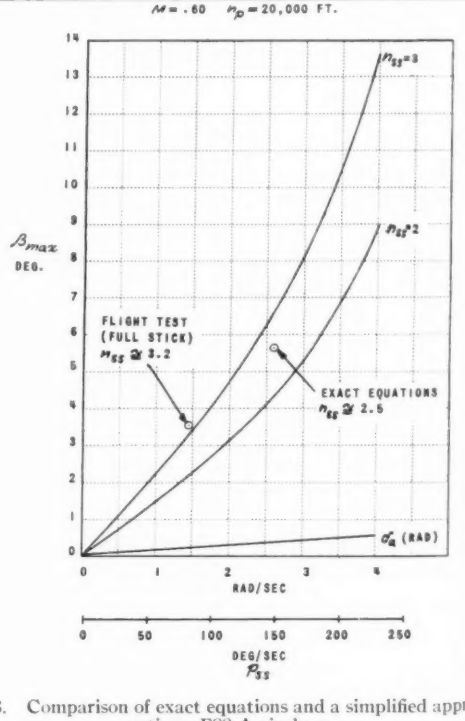

Fig. 8. Comparison of exact equations and a simplified approximation; F80-A airplane.

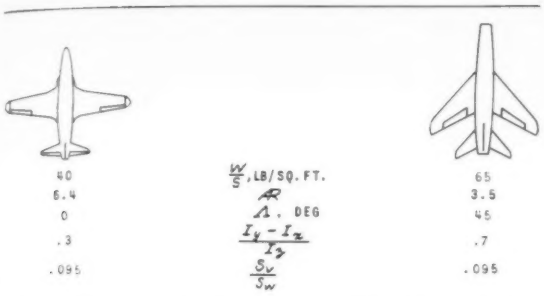

FIG. 9. Comparison of typical swept-wing fighter and F80-A.

$$\Delta C_n(\alpha) = C_{n_p}(\alpha)(pb/2U) + C_{n_{\delta_a}}(\alpha)\delta\alpha$$

The actual C_{n_p} and $C_{n_{\delta_a}}$ angle of attack functions must be determined for the individual airplane, and the angle of attack chosen must be commensurate with the steady state load factor chosen—i.e.,

$$\alpha = [(n_{ss} - 1)/C_{L_\alpha}](W/qS)$$

In addition, in the case of $C_{n_{\delta_a}}(\alpha)\delta_a$, a δ_a must be chosen commensurate with the roll rate, p. Such may be determined by calculation for the flight condition under consideration.

It may be noted from the expression for β_{max} that β goes to infinity when

$$[(I_y - I_x)/gSb]p_{ss}^2 = C_{n_\beta}$$

This may be caused by a combination of large $(I_y - I_x)$, p_{ss}, and low C_{n_β}—all characteristics of modern fighter airplanes. For a given airplane there exists a p_{ss} for which the above occurs. This has been termed the critical roll rate, and more will be noted about this condition later, on the basis of more recent work than that described above.

Very little work was done with this expression at the time of its derivation, except to note the effect of moment of inertia difference in comparison with those approximations which did not include this effect. It is apparent that the approximation is valid at least within respectable limits for what was then considered a conventional airplane. Fig. 8 shows a comparison of the approximation with the exact solution as described in a previous section, and with one of the flight conditions. Application to a swept-wing modern fighter with characteristics noted above indicates limitations which for practical purposes invalidates the approximation. However, in the case of other types of modern aircraft, such as a light or medium tactical bomber, possessing characteristics similar to the earlier fighter types, and required because of mission to perform large-disturbance maneuvers, the application of this approximation may be justifiable.

STUDY OF A HIGH-SPEED AIRPLANE

The modern fighter is a different airplane from the F-80A for which the five degree of freedom equations were developed. Present-day trends are toward low aspect ratio wings, high wing loadings, and mass concentrated in the fuselage. Accordingly, the dynamics of a typical swept-wing fighter were studied in general rolling maneuvers, emphasizing variations in wing plan form, vertical tail size, mass distribution, flight condition, aerodynamic derivatives, and control inputs. The remainder of this paper is concerned with the results of this study.[4]

The configuration chosen for study is compared in Fig. 9 with the F-80A and was based on a prototype version of a typical swept-wing fighter. Contemporary trends in geometry and mass characteristics are readily apparent. The aerodynamic derivatives were estimated for this configuration and include power effects and aeroelasticity. The results are presented in Fig. 10 for $M = 0.9$ and 20,000 ft. altitude. These derivatives are referred to stability axes. Only large nonlinearities are included, but no attempt is made to study the region of the stall. The variations of C_{l_β}, C_{n_p}, C_{y_p}, and C_{l_r}, with α are typical of airplanes with low aspect ratio swept wings. The forces and moments due to aileron deflection are peculiar to the particular lateral control system used. The equations of motion are written with respect to body axes as

$$mV(\dot\beta - \alpha p + r) = qSC_y + mg\cos\theta\sin\phi \quad (6a)$$

$$mV(\dot\alpha + \beta p - q) = qSC_z + mg\cos\theta\cos\phi \quad (6b)$$

$$I_x\dot p + (I_z - I_y)qr - I_{xz}(\dot r + pq) = qSbC_l \quad (6c)$$

$$I_y\dot q + (I_x - I_z)pr + I_{xz}(p^2 - r^2) = qScC_m \quad (6d)$$

$$I_z\dot r + (I_y - I_x)pq - I_{xz}(\dot p - qr) = qSbC_n \quad (6e)$$

These are Eqs. (1) with the following simplifications:

$$\alpha \cong w/u, \qquad \beta \cong v/V, \qquad u \cong V = \text{constant}$$

where u is the total component of velocity along the x axis. Airplane orientation in space (ψ, θ, and ϕ) is given by Eqs. (3). The incremental reading from level flight of a normal accelerometer placed at the center of gravity of the airplane is given by

$$-\Delta n_z = -(V/g)(\dot\alpha + \beta p - q) + \cos\theta\cos\phi - 1 \quad (7)$$

where the negative, $-\Delta n_z$, is used so that a positive "g" will correspond to a pull-up. In level flight $-\Delta n_z = 0$.

The equations may be conveniently written as

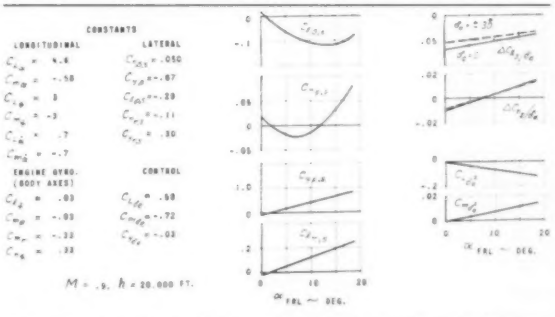

FIG. 10. Aerodynamic derivatives for the swept-wing fighter.

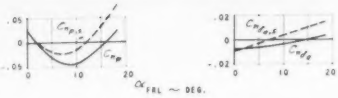

FIG. 11. Comparison of derivatives in stability and body-axis systems.

$$\dot{\beta} - \alpha p + r = y + (g/V)\cos\theta\sin\phi \quad (8a)$$

$$\dot{\alpha} + \beta p - q = z + (g/V)\cos\theta\cos\phi \quad (8b)$$

$$\dot{p} + [(I_z - I_y)/I_x]qr - (I_{xz}/I_x)(\dot{r} + pq) = l \quad (8c)$$

$$\dot{q} + [(I_x - I_z)/I_y]pr + (I_{xz}/I_y)(p^2 - r^2) = m \quad (8d)$$

$$\dot{r} + [(I_y - I_x)/I_z]pq - (I_{xz}/I_z)(\dot{p} - qr) = n \quad (8e)$$

where

$$y = Y/mV = (\rho SV/2m)C_y$$
$$z = Z/mV = (\rho SV/2m)C_z$$
$$l = L/I_x = (qSb/I_x)C_l$$
$$m = M/I_y = (qSc/I_y)C_m$$
$$n = N/I_z = (qSb/I_z)C_n$$

It is necessary to transform the aerodynamic forces and moments from stability axes, the system in which they are usually given, to body axes, the system in which the equations of motion are written. This subject, the transformation of data from one axis system to another, is a very important one and is discussed extensively in reference 4. The equations for transforming the derivatives are outlined in Appendix 1. In general, the derivatives in the stability axis system may be radically different from the corresponding derivatives in the body axis system. The derivatives which show the greatest difference are usually the yawing moment derivatives, and particularly C_{n_β}, C_{n_p}, and $C_{n_{\delta_a}}$ which are important ones. In order to illustrate this point the latter two derivatives are shown in Fig. 11 in both axis systems for the swept-wing airplane at $M = 0.9$ and 20,000 ft. altitude.

For the study airplane, the body axes are chosen so that they coincide with the stability axes for straight and level flight at the reference flight condition. After transforming the aerodynamic data to body axes, the aerodynamic forces and moments, including engine gyroscopic moments, may be expressed in nondimensional form as

$$y = y_p(\alpha)p + y_r r + y_\beta\beta + y_{\delta a}\delta_a \quad (9a)$$

$$z = z_q q + z_{\dot\alpha}\dot\alpha + z_{\delta a^2}(\alpha)\delta_a{}^2 + z_{\delta e}\delta_e \quad (9b)$$

$$l = l_p p + l_q q + l_r(\alpha)r + l_\beta(\alpha)\beta + l_{\delta a}(\alpha, \delta_a)\delta_a \quad (9c)$$

$$m = m_p p + m_q q + m_r r + m_{\dot\alpha}\dot\alpha + m_\alpha\alpha + m_{\delta a^2}(\alpha)\delta_a{}^2 + m_{\delta e}\delta_e \quad (9d)$$

$$n = n_p(\alpha)p + n_q q + n_r r + n_\beta\beta + n_{\delta a}(\alpha, \delta_a)\delta_a \quad (9e)$$

where the variable coefficients for the study airplane resulting from nonlinear aerodynamic derivatives are expressed in polynomials as

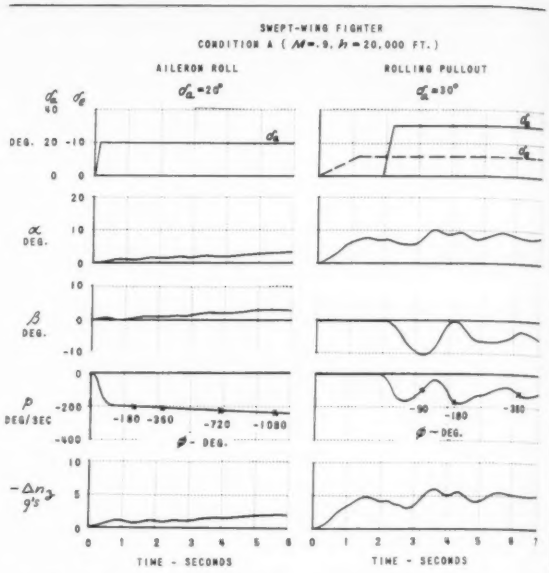

FIG. 12. Comparison of aileron roll and rolling pull-out from 5.11g pull-up.

$$y_p(\alpha) = y_p + y_{p\alpha}\alpha \quad (10a)$$

$$l_r(\alpha) = l_r + l_{r\alpha}\alpha \quad (10b)$$

$$l_\beta(\alpha) = l_\beta + l_{\beta\alpha}\alpha + l_{\beta\alpha^2}|\alpha|\alpha \quad (10c)$$

$$n_p(\alpha) = n_p + n_{p\alpha}\alpha + n_{p\alpha^2}|\alpha|\alpha \quad (10d)$$

$$z_{\delta_a{}^2}(\alpha) = z_{\delta_a{}^2} + z_{\delta_a{}^2\alpha}\alpha \quad (10e)$$

$$m_{\delta_a{}^2}(\alpha) = m_{\delta_a{}^2} + m_{\delta_a{}^2\alpha}\alpha \quad (10f)$$

$$l_{\delta_a}(\alpha) = (l_{\delta_a} + l_{\delta_a{}^2}|\delta_a|) + (l_{\delta_a\alpha} + l_{\delta_a{}^2\alpha}|\delta_a|)\alpha \quad (10g)$$

$$n_{\delta_a}(\alpha) = (n_{\delta_a} + n_{\delta_a{}^2}|\delta_a|) + (n_{\delta_a\alpha} + n_{\delta_a{}^2\alpha}|\delta_a|)\alpha \quad (10h)$$

Eqs. (8), (9), and (10) comprise the final five degree of freedom equations of motion for large disturbances from level flight, and the required kinematic relations for θ and ϕ are given by Eqs. (3). These are the equations used to compute F-80A solutions for comparison with flight test, except that the small angle approximations, $\sin\theta = \theta$ and $\cos\theta = 1$, were included and the nonlinear derivatives used for the F-80A were $l_r(\alpha)$, $m_\alpha(\alpha)$, $n_p(\alpha)$, $n_r(\alpha)$, and $n_{\delta a}(\alpha)$.

Three flight conditions were studies for the swept-wing fighter:

Condition A: M = 0.9, h = 20,000 ft.
Condition B: M = 0.7, sea level
Condition C: M = 0.7, h = 30,000 ft.

and the coefficients in the equations of motion are given in Appendix 2.

Analog solutions for condition A are presented in Fig. 12, comparing an aileron roll with a rolling pull-out initiated from a 5.11g pull-up (maximum unsymmetrical load factor). Aileron deflections are selected to give comparable maximum roll rates. The aileron roll solution is quite normal, but the rolling pull-out solution ex-

hibits extreme sideslip angles and noticeable coupling in the α and $-\Delta n_z$ records.

Solutions for condition B are presented in Fig. 13 comparing two rolling pull-outs initiated from a 5.11g pull-up. These solutions are even more extreme than those for condition A and show little resemblance to what one normally expects in a rolling maneuver, particularly for the 30° aileron deflection. The sideslip, β, oscillates about a steadily growing value and eventually reaches a very large steady state. Large amplitude longitudinal motions are excited, normal acceleration $-\Delta n_z$ varying between 0 and 8 g's, a severe maneuver by any standard. Comparing the two solutions in Fig. 13, we see that nonlinearity is the predominant characteristic.

Solutions for condition C are presented in Fig. 14 comparing two rolling pull-outs initiated from a 2g pull-up. The maximum load factor is limited by the angle of attack in this flight condition. The solution with 20° aileron deflection appears similar to the rolling pull-out solution shown in Fig. 12 for condition A, but the solution with 30° aileron deflection seems completely divorced from a rational maneuver. Just 2.5 sec. after the ailerons are deflected, the roll rate is −340°/sec., the angle of attack is −15°, normal acceleration ($-\Delta n_z$) is −3.5 g's, and the sideslip is 5°—having previously exceeded −10°. Comparing the two solutions, we find that for $\delta_a = 20°$ the average roll rate is about −60°/sec., whereas for $\delta_a = 30°$ the average roll rate is about −300°/sec.

The solutions presented in Figs. 12, 13, and 14 are typical of those obtained at the beginning of this investigation. The results were so different from anything previously encountered that their validity was questioned. Research airplanes were known to have experienced severe maneuvers at extreme altitudes, but the study airplane was a reasonable model with the external geometry of a current prototype fighter. However, investigation showed that the prototype had experienced severe uncontrollable motions in flight and that several other prototype airplanes were experiencing similar difficulties (see reference 9). A flight test record of a rolling maneuver was obtained for the prototype fighter. The appropriate inertial characteristics and flight condition were used but with the aerodynamic derivatives of this study to obtain the constants in the equations of motion. Satisfactory agreement between the flight record and the analog solution was obtained using a rough approximation for the control inputs recorded in flight. This shows that the unexpected nature of these computed responses is in fact reasonable. The question becomes, why do they occur?

Study of Large Amplitude Response

One method of obtaining an understanding of the solution of a set of differential equations is to examine the contributions of the individual terms. The rolling pull-out solution of Fig. 12 is substituted in Eqs. (8), rearranged with only the accelerations $\dot{\beta}$, $\dot{\alpha}$, $\dot{p}$, $\dot{q}$, and $\dot{r}$ on the left-hand side. The various terms in each equation, the inertial terms, the gravitational terms, and the lumped aerodynamic terms, are plotted in Fig. 15. The product of inertia terms are negligible in this solution because the body axes nearly coincide with the principal axes, so that $\eta \cong \alpha$ and $I_{xz} \cong 0$. The 57.3 factor is necessary because the results are presented in units of degrees. In order to complete the picture the components of the aerodynamic forces and moments, as given in Eqs. (9) and (10), are shown in Fig. 16.

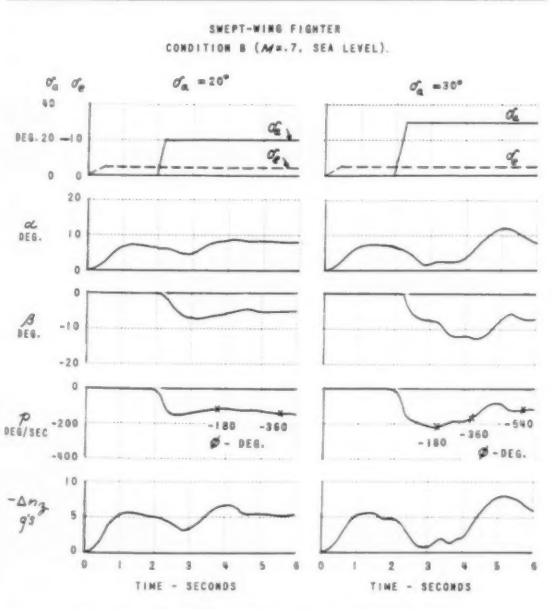

Fig. 13. Rolling pull-out from 5.11g pull-up.

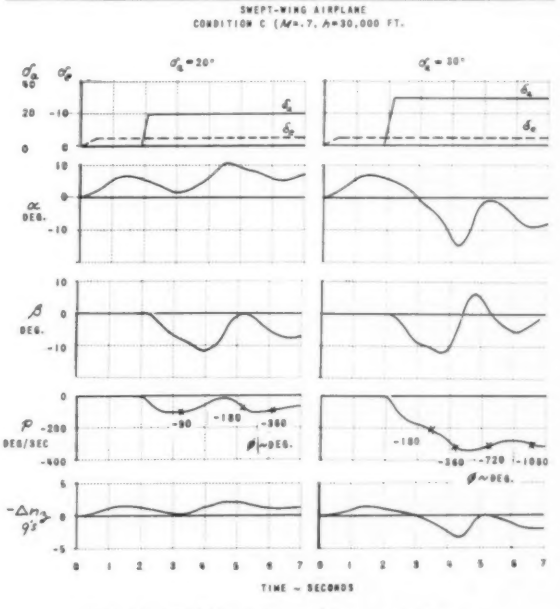

Fig. 14. Rolling pull-out from 2g pull-up.

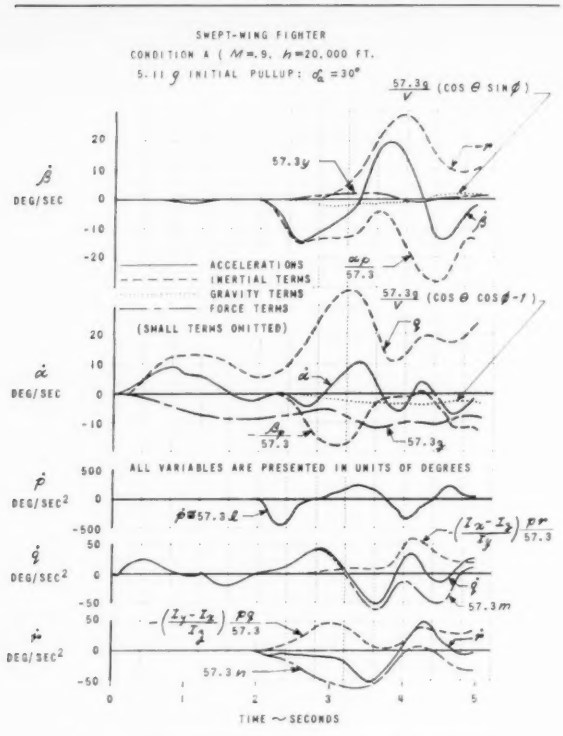

FIG. 15. Components in the equations of motion.

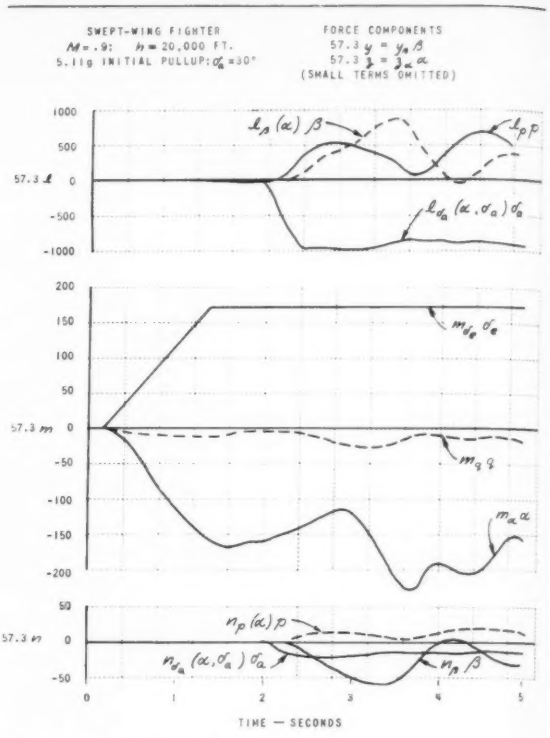

FIG. 16. Components of the aerodynamic forces and moments.

Terms not presented are of an order of magnitude smaller than the ones that are shown.

From the $\dot{\beta}$ equation we see that the force terms are small and that β is dominated by the αp and $-r$ terms. Similarly, $\dot{\alpha}$ is dominated by the $-\beta p$ and q terms. Since these four terms are essentially kinematic and just account for the rotation of the body axes, then the motion seems primarily one of rotation defined by the three rotational degrees of freedom. The roll rate is primarily a function of the aerodynamic rolling moments as seen from the $\dot{p}$ equation. However, the pitching and yawing velocities are heavily influenced by the $-[(I_x - I_z)/I_y]pr$ and $-[(I_y - I_x)/I_z]pq$ terms in the $\dot{q}$ and $\dot{r}$ equations, respectively. These two terms have been called the gyroscopic terms and are the real villains. Looking at the components of $\dot{r}$, we see that for $2.0 < t < 3.0$ sec. the $-[(I_y - I_x)/I_z]pq$ term almost exactly cancels the yawing moments, n. Examining the components of n, in Fig. 16, we see that n is largely $n_\beta\beta$ since $n_p(\alpha)p$ and $n_{\delta a}(\alpha, \delta_a)\delta_a$ about cancel. Thus, the gyroscopic term in the yawing moment equation tends to cancel the directional stability. Since the "net yawing moments" are nearly zero, the sideslip builds up to large values because of the αp term in the $\dot{\beta}$ equation. An important point is brought out. Since the body axes for this solution are principal axes, the α in the αp term represents the angle of attack of the x principal axis. Thus, the location of the principal axes with respect to the flight path has a direct bearing on the magnitude of the response in a rolling maneuver. If the principal axis coincides with the flight path ($\eta \cong 0$), this mode of generating sideslip does not exist. This is one reason why the sideslip is comparatively small in the aileron-roll solution in Fig. 12.

The results shown in Figs. 15 and 16 suggest that many terms in the equations of motion can be neglected without greatly affecting the solution. A simplified set of equations of motion is derived on the following bases: (1) all aerodynamic terms not shown in Fig. 16 are neglected, (2) the gravitational forces are neglected, and (3) the nonlinearity of rolling and yawing moments with aileron deflection is neglected. The equations are written with respect to principal axes as

$$\dot{\beta} - \alpha p + r = y_\beta \beta \tag{11a}$$

$$\dot{\alpha} + \beta p - q = z_\alpha \alpha \tag{11b}$$

$$\dot{p} + [(I_z - I_y)/I_x]qr = l_p p + l_\beta(\alpha)\beta + l_{\delta a}(\alpha)\delta_a \tag{11c}$$

$$\dot{q} + [(I_x + I_z)/I_y]pr = m_q q + m_\alpha \alpha + m_{\delta e}\delta_e \tag{11d}$$

$$\dot{r} + [(I_y - I_x)/I_z]pq = n_r r + n_\beta \beta + n_p(\alpha)p + n_{\delta a}(\alpha)\delta_a \tag{11e}$$

The damping in pitch and yaw are retained, even though their normal effect is small, since they are often the source of stability augmentation. This simplification of the equations is treated with considerable detail in reference 4, but these equations should give relatively good quantitative answers if the following conditions are met: (1) principal axes are used as the reference, otherwise product of inertia terms must be included; (2) the airspeed is high enough so that the wing angle of attack in level flight is small; and (3) $l_{\delta a}$ and $n_{\delta a}$ are

adjusted for the usual decrease in aileron effectiveness at large deflections. Obviously, if the magnitude of the motion exceeds the valid range for the aerodynamic representation, good results cannot be expected. Fig. 17 compares a solution computed using the full equations with one computed using the simplified equations. This is the rolling pull-out solution shown in Fig. 12 and the one used to prepare Figs. 15 and 16. These simplified equations will usually be more accurate than the numbers used in them. Not only are they comparatively easy to solve, requiring a minimum of numerical data and analog equipment, but they may be profitably studied using analytical techniques.

Analysis of the Effect of Roll Rate

Analysis of the equations of motion for steady rolling explains much of the behavior of airplanes in rolling maneuvers, and several references are available on the subject. This approach was first used, to the authors' knowledge, by White, Uddenberg, Murray, and Graham[5] who considered the stability, the frequency response, and the steady-state solution of the equations. A two degree of freedom approach (freedom in pitch and yaw) was developed by Phillips,[6] and Bergrun and Nickel[7] verified Phillips' results using a freely falling model (body-tail combination) with a roll-stabilization system. Phillips considered only the stability (linearized equations in pitch and yaw) for steady rolling about the flight path, but the analysis is quite complete. A comprehensive theory for the dynamics of rolling missiles was developed by Nicolaides[8] for bisymmetric configurations—i.e., $I_y = I_z$, $C_{z_\alpha} = C_{y_\beta}$, $-C_{m_\alpha} = (b/c)C_{n_\beta}$, etc. Nicolaides uses a complex variable notation—particularly applicable to bisymmetric aircraft—which presents the effects of rolling in a particularly clear manner, and his paper includes both steady rolling and roll dynamics. Since the effects of steady rolling are adequately covered in references 5–7, we will only include the important results as needed.

The first step is to put the equations of motion in a more meaningful form by eliminating some of the variables. If we solve Eqs. (11a) and (11b) for r and q, differentiate to obtain $\dot{r}$ and $\dot{q}$, then r and q can be eliminated from the pitch and yaw equations, (11d) and (11e), to yield

$$\ddot{\alpha} + (-z_\alpha - m_q)\dot{\alpha} + (-m_\alpha + z_\alpha m_q + Qp^2)\alpha + (1 - Q)p\beta + (Qy_\beta - m_q)p\beta + \dot{p}\beta = m_{\delta_e}\delta_e \quad (12a)$$

$$\ddot{\beta} + (-y_\beta - n_r)\dot{\beta} + (n_\beta + y_\beta n_r - Rp^2)\beta - (1 + R)p\dot{\alpha} + (R_{z_\alpha} + n_r)p\alpha - \dot{p}\alpha + n_p(\alpha)p = -n_{\delta_a}(\alpha)\delta_a \quad (12b)$$

where

$$Q = (I_x - I_z)/I_y \qquad R = (I_y - I_x)/I_z$$

If we constrain the motion to one of steady rolling about the x principal axis, with p_1 = steady roll rate, then the equations can be linearized for small disturbances in the remaining four degrees of freedom. If we assume that $n_p(\alpha)p$ and $n_{\delta a}(\alpha)\delta_a$ are the inputs to the yawing moment equation, then the pitch and yaw equations may be written as

$$\ddot{\alpha} + b_\alpha\dot{\alpha} + k_\alpha\alpha + (1 - Q)p_1\dot{\beta} + (Qy_\beta - m_q)p_1\beta = m_c \quad (13a)$$

$$\ddot{\beta} + b_\beta\dot{\beta} + k_\beta\beta - (1 - R)p_1\dot{\alpha} + (Rz_\alpha + n_r)p_1\alpha = -n_c \quad (13b)$$

where the following notation has been introduced:

$$\begin{aligned} b_\alpha &= -z_\alpha - m_q \\ k_\alpha &= m_\alpha + z_\alpha m_q + Qp_1^2 \\ b_\beta &= -y_\beta - n_r \\ k_\beta &= n_\beta + y_\beta n_r - Rp_1^2 \\ m_c &= m_{\delta_e}\delta_e \\ n_c &= n_p(\alpha)p + n_{\delta a}(\alpha)\delta_a \end{aligned}$$

We notice that, for $p_1 = 0$, b_α and k_α are the usual longitudinal short-period total damping and stiffness (usually includes m_α which is neglected in these equations), and b_β and k_β are the usual approximations for the Dutch-roll damping and stiffness.

Phillips, in reference 6, describes the stability of the system represented by Eqs. (13a) and (13b) in terms of the characteristic equation. Principal results are as follows. (1) For $p_1 = 0$ there is one frequency of oscillation in pitch and one frequency of oscillation in yaw. (2) For steady rolling, there are two frequencies of oscillation in pitch and the same two frequencies of oscillation in yaw. (3) One of these frequencies is higher than either of the nonrolling frequencies, and the

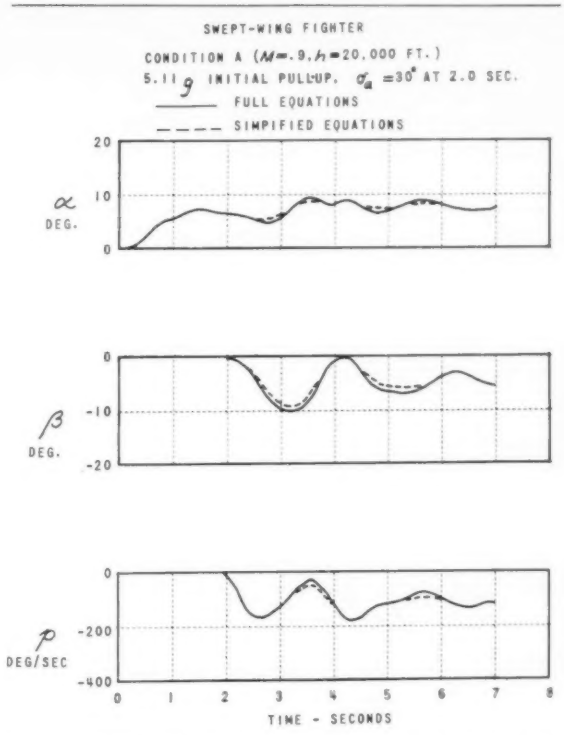

Fig. 17. Comparison of rolling pull-out computed using simplified and full equations of motion.

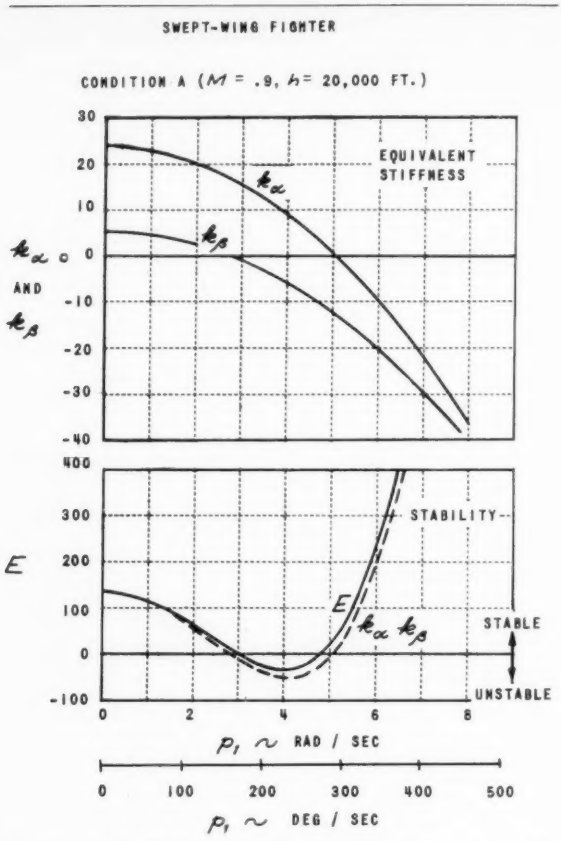

FIG. 18. Stability parameters in equations for steady rolling

other is lower than either of the nonrolling frequencies. (4) As the roll rate approaches zero, the high frequency approaches the higher nonrolling frequency, and the low frequency approaches the lower nonrolling frequency.

If the linear differential Eqs. (13a) and (13b) are solved for their characteristic equation, it is found to be of fourth degree. The constant term in this quartic, which equals the product of the undamped natural frequencies squared—i.e., the product of the roots—is designated by E and may be written as

$$E = k_\alpha k_\beta - (Qy_\beta - m_q)(Rz_\alpha + n_r)p_1^2 \qquad (14)$$

and the system is unstable if $E < 0$. The values of k_α, k_β, and E are plotted versus roll rate in Fig. 18 for the swept-wing airplane in condition A. For $3 < p_1 < 4.8$ rad./sec. (i.e., $170 < p_1 < 275$ deg./sec.) the system is unstable. The roll rates for which $E = 0$ are called the critical roll rates (p_{crit}).

The following simple criteria is proposed by Phillips. Since

$$E \cong k_\alpha k_\beta$$
$$k_\alpha \cong -m_\alpha + Qp_1^2$$
$$k_\beta \cong n_\beta - Rp_1^2$$

then for stability

$$-m_\alpha > -Qp_1^2 \qquad (15a)$$

and

$$n_\beta > Rp_1^2 \qquad (15b)$$

If these are reduced to more common notation, then the following criteria are obtained:

$$p < \sqrt{(1/2)\rho V^2 ScC_{m_\alpha}/(I_x - I_z)} \cong p_{crit} \qquad (16a)$$

$$p < \sqrt{(1/2)\rho V^2 SbC_{n_\beta}/(I_y - I_x)} \cong p_{crit} \qquad (16b)$$

Usually Eq. (16b) defines the lower critical roll rate. These can be considered as minimum criteria for C_{m_α} and C_{n_β} or they can be considered as criteria for the allowable roll rate. Zimmerman, in reference 9, discusses the trends in fighter development that have led to this problem. The trends may be summarized as higher wing-loadings, higher altitudes, and weight concentrated more in the fuselage.

The analysis of stability in pitch and yaw for steady rolling results in attractively simple expressions and criteria, but gives no knowledge of the amplitudes of motion in practical rolling maneuvers. More meaningful results can be obtained by considering the steady-state solution of the equations of motion—i.e., $\dot{\alpha} = \dot{\beta} = \dot{q} = \dot{r} = \dot{p} = 0$.

The steady-state solutions for α and β can be obtained from Eq. (13) as

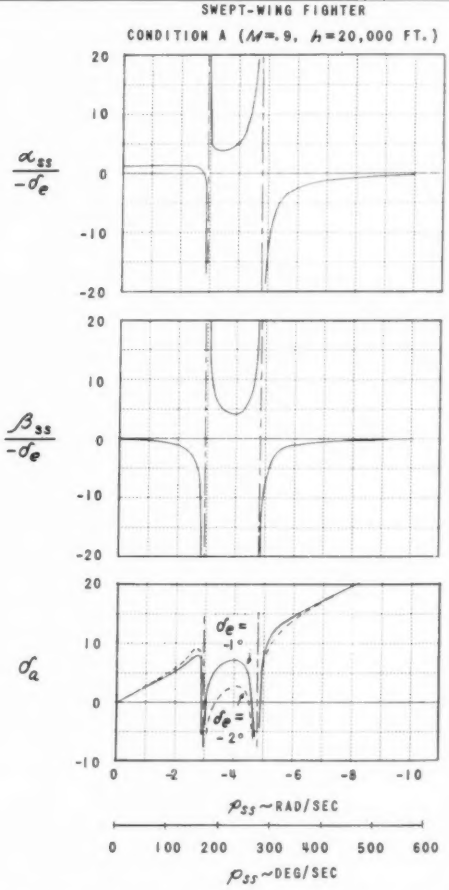

FIG. 19. Steady-state solution of equations of motion.

$$\alpha_{ss} = \frac{k_\beta m_c + (Qy_\beta - m_q)p_1 n_c}{k_\alpha k_\beta - (Qy_\beta - m_q)(Rz_\alpha + n_r)p_1^2} \quad (17a)$$

$$\beta_{ss} = \frac{-k_\alpha n_c - (Rz_\alpha + n_r)p_1 m_c}{k_\alpha k_\beta - (Qy_\beta - m_q)(Rz_\alpha + n_r)p_1^2} \quad (17b)$$

The yawing and pitching velocities are obtained from Eqs. (11a) and (11b) as

$$r_{ss} = \alpha_{ss}p_1 + y_\beta\beta_{ss} \quad (17c)$$

$$q_{ss} = \beta_{ss}p_1 - z_\alpha\alpha_{ss} \quad (17d)$$

The rolling equation may be written, with the qr term neglected since it is usually small, as

$$0 = l_p p_1 + l_\beta(\alpha)\beta + l_c \quad (17e)$$

We note that the denominator in Eqs. (17a) and (17b) is the constant term in the characteristic equation, E, of the steady-rolling analysis.

A complete solution of these steady-state equations, including the nonlinear derivatives $n_p(\alpha)$ and $n_{\delta a}(\alpha)$ in n_c and $l_\beta(\alpha)$, requires a lengthy iterative procedure. For illustrative purposes the steady state is computed using

$$m_c = m_{\delta e}\delta_e, \qquad n_c = 0, \qquad l_c = l_{\delta a}\delta_a$$

This allows the steady state to be presented as $\alpha_{ss}/-\delta_e$ and $\beta_{ss}/-\delta_e$, though δ_a is still not proportional to δ_e for any given value of p_1. The results are presented in Fig. 19 for the swept-wing airplane in condition A.

The instability predicted by the linearized equations for steady rolling ($E < 0$ as shown in Fig. 18) appears in the full equations as a new equilibrium state, characterized by large α_{ss} and β_{ss}. Discontinuities are found at two roll rates corresponding to $E = 0$, and are the critical roll rates. The steady-state solution is indeterminate at the critical roll rates and the dynamic solution tends to "jump" from one branch to the next.

A number of important aspects of the dynamic response are explained by the steady-state solution. In general, the origin of the large amplitude motions encountered at high roll rates is seen to be primarily the nonlinear inertial terms in the pitch and yaw equations. We see from Fig. 18 that if $k_\alpha = 0$ and $k_\beta = 0$ at the same roll rate, then the amplitude of the steady state is minimized, though it still may be large. This corresponds to the condition that

$$(-cC_{m_\alpha})/(I_z - I_x) \cong bC_{n_\beta}/(I_y - I_x)$$

or, approximating further, that the natural frequencies in pitch and yaw are equal. In addition, Fig. 18 shows that increasing the overall damping through any of the derivatives m_q, n_r, z_α, or y_β will decrease the steady-state response, since the increment between E and $k_\alpha k_\beta$ is thus increased [see Eq. (17)].

The aspects dealt with so far concern factors in the denominator of Eqs. (17a) and (17b). The numerators of these two equations are comprised of two types of terms: (1) the pitching moment due to longitudinal control, and (2) the yawing moments due to roll and due to ailerons (also the rudder control, which is neglected in this study). The longitudinal control in effect defines the angle of attack of the x principal axis for the nonrolling airplane, and the adverse yaw derivatives are known to be very sensitive to the location of the reference axes (principal axes in these equations). Thus the angle of attack of the principal axes and the adverse yaw derivatives with respect to these axes are determining factors in the response.

The steady-state relationship between roll rate and aileron deflection as shown in Fig. 19 demonstrates one of the most significant aspects of the problem—namely, that the roll rate is not uniquely defined by the aileron deflection. In fact, four possible autorotational roll rates exist—i.e., conditions of steady rolling with no aileron deflection. From Eq. (17e) it is apparent that $l_\beta(\alpha)$ is responsible for this behavior. No extensive study has been made of these autorotational conditions, but it has been noticed that once the lower critical roll rate is exceeded, there is a marked tendency for the roll rate to jump to the higher critical roll rate. This indicates that the lower autorotational roll rates are unstable whereas at least one of the higher roll rates may be stable. The important point is that aileron control power does not limit the roll rate and that a dynamic solution including both inertial and aerodynamic nonlinearities is required to estimate the roll rates in a rolling maneuver.

Stability in steady-rolling flight and the steady-state solution of the simplified equations [Eq. (11)] are seen to be concepts useful in understanding the nature of the equations of motion and their solution. Though their application to quantitative calculation of dynamic responses is limited, these two concepts are good tools for studying the qualitative effects of various parameters. However, the steady-rolling equations and the steady-state solution can yield quantitative answers for some problems.

Referring back to Fig. 8, we see that Eq. (5) predicted β_{max} in a rolling maneuver for the F-80A airplane with creditable accuracy. β_{max}, as given by Eq. (5), is just twice β_{ss} as given by Eq. (17b) with $m_q = n_r = Q = 0$. The simple expression for β_{max} can be expected to give good results if (1) the two critical roll rates are well separated—i.e., if the natural frequency in pitch is much higher than the natural frequency in yaw—and (2) if the roll rates are well below critical. These conditions will be met by most airplanes having straight wings with high aspect ratios.

The equations of motion written for small disturbances from steady rolling may also be profitably used in the design of automatic stabilization and flight control systems. Since presumably the stabilization system will restrict the motion to small amplitudes, then the linearized equations should be valid. The root-locus technique can be used to plot the loci of the zeroes and poles with roll rate as a parameter. The stabilization system must then provide satisfactory response throughout the range of applicable roll rates. Roll dynamics may be included by allowing small per-

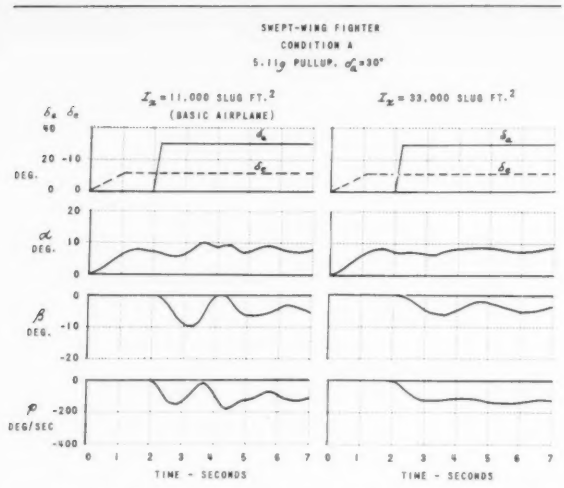

FIG. 20. Effect of increasing I_x on rolling pull-out response.

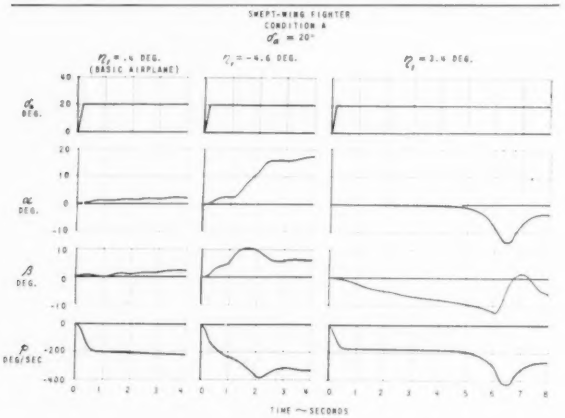

FIG. 21. Effect of varying the location of the principal axes on roll response.

turbations in the roll rate. This linear approach does not provide means for computing actual responses in a given maneuver. Only the full equations of motion can provide such responses.

ANALOG SOLUTIONS

Means for understanding and interpreting the dynamic response in rolling maneuvers have been developed in the previous section. In this section we will examine the effects of various parameters on the computed responses for the swept-wing airplane in flight condition A. The full equations of motion [Eqs. (8)] have been used to compute these responses.

The source of the large-amplitude motions in rolling maneuvers has been traced to the nonlinear inertial terms (inertial coupling) in the pitch and yaw equations:

$$[(I_x - I_z)/I_y]pr \quad \text{in the pitch equation}$$
$$[(I_y - I_z)/I_z]pq \quad \text{in the yaw equation}$$

The effect of increasing I_x by a factor of three is shown in Fig. 20. Coupling of pitch and yaw is greatly reduced and the response is similar to what would be expected from linear equations.

The location of the principal axes has been stressed as important. The steady-state solution indicates that η (angle of attack of the x principal axis) acts like an input in a roll and dominates the magnitude of the response. Aileron rolls for three locations of the principal axes are compared in Fig. 21. These variations, $+3°$ and $-5°$ from the basic airplane, are not large, and their effect on the response is nothing short of startling. In all three cases the roll rate is near the critically roll rates, but for the basic airplane there is no mechanism for exciting large amplitude motions.

The rolling responses for a series of initial pull-ups are summarized in Fig. 22 by giving the extreme values (after the first maximum) of α, β, and p obtained in each solution. The reference values of α and p—i.e., α_{ref} and p_{ref}—are essentially the angle of attack and roll rate that would be obtained from the uncoupled lateral and longitudinal equations. The largest excursions in α and β are seen to correspond with roll rates near critical, large β occurring for p_{ref} near the low p_{crit} (4 g's), and large α occurring for p_{ref} near the high p_{crit} (0 g's) and where the roll rate oscillates about the high critical roll rate (3 g's). These results correlate with the steady-state results shown in Fig. 19. The extreme roll rates obtained for 3g reflect the autorotational tendency.

Variations in wing and tail geometry have been studied and the most significant parameter was found to be the vertical tail size. Results for this variation are

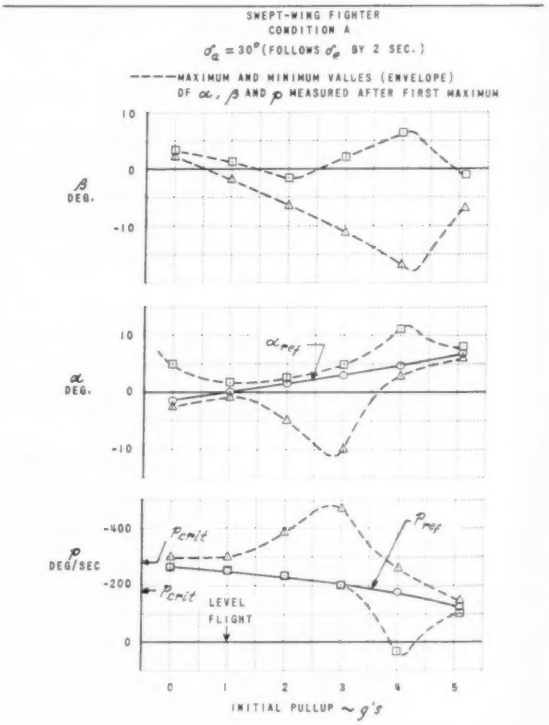

FIG. 22. Effect of initial pull-up on rolling pull-out response.

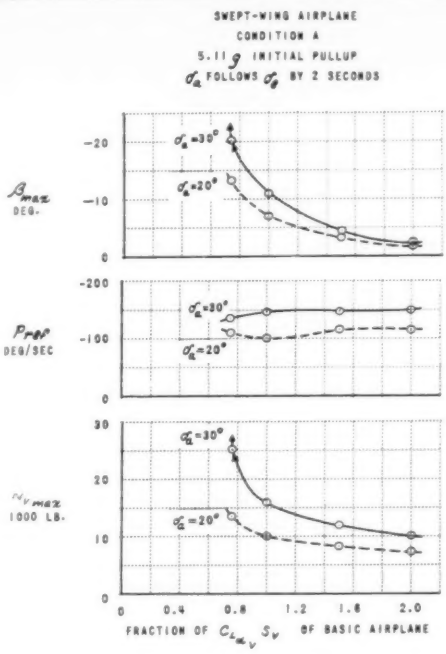

FIG. 23. Effect of vertical tail size on rolling pull-out response.

summarized in Fig. 23. The principal result of increasing the vertical tail size is to increase the critical roll rate through C_{n_β} [see Eq. (16b)].

Arbitrary variations in the aerodynamic derivatives have been made and results showed that the following derivatives are particularly important: C_{n_β}, C_{l_β}, C_{m_α}, C_{l_p}, C_{n_p}, $C_{l_{\delta_a}}$, $C_{n_{\delta_a}}$, and $C_{m_{\delta_e}}$. In addition, C_{y_β} and C_{L_α} determine the lateral and normal accelerations on the airplane though they have only a secondary effect on the overall motion. The effect of varying C_{n_β} and C_{l_β} are shown in Fig. 24, where the extreme values of α, β, and p for a 5.11g rolling pull-out are given. The effect of varying C_{n_p} is shown in Fig. 25 by comparing the response of the normal airplane to that with a positive C_{n_p}. In addition, the effect of varying C_{m_α}, C_{n_β}, and $C_{n_{\delta_a}}$ for the F-80A airplane may be seen in Figs. 4 and 5.

The influence of the inertia-coupling terms may be shown particularly well if the yawing moment due to roll is favorable and large. In Figs. 26 three solutions are compared for the swept-wing airplane but with a positive C_{n_p} as in Fig. 25. In the first solution, the inertia-coupling terms

$$[(I_x - I_z)/I_y]pr \qquad [(I_y - I_z)/I_z]pq$$

are set to zero and the response is what one might expect from a linear airplane. In the second solution the inertia coupling term in the yawing moment equation (pq term) is introduced. This term is seen to be responsible for the large excursions and the solution appears divergent as predicted by Phillips' stability analysis. In the third solution both inertia-coupling terms are included. The term in the pitching moment equation (pr term) is seen to stabilize or limit the divergence to a new steady state. This demonstrates the essence of the problem, for small disturbances from steady rolling the system appears to be unstable in the range of critical roll rates, but the complete equations show that the divergences or large excursions are actually caused by a change in the steady state.

So far we have studied parameters in the equations and no emphasis has been placed on particular control motions or maneuvers other than roll rate and initial

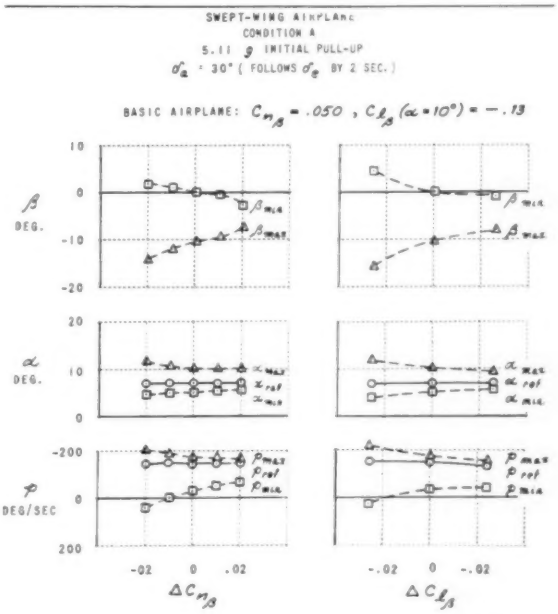

FIG. 24. Effect of varying $C_{n\beta}$ and $C_{l\beta}$ on rolling pull-out response.

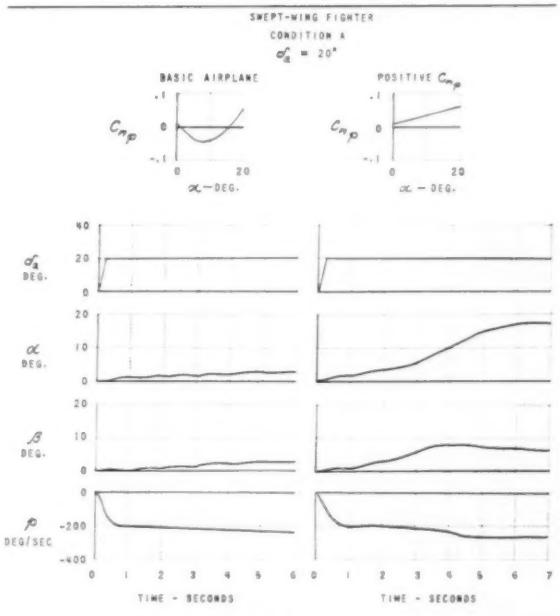

FIG. 25. Effect of varying C_{n_p} on the rolling response.

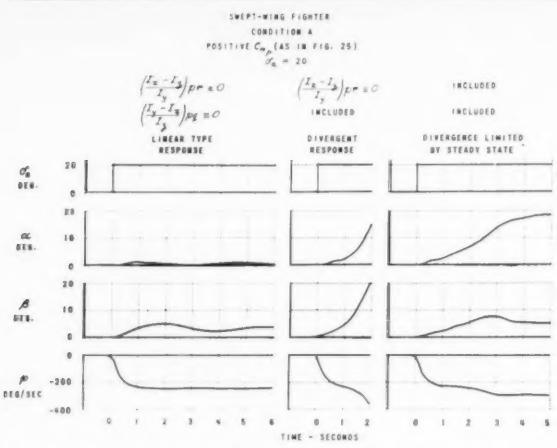

FIG. 26. Effect of inertia-coupling terms in pitch and yaw equations.

normal acceleration. Control motions are also critical quantities. In Fig. 27 three relative time lags between the elevator and aileron inputs are shown. The elevator reversal at high roll rates—i.e., change in sign of α/δ_e—that was noted in the steady-state solution is clearly demonstrated by these responses. Elevator deflections applied during the roll are generally found to be critical. This also applies to aileron deflections since in some maneuvers the largest sideslip angles have been encountered after the ailerons have been neutralized to stop the roll. Though control motions are important, the airplane's orientation in space is of secondary significance. In reference 4 two solutions are compared, one for a roll initiated from a pull-up and one initiated from a steady turn, and the two solutions are identical except for spacial orientation—i.e., ψ, θ, and ϕ. Of course, this result might be expected since the simplified equations [Eqs. (11)], which neglect gravity, agree well with the complete equations.

Basic Nature of Motion

The basic nature of motions in a rolling maneuver is to some extent described by the steady-rolling and steady-state analyses developed earlier. However, a clear understanding of the nonlinear phenomena and the relationship between the aerodynamic and inertial forces may be gained by examining the force-free motions of a rigid body—e.g., motions in a vacuum.

For symmetrical bodies ($I_y = I_z$), the force-free equations can be solved using elementary functions.

$$I_y\dot{q} = (I_y - I_x)pr$$

$$I_y\dot{r} = -(I_y - I_x)pq$$

$$I_x\dot{p} = 0$$

The variables may be separated by differentiation and substitution to yield

$$\ddot{q} = -\{[(I_y - I_x)/I_y]p\}^2 q$$

$$\ddot{r} = -\{[(I_y - I_x)/I_y]p\}^2 r$$

These equations describe simple harmonic motion

$$q = A\cos\omega t, \qquad r = A\sin\omega t$$

where

$\omega = [(I_y - I_x)/I_y]p$
p = constant
A = constant

The magnitude of the total angular velocity is a constant but the position of the angular velocity vector rotates (precesses) in the body with frequency ω. Thus steady rotation can occur only about a principal axis ($A = 0$), and rolling about a nonprincipal axis will introduce precession, causing excursions in α and β. An important point is made—the force-free motion is neutrally stable. The body is no more prone to rotate about a principal axis than it is to rotate with precession.

For unsymmetrical bodies ($I_x \neq I_z$), the equations may be solved in terms of elliptic functions, but a geometrical construction in three dimensions, known as Poinsot's construction, can be used to show the character of the motion. For the details of this Poinsot motion one may refer to reference 10 where the equations are discussed and a pictorial description of Poinsot's model is shown. The principal result is the same as for the symmetrical body, steady rotation can exist only about a principal axis. For any other condition the body will rotate in a predictable but nonuniform fashion, causing excursions in α and β. If I_y is nearly equal to I_z, as in many recent airplanes, then the motion will be nearly periodic and very similar to the symmetrical case.

The essence of the motion in rolling maneuvers can be described by considering two extremes (force-free and inertialess).

(1) For a rolling airplane with aerodynamic forces but zero moments of inertia:

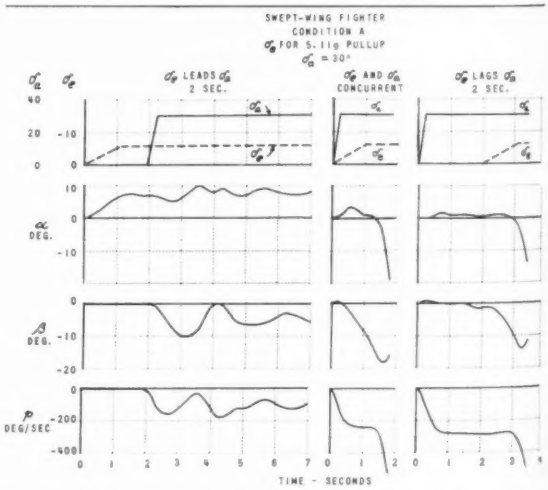

FIG. 27. Effect of varying the time lag between the elevator and the ailerons.

$$\alpha \cong (C_{m_{\delta e}}/C_{m_\alpha})\delta_e \tag{18a}$$

$$\beta \cong [C_{n_{\delta_a}}\delta_a + (b/2V)C_{n_p}p]/C_{n_\beta} \tag{18b}$$

(2) For a rolling airplane with inertia but with zero forces:

$$\dot{\alpha} = -\beta p + q \tag{19a}$$

$$\dot{\beta} = \alpha p - r \tag{19b}$$

and α and β can be constant only if p is about a principal axis and q and r are zero.

Thus, for a rolling airplane, if the principal axis coincides with the flight path, as described by Eq. (18) steady rolling is possible without otherwise disturbing the airplane. However, for any other condition Eqs. (18) and (19) represent a conflict, and the airplane will experience lateral and longitudinal disturbances. The magnitude of these disturbances will depend primarily on the roll rate and the static stabilities.

Two very simple models may be used to demonstrate the inertia-coupling phenomena. The first is a rod, pin-connected to a shaft or axis of rotation and restrained to the shaft by a spring. The rod represents the airplane, the spring represents static stability, and the shaft represents the component of rotation along the flight path. By rotating the shaft at various speeds the existence of a critical roll rate and large-amplitude steady states can be shown. The equation of motion for this model is very simple and demonstrates stability and steady state as a function of roll rate.

The second model may be made by hanging a small toy airplane (preferably metal and with short wings) by its tail with a rubber band. The rubber band and gravity supply static stability in pitch and yaw. If the model is wound up on the rubber band and released, it will demonstrate the inertia-coupling phenomena by revealing the different modes of motion associated with different roll rates.

Time and space do not allow a complete presentation here of this type of approach which utilizes elemental equations. However, recent studies at Cornell Laboratory suggest that further effort along these lines may prove very valuable.

Conclusion

In this paper we have presented a five degree of freedom approach to the dynamics of large-disturbance maneuvers with particular emphasis on the nonlinearities associated with high rates of roll. We have tried to show what factors are important; (1) by comparing calculated responses, (2) by simplified equations and techniques, and (3) by study of simple models such as the force-free body.

The problem is important and complex. It is one that the designer is faced with now and will be faced with in the future. For detailed calculations the complete equations of motion must be used and practical solution requires large digital or analog computers.

Present results are based on five degrees of freedom. However, even the five degree of freedom approach is open to question. It is obvious that maneuvers performed at slightly greater than sonic speeds will result in deceleration into or through the transonic regime. The aerodynamic nonlinearities so introduced may have very large effects in rolling maneuvers and for such cases six degrees of freedom may be required. Other large disturbance motions are prevalent in aircraft which may be just as important as rolling—namely, large pitching velocities and large forward accelerations. Studies have been made which show these too have destabilizing effects similar to those of rolling.[11,12] Thus, there is much work still to be done in the study of the dynamics of large-disturbance motions from the theoretical standpoint.

There are a host of related problems that need solution. Aerodynamic data for use in large-disturbance calculations is meager, particularly in terms of nonlinearity with sideslip and rolling velocity. Schemes for automatically controlling the airplane in nonlinear maneuvers are needed, as are methods for design and synthesis of such systems. Design criteria are needed, not only in terms of the airplane control and structural limitations, but also in terms of acceptable rate and acceleration limits on the pilot. Even in the missile and ballistics field, where rolling has been a recognized problem for several years, there are many unanswered questions.

However, the complexity of this problem in no way obviates the necessity for an elemental approach or a need for understanding its mechanics. Simple methods of approach are required not only for preliminary design studies but also for directing analog or digital calculations used in detailed design and analysis. Without such a guide the study of so complex a nonlinear system will become a hopeless hit or miss process.

Various simplified approaches have been presented in this paper which show the effects of rolling velocity. These represent only a first attack of the problem. The overall domain of large-disturbance motions remains still primarily uncharted and the real need is for a clear understanding of these problems and simple methods of treating them which retain only essentials.

APPENDIX 1

Equations for Transforming From Stability to Body Axes

(1) *Components*

$$X = X_s \cos\alpha - Z_s \sin\alpha$$
$$Y = Y_s$$
$$Z = X_s \sin\alpha + Z_s \cos\alpha$$

The moments (L_s, M_s, and N_s), the moment coefficients (C_{l_s}, C_{m_s}, C_{n_s}), the angular velocities (p_s, q_s, r_s), etc., all transform in similar manner.

(2) *Selected Derivatives*

$$
\begin{aligned}
C_{yp} &= C_{yp,s}\cos\alpha - C_{yr,s}\sin\alpha \\
C_{yr} &= C_{yp,s}\sin\alpha + C_{yr,s}\cos\alpha \\
C_{lp} &= C_{lp,s}\cos^2\alpha - (C_{lr,s} + C_{np,s}) \times \\
&\qquad \sin\alpha\cos\alpha + C_{nr,s}\sin^2\alpha \\
C_{lr} &= C_{lr,s}\cos^2\alpha + (C_{lp,s} - C_{nr,s}) \times \\
&\qquad \sin\alpha\cos\alpha - C_{np,s}\sin^2\alpha \\
C_{mq} &= C_{mq,s} \\
C_{nq} &= C_{np,s}\cos^2\alpha + (C_{lp,s} - C_{nr,s}) \times \\
&\qquad \sin\alpha\cos\alpha - C_{lr,s}\sin^2\alpha \\
C_{nr} &= C_{nr,s}\cos^2\alpha + (C_{lr,s} + C_{np,s}) \times \\
&\qquad \sin\alpha\cos\alpha + C_{lp,s}\sin^2\alpha
\end{aligned}
$$

The transformation of derivatives where both quantities are affected by the transformation requires a double operation.

REFERENCES

[1] Rhoads, D. W., and O'Hara, J. C., *Rolling Pullout Study—Part I, Development of Large Disturbance Theory for Calculating Airplane Motions and Tail Loads in a Rolling Pullout Maneuver*, AFTR-6701 Part I, Cornell Aeronautical Laboratory Report TB-541-F-1, April, 1954.

[2] Rhoads, D. W., *Rolling Pullout Study—Part II, Flight Test Measurement of Vertical and Horizontal Tail Loads During a Rudder Locked Rolling Pullout Maneuver*, AFTR-6701 Part II, Cor-

(Continued on page 532)

APPENDIX 2

SUMMARY OF CONSTANTS IN EQUATIONS OF MOTION FOR THE SWEPT-WING FIGHTER

FLIGHT CONDITION	A	B	C
$(I_z - I_y)/I_x$	.727	.727	.695
$(I_x - I_z)/I_y$	-.949	-.949	-.946
$(I_y - I_x)/I_z$	.716	.716	.716
I_{xz}/I_x	-.037	-.042	-.314
I_{xz}/I_y	-.007	-.007	-.060
I_{xz}/I_z	-.006	-.006	-.053
y_p	.0002	.0003	.0007
$y_{p\alpha}$	.0139	.027	.011
y_r	.0017	.0033	.0013
y_β	-.196	-.280	-.098
y_{δ_a}	.0071	.0119	.0048
z_q	-.0060	-.0089	-.0040
$z_{\dot\alpha}$	-.0012	-.0018	-.0009
z_α	-1.329	-1.746	-.618
$z_{\delta_a{}^2}$	.0028	.0059	.0071
$z_{\delta_a{}^2\alpha}$	.110	.223	.088
z_{δ_e}	-.168	-.224	-.092
n_p	.002	.013	-.024
$n_{p\alpha}$	-1.578	-1.583	-.459
$n_{p\alpha^2}$	6.062	3.160	1.165
n_q	.223	.222	.211
n_r	-.235	-.377	-.136
n_β	5.67	8.88	3.16
n_{δ_a}	-.921	-1.282	-.215
$n_{\delta_a\alpha}$	1.132	2.459	1.075
$n_{\delta_a{}^2}$	.148	.207	.041
$n_{\delta_a{}^2\alpha}$	1.445	.346	.091

FLIGHT CONDITION	A	B	C
ℓ_p	-3.933	-5.786	-2.101
ℓ_q	.107	.108	.170
ℓ_r	.126	.221	.341
$\ell_{r\alpha}$	8.39	13.16	4.78
ℓ_β	-9.99	-20.91	-15.19
$\ell_{\beta\alpha}$	-684.4	-543.8	-146.4
$\ell_{\beta\alpha^2}$	1,358	1,456	198
ℓ_{δ_a}	-45.83	-60.27	-19.60
$\ell_{\delta_a\alpha}$	63.5	64.6	22.3
$\ell_{\delta_a{}^2}$	15.85	12.27	4.01
$\ell_{\delta_a{}^2\alpha}$	-30.53	-11.45	-3.97
m_p	-.020	-.020	-.032
m_q	-.814	-1.168	-.452
m_r	-.254	-.252	-.240
$m_{\dot\alpha}$	-.173	-.251	-.103
m_α	-23.18	-10.70	-5.86
$m_{\delta_a{}^2}$	.043	.136	1.46
$m_{\delta_a{}^2\alpha}$	1.666	5.109	1.797
m_{δ_e}	-28.37	-31.64	-11.55
τ	1.714	1.089	3.268
I_x/qSb	.00145	.00110	.00378
I_y/qSC	.02520	.01914	.06455
I_z/qSb	.00884	.00671	.02256
q	551	725.7	215.1
$b/2V$	.0196	.0234	.0263
$c/2V$	.00605	.00723	.00811
g/V	.0345	.0412	.0462

Optimum Nose Shapes for Missiles in the Superaerodynamic Region

W. J. CARTER*
University of Texas

SUMMARY

The mechanics of the kinetic theory of gases is employed to describe the drag force on the nose of a missile moving in the superaerodynamic region of the atmosphere. Three separate cases are considered—ideal specular reflection, specular-type reflection from a slightly rough surface, and surface absorption followed by random emission of the striking molecules. The calculus of variations is employed to obtain the differential equation of the nose shape which minimizes the drag force for each of the three cases. The resulting differential equations are then solved by a numerical procedure. The drag coefficients for the optimum nose shapes are likewise determined and these are compared with the drag coefficients given by other nose shapes. It is further shown that the drag coefficients arising when specular-type reflections occur are significantly dependent on the nose shape. When surface absorption followed by random emission occurs, the drag coefficient is not strongly dependent on either the missile nose shape or the fineness ratio of the nose.

(1) INTRODUCTION

AT VERY HIGH ALTITUDES, the mean free path of the air molecules will be of the same order of magnitude as the dimension of a missile moving through that region. When the mean free path is large, the drag force on the nose of a projectile may be computed, assuming that there is little mutual interference between the air molecules as they strike the nose and then rebound.

In the classic formulation of the kinetic theory of gases, the molecules are imagined as being smooth, perfectly elastic spheres which will rebound from a smooth surface at the same angle at which they strike. This type of behavior is called specular reflection. The concept is obviously an overidealization of the matter in general. If all rebounds were of specular type, no viscous type forces could be generated at a surface. Even though the classic picture is an oversimplification, it does account very well for many things. Experiments have shown that an appreciable percentage of specular-type reflections can occur when a stream of gas molecules strike a smooth surface, especially when the impacts are at an acute angle.

For specular reflection, it is assumed that the duration of impact is very short and that there is no opportunity for the striking molecules to achieve thermal equilibrium with the vibrating molecules on the surface of the solid. Under these conditions the magnitude of the rebound velocity is the same as that of the striking velocity. In such a case, the drag force may be ascribed to the momentum change of the rebounding molecules.

A slightly more realistic picture may be obtained by combining the concept of the smooth elastic sphere for the molecule with that of a surface having appreciable roughness. Fig. 1 shows such an idealized rough surface. The molecules rebounding from this surface are considered to be individually of specular type and scattering occurs as a result of the surface irregularity. Likewise, it may be seen that more molecules will strike the forward surfaces of the irregularities than will strike the rear surfaces. This action causes the average angle of reflection to be somewhat greater than that which would occur with specular reflection from the mean surface. Some experimental evidence indicates that this sort of behavior occurs.

Many of the gas molecules which strike a surface will be absorbed on the surface for a brief time interval and will then be emitted. The dwell time allows the gas molecule, on the average, to achieve thermal equilibrium with the surface. The average emission velocity corresponding to the kinetic temperature, will have a random direction. Loeb[1] gives a thorough discussion of this and other types of gas-surface phenomena.

(2) OPTIMUM NOSE SHAPE FOR A MISSILE ASSUMING SPECULAR MOLECULAR REFLECTION FROM A SMOOTH SURFACE

The curve of Fig. 2, when rotated about the x-axis, will form the nose of a missile. If the air molecules which strike the nose undergo specular reflection, the drag force on the missile may be deduced in a simple way by considering the momentum change which occurs as the molecules rebound from the nose.

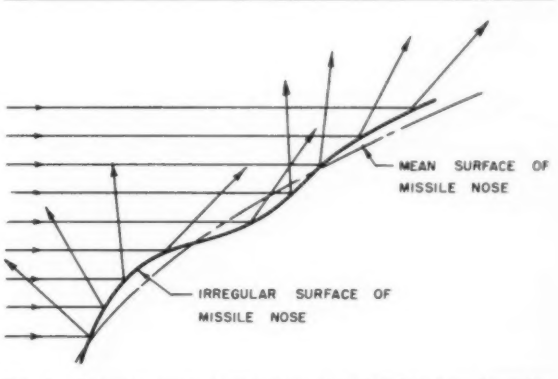

FIG. 1. Specular type of reflection of molecules from irregular surface.

Received December 28, 1955. Revised and received April 19, 1957.

* Associate Professor of Mechanical Engineering.

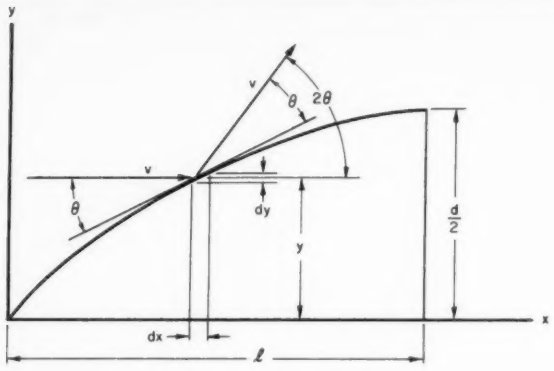

FIG. 2. Nose shape of missile.

The Eulerian point of view is taken here—the missile is assumed to be at rest and the air molecules are considered to be streaming past the missile nose in a direction parallel to the axis of the nose. The magnitude of the streaming velocity is v. The air molecules also have thermal velocities corresponding to their mean kinetic temperature. It is usually assumed that the thermal velocities are random as to direction and have a Maxwellian distribution of magnitude.

One of the significant parameters of free molecule flow is the "free molecule Mach Number," M_∞, which has the definition

$$M_\infty = v/c$$

where c is the most probable thermal velocity of the molecules. Ashley[2] has shown that the thermal velocities may be disregarded in determining the force exerted by the striking molecules, provided that $v \gg c$. For missile flight at very great altitudes this is the likely case. In the analysis which follows, it is assumed that M_∞ is large enough so that only the streaming velocity need be considered.

Referring to Fig. 2, it may be seen that the mass flux against the differential area $2\pi y dy$ is

$$dm = 2\pi\rho v\, y dy = 2\pi\rho v\, yy' dx$$

where ρ is the mass density of the air and $y' = dy/dx$. For specular reflection the rebound angle θ is the same as the angle of incidence. The total direction change relative to the axis of the nose is 2θ.

The differential drag force due to the momentum change of the mass flux on the differential area is

$$dD = 2\pi\rho v^2(1 - \cos 2\theta)yy' dx$$

from which the drag force may be obtained by integration,

$$D = 2\pi\rho v^2 \int_0^l (1 - \cos 2\theta)yy' dx \qquad (1)$$

It follows that

$$1 - \cos 2\theta = 2\sin^2\theta = 2y'^2/(1 + y'^2)$$

thus, Eq. (1) may be written

$$D = 4\pi\rho v^2 \int_0^l [yy'^3/(1 + y'^2)]dx \qquad (2)$$

For the shape of the nose to be such that the drag force is minimum it is necessary that the integrand of Eq. (2) satisfy the Euler-Lagrange differential equation

$$(\partial F/\partial y) - (d/dx)(\partial F/\partial y') = 0 \qquad (3)$$

where $F = yy'^3/(1 + y'^2)$. A further requirement is that y and y' be continuous and bounded in the interval of integration. It may be shown that

$$\partial F/\partial y = y'^3/(1 + y'^2)$$

$$\partial F/\partial y' = [3yy'^2/(1 + y'^2)] - [2yy'^4/(1 + y'^2)^2]$$

$$(d/dx)(\partial F/\partial y') = [6yy'y''/(1 + y'^2)] + [3y'^3/(1 + y'^2)] - [14yy'^3y''/(1 + y'^2)^2] - [2y'^5/(1 + y'^2)^2] + [8yy'^5y''/(1 + y'^2)^3]$$

Substitution in Eq. (3) and simplification yields the differential equation of the minimizing curve

$$y'' = -(y'^2/y)[(y'^2 + 1)/(3 - y'^2)] \qquad (4)$$

There is little hope of finding an analytic solution to Eq. (4) in terms of known functions, but a numerical solution may be readily determined. It may be seen that the differential equation has a singularity at $y' = \sqrt{3}$. For $y' < \sqrt{3}$, the nose curve is concave down, as indicated in Fig. 3. For $y' > \sqrt{3}$ the curve of y is concave up. It may be shown that y does not approach zero for any finite x. This means that the missile nose prefers to have a hole through the center. This is of small practical concern since the point of curvature change occurs very near the nose centerline for nose

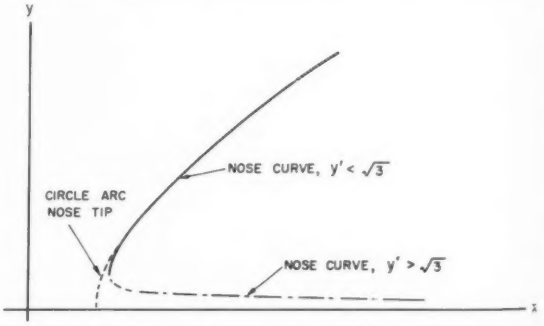

FIG. 3. Nose curve for minimum drag with specular reflection.

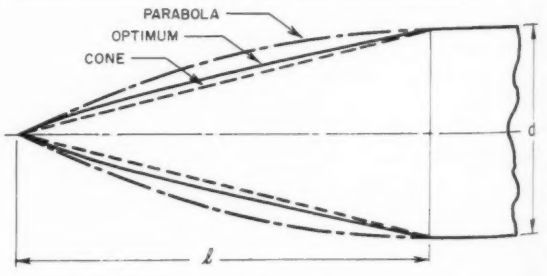

FIG. 4. Comparison of nose shapes for $l/d = 2$.

shapes having a reasonable fineness ratio. The tip of the missile nose from say $y' = 1$ to the x-axis may be formed by some suitable curve. In this case a circle arc is taken to form the nose tip.

The procedure for obtaining the numerical solution of Eq. (4) may be outlined as follows by (a) choosing any convenient y_1 and y_1' as starting values (in this case, $y_1 = 10$ and $y_1' = 1.000$); (b) computing y_1'' from Eq. (4); (c) choosing some appropriate interval Δx and computing

$$y_2 = y_1 + y_1'\Delta x + y''(\Delta x^2/2)$$
$$y_2' = y_1' + y_1''\Delta x$$

and (d) repeating the process of (b) and (c) until the curve has been adequately mapped.

Table 1 gives a few of the values of y, y', and l/d for the minimizing curve. A graphic comparison of the curve with a cone and a parabola having its vertex at the junction of nose and body is shown in Fig. 4.

It is of interest to compare the drag coefficients at various values of l/d for the three nose shapes shown in Fig. 4. The drag coefficient will be defined by the relation

$$C_D = 2D/A\rho v^2 \tag{5}$$

Eq. (2) gives D in terms of the nose shape. When this is substituted in Eq. (5) the result is

$$C_D = (32/d^2)\int_0^l [yy'^3/(1 + y'^2)]dx \tag{6}$$

Eq. (6) has also been solved by a numerical procedure in the case of the optimum curve and by analytic methods for the cone and parabolic shape. These results are shown in Fig. 5. It may be seen that the optimum nose shape gives a somewhat lower drag coefficient for all values of l/d.

(3) Optimum Nose Shape for a Missile Assuming Specular Reflection of the Molecules from a Slightly Rough Surface

The Introduction has discussed the manner in which a molecule would rebound from a nonideal surface. It is further suggested that the smoothest of realizable surfaces have irregularities that are of the same order of magnitude as a molecular dimension. Most of the air molecules rebounding from the rough surface would undergo a change of direction greater than that considered in Section (2).

Some idea may be obtained of the effect of surface roughness on the optimum nose shape by assuming that the molecules rebound from the surface as shown

Table 1

x	y	y'	l/d	x	y	y'	l/d
4.14	10.00	1.000	0.207	500	152.7	0.203	1.64
5	10.52	0.949	0.238	1,000	243.7	0.165	2.05
13	16.60	0.645	0.392	3,000	517.7	0.119	2.90
30	34.98	0.415	0.715	6,000	838.5	0.097	3.58
100	53.50	0.335	0.935	15,000	1585	0.072	4.73
220	88.70	0.262	1.24	35,000	2836	0.056	6.17

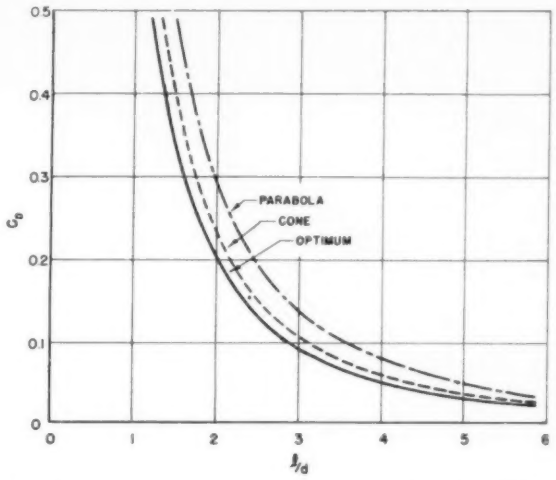

Fig. 5. Drag coefficients for spectral reflection of molecules.

in Fig. 6. The average rebound angle is assumed to be larger than the angle of incidence by the amount ϵ.

In the same manner as for the case of the perfectly smooth surface, the differential drag force is found to be

$$dD = 2\pi\rho v^2[1 - \cos(2\theta + \epsilon)]yy'dx$$

from which

$$D = 2\pi\rho v^2\int_0^l [1 - \cos(2\theta + \epsilon)]yy'dx \tag{7}$$

It may be also shown that

$$\cos(2\theta + \epsilon) = \cos 2\theta\cos\epsilon - \sin 2\theta\sin\epsilon$$

To expedite the subsequent work, ϵ will be assumed to be of such smallness that $\cos\epsilon \doteq 1$ and $\sin\epsilon \doteq \epsilon$—thus,

$$\cos(2\theta + \epsilon) = \cos 2\theta - \epsilon\sin 2\theta$$

$$D = 2\pi\rho v^2\int_0^l (1 - \cos 2\theta + \epsilon\sin 2\theta)yy'dx \tag{8}$$

It may be shown that

$$1 - \cos 2\theta = 2y'^2/(1 + y'^2)$$

$$\sin 2\theta = 2y'/(1 + y'^2)$$

$$D = 4\pi\rho v^2 \times \int_0^l \{[yy'^3/(1 + y'^2)] + [\epsilon yy'^2/(1 + y'^2)]\}dx \tag{9}$$

As in Section (2), the differential equation of the minimizing curve is found by substitution of the integrand of Eq. (9) in the Euler-Lagrange relation, Eq. (3). A tedious bit of algebra discloses that

$$y'' = -\frac{y'^2}{y}\frac{[(1 + y'^2)^2 - \epsilon(1 - y'^4)]}{[(3 - y'^2)(1 + y'^2)^2 + \epsilon(2 - 6y'^2)]} \tag{10}$$

It will be seen that Eq. (10) reduces to Eq. (4) when $\epsilon = 0$. Eq. (10) has been solved by the same type of numerical procedure used in obtaining the solution to Eq. (4). The solution is started at $y = 10$ and $y' = 1.000$. A circle arc is used to form the end of the nose shape and ϵ was chosen to be 0.07 radian.

The roughness of the surface has very little effect on the optimum nose shape for $\epsilon = 0.07$ radian. This becomes obvious by comparing the two curves shown in Fig. 7. It should be noted that the y-axis must be considerably stretched to show much difference in the two curves.

Although the surface roughness has little effect on the optimum nose shape—at least for the mechanism assumed here—it does have a significant effect on the drag coefficient. The drag coefficient is defined in the same manner as before:

$$C_D = (32/d^2) \times \int_0^l \{[yy'^3/(1+y'^2)] + \epsilon\,[yy'^2/(1+y'^2)]\}\,dx \quad (11)$$

Eq. (11) has been solved by a numerical procedure for the optimizing curve defined by Eq. (10), and the result is shown in Fig. 8 together with the drag coefficients that would result if the rebound angle equaled the angle of incidence—that is, $\epsilon = 0$.

(4) Optimum Nose Shape Assuming Molecules Are Randomly Reflected From the Missile Nose Surface

Experimental evidence indicates that many of the gas molecules which strike a surface are absorbed on the surface for a brief time interval and are then emitted. The percentage of gas molecules which will undergo this action is dependent on the temperature of the surface and the chemical nature of the gas and the surface.

It is assumed that the molecules which are absorbed on the surface and are later emitted will leave the surface in a random direction with an average magnitude of velocity corresponding to the surface temperature. The average velocity of emission is assumed to be bv, where v is the missile velocity through the atmosphere. Fig. 9 illustrates that random emission implies that the probability density of emission is uniform in the unit hemisphere above the point at which the molecule strikes the surface. The percentage of molecules emitted in the solid angle formed by the rotation of $d\phi$ around the normal to the surface is

$$(2\pi \cos\phi d\phi)/2\pi = \cos\phi d\phi$$

The velocity component of these molecules in the direction of the normal to the surface is

$$dv_n = bv \sin\phi \cos\phi d\phi = (1/2)\, bv \sin 2\phi d\phi$$

The net velocity component in the normal direction for all of the molecules emitted above the point is given by the integral

$$v_n = (1/2)\, bv \int_0^{\pi/2} \sin 2\phi d\phi = bv/2 \quad (12)$$

The conclusion derived from the foregoing analysis is that the average velocity vector of the emitted molecules is normal to the surface and that it has a magnitude

$$cv = bv/2$$

TABLE 2

x	y	y'	l/d	x	y	y'	l/d
4.14	10.00	1.000	0.207	300	82.58	0.157	1.8
7	12.35	0.709	0.283	650	129.3	0.116	2.5
12	15.46	0.552	0.388	1,500	211.7	0.083	3.5
30	23.59	0.385	0.636	3,000	319.8	0.064	4.7
60	33.91	0.295	0.885	4,000	380.4	0.057	5.2
130	51.50	0.218	1.26	5,500	461.5	0.051	5.9

The mass flux on the dy strip is given by the expression:

$$dm = 2\pi\rho v y dy = 2\pi\rho v y y' dx$$

from which is obtained the differential drag force

$$dD = 2\pi\rho v(v + cv \sin\theta) y y' dx$$

The total drag force is given by the integral

$$D = 2\pi\rho v^2 \int_0^l (1 + c \sin\theta) y y' dx \quad (13)$$

It may likewise be shown that

$$\sin\theta = y'/(1+y'^2)^{1/2}$$

Thus Eq. (13) may be written

$$D = 2\pi\rho v^2 \int_0^l yy' + [cyy'^2/(1+y'^2)^{1/2}]\,dx \quad (14)$$

The integral

$$\int_0^l yy'dx = \int_0^{l/2} ydy$$

is independent of the nose shape, and thus this part of the integral of Eq. (14) need not be considered in the minimization procedure. The expression to be minimized in this case is

$$\bar{D} = 2\pi\rho v^2 c \int_0^l [yy'^2/(1+y'^2)^{1/2}]dx \quad (15)$$

For a minimum drag the integrand of Eq. (15) must satisfy the Euler-Lagrange differential equation which yields the differential equation of the minimizing curve. In this case,

$$y'' = -(y'^2/y)[(1+y'^2)/(2-y'^2)] \quad (16)$$

Eq. (16) has a singularity at $y' = \sqrt{2}$ which need cause no concern here. As before, the solution is started at $y = 10$, $y' = 1.000$, and the extreme tip of the nose shape is formed with a circle arc. Eq. (16) has been solved by the numerical procedure described in Section (2). Table 2 gives values of x, y, y', and l/d for this curve. The shape of the curve is very nearly that of a parabola which has its vertex at the nose.

It is convenient to define a coefficient $\bar{C}_D$ which is dependent on $\bar{D}$ [see Eq. (15)] thus,

$$\bar{C}_D = 2\bar{D}/\rho A v^2 = (16c/d^2)\int_0 [yy'^2/(1+y'^2)^{1/2}]dx \quad (17)$$

Eq. (17) shows that the portion of the drag coefficient which is affected by the nose shape is also dependent on c which is a function of the surface temperature of the

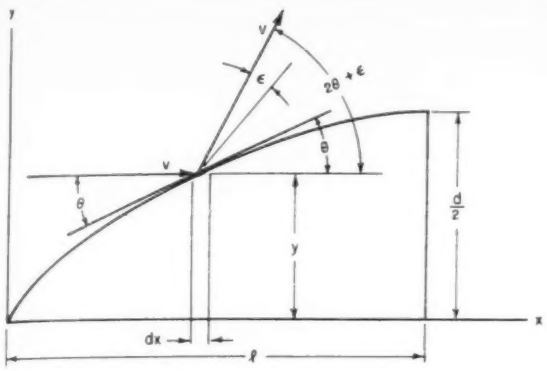

FIG. 6. Rebound of molecules from slightly rough surface.

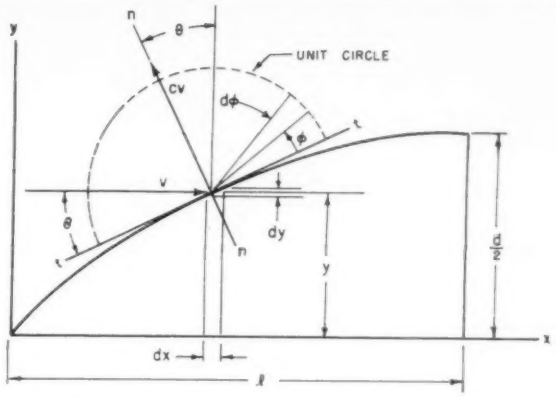

FIG. 9. Random emission of molecules from missile nose surface.

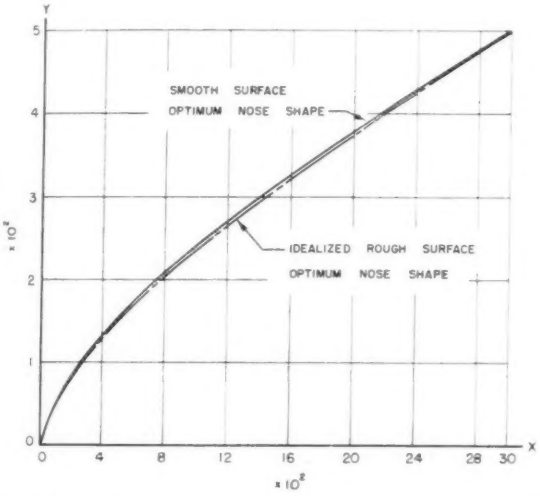

FIG. 7. Comparison of optimum nose shapes for idealized smooth surface and for partially rough surface; $l/d = 3$, $\epsilon = 0.07$.

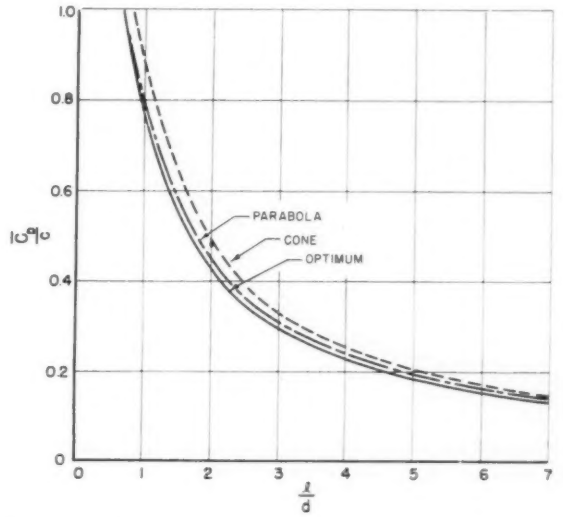

FIG. 10. $\bar{C}_D/c$ versus l/d for random reflection of air molecules.

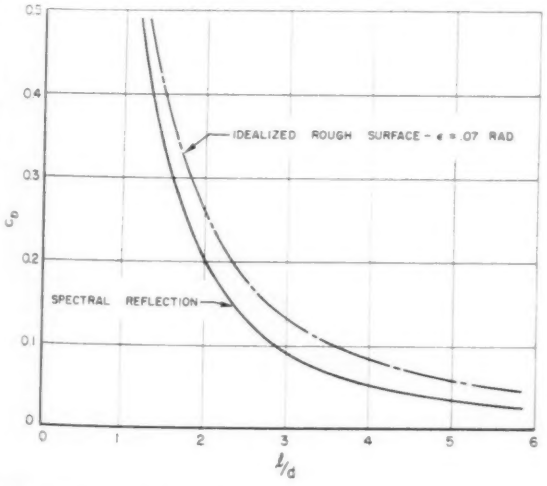

FIG. 8. Drag coefficients of optimum nose shape with roughness effects considered.

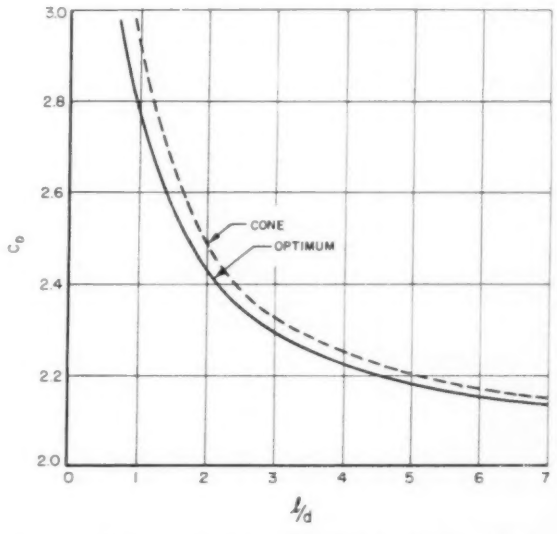

FIG. 11. $\bar{C}_D$ versus l/d for random reflection of air molecules.

nose or more exactly a function of the difference of the kinetic temperatures corresponding to the missile velocity v and the surface temperature of the nose.

For the purpose of comparing the drag of various nose shapes with random reflection, the coefficient may be defined as

$$\bar{C}_D/c = (16/d^2) \int_0^l [yy'^2/(1 + y'^2)^{1/2}]\, dx \quad (18)$$

This coefficient has been computed by a numerical procedure for the optimum nose shape defined by Eq. (16). The coefficient has also been determined for a parabolic nose shape, having the vertex at the missile nose tip, and for a cone. A comparison of the values for these shapes is shown in Fig. 10. The values for the parabola are very near those for the optimum curve since the optimum curve has very nearly a parabolic shape.

The total drag coefficients do not differ very much when random reflection occurs. The total drag coefficient may be defined by the relation

$$C_D = 2DAv^2 = (16/d^2) \int_0^l \{yy' + [cyy'^2/(1 + y'^2)^{1/2}]\}\, dx \quad (19)$$

This coefficient has been evaluated for c equal to unity for the optimum curve and the cone. The results are shown in Fig. 11. These curves show clearly that neither nose shape nor the l/d ratio have much effect on the total drag when random reflection occurs.

(5) Conclusion

The fundamental information now available is not complete enough to permit one to determine exactly the aerodynamic drag of objects moving in a rarefied gas. As noted in the Introduction, the drag force may well be dependent on factors other than the geometry of the body. This study then should be regarded as one which defines the limits between which the actual drag forces must lie.

References

[1] Loeb, Leonard B., *The Kinetic Theory of Gases*, pp. 278–388, McGraw-Hill Book Company, Inc., New York, 1934.

[2] Ashley, Holt, *Applications of the Theory of Free Molecule Flow to Aeronautics*, Journal of the Aeronautical Sciences, Vol. 16, No. 2, pp. 95–104, February, 1949.

. . . Airplane Dynamics in Large-Disturbance Maneuvers

(*Continued from page 526*)

nell Aeronautical Laboratory Report TB-541-F-4, January 4, 1952.

[3] Rhoads, D. W., *Rolling Pullout Study—Part III, Comparison of Calculated and Measured Airplane Motions and Tail Loads During Typical Rolling Pullout Maneuvers*, AFTR-6701 Part III, Cornell Aeronautical Laboratory Report TB-541-F-3, September, 1954.

[4] Schuler, John M., *Analytical Study of Airplane Dynamics and Tail Loads in Rolling Pullout Maneuvers*, WADC TR 56-403, Cornell Aeronautical Laboratory Report TB-916-F-1, September, 1956.

[5] White, R. J., Uddenberg, R. C., Murray, D., and Graham, F. D., *The Dynamic Stability and Control Equations of a Pivoted-Wing Supersonic Pilotless Aircraft, with Downwash, Wake and Interference Effects Included*, Boeing Aircraft Company Document No. D-8510, January 9, 1948.

[6] Phillips, William H., *Effect of Steady Rolling on Longitudinal and Directional Stability*, NACA TN 1627, June, 1948.

[7] Bergrun, Norman R., and Nickel, Paul A., *A Flight Investigation of the Effect of Steady Rolling on the Natural Frequencies of a Body-Tail Combination*, NACA TN 2985, August, 1953.

[8] Nicolaides, J. D., *On the Free Flight Motion of Missiles Having Slight Configurational Asymmetries*, Institute of the Aeronautical Sciences, presented at the 21st Annual Meeting, IAS, New York, January 26–29, 1953. (Preprint No. 395.)

[9] Zimmerman, Charles H., *Recent Stability and Aerodynamic Problems and Their Implication as to Load Estimation*, NACA RM L55E11a, June 28, 1955.

[10] Goldstein, Herbert, *Classical Mechanics;* Addison-Wesley Press, Inc., Cambridge, Mass., 1950.

[11] Abzug, M. J., *Effects of Certain Steady Motions on Small-Disturbance Airplane Dynamics*, Journal of the Aeronautical Sciences, Vol. 21, No. 11, pp. 749–752, November, 1954.

[12] Collar, A. R., *On the Stability of Accelerated Motion*, Aeronautical Research Council Report No. 16, 831 (S. and C. 2908), May, 1954.

[13] *Letter Symbols for Aeronautical Sciences*, American Standards Association Y10.7-1954, published by the American Society of Mechanical Engineers, New York, 1954.

[14] Yowell, E. C., *Report on the Solution of the Equations of Flight During a Rolling Pullout Maneuver*, National Bureau of Standards Report 2983, December 17, 1953.

[15] Kelly, D. V., Skelly, E. T., *Instrumentation of an F-80A Airplane for Dynamic Stability and Tail Load Flight Tests, Part I—Recording Instrumentation and Autopilot Instrumentation*, Cornell Aeronautical Laboratory Report TB-495-F-8, December 15, 1949.

Nonlinear Deflections of Shallow Spherical Shells†

EDWARD L. REISS, HERBERT J. GREENBERG, AND HERBERT B. KELLER
Institute of Mathematical Sciences, New York University

SUMMARY

The equations obtained by Chien for the nonlinear deflection of shallow spherical shells under uniform external pressure are solved by means of power series expansions, following procedures introduced by Friedrichs and Stoker in their treatment of buckling of circular plates. These equations depend upon two parameters. One of these parameters is related to the external pressure, while the other depends upon the dimensions of the shell. The equations are solved for several ranges of the parameters under boundary conditions corresponding to a fixed edge.

The solution, carried out numerically on the AEC UNIVAC at New York University, yields a complete description of the stresses and deflections as functions of the polar angle over a wide range of values of the loading parameter and the dimensional parameter. Prediction of the upper buckling load is then made by means of a numerical criterion based on the load vs. deflection curve. For some cases, the postbuckling behavior is investigated. The results agree well with existing experimental and theoretical studies and cover a wide range of cases not previously treated.

SYMBOLS

D = flexural rigidity of shell $2Eh^3/3(1-\nu^2)$
E = Young's modulus
F, G = boundary functions, see Eq. (19)
$2h$ = shell thickness
k = $2/3(1-\nu^2)$
N = number of terms in power series required for convergence
p = external pressure, positive inwards
P = loading parameter, see Eq. (12)
r = radial variable, distance to any point in shell
R = radius of middle surface of shell
S = surface of shell
u = tangential component of displacement
u^0 = tangential component of displacement on middle surface
V = volume of shell
w = radial component of displacement
w^0 = radial component of displacement on middle surface
$\bar{\alpha}$ = slope of tangent plane to deformed surface with the horizontal plane
α = $\bar{\alpha}/\Lambda$
$\bar{\gamma}$ = stress function, see Eq. (10)
γ = reduced stress function, see Eq. (12)
ϵ_β = longitudinal strain
$\epsilon_{\bar{\varphi}}$ = circumferential strain
ϵ = a small number
ϵ_{ij} = components of strain tensor
ζ = $R - r$
η = a small number
$\bar{\theta}$ = polar angle
θ = $\bar{\theta}/\Lambda$
Λ = semiangle of shell opening
λ = Kaplan and Fung geometric parameter
ν = Poisson's ratio
Π = potential energy
ρ = geometric parameter, see Eq. (12)
$\sigma_{\bar{\theta}}, \sigma_{\bar{\theta}}^0$ = longitudinal stress; value on middle surface
$\sigma_{\bar{\varphi}}; \sigma_{\bar{\varphi}}^0$ = circumferential stress; value on middle surface
τ^{ij} = components of stress tensor
$\bar{\varphi}$ = azimuthal angle

Presented at the Structures Session, Twenty-Fifth Annual Meeting, IAS, New York, January 28–31, 1957.

† The research reported in this paper was performed under Contract AT(30-1)-1480 with the United States Atomic Energy Commission. A partial summary of the results contained in this paper was presented at the Ninth International Congress of Applied Mechanics in Brussels, September, 1956.

The authors wish to express their appreciation to Prof. J. J. Stoker for suggesting this investigation.

INTRODUCTION

CONSIDER a thin hollow sphere of wall thickness $2h$ and mean radius R loaded by a uniform external pressure p directed toward the center. It is observed experimentally that as the pressure increases from zero, the shell apparently deforms by contracting into a smaller sphere. This mode of deformation continues until some critical value of the pressure is reached. At this value the shell suddenly jumps, or buckles into a nonspherical buckled state consisting of a round, rotationally symmetric, inward "dimple" of small solid angle at some point on the surface of the shell, while the remainder of the shell remains apparently spherical.

These experimentally observed facts are entirely at variance with the linear theory of buckling.[1] Characteristically, the linear theory predicts a wave form extending over the whole surface, with the amplitude undetermined—e.g., the shell could buckle inward or outward under the same load. This is to be contrasted with the experimentally observed "dimpling" behavior. Furthermore, the experimental buckling load is found, in some cases, to be as low as one quarter of that predicted by the linear buckling theory.

In a similar type of phenomenon observed in the case of buckling of thin cylindrical shells under axial compression attempts were made to explain the discrepancy between theory and experiment on the basis of initial imperfections from the cylindrical shape of the model, and deviation of the boundary conditions from those assumed in the theoretical calculations. Although important, these effects were not sufficient to account for the lack of agreement (see the discussion in reference 2).

Von Kármán and Tsien[2] recognized that this must be the result of a nonlinear behavior of the structure. Based upon the minimization of a potential energy expression, they showed that for values of p below the buckling load predicted by the linear theory there exist

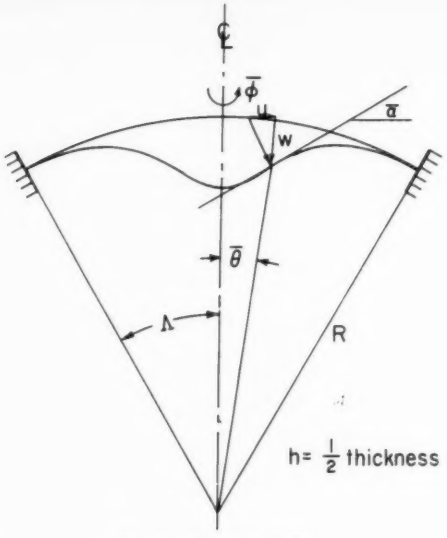

FIG. 1. Shell geometry.

other, nonadjacent, stable states of equilibrium. The greatest lower bound of such loads p is called the "minimum" or "lower" buckling load p_K. If p exceeds p_K there is a possibility that buckling will occur.

Friedrichs[3] pointed out some shortcomings and suggested improvements in the Kármán-Tsien theory. He also treated the buckling of a thin sphere as a "boundary-layer" phenomenon; where the "boundary layer" is considered as occurring in the dimpled region of the sphere. Tsien,[4] adopting some of the suggestions of Friedrichs,[3] presented an improved version of the Kármán-Tsien[2] theory. Altshuler[5] attempted to determine the buckling load by solving the differential equations by asymptotic expansion techniques. Although none of these approaches are entirely satisfactory, they do reveal the essential nature of the phenomena that are involved in the buckling process.

Closely related to the problem of the buckling of a thin sphere is that of the buckling of a shallow* spherical shell under uniform external pressure. Physically as well as mathematically, both problems reveal a similar nonlinear behavior. The shallow spherical shell is of interest both as a structural entity in itself, and as representing that portion of a complete sphere in which the dimpling occurs.

Solutions for the nonlinear deformations of shallow spherical shells under various external pressures and edge moments have been obtained by Chien and Hu[12] and Feodosyev.[13] In reference 6, Kaplan and Fung present a theoretical and experimental treatment for the clamped shallow spherical shell under uniform external pressure. Their theoretical work is based upon a perturbation solution of the nonlinear equations, where the nondimensional radial deflection at the center of the shell serves as the perturbation parameter. Unfortunately, solutions to the resulting linear perturbation equations could be obtained only for very shallow shells. However, their experiments as observed in reference 7 revealed some new and interesting phenomena concerning the buckling of curved structures. Archer,[15] using a similar set of equations derived by Reissner,[16] extended and improved the perturbation technique, and was able to obtain solutions for a greater range of shells than Kaplan and Fung. The agreement with experiments of the buckling loads predicted from the perturbation solution becomes poorer as the value of the geometric shell parameter ($\rho = A^2R/\sqrt{k}h$) increases. Furthermore, the perturbation solution, based upon a one parameter expansion, fails to reveal the nonmonotone dependence of buckling loads on ρ as indicated in reference 7. Simons[14] proposes solving the nonlinear equations[16] by a power series technique similar to that presented in this paper. His calculations, however, cover only a small range of parameters.

The physical problem treated in this paper is that of a thin shallow spherical shell under the action of uniform external pressure. This shell is assumed fixed and clamped along the edge. Only rotationally symmetric deformations will be considered. The problem is considered as one in the nonlinear theory of elasticity with small strains and small, but finite, deflections. Nonlinear load vs. deformation characteristics of the shell are expected to have the form shown in Fig. 2. Here, p represents the external pressure and w the radial deflection at some point—i.e., the center. Point A represents the "upper" or "initial" buckling load. Point B represents the "final" or "minimum" buckling load.

The present investigation has been successful in obtaining solutions including deflections and stresses for a large range of shell geometries for pressures from zero to those in the vicinity of point A of Fig. 2. Unfortunately, only meager results have been obtained so far for the "postbuckling" region—i.e., the portion of the curve ABC in Fig. 2.

The technique of solution employed was that of power series expansions inspired by the success of Friedrichs

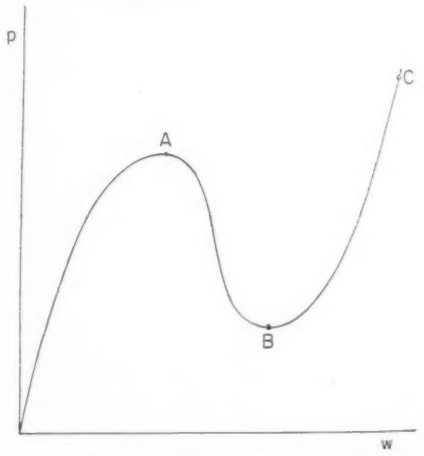

FIG. 2. Load vs. deformation characteristics.

* By shallow it is implied that the semiangle of opening A of the spherical segment is a small angle (see Fig. 1).

and Stoker,[10] and Bromberg[11] in the problems of bending and buckling of circular plates. The use of this approach in the present problem, however, was only possible due to the availability of a high-speed digital computer.

Derivation of Differential Equations

The nonlinear equations for the deformation of spherical shells of small curvature, based upon an assumption of small strains and linear stress-strain law, were originally obtained by Chien[8] from static considerations. These equations can also be derived from a variational principle. In this case we employ the principle of minimum potential energy and seek Euler's equations for the functional,

$$\Pi = \iiint_v (1/2)\tau^{ij}\epsilon_{ij}dV + \iint_S pwdS \qquad (1)$$

where Π is the potential energy, τ^{ij} are the components of the stress tensor, ϵ_{ij} are the components of the strain tensor, w is the radial displacement, and p is the external pressure, positive inwards. See Fig. 1 for the shell geometry.

The functional, Eq. (1), may be expressed in terms of the components of displacement through the following relations.

Stress Strain

$$\left.\begin{aligned} \tau^{11} \equiv \sigma_\theta &= [E/(1-\nu^2)](\epsilon_\theta + \nu\epsilon_\varphi) \\ \tau^{22} \equiv \sigma_\varphi &= [E/(1-\nu^2)](\epsilon_\varphi + \nu\epsilon_\theta) \end{aligned}\right\} \qquad (2)$$

From the assumption of rotational symmetry all other stress and strain components vanish.

Strain Displacement

Let r be the radial distance to any point in the shell and R the radius of the middle surface. The exact nonlinear strain displacement relations for rotationally symmetric deformations in a spherical coordinate system are then

$$\epsilon_{11} \equiv \epsilon_\theta = [(u_\theta - w)/r] + (1/2)[(w_\theta + u)/r]^2 + (1/2)[(u_\theta - w)/r]^2 \qquad (3a)$$

$$\epsilon_{22} \equiv \epsilon_\varphi = [(u\cot\bar\theta - w)/r] + (1/2)[(u\cot\bar\theta - w)/r]^2 \qquad (3b)$$

where subscripts on u and w denote differentiation.

For the case of small finite deflections, u and w (analagous to the Foppl-Kármán nonlinear plate theory) and shallow shells (small $\bar\theta$, $u_\theta{}^2$ is negligible compared to u_θ and $w_\theta{}^2$, and u is negligible compared to w_θ), Eqs. (3a) and (3b) reduce to

$$\epsilon_\theta = (1/r)(u_\theta - w) + (1/2)(w_\theta/r)^2 \qquad (4a)$$

$$\epsilon_\varphi = (1/r)(u/\bar\theta - w) \qquad (4b)$$

Eqs. (4a) and (4b) are the strain displacement relations that will be employed in the variational expression. It is not clear to what extent these equations are adequate for nonshallow shells without retaining additional terms from Eqs. (3a) and (3b); for example, see page 260 of reference 3.

As is customary in thin shell theory, the following assumptions are made concerning the distribution of the displacements through the shell thickness:

$$u = u^0 - (\zeta/R)w_\theta{}^0; \quad w = w^0 \qquad (5)$$

where $\zeta = R - r$ and u^0 and w^0 are the displacements of the middle surface $\zeta = 0$.

Substituting Eqs. (2), (4a), (4b), and (5) into Eq. (1), and performing the ζ and $\bar\varphi$ integrations, the potential energy Π may be written as

$$\Pi/2\pi R^2 = \int_0^\Lambda [Eh/(1-\nu^2)](\epsilon_\theta{}^{02} + \epsilon_\varphi{}^{02} + 2\nu\epsilon_\varphi{}^0\epsilon_\theta{}^0)\bar\theta d\bar\theta + \int_0^\Lambda [E\,3(1-\nu^2)] \times (h^3/R^4)[w_{\theta\theta}{}^2 + (1/\bar\theta^2)w_\theta{}^2 + (2\nu/\bar\theta)w_\theta w_{\theta\theta}]\bar\theta d\bar\theta + \int_0^\Lambda pw\bar\theta d\bar\theta \qquad (6)$$

where $\epsilon_\theta{}^0$ and $\epsilon_\varphi{}^0$ are the strains on the middle surface.

Setting the first variation of Eq. (6) equal to zero, the following equilibrium equations result:

$$\sigma_\varphi{}^0 = (d/d\bar\theta)(\bar\theta\sigma_\theta{}^0) \qquad (7a)$$

$$-(2h/R)\{(\sigma_\theta{}^0 + \sigma_\varphi{}^0)\bar\theta + (1/R)(d/d\bar\theta)(\bar\theta w_{\bar\theta}\sigma_\theta{}^f)\} + (D/R^4)\{(d/d\bar\theta)\bar\theta(d/d\bar\theta)(1/\bar\theta)(d/d\bar\theta)\bar\theta w_{\bar\theta}\} - p\bar\theta = 0 \qquad (7b)$$

where $\sigma_\theta{}^0$ and $\sigma_\varphi{}^0$ are stresses on the middle surface, and

$$D = 2Eh^3/3(1-\nu^2)$$

Eqs. (7a) and (7b) are a set of two equations in the three unknowns, $\sigma_\theta{}^0$, $\sigma_\varphi{}^0$, and w. It is also necessary to satisfy the compatibility equation for the middle surface. This equation can be obtained by eliminating u from Eqs. (4a) and (4b) for $r = R$. There results

$$(d/d\bar\theta)\bar\theta(\sigma_\varphi{}^0 - \nu\sigma_\theta{}^0) - \sigma_\theta{}^0 + \nu\sigma_\varphi{}^0 + (E/R)\bar\theta w_{\bar\theta} + (E/2)(w_{\bar\theta}/R)^2 = 0 \qquad (8)$$

In addition to yielding the differential equations (7a) and (7b), the variational problem leads to the following boundary conditions:

$$[(2h/R)\sigma_\theta{}^0\bar\theta\delta u^0 + (\bar\theta/R^2) \times \{(D/R^2)[-(d/d\bar\theta)(1/\bar\theta)(d/d\bar\theta)\bar\theta w_{\bar\theta} + \nu w_{\bar\theta}] + 2h\sigma_\theta{}^0 w_\theta\}\delta w + (D/R^4)(\bar\theta w_{\bar\theta\bar\theta} + \nu w_{\bar\theta})\delta w_{\bar\theta}]_0^\Lambda = 0 \qquad (9)$$

The first equation of equilibrium, (7a), is identically satisfied if we set

$$\sigma_\theta{}^0 = (E/2h)(\bar\gamma/\bar\theta) \qquad (10a)$$

$$\sigma_\varphi{}^0 = (E/2h)\bar\gamma_{\bar\theta} \qquad (10b)$$

Also, let us introduce the more convenient variables

$$\bar\alpha = (1/R)(dw/d\bar\theta) + \bar\theta \qquad (11)$$

$$\left.\begin{aligned} &\bar\alpha = \Lambda\alpha; \quad \bar\theta = \Lambda\theta; \quad k = 2/3(1-\nu^2); \\ &\bar\gamma = (k)^{1/2}(\Lambda h^2/R)\gamma; \quad p = 2E(k)^{1/2}(h/R)^2 P; \\ &\qquad\qquad \rho = (k)^{-1/2}\Lambda^2(R/h) \end{aligned}\right\} \qquad (12)$$

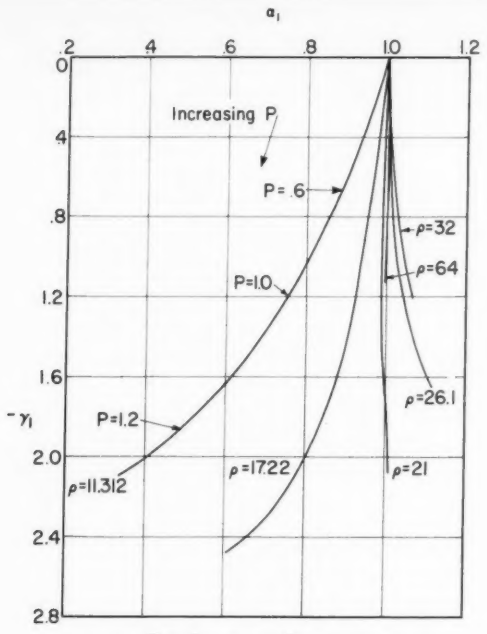

FIG. 3. α_1, γ_1 plane.

Geometrically, the independent variable $\bar{\alpha}$ defined in Eq. (11) is the angle that the tangent plane to the deformed surface makes with the horizontal plane, see Fig. 1.

The parameter ρ, hereafter referred to as the "geometrical parameter," is proportional to the ratio of the shell rise and the thickness. The shell rise is defined as the height of the center of the shell above the horizontal plane through the edge. ρ is also roughly proportional to the ratio of membrane and bending stiffness. The relation between ρ and Kaplan and Fung's geometrical parameter λ is

$$\rho = (2)^{-1/2}\lambda^2 \tag{12a}$$

Substituting Eqs. (10a), (10b), (11), and (12) into Eqs. (7a), (7b), and (8), and integrating Eq. (7b) once (employing the fact that from rotational symmetry $dw/d\theta = 0$ at $\theta = 0$), the following differential equations are obtained:

$$L\alpha = \rho(\alpha\gamma + P\theta^2) \tag{13a}$$

$$L\gamma = \rho(\theta^2 - \alpha^2) \tag{13b}$$

where L is the linear differential operator,

$$L = \theta(d/d\theta)\ (1/\theta)\ (d/d\theta)\theta \tag{14}$$

The boundary conditions corresponding to the differential equations (13a) and (13b) are as follows. At the center, $\theta = 0$, from rotational symmetry,

$$\alpha = 0; \quad u = 0$$

From Eqs. (2), (4a), (4b), (10a), and (10b), this is equivalent to

$$\alpha(0) = 0; \quad \gamma(0) = 0 \tag{15}$$

At the edge, $\theta = 1$, we assume that the plate is held fixed and clamped. This condition can also be considered as simulating the boundary separating the region of dimpling from that of uniform contraction of a complete sphere. Therefore, the conditions are

$$\alpha = 1; \quad u = 0; \quad w = 0$$

This is equivalent to

$$\alpha(1) = 1; \quad [\gamma_\theta - \nu\gamma]_{\theta=1} = 0 \tag{16}$$

It should be observed that, if conditions (15) and (16) are imposed, then the boundary conditions (9), resulting from the variational problem, are identically satisfied.

Thus, the complete formulation of the problem consists of the differential equations (13a) and (13b) subject to the boundary conditions (15) and (16). These equations—a pair of second-order coupled ordinary nonlinear differential equations—are quite similar to the equations governing the nonlinear deflections of circular plates,[9–11] except for the addition of extra terms resulting from the initial curvature. However, the physical phenomena that these equations describe are quite different. Mathematically, the buckling problem for the circular plate, or the bending problem, differ in their parametric dependence from the spherical shell problem. The plate problems depend upon one parameter, either a reduced edge load (the "thrust ratio," see reference 10) or a reduced lateral load (see reference 11); while, on the other hand, the equations governing the shell problem depend upon two parameters, P and ρ. From this point of view, it would seem that to obtain a more reasonable perturbation solution for the shell problem a two-parameter expansion should be attempted.

TECHNIQUE OF SOLUTION

The technique of solution to be employed for the boundary value problem posed by Eqs. (13a), (13b), (15), and (16) is to expand the dependent variables α and γ in power series in θ. This approach has been used in nonlinear circular plate problems by Way,[9] Friedrichs and Stoker,[10] and Bromberg.[11]

From Eqs. (13a) and (13b) and the boundary conditions at $\theta = 0$, the power series for α and γ must contain odd powers only, so that

$$\alpha = \sum_{n=1}^{\infty} \alpha_n \theta^{2n-1}; \quad \gamma = \sum_{n=1}^{\infty} \gamma_n \theta^{2n-1} \tag{17}$$

By substitution of these power series into Eqs. (13a) and (13b), the following recurrence relations for the coefficients α_n and γ_n are obtained:

$$\left.\begin{aligned} &\alpha_2 = \rho/8(\alpha_1\gamma_1 + P); \quad \gamma_2 = \rho/8(1 - \alpha_1^2); \\ &\text{for } n > 2 \\ &\alpha_n = \frac{\rho}{4n(n-1)} \sum_{i=1}^{n-1} \alpha_i\gamma_{n-i}; \\ &\gamma_n = -\frac{\rho}{4n(n-1)} \sum_{i=1}^{n-1} \alpha_i\alpha_{n-i} \end{aligned}\right\} \tag{18}$$

Again, by insertion of the power series into Eq. (16), the boundary conditions at $\theta = 1$ can be written as

$$\sum_{n=1}^{\infty} \alpha_n = 1; \quad \sum_{n=1}^{\infty} (2n - 1 - \nu)\gamma_n = 0$$

Since it is possible through the recurrence relations (18) to express all α_n and γ_n in terms of α_1 and γ_1 the above conditions constitute a pair of simultaneous equations in α_1 and γ_1—i.e.,

$$\left.\begin{aligned} F(\alpha_1, \gamma_1) &\equiv \sum_{n=1}^{\infty} \alpha_n - 1 = 0 \\ G(\alpha_1, \gamma_1) &\equiv \sum_{n=1}^{\infty} [2n - (1 + \nu)]\gamma_n = 0 \end{aligned}\right\} \quad (19)$$

The problem thus reduces, for given P and ρ, to solving the two simultaneous equations (19) for the unknowns α_1 and γ_1. Once the root or roots of these equations are obtained all the α_n and γ_n and, hence, all the stresses and displacements, are then determined (see Appendix A).

Computational Technique

The computational problem is, for a given set of parameter values (P, ρ) to determine the roots (α_1, γ_1) satisfying Eqs. (19). For computing purposes, it is necessary to replace the exact Eqs. (19) by the approximate conditions,

$$\left.\begin{aligned} |F(\alpha_1, \gamma_1)| &\doteq \left|\sum_{n=1}^{N} \alpha_n - 1\right| < \eta \\ |G(\alpha_1, \gamma_1)| &\doteq \left|\sum_{n=1}^{N} [2n - (1 + \nu)]\gamma_n\right| < \eta \end{aligned}\right\} \quad (19')$$

where η is a small number and N is an integer determined on the basis of a convergence criterion for the series. In the majority of the computations η was chosen as 1×10^{-4}. N is never greater than 99.

For a fixed P and ρ the procedure starts from a reasonable guess for (α_1, γ_1), say $(\alpha_1, \gamma_1)^0$. Then from Eq. (18) α_n and γ_n corresponding to $(\alpha_1, \gamma_1)^0$ are computed for $n \leq N$. As a convergence criterion for the series (17), it is prescribed that the sum of the absolute magnitudes of the last three computed α_n and γ_n be less than a certain small number, ϵ. That is, the computation of α_n and γ_n in Eqs. (18) ceases for $n = N$ such that

$$\left.\begin{aligned} |\alpha_N| + |\alpha_{N-1}| + |\alpha_{N-2}| &< \epsilon \\ |\gamma_N| + |\gamma_{N-1}| + |\gamma_{N-2}| &< \epsilon \end{aligned}\right\} \quad (20)$$

In the majority of the computations ϵ was set equal to 1×10^{-4}.

When the α_n and γ_n satisfy Eqs. (20), they are inserted into the expressions for $F(\alpha_1, \gamma_1)$ and $G(\alpha_1, \gamma_1)$. If F and G satisfy Eqs. (19′), the stress and displacement distribution throughout the shell are computed from the relations listed in Appendix A. In general, however, F and G do not satisfy Eqs. (19′), and it is necessary to obtain an improved approximation to (α_1, γ_1). This is done systematically by means of the Newton-Raphson iteration process. The partial derivatives of F and G in the Newton-Raphson process are approximated by forward difference quotients. This iteration process is repeated until Eqs. (19′) are satisfied. The displacements and stresses are then computed from the equations of Appendix A. The number of iterations required for convergence varies with the (P, ρ) selection and the initial guess $(\alpha_1, \gamma_1)^0$. For most of the cases encountered, two to six Newton-Raphson iterations were necessary. The number of coefficients, N, that were required for convergence varied with the (P, ρ) selection; Table 1 gives some representative values. The computation of coefficients, the iteration process, and the calculation of stresses and displacements are all performed on the AEC UNIVAC at New York University.*

Table 1
The Number N, of Coefficients Required for Convergence

	P			
ρ	0.2	0.8	1.0	1.4
12.23	11	13	14	19
17.22	13	17	19	23
32.0	16	26	31	—
52.2	20	36	46	—
64.0	22	42	54	—

The method for calculating with fixed P and ρ has thus been described. The computations proceed, for fixed ρ, by obtaining a sequence of roots (α_1, γ_1) for a corresponding sequence of increasing values of P. A first guess for (α_1, γ_1) is determined by selecting a low value for P, usually $P = 0.1$. For such low values of P, the deformed state, and hence the first (α_1, γ_1) guess, should be nearly spherical. The Newton-Raph-

* The authors are indebted to Miss M. Weissner and Messrs. A. Paster and S. B. Weinberg for their aid in coding and programing this problem.

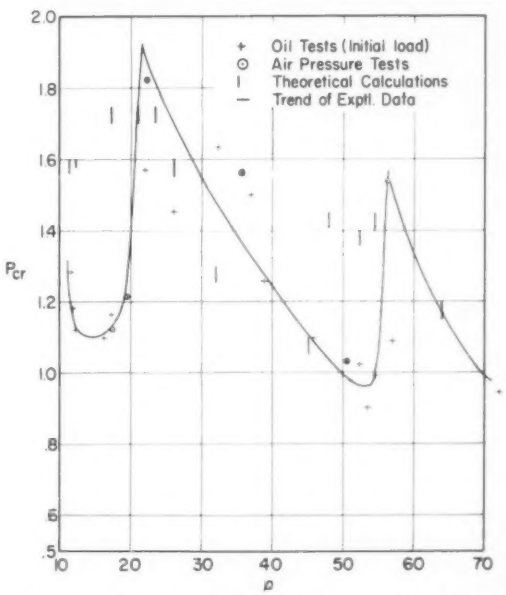

Fig. 4. Comparison of theoretical and experimental initial buckling loads.

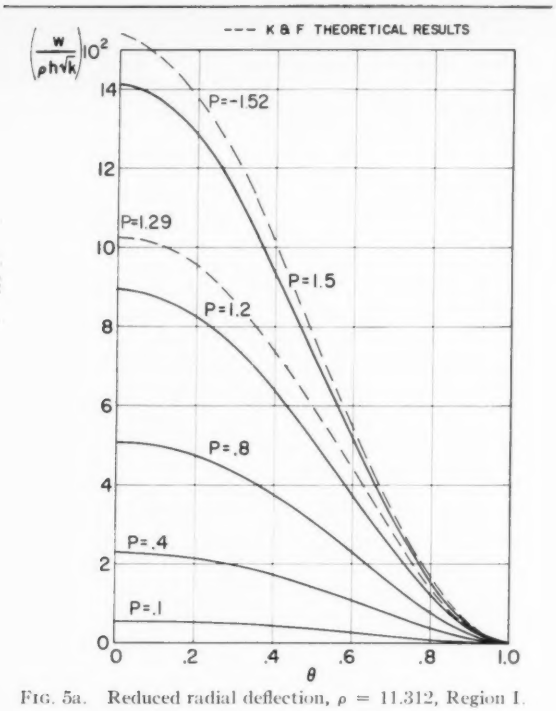

FIG. 5a. Reduced radial deflection, $\rho = 11.312$, Region I.

son process then rapidly yields the root (α_1, γ_1) to the required accuracy. The initial guess of the roots for successively higher values of P is obtained by extrapolation of the preceding roots in the sequence. This is done with the aid of a plot of α_1 vs. γ_1 as shown in Fig. 3. This procedure is terminated for either of two reasons—the Newton-Raphson iteration process fails to converge to a root in a large number of iterations (usually 10), or the coefficients fail to converge according to Eqs. (20). As an example of the first reason for termination, with $\rho = 32$ and $P = 1.25$ the procedure converged in 3 iterations. However, with $P = 1.3$ there was no indication of convergence in 10 Newton-

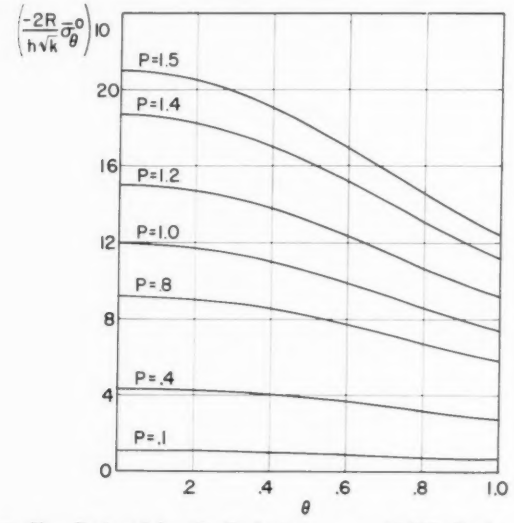

FIG. 5b. Reduced longitudinal stress, $\rho = 11.312$, Region I.

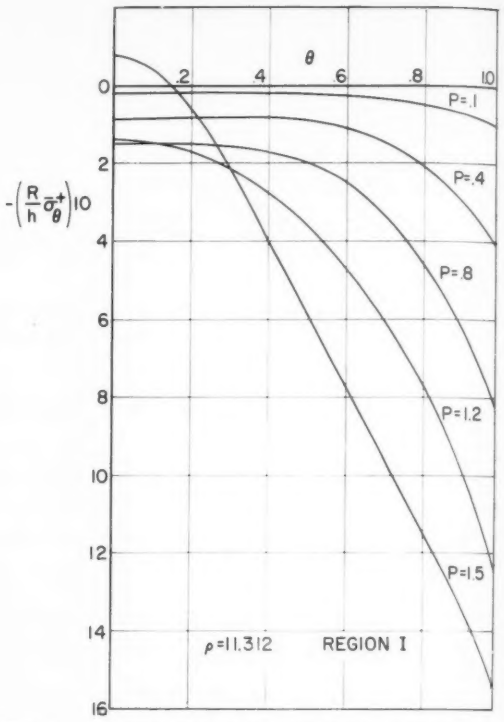

FIG. 5c. Reduced longitudinal total stress—top surface.

Raphson iterations. An illustration of the second reason for termination is for $\rho = 26.1$ and $P = 1.55$. Here convergence occurred in 2 iterations and 40 terms of the power series. But, for $P = 1.6$, 99 terms were computed with Eqs. (20) not being satisfied. In fact, the terms were steadily growing in absolute magnitude.

The criterion for the initial buckling that is used in this investigation is based on this terminating value of P. Direct application of the "classical" criterion (the load at which $dP/dw = 0$) for buckling seems im-

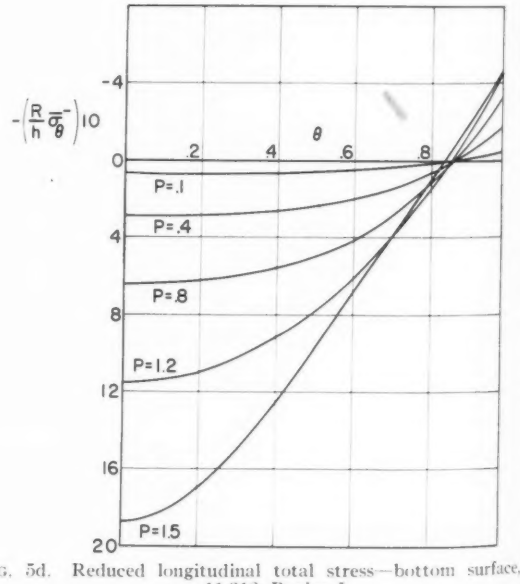

FIG. 5d. Reduced longitudinal total stress—bottom surface, $\rho = 11.312$, Region I.

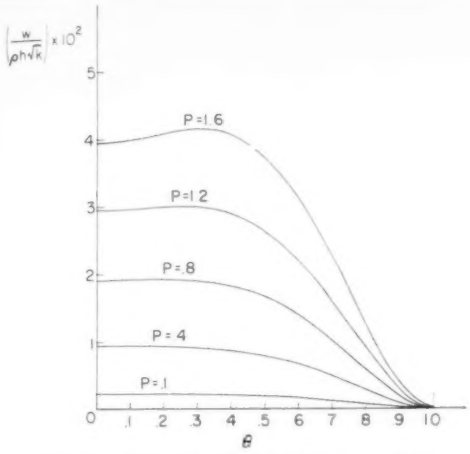

FIG. 6. Reduced radial deflection, $\rho = 23.5$.

practicable with the present technique of solution Instead, the numerical equivalent of the buckling phenomena is used as the criterion for determining the buckling load—i.e., the failure of the computing process to produce a neighboring solution corresponding to a small increment in the load. If P_1 represents the last value of P for which convergence occurs, and P_2 represents the next value of P attempted, then the initial buckling load, P_{cr}, is assumed to lie in the interval $P_1 \leq P_{cr} \leq P_2$.

DISCUSSION OF RESULTS

Before proceeding to a discussion of the results of our calculations, a brief review of the experimental results of Kaplan and Fung and the interpretation given in reference 7 will be presented.

Kaplan and Fung constructed a series of shallow spherical domes of varying radii and thickness. These domes were placed in a clamping jig and loaded under uniform external pressure. In addition to measuring the initial and final buckling pressures, they measured the vertical deflections at various points for several different values of the pressure.

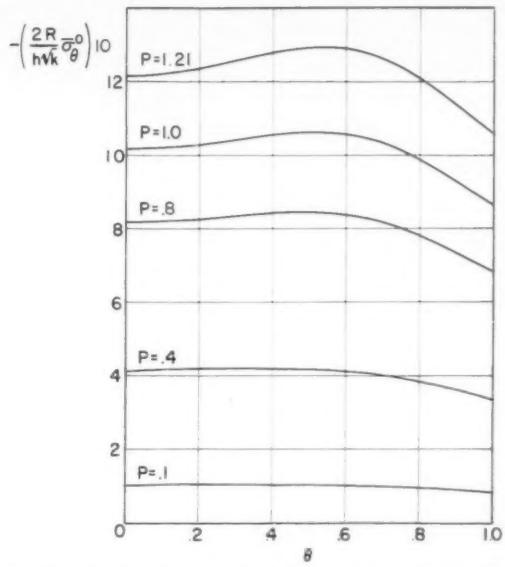

FIG. 7b. Reduced longitudinal stress, $\rho = 32$, Region II.

For low values of the geometric parameter ρ [or equivalently Kaplan and Fung's λ as related by Eq. (12a)] the experiments showed that the form of the deflections are such that the maximum deflection is at the center of the shell, and decreases steadily toward the edge. This will be called mode of deformation I. As ρ increases, it was observed that the peak deflection at the center gradually flattened out, until, at ρ equal to approximately 21, the maximum deflection occurs at some point between the center and edge;

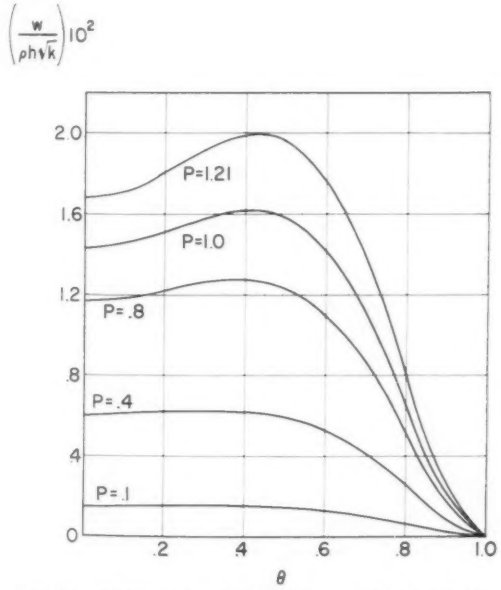

FIG. 7a. Reduced radial deflection, $\rho = 32$, Region II.

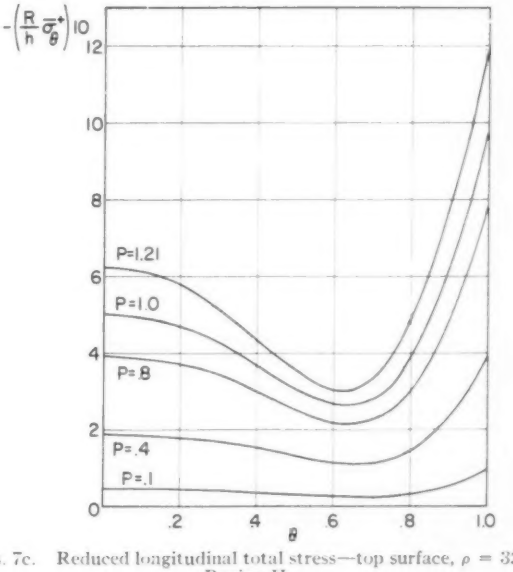

FIG. 7c. Reduced longitudinal total stress—top surface, $\rho = 32$, Region II.

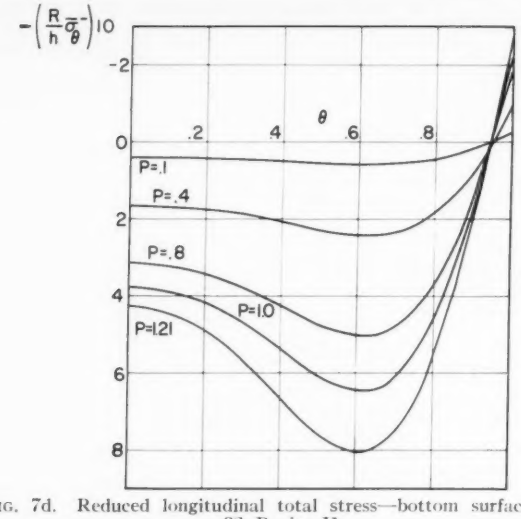

FIG. 7d. Reduced longitudinal total stress—bottom surface, $\rho = 32$, Region II.

so that there is also a local minimum point at the center. This will be called mode of deformation II. With a further increase in ρ the maximum point moved toward the edge until approximately $\rho = 55$. Then the shell deformed in a third mode. This mode has two local maximum points, one at the center and the other between the center and the edge (see Fig. 16 of reference 6).

When the experimental buckling loads are plotted against ρ rather than λ, it is found[7] that there is an interesting peaking behavior in these loads as a function of ρ—e.g., see Fig. 4. In Fig. 4 the crosses and circles indicate the experimental values of Kaplan and Fung, while the solid line indicates the apparent trend of the experimental data. It is significant to note that these peaks in the buckling loads occur at those values of ρ at which a change of mode of deformation had been observed.

In proceeding with our numerical solutions on the UNIVAC we have in a real sense conducted "experiments" on shallow spherical shells. For each given value of ρ—i.e., a particular shell configuration—deflection and stress "measurements" are made for increasing values of load P. As in a physical experiment, the initial buckling load is considered to be reached, when for a small increment in P no neighboring solution to the previously attained solution can be found—i.e., the iteration process suddenly fails to converge.

For low values of ρ, $\rho < 23$, the numerical results confirm Kaplan and Fung's experiments. In Figs. 5a, 5b, 5c, and 5d, are plotted some values of the deflections and stresses as a function of θ. The plots are for increasing load P at a constant value of ρ. In this case $\rho = 11.312$ was selected as representative of the mode of deformation of type, or region I. In Fig. 5a the radial deflection w can be seen to peak at the center and fall off toward the edge. The dotted lines indicating the results from the perturbation solution of Kaplan and Fung.[6] It can also be noted from Figs. 5b, 5c, and 5d that the stresses exhibit a similar behavior.

For increasing values of ρ, the graphs of these functions tend to flatten out in the central region of the shell ($\theta = 0$). This process continues until $\rho = 23.5$. See Fig. 6, where only the results for the radial deflection are presented. For this value of ρ and for low values of load, say $P \leq 0.4$, the shell deforms in mode I with maximum deflection at the center. However, for higher load the mode of deformation gradually changes into type II, with the maximum deflection located somewhere between the center and the edge (in this case, $\theta \approx 0.3$). It is to be noted from Fig. 4 that the shell $\rho = 23.5$ falls in the peaking region of the buckling loads. Thus, the mode of deformation for constant ρ may change with increasing load. This clearly illustrates the two parameter dependence of the character of the solutions.

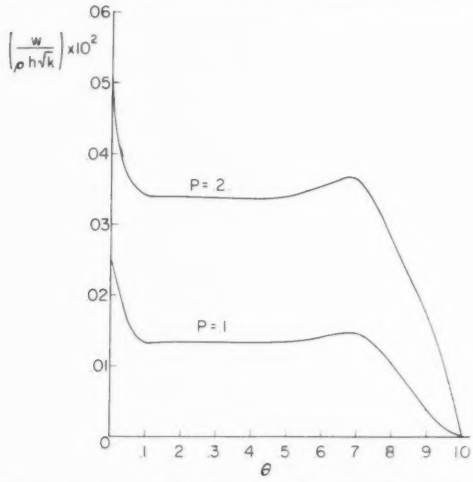

FIG. 8. Reduced radial deflection, $\rho = 176$, Region III.

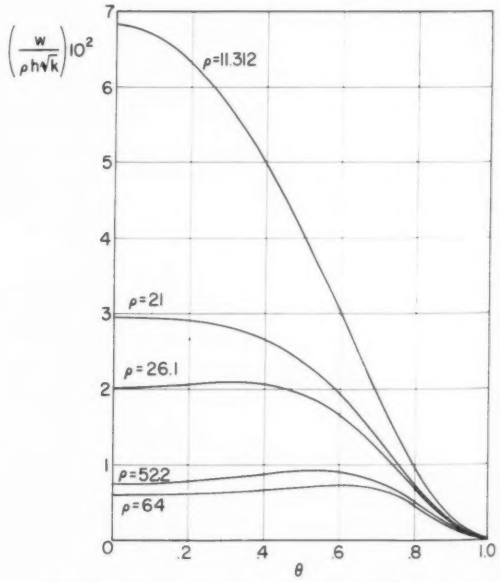

FIG. 9a. Reduced radial deflection, at $P = 1.0$.

In Figs. 7a, 7b, 7c, and 7d are shown plots of deflections and stresses for a typical shell, $\rho = 32$, of mode II of deformation for increasing values of load. Notice that the longitudinal membrane stress of Fig. 7b also has a maximum located between the center and edge (compare to Fig. 5b). The behavior of the total stresses for mode II (see Figs. 7c and 7d) shows a marked difference from that of mode I (see Figs. 5c and 5d). For mode I, the total stresses fall off in a smooth manner from the center to the edge, while for mode II there is a local minimum near $\theta = 0.6$ and then the stresses change rapidly toward the edge. This is reminiscent of the boundary-layer phenomena found by Friedrichs and Stoker[10] for the buckling of circular plates.

A further increase in ρ results in a flattening of the deflection and stress distributions in the central portion of the shell, and a movement of the maximum point toward the edge. Mode II persists until $\rho \approx 52$, when a transition case similar to $\rho = 23.5$ is detected. However, this time the transition is from mode II to mode III. In the radial deflection plot, the mode III form is barely visible, but it can clearly be observed in the total stress graphs. It is not until large ρ, say $\rho = 176$, that there is a sharp appearance of mode III in the radial deflection graph (see Fig. 8). Again from Fig. 4 it can be observed that the transition of modes occurs at the peaking of the buckling loads.

In Figs. 9a, 9b, 9c, and 9d the deflections and stresses are again plotted against θ, but this time for constant P and increasing ρ. In Fig. 9a the motion of the maximum deflection point toward the edge with increasing ρ is clearly indicated. This is again reminiscent of boundary-layer phenomena. In the plots for the longitudinal membrane stress of Fig. 9b, and in particular the total stresses of Figs. 9c and 9d, the change in mode shape is clearly illustrated.

The load vs. deflection at the center characteristics for various values of ρ are plotted in Fig. 10 and com-

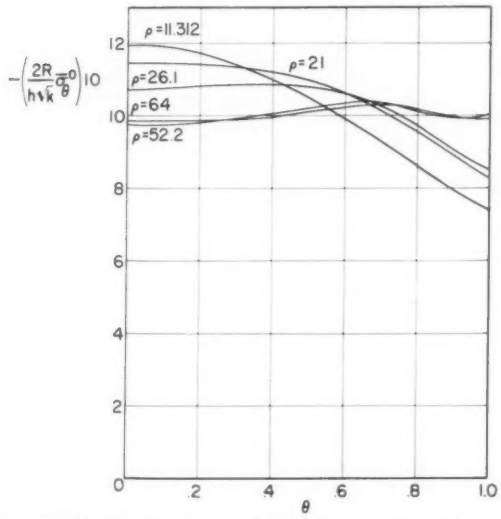

FIG. 9b. Reduced longitudinal stress, at $P = 1.0$.

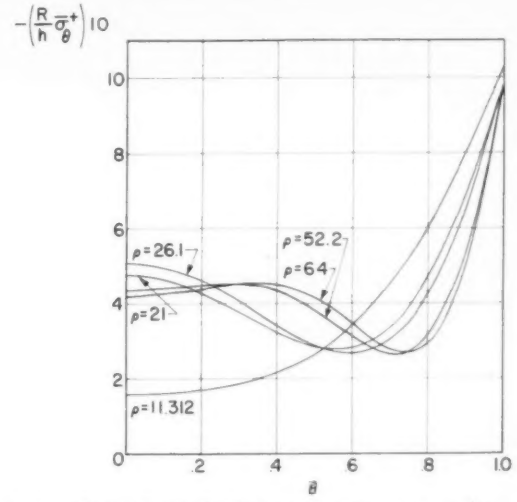

FIG. 9c. Reduced longitudinal total stress—top surface, at $P = 1.0$.

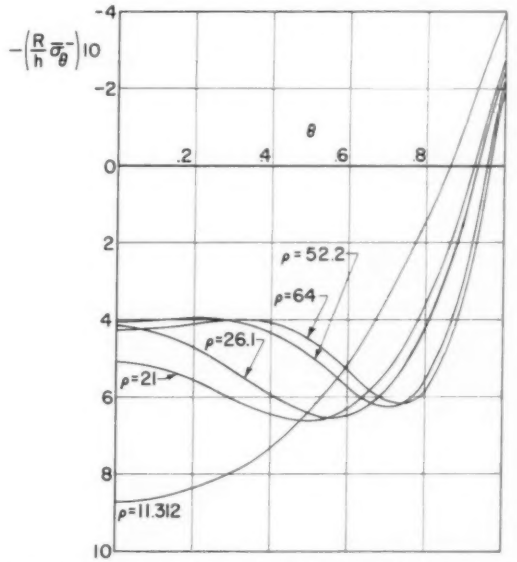

FIG. 9d. Reduced longitudinal total stress—bottom surface, at $P = 1.0$.

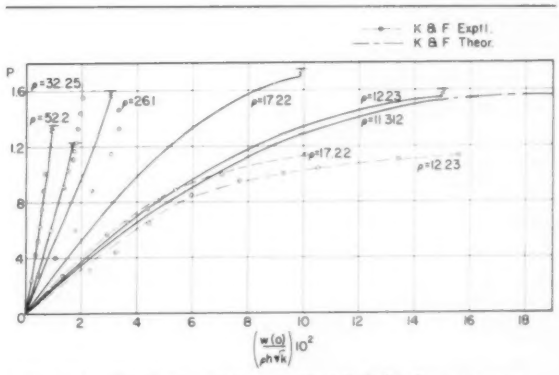

FIG. 10. Load parameter vs. reduced deflection at center.

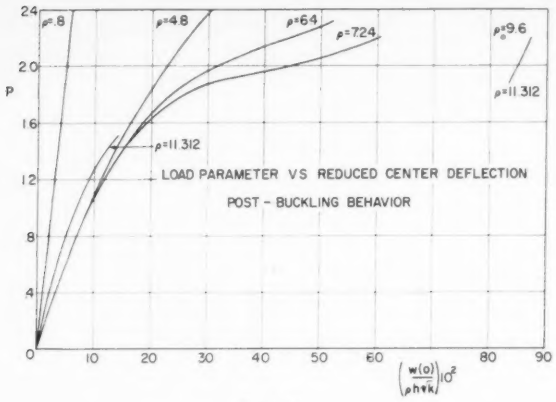

FIG. 11.

pared with the theoretical and experimental results obtained by Kaplan and Fung. For low values of ρ the agreement with the experiments is only fair, while for increasing ρ the agreement between the physical and numerical experiments becomes uniformly better. This is probably caused by the fact that for shallow shells (small ρ) the effect of initial imperfections is more pronounced, and that the shallower the shell the more difficult it is to measure the radius properly.

Initial Buckling Loads

The results of the numerical computation of P_{cr} as well as the experimental results of Kaplan and Fung are presented in Fig. 4. The intervals, P_1P_2, in which the P_{cr} lie are indicated by short vertical lines. It can be observed that the computed P_{cr} follow the same general trend as the experimental data, indicating a peaking behavior as a function of ρ. The agreement between experiment and theory is least satisfactory in the region of peaking [$18 \leq \rho \leq 25$, $50 \leq \rho \leq 60$]. In this region a small error in the experimental determination of ρ may lead to a large error in P_{cr} for a particular shell. It can also be observed from Fig. 4 that in some cases the numerical results predict greater P_{cr} than the experiments, while in other cases it is just the opposite. There is no apparent trend in this respect.

Postbuckling Behavior

The postbuckling region is defined as the region ABC of Fig. 2—i.e., the behavior of the shell after $P = P_{cr}$. The primary purpose of investigating this region is to determine the lowest value of P—($P = P_B$)—for which there exists non-unique solutions to the boundary value problem described by Eqs. (13a), (13b), (15), and (16). The procedure previously outlined does not enable us to continuously obtain solutions beyond point A. However, starting from a solution in the neighborhood of point C we may apply the previous procedure with a decreasing sequence of P values to obtain the point B.

To obtain a solution in the neighborhood of point C we select a sufficiently *large* value of P (say $P = 2.2$). For a sufficiently *small* value of ρ it is possible to obtain a solution, using the previous procedure, for this value of P, since, for a "flat" shell, the load vs. deformation characteristics must be monotone—i.e., there will be no buckling. Then, starting with the solution for this value of ρ, we obtain a sequence of solutions for an increasing sequence of ρ values and fixed P (see Fig. 11; $\rho = 0.8$, 4.8, 6.4, and 7.24). This procedure is analogous to the original procedure where the roles of P and ρ are interchanged. We note how, for increasing ρ values, the characteristics depart more and more from the initial linear relation and approach the buckling type of curve.

A solution is thus obtained for $P = 2.2$ and $\rho = 11.312$. This load is higher than that previously used and corresponds to much larger deflections. Keeping ρ fixed, a decreasing sequence of P values is selected in an attempt to locate point B. Unfortunately, convergence of the computations becomes increasingly poor as P decreases. Solutions are obtained only for the range $1.8 \leq P \leq 2.2$, see Fig. 11. The initial portion of the curve for $\rho = 11.312$ is also shown in Fig. 11. Fig. 12 represents the radial deflection over the shell for one value of P in the postbuckling region.

Conclusions

Numerical solutions of the nonlinear equations governing the deflections of clamped shallow spherical shells under a uniform external pressure have been obtained by power series technique. The computations were conducted on the AEC UNIVAC at N.Y.U. These solutions yield stress and deflection distributions

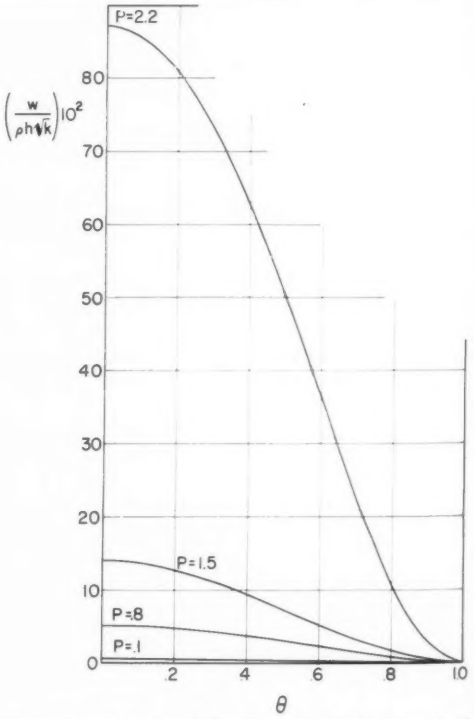

FIG. 12. Reduced radial deflection, $\rho = 11.312$, postbuckling behavior.

over the shell as well as estimates of the initial buckling loads for a wide range of values of the shell parameters. The two parameter dependence of the solutions and the various modes of deformation have been clearly shown. Only a limited number of solutions for the postbuckling region have been obtained. It is anticipated that some improvements in the numerical method may yield additional results in this region.

Appendix

Once the roots (α_1, γ_1) are obtained for a given set of parameter values (P, ρ), the stresses and deflections may be computed from the following relations:

$$\alpha(\theta) = \sum_{n=1}^{N} \alpha_n \theta^{2n-1} \tag{A-1}$$

$$w(\theta)/\rho h\sqrt{k} = (1/2)\left[1 - \sum_{n=1}^{N} (\alpha_n/n) + \sum_{n=1}^{N} (\alpha_n/n)\theta^{2n} - \theta^2\right] \tag{A-2}$$

$$w(0)/\rho h\sqrt{k} = (1/2)\left[1 - \sum_{n=1}^{N} (\alpha_n/n)\right] \tag{A-3}$$

Membrane stresses: $\bar{\sigma} = \sigma/E$,

$$2(k)^{-1/2}(R/h)\bar{\sigma}_\theta{}^0 = \sum_{n=1}^{N} \gamma_n \theta^{2n-2} \tag{A-4}$$

$$2(k)^{-1/2}(R/h)\bar{\sigma}_\varphi{}^0 = \sum_{n=1}^{N} (2n-1)\gamma_n \theta^{2n-2} \tag{A-5}$$

Total stresses: at upper and lower surfaces,

$$(R/h)\bar{\sigma}_\theta\big|_{\mp h} = (\sqrt{k}/2)\sum_{n=1}^{N} \gamma_n \theta^{2n-2} \pm (1-\nu^2)^{-1} \times \left[\sum_{n=1}^{N} (2n-1+\nu)\alpha_n \theta^{2n-2} - (1+\nu)\right] \tag{A-6}$$

$$(R/h)\bar{\sigma}_\varphi\big|_{\mp h} = (\sqrt{k}/2)\sum_{n=1}^{N} (2n-1)\gamma_n \theta^{2n-2} \pm (1-\nu^2)\left[\sum_{n=1}^{N} (2\nu n + 1 - \nu)\alpha_n \theta^{2n-2} - (1+\nu)\right] \tag{A-7}$$

References

[1] Timoshenko, S., *Theory of Elastic Stability*, McGraw-Hill Book Company, Inc., New York, 1936.

[2] von Kármán, T., and Tsien, H. S., *The Buckling of Spherical Shells by External Pressure*, Journal of the Aeronautical Sciences, Vol. 7, No. 2, pp. 43–50, December, 1939.

[3] Friedrichs, K. O., *On the Minimum Buckling Load for Spherical Shells*, von Kármán Anniversary Volume, pp. 258–272, California Institute of Technology, Pasadena, 1941.

[4] Tsien, H. S., *A Theory for the Buckling of Thin Shells*, Journal of the Aeronautical Sciences, Vol. 9, No. 10, pp. 373–384, August, 1942.

[5] Altshuler, B., *Nonlinear Buckling of a Spherical Shell*, Doctoral thesis, New York University, 1953.

[6] Kaplan, A., and Fung, Y. C., *A Nonlinear Theory of Bending and Buckling of Thin Elastic Shallow Spherical Shells*, NACA TN 3212, 1954.

[7] Reiss, E. L., *On the Nonlinear Buckling of Shallow Spherical Domes*, Journal of the Aeronautical Sciences, Vol. 23, No. 10, pp. 973–975, October, 1956.

[8] Chien, W. Z., *The Intrinsic Theory of Thin Shells and Plates*, Quar. of Appl. Math., Vol. II, No. 2, pp. 120–135, July, 1944.

[9] Way, S., *Bending of Circular Plates With Large Deflection*, Trans. ASME, Vol. 56, p. 627, 1934.

[10] Friedrichs, K. O., and Stoker, J. J., *The Nonlinear Boundary Value Problem of the Buckled Plate*, Amer. Jour. of Math., Vol. LXIII, No. 4, pp. 839–888, October, 1941. *Buckling of the Circular Plate Beyond the Critical Thrust*, Jour. of Appl. Mech., Vol. 9, No. 1, pp. A7–A14, March, 1942.

[11] Bromberg, E., *Nonlinear Bending of a Circular Plate Under Normal Pressure*, Doctoral thesis, New York University, 1950.

[12] Chien, W. Z., and Hu, H. C., *On the Snapping of a Thin Spherical Cap*, paper presented before IX International Congress of Applied Mechanics, Brussels, Belgium, September, 1956.

[13] Feodosyev, V. I., *On the Stability of a Spherical Shell Under the Action of an External Uniform Pressure*, (In Russian), Prikl. Mat. Mek., Vol. 18, No. 1, pp. 35–42, 1954.

[14] Simons, R. M., *A Power Series Solution of the Nonlinear Equations for Axi-Symmetrical Bending of Shallow Spherical Shells*, Jour. Math. and Phys., Vol. 35, No. 2, pp. 164–176, 1956.

[15] Archer, R. R., *Stability Limits for a Clamped Spherical Shell Segment Under Uniform Pressure*, Doctoral thesis, Massachusetts Institute of Technology, May, 1956.

[16] Reissner, E., *On Axi-Symmetrical Deformations of Thin Shells of Revolution*, Proc. of Symp. on Appl. Math., Amer. Math. Soc., Vol. 3, p. 27, 1950.

Notice to Contributors

Manuscripts submitted for publication *must* be double- or triple-spaced originals. There should be wide margins on all sides of the sheets and triple spacing around formulas to allow for the marking of directions for the printer.

Original drawings (jet black India ink on white paper or tracing cloth) should accompany the manuscript. *(Blueprints are not acceptable.)* Photographs *must* be on glossy white paper. The smallest lettering on 8- by 10-in. figures should be no less than 1/4 in. high.

Only the simplest formulas should be typewritten; all others should be carefully written in pen and ink. The difference between capital and lower-case letters and Greek symbols should be clearly distinguished.

See Inside Back Cover of this issue for further details

Readers' Forum

BRIEF REPORTS of investigations in the aeronautical sciences and discussions of papers published in the JOURNAL are presented in this special department. Entries must be restricted to a maximum of 1,300 words or the equivalent of one JOURNAL page including formulas and illustrations. Publication is completed as soon as possible after receipt of the material. The Editorial Committee does not hold itself responsible for the opinions expressed by the correspondents.

Contents

Comments on "Investigation of the Temperature Distribution and Thermal Stresses in a Hypersonic Wing Structure" ..... SHIH-YUAN CHEN 544

Remarks Concerning Transition Reynolds Numbers on Cones and Flat Plates ..... NEAL TETERVIN 545

Sears Function in Unsteady Flows ..... HSUAN YEH 546

The Pressure Rise at Shock-Induced Turbulent Boundary-Layer Separation in Three-Dimensional Supersonic Flow ..... RAYMOND J. STALKER 547

Some General Properties of the Dynamic Amplification Spectra ..... Y. C. FUNG 547

Simplified Equations for Calculating Local and Total Heat Flux to Nonisothermal Surfaces ..... E. R. G. ECKERT, J. P. HARTNETT, AND ROLAND BIRKEBAK 549

Stress Concentration in Plexiglas as a Function of Loading Rate ..... LEO V. KLINE 551

Errata—"Vibration of Clamped Parallelogrammic Isotropic Flat Plates" ..... M. HASEGAWA 552

Errata—"Subsonic Oscillatory Control Surface Coefficients Computed by the Method of Reissner and Haskind" ..... HENRY E. FETTIS 552

Comments on "Investigation of the Temperature Distribution and Thermal Stresses in a Hypersonic Wing Structure"[1]

Shih-Yuan Chen
Design Specialist, Republic Aviation Corporation, Farmingdale, N.Y.

March 11, 1957

RECENTLY, Goldberg presented a paper[1] in the JOURNAL OF THE AERONAUTICAL SCIENCES. He first introduced the dimensionless variables into the heat-transfer equations

$$(\partial^2 t_1/\partial x^2) + (q/k\tau_s) = (1/\alpha)\,(\partial t_1/\partial \theta)^{\dagger} \tag{1}$$

for $b_w \leq x \leq (bs/2) + bw$ and $y = \tau_s$, and

$$\partial^2 t_{11}/\partial x^2 = (1/\alpha)\,(\partial t_{11}/\partial \theta) \tag{2}$$

for $0 \leq x \leq b_w$ and $Y = \tau_w/2$ and obtained Eqs. (3) and (4) below:

$$(\partial^2 u_1/\partial \underline{x}^2) + \bar{q}\,\sin(\pi\theta/\theta_F) = \partial u_1/\partial \underline{\theta} \tag{3}$$

for $\bar{R} \leq \underline{x} \leq 1$, and

$$\partial^2 u_{11}/\partial \underline{x}^2 = \partial u_{11}/\partial \underline{\theta} \tag{4}$$

for $0 \leq \underline{x} \leq \bar{R}$.

Then he applied the Laplace transform, employed p as the transform parameter, and obtained

$$(d^2 u_1{}^*/d\underline{x}^2) + [\bar{q}M/(p^2 + M^2)] = pu_1{}^* - u_a \tag{5}$$

$$d^2 u_{11}{}^*/d\underline{x}^2 = pu_{11}{}^* - u_a \tag{6}$$

The transformed boundary conditions are

$$\left.\begin{array}{ll} \underline{x} = 1 & du_1{}^*/d\underline{x} = 0 \\ \underline{x} = \bar{R} & u_1{}^* = u_{11}{}^* \\ \underline{x} = \bar{R} & (1/S)\,(du_1{}^*/d\underline{x}) = du_{11}{}^*/d\underline{x} \\ \underline{x} = 0 & du_{11}{}^*/d\underline{x} = 0 \end{array}\right\} \tag{7}$$

† Same symbols as in reference 1 are used throughout.

Contributors Please Note

Readers' Forum items must be confined to the equivalent of one page in the *Journal*. Contributions that exceed this limit will be returned to the authors for condensation and rewrite. To avoid inconvenience and delay, please adhere to the following specifications:

(1) Five, double-spaced, typewritten, manuscript pages ($8\frac{1}{2}$ by 11 in.), including wide margins, formulas, and headings equal one printed page.

(2) For every illustration, deduct at least one-half or as much as one manuscript page, depending on the size of the illustration.

Letting $r^2 = p$, the general solutions for Eqs. (5) and (6) are

$$u_I^* = C \cosh r\underline{x} + D \sinh r\underline{x} + [\bar{q}M/p(p^2 + M^2)] + (1/p) \tag{8}$$

for $\bar{R} \leq \underline{x} \leq 1$, and

$$u_{II}^* = A \cosh r\underline{x} + B \sinh r\underline{x} + (1/p) \tag{9}$$

After substituting the boundary conditions and performing the necessary simplifications, one obtains

$$u_I^* = \frac{-\bar{q}MS \sinh r\bar{R} \cosh r(1 - \underline{x})}{p(p^2 + M^2)\ [S \cosh r(1 - \bar{R}) \sinh r\bar{R} + \sinh r(1 - \bar{R}) \cosh r\bar{R}]} + \frac{\bar{q}M}{p(p^2 + M^2)} + \frac{1}{p} \tag{10}$$

$$u_{II}^* = \frac{\bar{q}M \sinh r(1 - \bar{R}) \cosh r\underline{x}}{p(p^2 + M^2)\ [S \cosh r(1 - \bar{R}) \sinh r\bar{R} + \sinh r(1 - \bar{R}) \cosh r\bar{R}]} + \frac{1}{p} \tag{11}$$

These are different in form as compared to the original paper. Goldberg then applied the Inversion Theorem and obtained residues at the poles:

$$\left.\begin{aligned} \psi &= 0 \\ \psi &= \pm iM \\ \psi &= -[(n + 1)^2 \pi^2/4\bar{R}^2] \qquad \text{with } n = 0, 2, 4, \ldots \\ \psi &= -\phi_n^2 \end{aligned}\right\} \tag{12}$$

where $-\phi_n^2$'s are roots of

$$\tan \phi_n (1 - \bar{R}) + S \tan \phi_n \bar{R} = 0 \tag{13}$$

for Eq. (10) and obtained residues at the poles

$$\left.\begin{aligned} \psi &= 0 \\ \psi &= \pm iM \\ \psi &= -[(n + 1)^2 \pi^2/4(1 - \bar{R})^2] \qquad \text{with } n = 0, 2, 4, \ldots \\ \psi &= -\phi_n^2 \end{aligned}\right\} \tag{14}$$

where $-\phi_n^2$'s are also roots of Eq. (13) for Eq. (11).

It is evident that neither

$$\psi = -[(n + 1)^2 \pi^2/4\bar{R}^2] \qquad \text{with } n = 0, 2, 4, \ldots$$

nor

$$\psi = -[(n + 1)^2 \pi^2/4(1 - \bar{R})^2] \qquad \text{with } n = 0, 2, 4, \ldots$$

are the poles of Eqs. (10) and (11), respectively. The correct poles for Eqs. (10) and (11) are at (see reference 2, page 120, and reference 3, page 139)

$$p = \psi = 0, \quad p = \psi = \pm iM, \quad p = \psi = -\phi_n^2$$

where $-\phi_n^2$'s are roots of the transcendental equation

$$S \cosh r(1 - \bar{R}) \sinh r\bar{R} + \sinh r(1 - \bar{R}) \cosh r\bar{R} = 0$$

For the case where

$$\cosh r(1 - \bar{R}) \cosh r\bar{R} \neq 0 \tag{15}$$

Eq. (13) can be rewritten as

$$S \tan \phi_n \bar{R} = -\tan \phi_n (1 - \bar{R}) \tag{16}$$

For some particular values of S and $\bar{R}$, such as

$$\tan \beta = -2 \tan 2.9\beta \tag{17}$$

one can find the first 14 roots given in reference 4, page 10.

Therefore, the general solutions given in the paper should be corrected by simply neglecting terms that involve

$$-[(n + 1)^2\pi^2/4\bar{R}^2] \qquad \text{and} \qquad -[(n + 1)^2\pi^2/4(1 - \bar{R})^2]$$

with $n = 0, 2, 4, \ldots$

References

[1] Goldberg, Martin A., *Investigation of the Temperature Distribution and Thermal Stresses in a Hypersonic Wing Structure*, Journal of the Aeronautical Sciences, Vol. 23, No. 11, pp. 981–990, November, 1956.

[2] Churchill, R. V., *Introduction to Complex Variables and Applications*, 1st Ed., McGraw-Hill Book Company, Inc., New York, 1948.

[3] Churchill, R. V., *Modern Operational Mathematics in Engineering*, McGraw-Hill Book Company, Inc., New York, 1944.

[4] Pohle, F. V., and Berman, I., *Thermal Stresses in Airplane Wings Under Constant Heat Input*, WADC TN 55-330, July, 1956.

Remarks Concerning Transition Reynolds Numbers on Cones and Flat Plates

Neal Tetervin

Langley Aeronautical Laboratory, NACA, Langley Field, Va.

March 26, 1957

RECENTLY, it has been conjectured (for example, reference 1) that, because the minimum critical Reynolds Number—the Reynolds Number below which all disturbances of very small amplitude are damped—is three times as large on a cone as on a plate, the transition Reynolds numbers may also be in the ratio three. To examine this conjecture, the linear theory of boundary-layer stability[2] is used to derive an approximate relation between the Reynolds Number on a cone and the Reynolds Number on a flat plate for equal closeness to transition; the assumption is made that the ratio of the shear caused by the velocity fluctuations in the laminar boundary layer to the laminar shear is an indication of the closeness to transition.[3] An analysis based on the linear stability theory cannot, of course, provide a relation between transition Reynolds Numbers on cones and those on plates because, when transition occurs, the disturbances are too large for their behavior to be described by the linear stability theory. The relations for equal closeness to transition can thus be useful in a comparison of cone and plate transition Reynolds Numbers only if there is not an appreciable difference between the Reynolds Numbers at which the relations for equal shear ratio become inapplicable and the transition Reynolds Numbers.

The examination is restricted to a thin boundary layer in which the disturbances on plate and cone are assumed to be of the same type and to be periodic in the direction of flow; the equations that describe the local stability characteristics are then also the same on plate and cone.[4] Moreover, the amplification of the disturbance as it proceeds downstream on the cone is calculated in the same way as on the plate. This, however, is an approximation because the effect on the disturbance of the change in surface area of the cone with increase in distance downstream is not available from the equations for a vanishingly thin boundary layer.

At present, no data on the behavior of amplified oscillations in the laminar boundary layer in supersonic flow are available; therefore, Schlichting's calculated amplification ratios for incompressible flow[5] are used. The use of these data leads to the approximate result that, at equal ratio of oscillation shear to laminar shear, the cone Reynolds Number based on the distance to the tip exceeds the plate Reynolds Number based on the distance to the leading edge by twice the minimum critical Reynolds Number on the plate. This relation requires that the amplitude of the disturbance be equal on cone and plate where amplification begins. The frequency on the cone is the frequency for maximum amplification to a Reynolds Number; the frequency on the plate is the frequency for maximum amplification to the corresponding Reynolds Number on the plate and is, in general, not the same as the frequency on the cone.

Although the present state of development of the theory does not permit the calculation of transition Reynolds Numbers, the indication is that the ratio of the cone Reynolds Number for

transition based on the distance to the cone tip divided by the plate Reynolds Number for transition based on the distance to the leading edge is not, in general, equal to three. The indication is that the ratio of transition Reynolds Numbers will be near three only when transition occurs near the minimum critical Reynolds Number. When transition occurs at a much larger Reynolds Number, the indication is that the ratio will be near unity. Because these remarks apply only when transition is caused by the amplification of very small disturbances, they are not applicable when local surface imperfections or distributed roughness cause transition by generating large disturbances.

References

[1] Probstein, Ronald F., and Lin, C. C., *A Study of the Transition to Turbulence of the Laminar Boundary Layer at Supersonic Speeds*, Paper presented at the 24th Annual Meeting, Institute of the Aeronautical Sciences, New York, January 23–26, 1956.

[2] Lin, C. C., *The Theory of Hydrodynamic Stability;* Cambridge University Press, 1955.

[3] Liepmann, H. W., *Investigation of Boundary Layer Transition on Concave Walls*, NACA Wartime Report W-87, 1945.

[4] Battin, R. H., and Lin, C. C., *On the Stability of the Boundary Layer Over a Cone*, Journal of the Aeronautical Sciences, Vol. 17, No. 7, pp. 453, 454, July, 1950.

[5] Schlichting, H., *On the Production of Turbulence in Flow Along a Plate*, Nachr. Gottingen M. P. K., S181–208, 1933 (also Translation No. 6, Australian Division of Aeronautics).

Sears Function in Unsteady Flows

Hsuan Yeh

Professor of Mechanical Engineering, University of Pennsylvania, Philadelphia, and Consultant, Garfield Thomas Water Tunnel, Ordnance Research Laboratory, University Park, Pa.

April 1, 1957

In a previous note in the Readers' Forum,[1] Sears function* $S(\omega)$ was tabulated for ω up to 15. As was pointed out in reference 1, this function (first used by Sears[2]) can be identified as

$$S(\omega) = (2/\pi\omega)\{1/[J_0(\omega) - Y_1(\omega)] - i[J_1(\omega) + Y_0(\omega)]\} \qquad (1)$$

* The same function was denoted by $F(\omega)$ in reference 2 and $\varphi(k)$ in reference 3.

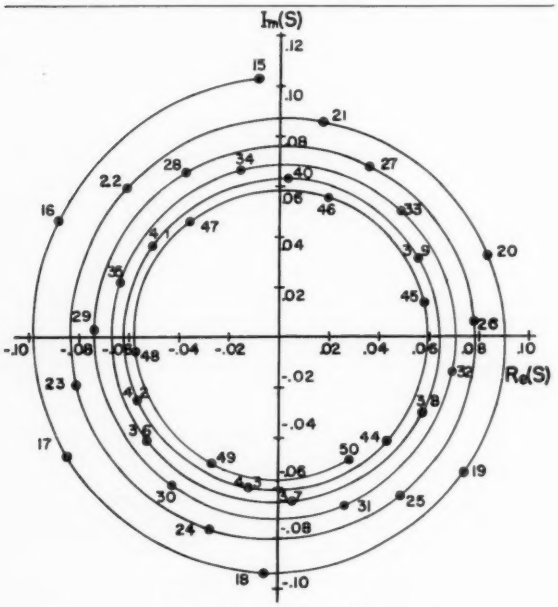

Fig. 1. Function $S(\omega)$.

Table 1
Function $S(\omega)$

ω	Re(S)	Im(S)	ω	Re(S)	Im(S)
0	1.00000	0	26	+.07793	+.00678
1	+.36865	+.12594	27	+.03573	+.06795
2	+.08157	+.26797	28	−.03719	+.06559
3	−.14479	+.17727	29	−.07403	+.00341
4	−.19802	+.02067	30	−.04266	−.05904
5	−.08116	−.15863	31	+.02620	−.06671
6	+.08127	−.14098	32	+.06915	−.01380
7	+.15050	−.00765	33	+.04883	+.05004
8	+.08235	+.11443	34	−.01575	+.06657
9	−.04863	+.12373	35	−.06360	+.02241
10	−.12365	+.02477	36	−.05246	−.04081
11	−.08367	−.08635	37	+.00587	−.06534
12	+.02618	−.11212	38	+.05735	−.03000
13	+.10421	−.03712	39	+.05550	+.03162
14	+.08439	+.06512	40	+.00335	+.06301
15	−.00882	+.10261	41	−.05061	+.03639
16	−.08820	+.04654	42	−.05647	−.02345
17	−.08420	−.04760	43	−.01175	−.05970
18	−.00539	−.09390	44	+.04355	−.04170
19	+.07404	−.05380	45	+.05785	+.01384
20	+.08312	+.03240	46	+.01937	+.05554
21	+.01728	+.08530	47	−.03589	+.04582
22	−.06101	+.05930	48	−.05715	−.00536
23	−.08101	−.01887	49	−.02627	−.05056
24	−.02730	−.07670	50	+.02815	−.04888
25	+.04875	−.06311			

Recently, it was found that the values of $S(\omega)$ up to ω = 50 or more (see below) were required. The staff of the Garfield Thomas Water Tunnel made such a calculation. The results are shown in Table 1. Since the accuracy of the values given in reference 1 was found to be insufficient, $S(\omega)$ for ω up to 15 was recalculated. In so doing an error in the previous reference (for $\omega = 10$) was discovered. This was corrected in the present table.

For values of ω larger than 50, $S(\omega)$ may be obtained by the following approximate relations:

$$J_0(\omega) \to \sqrt{2/\pi\omega}\cos[\omega - (\pi/4)]$$

$$Y_0(\omega) \to \sqrt{2/\pi\omega}\sin[\omega - (\pi/4)]$$

$$J_1(\omega) \to \sqrt{2/\pi\omega}\cos[\omega - (3\pi/4)]$$

$$Y_1(\omega) \to \sqrt{2/\pi\omega}\sin[\omega - (3\pi/4)]$$

Using these relations, it follows that, for large values of ω,

$$S(\omega) \to (1/2\sqrt{\pi\omega})[(\sin\omega + \cos\omega) + i(\sin\omega - \cos\omega)] = [(1 - i)/2\sqrt{\pi\omega}]e^{i\omega} \qquad (2)$$

$$|S(\omega)| \to 1/\sqrt{2\pi\omega} \qquad (3)$$

Eq. (3) was first suggested in reference 3 (which was concerned with the power spectrum and therefore required only the magnitude but not the complete calculation of this function). A comparison using the exact formula (1) and the approximate formula (2) shows that the discrepancy is negligible for $\omega > 50$.

Eq. (2) not only facilitates the calculation of $S(\omega)$ for large values of ω but also points out the now obvious fact that, for large values of ω, $S(\omega)$ rotates in the same manner as ω—i.e., $S(\omega)$ makes one revolution in the vector diagram (see Fig. 1) when ω increases by 2π. (A similar diagram for $0 < \omega < 10$ was given in reference 2.) Furthermore, Eq. (3) shows that the magnitude of $S(\omega)$ decreases slowly with increasing ω. Physically, this means that the response of an airfoil to a sinusoidal gust drops off only gradually

with increasing frequency of the unsteadiness. This is the reason that terms up to $\omega = 50$ or more may be actually necessary in the calculation of a practical problem (such as the problem of pressure perturbation due to sinusoidal upstream velocity disturbances). It is hoped that Table 1 may prove helpful to other investigators in similar problems.

References

[1] Kemp, N. H., *On the Lift and Circulation of Airfoils in Some Unsteady-Flow Problems*, Readers' Forum, Journal of the Aeronautical Sciences, Vol. 19, No. 10, pp. 713, 714, October, 1952.

[2] Sears, W. R., *Some Aspects of Non-Stationary Airfoil Theory and Its Practical Applications*, Journal of the Aeronautical Sciences, Vol. 8, No. 3, pp. 104–108, January, 1941.

[3] Liepmann, H. W., *On the Application of Statistical Concepts to the Buffeting Problem*, Journal of the Aeronautical Sciences, Vol. 19, No. 12, pp. 793–800, 822, December, 1952.

The Pressure Rise at Shock-Induced Turbulent Boundary-Layer Separation in Three-Dimensional Supersonic Flow*

Raymond J. Stalker

William and Agnes Bennett Supersonics Laboratory, The University of Sydney, Sydney, N.S.W., Australia

April 1, 1957

Summary

Experiments are reported which indicate that the peak-pressure ratio for supersonic turbulent free separation depends only on the Mach Number component normal to the line of separation.

Experiment

Experiments were undertaken to study the three-dimensional, shock-induced turbulent boundary-layer separation process at supersonic speeds. Some results obtained regarding the peak-pressure ratio attained in fully developed or "free" separation are sufficiently important to warrant immediate publication as this interim note.

The results were obtained with a straight step at angles of sweepback from 0° to 57° on the 6-in.-wide sidewall of a blow-down tunnel operating at $M = 2.36$ and at a Reynolds Number of 9×10^5 per in.

Schlieren observation indicated a boundary-layer thickness of about 0.25 in. in the empty test section, and a step height of 0.31 in. was chosen to ensure that, in the absence of sweepback, free separation would be obtained—that is, separation with pressure distribution independent of the agency provoking it. With sweepback, the wall pressure distribution along a line normal to the separation line was characteristically similar in shape to that obtained at zero sweepback, and the separation line was just as far ahead of the step, so that it would appear reasonable to conclude that free separation was again achieved.

At each sweepback angle the streak patterns obtained from applying the China film technique showed no variation along any straight line parallel to the separation line for at least 1 in. on either side of the line of wall pressure transverse. It was therefore concluded that there were no changes in the flow in the direction parallel to the separation line.

Fig. 1 shows the measured ratio of peak static pressure to free-stream static pressure plotted against the component normal to the separation line of the main-stream Mach Number upstream of separation. The Figure also includes a point from an experiment where a state approaching free† separation with sweepback

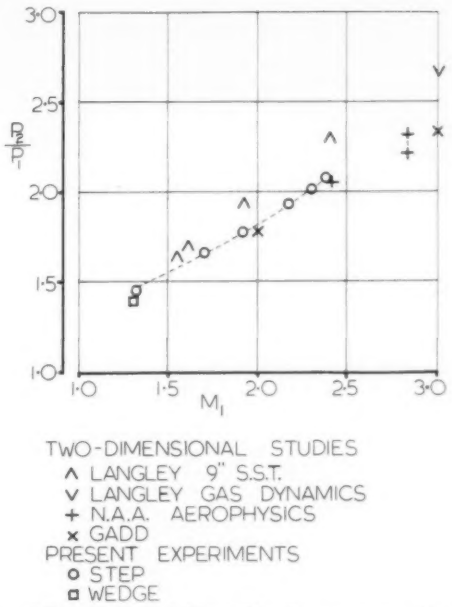

Fig. 1. Effect of normal Mach Number on separation peak-pressure ratio.

was obtained on the sidewall by means of the nose shock from a wedge on the tunnel floor; the peak pressure in this case was taken to be the pressure at the characteristic inflection point of the pressure distribution between the separation and reattachment processes.

Comparison with results of previous investigations[1, 2] for the two-dimensional free separation shows that, within the margin of uncertainty of those results, a sweepback principle may be enunciated—namely, that the peak-pressure ratio for turbulent, free separation depends only on the Mach Number component normal to the separation line.

This conclusion has been shown to be plausible by extending to three dimensions the model used successfully by Crocco and Probstein[3] to estimate the peak-pressure ratio at turbulent separation in two-dimensional supersonic flow. This will be published in a later paper.

References

[1] Lange, R. H., *Present Status of Information Relative to the Prediction of Shock-Induced Boundary-Layer Separation*, NACA TN 3065, February, 1954.

[2] Gadd, G. E., Holder, D. W., and Regan, J. D., *An Experimental Investigation of the Interaction between Shock Waves and Boundary Layers*, Proc. Roy. Soc., Series A, No. 1165, Vol. 226, pp. 227–253, November, 1954.

[3] Crocco, L., and Probstein, R. F., *The Peak Pressure Rise Across an Oblique Shock Emerging from a Turbulent Boundary Layer Over a Plane Surface*, Princeton Aero. Lab. Report 254, March, 1954.

Some General Properties of the Dynamic Amplification Spectra

Y. C. Fung

Associate Professor, Guggenheim Aeronautical Laboratory, California Institute of Technology, Pasadena, Calif.

February 25, 1957

When a more or less rapidly applied force acts on an elastic structure, the concept of *dynamic amplification* is of great importance. In the following we shall consider simple pulses of the nature of the landing impact loads; they rise monotonically from zero to a peak value at time t_m, then fall off back to zero at time t_0. A plot of the maximum response versus fre-

* This investigation was conducted under a research grant from the University of Sydney during leave of absence granted the author by Australian National Airways. The guidance of Dr. R. E. Meyer is gratefully acknowledged.

† The China film pattern showed a separated region about six initial boundary-layer thicknesses wide.

quency, of a variable frequency single degree of freedom linear oscillator to such a pulse, normalized in some specific manner, is called a "shock spectrum." Such a shock spectrum can be obtained experimentally, for example, by multifrequency reed gages. Since the idea of shock spectrum has been used broadly in specifying the nature of shocks in many engineering design problems (see references 1 and 2 where a survey of literature is given), it seems of interest to study the general features of such a spectrum that are not particularly sensitive to the specific details of the pulse history.

Let $\mathfrak{F}(t)$ be a pulse for which

$$\begin{aligned} \mathfrak{F}(t) &= 0 \quad \text{for} \quad t \leq 0 \text{ and } t \geq t_0 \\ &\geq 0 \quad \text{for} \quad t \text{ in } (0, t_0) \end{aligned}$$

$$\max_{0 \leq t \leq t_0} \mathfrak{F}(t) = \mathfrak{F}(t_m) = 1 \tag{1}$$

Then the positive dynamic amplification spectrum with a small damping parameter, ϵ, $(0 \leq \epsilon \ll 1)$, is defined as

$$q_{max}/q_0 = max\ [q(t)/q_0] = \max_{0 \leq t \leq \infty} \left\{ \omega \int_0^t \mathfrak{F}(\tau) e^{-\epsilon\omega(t-\tau)} \sin \omega(t-\tau) d\tau \right\} \tag{2}$$

The negative amplification spectrum is obtained by the same expressions through replacing *max* by *min*. These spectra are considered as functions of the dimensionless parameter $\omega\, t_m/\pi$.

Expanding the sine term in Eq. (2), one can rewrite the result as

$$q/q_0 = R\, e^{-\epsilon\omega t} \sin(\omega t - \phi) \tag{3}$$

where

$$R = \omega \left\{ \left(\int_0^t \mathfrak{F}(\tau) e^{\epsilon\omega\tau} \cos \omega\tau\, d\tau \right)^2 + \left(\int_0^t \mathfrak{F}(\tau) e^{\epsilon\omega\tau} \sin \omega\tau\, d\tau \right)^2 \right\}^{1/2} \tag{4}$$

$$\phi = \arctan \left\{ \int_0^t \mathfrak{F}(\tau) e^{\epsilon\omega\tau} \sin \omega\tau\, d\tau \div \int_0^t \mathfrak{F}(\tau) e^{\epsilon\omega\tau} \cos \omega\tau\, d\tau \right\} \tag{5}$$

Properties of the Amplification Spectrum at Small Values of Frequency

Now it can be shown that when $\omega t_m/\pi$ is sufficiently small, the absolute maximum of q occurs at $t > t_0$—i.e., after the pulse has fallen back to zero. For instance, for a trapezoidal pulse this occurs when $\omega t_m/\pi \leq 1/3$. That this is in general the case can be seen from Eqs. (4) and (5) which show that $\phi \to 0$ when $\omega \to 0$ and that, for small ω,

$$R \to \omega \int_0^t \mathfrak{F}(\tau)\, d\tau$$

which increases monotonically with increasing t if $\mathfrak{F}(t)$ is a simple pulse defined by Eq. (1). Hence, the peak of $q(t)$ is controlled, as in Eq. (3), by $\sin \omega t$ when ω is small. If t_p denotes the time at which the first peak of $q(t)$ is reached, we have $t_p \to \pi/(2\omega)$, which can be made $> t_0$ by choosing a sufficiently small ω.

Since $\mathfrak{F}(\tau) = 0$ for $\tau > t_0$, R and ϕ become constant for $t \geq t_0$. Hence, when $\omega t_m/\pi$ is sufficiently small so that the first maximum of $q(t)$ occurs at $t > t_0$, Eq. (3) shows that the peak time, t_p, and the peak value of q/q_0 are given by

$$\omega t_p - \phi_0 = \pi/2 \tag{6}$$

$$q_{max}/q_0 = \exp\{-\epsilon[(\pi/2) + \phi_0]\}\, R(t_0) \tag{7}$$

respectively, where ϕ_0 and $R(t_0)$ are the values of ϕ and $R(t)$ evaluated at t_0. Expanding $e^{\epsilon\omega\tau} \cos \omega\tau$ and $e^{\epsilon\omega\tau} \sin \omega\tau$ into Taylor's series in ω and defining the successive "moments" of the pulse $\mathfrak{F}(\tau)$ about the origin as μ_k,

$$\mu_k = \int_0^\infty \tau^k \mathfrak{F}(\tau)\, d\tau, \qquad (k = 0, 1, 2, \ldots) \tag{8}$$

we obtain from Eqs. (4), (5), and (7)

$$R(t_0) = \omega\{\mu_0 + \epsilon\mu_1\omega + (1/2)[(\mu_1^2/\mu_0) + (\epsilon^2 - 1)\mu_2]\omega^2 + (1/2)\{[(\epsilon^3/3) - \epsilon^2]\mu_3 + 2\epsilon(\mu_1\mu_2/\mu_0) - \epsilon(\mu_1^3/\mu_0^2)\}\omega^3 + \ldots\} \tag{9}$$

$$\phi_0 = (\mu_1/\mu_0)\,\omega + \epsilon[(\mu_2/\mu_0) - (\mu_1^2/\mu_0^2)]\omega^2 + \{[(\epsilon^2/2) - (1/6)]\,(\mu_3/\mu_0) - (\mu_1\mu_2/\mu_0^2) \times [(3/2)\epsilon^2 - (1/2)] - (1/3)\,(\mu_1^3/\mu_0^3)\}\omega^3 + \ldots \tag{10}$$

$$q_{max}/q_0 = \exp[-\epsilon(\pi/2)]\{\mu_0\omega + \{(\mu_1^2/2\mu_0) - (\mu_2/2) + \epsilon^2[(1/2) - \mu_2 + (1/2)\,(\mu_1^2/\mu_0)]\}\omega^3 + \{[(\epsilon/6) - (\epsilon^2/2) - (\epsilon^3/3)]\mu_3 + (\epsilon + \epsilon^3)\,(\mu_1\mu_2/\mu_0) + [-(7/6)\epsilon + (1/3)\epsilon^3]\,(\mu_1^3/\mu_0^2)\}\omega^4 + \ldots\} \tag{11}$$

Eq. (6) shows again $t_p \to \pi/2\omega$ as $\omega \to 0$. Eq. (11) shows that the slope of the spectrum at the origin ($\omega = 0$) is equal to the total impulse (μ_0) multiplied by the numerical factor π/t_m:

$$\lim_{\omega \to 0} [d/d(\omega t_m/\pi)]\ (q_{max}/q_0) = (\pi/t_m) \int_0^{t_0} \mathfrak{F}(\tau)\, d\tau \tag{12}$$

It is clear that the curvature of an amplification spectrum at the origin ($\omega = 0$) always vanishes and that the higher order terms can be expressed in terms of the successive moments of the pulse about the origin.

The Inverse Problem

To the inverse problem of determining $\mathfrak{F}(t)$ from the spectrum q_{max}/q_0, the following question may be asked: Can μ_k be determined from q_{max}/q_0? Expanding q_{max}/q_0 into a power series in ω and comparing coefficients in Eq. (11), one obtains, in the case $\epsilon = 0$,

$$\left.\begin{aligned} \mu_0 &= (d/d\omega)\,(q_{max}/q_0) \\ \mu_2 - (\mu_1^2/\mu_0) &= -(1/3)\,(d^3/d\omega^3)\,(q_{max}/q_0) \end{aligned}\right\} \tag{13}$$

etc. In general, for $m = 0, 1, 2, \ldots$

$$\sum_{i=0}^{m} \frac{\mu_{2i}\,\mu_{2m-2i}}{(2i)!(2m-2i)!} - \sum_{i=0}^{m-1} \frac{\mu_{2i+1}\,\mu_{2m-2i-1}}{(2i+1)!(2m-2i-1)!} = [(-1)^m/(2m+1)!]\,(d^{2m+1}/d\omega^{2m+1})\,(q_{max}/q_0)^2$$

Here all the derivatives of q_{max}/q_0 or $(q_{max}/q_0)^2$ must be evaluated at $\omega = 0$. It is seen that any m equations of the type (13) involve more than m μ's; thus the possibility of determining an inverse becomes uncertain. The same is true for the case $0 < \epsilon \ll 1$. However, it is yet unknown whether detailed information of q_{max}/q_0 at larger values of ω will uniquely define an inverse. The negative spectrum, q_{min}/q_0, and the acceleration spectra, $\ddot{q}_{max}$, etc., are much more sensitive to the pulse history; an interesting theoretical question is, therefore, the possibility of determining the inverse from such spectra.

Large Values of Frequency

In what follows we will consider the no-damping case, $\epsilon = 0$. Since

$$q(t)/q_0 = \int_0^t \mathfrak{F}(t-\tau)\,\omega \sin \omega\tau\, d\tau = \mathfrak{F}(t) - \int_0^t [d\mathfrak{F}(t-\tau)/d(t-\tau)] \cos \omega\tau\, d\tau \tag{14}$$

so

$$\lim_{\omega \to \infty} [q(t)/q_0] = \mathfrak{F}(t) \tag{15}$$

which shows that, if the applied load varies slowly in comparison with the natural vibration frequency of the oscillator, the response tends to be identical with the pulse.

Asymptotic formulas for large values of ω can be derived by a method given by Willis.[3] Consider the following integral which is related to the last term in Eq. (14):

$$I(\alpha, \omega) = \int_0^t f(t-\tau) \cos \omega\tau\, e^{-\alpha(t-\tau)} d\tau \tag{16}$$

Expand $f(t-\tau)$ into a Taylor's series with remainder,

$$I(\alpha,\omega) = \int_0^t \left\{ \sum_{r=0}^{n-1} [(t-\tau)^r/r!]\, f^{(r)}(0) + [(t-\tau)^n/n!]\, f^{(n)}(\theta t) \right\} \cos \omega\tau\, e^{-\alpha(t-\tau)}\, d\tau \quad (17)$$

where $0 \le \theta \le 1$. Expanding the following integral into a Taylor's series in α:

$$\int_0^t \cos \omega\tau\, e^{-\alpha(t-\tau)}\, d\tau = \psi(t,\alpha) \quad (18)$$

say,

$$\psi(t,\alpha) = \sum_{r=0}^{\infty} A_r(t)\alpha^r \quad (19)$$

then

$$A_r(t) = (1/r!)\,(\partial^r\psi/\partial\alpha^r)_{\alpha=0} \quad (20)$$

By differentiating Eq. (18) r times with respect to α, we obtain

$$\int_0^t (t-\tau)^r \cos \omega\tau\, e^{-\alpha(t-\tau)}\, d\tau = (-1)^r(\partial^r\psi/\partial\alpha^r) \quad (21)$$

Substituting into Eq. (17) and passing to the limit $\alpha = 0$, we have

$$I(0,\omega) = \sum_{r=0}^{n-1} f^{(r)}(0)\,(-1)^r A_r + (-1)^n f^{(n)}(\theta t)\, A_n \quad (22)$$

Now

$$\psi(t,\alpha) = \int_0^t \cos \omega\tau\, e^{-\alpha(t-\tau)}\, d\tau = [\omega/(\omega^2+\alpha^2)]\,[\sin \omega t + (\alpha/\omega)\cos \omega t - (\alpha/\omega)e^{-\alpha t}]$$

Hence

$$\left.\begin{aligned} A_0 &= (1/\omega)\sin \omega t \\ A_1 &= (1/\omega^2)(\cos \omega t - 1) \\ A_2 &= (1/\omega^3)(\omega t - \sin \omega t) \\ A_3 &= -(1/\omega^4)[(\omega^2 t^2/2!) + \cos \omega t - 1] \end{aligned}\right\} \quad (23)$$

etc. From Eqs. (22), (23), and (14), we obtain the asymptotic formula

$$q(t)/q_0 = \mathfrak{F}(t) - (1/\omega)\sin \omega t\, \dot{\mathfrak{F}}(0) + (1/\omega^2) \times [(\cos \omega t - 1)\, \ddot{\mathfrak{F}}(0) - t\, \mathfrak{F}^{(3)}(\theta t)] + (1/\omega^3)\sin \omega t\, \mathfrak{F}^{(3)}(\theta t), \quad (0 \le \theta \le 1) \quad (24)$$

or

$$q(t)/q_0 = \mathfrak{F}(t) - (1/\omega)\sin \omega t\, \dot{\mathfrak{F}}(0) + (1/\omega^2)[(\cos \omega t - 1)\, \ddot{\mathfrak{F}}(0) - t\, \mathfrak{F}^{(3)}(0) - (t^2/2!)\, \mathfrak{F}^{(4)}(\theta t)] + (1/\omega^3)\sin \omega t\, \mathfrak{F}^{(3)}(0) - (1/\omega^4)(\cos \omega t - 1)\, \mathfrak{F}^{(4)}(\theta t), \quad (0 \le \theta \le 1) \quad (25)$$

etc. The indeterminacy of the factor θ can be removed if $\mathfrak{F}(t)$ can be approximated by a polynomial of degree n. Then $\mathfrak{F}^{(n+1)}(t)$ vanishes, and an expansion of the following form may be obtained:

$$q(t)/q_0 = \mathfrak{F}(t) - (1/\omega)\sin \omega t\, \dot{\mathfrak{F}}(0) + (1/\omega^2)\left[(\cos \omega t - 1)\, \ddot{\mathfrak{F}}(0) - \sum_{r=1}^{n-2}(t^r/r!)\, \mathfrak{F}^{(r+2)}(0)\right] + (1/\omega^3)\sin \omega t\, \mathfrak{F}^{(3)}(0) + \ldots \quad (26)$$

Eq. (26) shows that the time t_p at which q_{max} is reached approaches t_m when ω is large:

$$t_p \to t_m \quad (27)$$

Hence,

$$q_{max}/q_0 \cong 1 - [\dot{\mathfrak{F}}(0)/\omega]\sin \omega t_m + 0(1/\omega^2) \quad (28)$$

This shows that the wavy curve of the spectrum that converges to 1 as ω increases has a "period"

$$\omega t_m \cong 2\pi \quad (29)$$

References

[1] Shapiro, H., and Hudson, D. E., *The Measurement of Acceleration Pulses with the Multi-Frequency Reed Gage*, J. Appl. Mech., Vol. 20, No. 3, pp. 422–426, 1953.

[2] Fung, Y. C., and Barton, M. V., *Some Characteristics and Uses of Shock Spectra*, Report No. GM-TR-82, The Ramo-Wooldridge Corp.

[3] Willis, H. F., *A Formula for Expanding an Integral as a Series*, Phil. Mag., Ser. 7, Vol. 39, pp. 455–459, 1948.

Simplified Equations for Calculating Local and Total Heat Flux to Nonisothermal Surfaces†

E. R. G. Eckert,* J. P. Hartnett,** and Roland Birkebak***

University of Minnesota, Minneapolis

March 14, 1957

Symbols

- b = width of surface, ft.
- h = local heat-transfer coefficient, $q = h(T_w - T_r)$, B.t.u./hour ft.^{2} F.
- k = thermal conductivity, B.t.u./hour ft. F.
- m = exponent in equation describing velocity variation
- Pr = Prandtl Number, $Pr = \mu c_p/k$
- q = local heat flow per unit area and unit time, B.t.u./hour ft.^{2}
- Q = total heat flow per unit time, B.t.u./hour
- Re_x = local Reynolds Number based on x, $Re_x = u_\infty x/\nu$
- T = absolute temperature, R.
- u = velocity in x direction
- x = coordinate measured along the surface indicating location of $q(x)$
- ϑ = difference between wall and recovery temperature, F.
- ζ = coordinate measured along surface, indicating location of step in wall temperature, ft.

Subscripts

- *iso* = isothermal wall
- 0 = value at leading edge
- r = refers to adiabatic wall or recovery temperature, T_r
- w = refers to conditions at the surface
- ∞ = refers to conditions at location x outside the boundary layer

Introduction

Up to the present time, the major efforts in the study of heat transfer to external surfaces have been directed to a constant wall-temperature condition. Unfortunately, in many practical cases, the wall temperature is not constant but is varying along the surface. The question then arises of how much the heat transfer in this case deviates from that on a constant wall-temperature surface. Contributions to the clarification of this problem have been made by Fage and Falkner, Rubesin and Chapman, Bond, Eckert, Seban, Tribus, and others. An excellent review of such solutions is available.[1] The results of these analyses are somewhat difficult to apply to a completely arbitrary wall-temperature distribution. Consequently, there has been a demand for interpretation of these results in such a form that may be readily utilized by design engineers. The primary purpose of this note is to present such a simplified method for calculating the heat transfer to surfaces for either completely laminar or turbulent boundary-layer flows with and without pressure gradients over surfaces with arbitrarily prescribed nonuniform temperature.

Basic Results

It has previously been shown[1] that the local heat rate $q(x)$ for a constant property boundary layer with arbitrarily varying wall temperature is rigorously given by the following expression:

$$q(x) = \int_0^x h(x,\zeta)\,(d\vartheta_w/d\zeta)\, d\zeta + \sum_i h(x,\zeta_i)\,[\vartheta_w(\zeta_i^+) - \vartheta_w(\zeta_i^-)] \quad (1)$$

In this equation, $\vartheta_w = (T_w - T_r)$ indicates the difference between the wall temperature and the recovery temperature, both taken at position ζ; $h(x,\zeta)$ is the heat-transfer coefficient existing at

† Publication from the Heat Transfer Laboratory, University of Minnesota.

Support by the Aeronautical Research Laboratory of the Wright Air Development Center, Wright-Patterson AFB, Ohio, is acknowledged.

* Professor of Mechanical Engineering.

** Associate Professor of Mechanical Engineering.

*** Graduate Research Assistant.

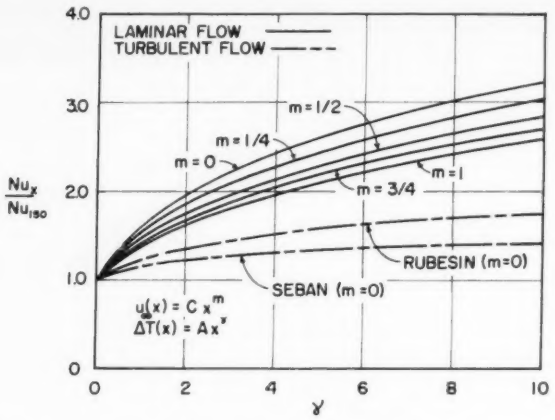

FIG. 1. Laminar and turbulent heat transfer from surface with pressure gradient and variable wall temperature.

location x when the surface is unheated upstream of position ζ and heated to a constant temperature downstream of position ζ. The integral portion is evaluated without taking into consideration any discontinuities in the wall temperature. Such discontinuities are accounted for by the summation expression, with each discontinuity giving a separate contribution to the local heat flow. The symbol $\vartheta_w(\zeta_i^+)$ indicates the temperature difference just upstream and $\vartheta_w(\zeta_i^-)$ the value just downstream of the temperature discontinuity.

The required expressions for the local heat-transfer coefficient $h(x, \zeta)$ for a step in the wall temperature as obtained by approximate methods are available.[1] They will be referred to the heat-transfer coefficient h_{iso} of a surface with locally constant temperature. For laminar flow,

$$h(x, \zeta)/h_{iso} = [1 - (\zeta/x)^{\alpha}]^{-1/3} \tag{2}$$

The value of α is dependent on the pressure gradient. For wedge-type flows described by $u_\infty = cx^m$, the following results apply:

m	0	1/4	1/2	3/4	1
α	3/4	15/16	9/8	21/16	3/2

In the case of turbulent flow with constant velocity over a flat plate, two approximate expressions are available. Both will be reported here since experimental data are not sufficient to decide which one is better.

Seban: $$h(x, \zeta)/h_{iso} = [1 - (\zeta/x)^{9/10}]^{-1/9} \tag{3}$$

Rubesin: $$h(x, \zeta)/h_{iso} = [1 - (\zeta/x)^{39/40}]^{-7/39} \tag{4}$$

When the only temperature discontinuity occurs at the leading edge, the expression for the local heat rate is

$$q(x) = h_{iso}\left[\vartheta_{w_0} + \int_0^x \frac{h(x, \zeta)}{h_{iso}} \frac{d\vartheta_w}{d\zeta}\, d\zeta\right] \tag{5}$$

A rather significant result is readily obtained if one assumes a wall-temperature distribution given by the expression $\vartheta_w = Ax^y$. For this case the integral in Eq. (5) may be evaluated. The results are shown on Fig. 1. It is seen that the influence of the nonisothermal wall conditions is more pronounced in laminar than in turbulent flow. It may, however, be significant even in turbulent flow if severe temperature gradients are present. A pressure gradient slightly decreases the influence of the variable wall temperature as demonstrated in Fig. 1 for laminar wedge flow.

The present note utilizes a method suggested in reference 2. The actual wall-temperature distribution is approximated by a series of sloping segments as shown in Fig. 2, thereby making $d\vartheta_w/d\zeta$ a constant value over any interval Δx and allowing its removal from the integral sign. Eq. (5) then reads

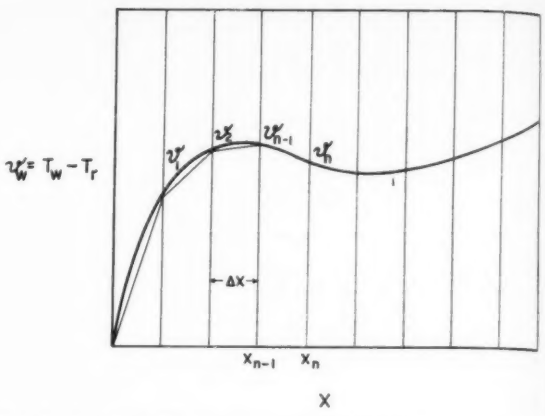

FIG. 2. Laminar sloping segment approximation for temperature distribution.

$$q(x_n) = h_{iso}\left[\vartheta_{w_0} + \left(\frac{d\vartheta_w}{dx}\right)_{0-x_1}\int_0^{x_1}\frac{h(x, \zeta)}{h_{iso}}\, d\zeta + \left(\frac{d\vartheta_w}{dx}\right)_{x_1-x_2}\int_{x_1}^{x_2}\frac{h(x, \zeta)}{h_{iso}}\, d\zeta + \cdots \left(\frac{d\vartheta_w}{dx}\right)_{x_{n-1}-x_n}\int_{x_{n-1}}^{x_n}\frac{h(x, \zeta)}{h_{iso}}\, d\zeta\right] \tag{6}$$

The general form of the integrals in this equation may be written as follows:

$$\int_{x_{i-1}}^{x_i}\frac{h(x, \zeta)}{h_{iso}}\, d\zeta = x\left[\int_0^{x_i/x}\frac{h(x, \zeta)}{h_{iso}}\, d\left(\frac{\zeta}{x}\right) - \int_0^{x_{i-1}/x}\frac{h(x, \zeta)}{h_{iso}}\, d\left(\frac{\zeta}{x}\right)\right] \tag{7}$$

Since the expressions for $h(x, \zeta)/h_{iso}$ are known functions of (ζ/x) for laminar and turbulent flow, it is possible to evaluate the integrals once and for all.

The values of the integral on the right side have been obtained and tabulated in reference 3 for values of (x_i/x) from 0 to 1 in steps of 0.01. A further simplification results from the fact that the tabulated values of the integral can be approximated with good accuracy by the following expression:

$$\int_0^{x_i/x}\frac{h(x, \zeta)}{h_{iso}}\, d\left(\frac{\zeta}{x}\right) = A\left(\frac{x_i}{x}\right) + B\left(\frac{x_i}{x}\right)^2 \tag{8}$$

When this relationship is substituted into Eq. (6) under the assumption that the length x is subdivided into n equal intervals—i.e., Δx = constant—we arrive at the fiaal relatively simple expression for the local heat flux $q(x)$.

$$q(x_n) = h_{iso}\{\vartheta_{w_0} + A(\vartheta_{w_n} - \vartheta_{w_0}) + B(\Delta x/x) \times [-\vartheta_{w_0} - 2\vartheta_{w_1} - 2\vartheta_{w_2} \cdots -2\vartheta_{w_{n-1}} + (2n - 1)\vartheta_{w_n}]\} \tag{9}$$

The dimensionless parameters in this equation and in the equation $h_{iso} = C(k/x)Re_x^n Pr^{1/3}$ for the isothermal heat-transfer coefficient are collected in Table 1.

It is estimated that Eq. (9) will yield results which are within 5 per cent of those obtained by using the more exact value of the integral as reported in reference 3.

TABLE 1

	m	A	B	C	n
Laminar	0	0.895	0.690	0.332	1/2
	1/4	0.837	0.635	0.412	1/2
	1/2	0.840	0.572	0.469	1/2
	1	0.792	0.538	0.560	1/2
Turbulent					
Seban	0	0.991	0.117	0.0296	0.8
Rubesin	0	0.967	0.256	0.0296	0.8

TABLE 2

	A'	B'	C'	n
Laminar ($m = 0$)	0.696	0.432	0.664	1/2
Turbulent				
Schan	0.982	0.478	0.0370	0.8
Rubesin	1.018	0.475	0.0370	0.8

EVALUATION OF THE TOTAL HEAT FLUX $Q(x)$

It may be desirable to evaluate the total heat transfer up to a given location along the surface. This may be accomplished by integrating the local heat flux as determined above. A direct approach can be made for the flat plate by performing this integration with the same basic procedure as outlined in the preceding section. The resulting expression for the total heat flow up to a position x_n may be expressed.

$$Q(x_n) = h_{iso}\, xb\{(\vartheta_{w_n}) + A'(\vartheta_{w_n} - \vartheta_{w_0}) - B'(\Delta x/x) \times [-\vartheta_{w_0} - 2\vartheta_{w_1} \ldots - 2\vartheta_{w_{n-1}} + (2n - 1)\ \vartheta_{w_n}]\} \quad (10)$$

The dimensionless parameters in this equation and in the expression $h_{iso} = C'(k/x)Re^n Pr^{1/3}$ are contained in Table 2.

The results obtained with Eq. (10) are in substantial agreement (within 1 per cent) with those obtained with the tabulated integrals for both laminar and turbulent flow.

REFERENCES

[1] Klein, J., and Tribus, M., *Forced Convection from Non-Isothermal Surfaces*, Heat Transfer Symposium, Engineering Research Institute, University of Michigan, August, 1952.

[2] Shoulberg, R. H., et al., *Wind Tunnel Reports 36 and 39*, Naval Supersonic Laboratory, Massachusetts Institute of Technology, June, 1953.

[3] Hartnett, J. P., Eckert, E. R. G., Birkebak, Roland, and Sampson, R. L., *Simplified Procedures for the Calculation of Heat Transfer to Surfaces with Non-Uniform Temperatures*, WADC TR 56-373, July, 1956.

Stress Concentration in Plexiglas as a Function of Loading Rate

Leo V. Kline*

Assistant Professor, Division of Engineering Sciences, Purdue University, Lafayette, Ind.

April 4, 1957

SUMMARY

A study is made of stress concentration effects as functions of loading rate. Polymethyl methacrylate is chosen as the working medium. The loading conditions used are uniform crosshead velocities ranging from 0.02 in. per min. to approximately 6,600 in. per min. It is shown that failure to recognize the dependence of the stress concentration on the loading rate may result in serious underdesign.

INTRODUCTION

THE EFFECT of the loading rate on the ultimate strength and modulus of elasticity of plastics has been the subject of considerable research. The results of this research cannot be intelligently used in designing plastic-like items such as rocket motor propellant grains until the dependence of stress concentration on loading rate is also established. This work supplies information on how stress concentration effects are influenced by loading rate.

EXPERIMENTAL WORK

Polymethyl methacrylate (Plexiglas IA, UVA) was tested in tension with seven different crosshead velocities ranging from 0.02 in. per min. to approximately 6,600 in. per min. An Instron machine was used to obtain velocities from 0.02 to 2 in. per min. A rapid rate machine designed at Redstone Arsenal[1] was used for obtaining the higher velocities. Although this machine is not a constant crosshead velocity machine, the crosshead velocities

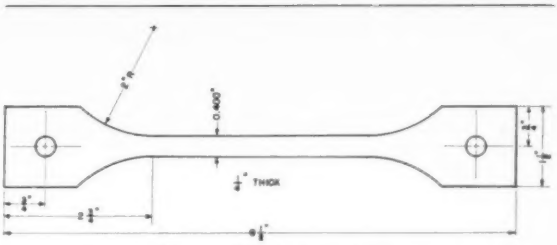

FIG. 1. Sketch of specimen.

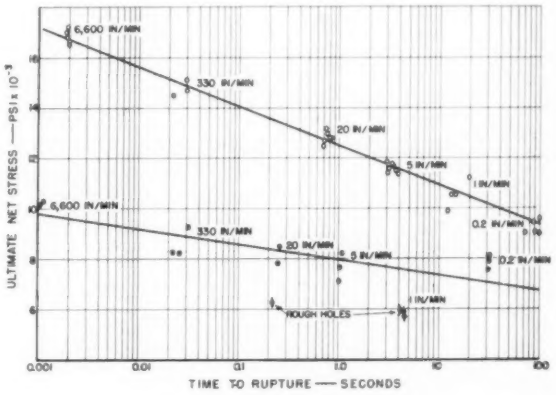

FIG. 2. Data for 1/8-in. hole.

obtained were nearly constant values of 330 and 6,600 in. per min. Load-time data were obtained by feeding the amplified signal of strain-gage load cells into a standard pen recorder, a recording oscillograph, or a cathode ray oscilloscope, depending on the response needed. Specimens were prepared by drying for 48 hours at 122°F. followed by at least 5 hours in a desiccator at room temperature. Room temperature was maintained between 74 and 78°F. for all tests.

A total of 70 specimens designed as shown in Fig. 1 were used by Ely of Redstone Arsenal to establish the upper curve of Fig. 2. For the present study, specimens were modified from the design shown in Fig. 1 by drilling a centrally located hole parallel to the 0.25-in. dimension. Specimens with hole diameters of $^1/_{16}$, $^1/_8$, $^7/_{32}$, and $^1/_4$ in. were studied. The net rupture stresses S_{nr} for the specimens with $^1/_8$-in. holes are plotted on the lower portions of Fig. 2 as functions of the rupture times. The net rupture stress is considered to be the quotient of the rupture load and the net area measured at the cross section through the hole. The lower curve of Fig. 2 represents a reasonable fit for the experimental data.

DISCUSSION

Using curves similar to Fig. 2, a strength-reduction factor K_r can be calculated for the geometries included in this study. This factor is defined to be

$$K_r = S_r/S_{nr} \quad (1)$$

where S_r is the rupture stress for the material as determined from specimens with no stress concentration. This factor is to be distinguished from the theoretical stress concentation factor K_t, a function of geometry only, which is defined by

$$K_t = S_m/S_n \quad (2)$$

where S_m is the maximum stress in the stressed body and S_n is the average stress over the net cross section of the stressed body. Although the theoretical stress concentration factor is of considerable value, the designer is usually more interested in the strength-reduction factor K_r. For a given combination of hole size and loading rate, the value of K_r can be obtained with the aid of the curves similar to Fig. 2. For example, to find K_r for

* Formerly, Research Engineer, Research Laboratories, Ordnance Missile Laboratories, Redstone Arsenal.

TABLE 1
Stress Concentration Values

Crosshead Velocity in./min.	S_r psi	1/16 in. hole K_r	1/16 in. hole ΔK*	1/8 in. hole K_r	1/8 in. hole ΔK*	7/32 in. hole K_r	7/32 in. hole ΔK*	1/4 in. hole K_r	1/4 in. hole ΔK*
0.02	7,900	1.25	1.42	1.25	1.11	1.25	0.88	1.28	0.75
0.2	9,400	1.56	1.09	1.56	1.00	1.42	0.69	1.38	0.71
1.0	10,600	1.49	1.16	1.40	0.96	1.47	0.80	1.47	0.68
5.0	11,700	1.58	1.07	1.47	0.87	1.54	0.57	1.51	0.68
20.0	12,600	1.64	1.02	1.52	0.82	1.59	0.52	1.57	0.62
300	14,900	1.86	0.79	1.67	0.67	1.79	0.52	1.71	0.62
1,660	16,700	1.94	0.71	1.74	0.60	----	----	1.74	0.55

* $\Delta K = K_t - K_r$.

the 5-in per min. crosshead velocity and the 1/8-in. diameter hole, the value of 11,700 psi for S_r is read from the top curve of Fig. 2 while the value of 7,950 psi for S_{nr} is read from the lower curve. Thus

$$K_r = 11{,}700/7{,}950 = 1.47 \tag{3}$$

Table 1 includes the calculated values of K_r for each combination of stress concentration and loading rate.

Values of the theoretical stress concentration factor[2] K_t for the hole sizes studied are included in Table 1. If, for a particular geometry, K_t is assumed to be constant for all values of maximum normal stress S_m, then it is permissible to write

$$K_t = S_{mr}/S_{nr} \tag{4}$$

where S_{mr} is the maximum normal stress at rupture. If the furthur assumption is made that the maximum normal stress theory of failure accurately predicts the behavior of the material, then $S_{mr} = S_r$, and the theoretical stress concentration factor becomes

$$K_t = S_r/S_{nr} \tag{5}$$

which is the definition of K_r. Since the experimentally obtained values of K_r do not equal K_t, it follows that the assumptions made in arriving at Eq (5) are not accurate. The first of these assumptions (that K_t is constant) is accurate if the material exhibits elastic behavior. All of the specimens with stress concentrations experience sufficiently high strain rates in the vicinity of the concentration so that the assumption of a linear stress-strain relation is reasonable. It is felt, therefore, that the first assumption used in arriving at Eq. (5) is a good assumption. Thus, the second of the above assumptions (concerning the theory of failure) is primarily responsible for the difference $K_t - K_r$. This difference can therefore be considered as a measure of the inability of the maximum normal stress theory of failure to predict the behavior of the material. The values of $K_t - K_r$ are included in Table 1. As the loading rate is increased, the material loses ductility. Since the maximum normal stress theory of failure is most accurate for brittle materials, it might be expected that $K_t - K_r$ would decrease as the loading rate increases. This is the case as can be seen from the tabulated values of $K_t - K_r$.

Conclusions

Failure to recognize the dependence of K_r on the loading rate may result in serious underdesign. Consider the case where the stress distribution around a point in a propellant grain can be considered comparable to the distribution around a 1/8-in. hole in a tensile specimen loaded with a crosshead velocity of 330 in. per min. Using the value of K_r for a commonly employed crosshead rate, 0.02 in. per min., gives a design rupture stress of

$$S = 14{,}900/1.23 = 12{,}100 \text{ psi} \tag{6}$$

Using the value of K_r which should be associated with a crosshead velocity of 330 in. per min. gives a design rupture stress of

$$S = 14{,}900/1.67 = 8{,}920 \text{ psi} \tag{7}$$

For this example, failure to recognize the dependence of K_r on the loading rate would cause one to predict a design stress 36 per cent higher than the correct value.

The results of this study show that the strength reduction factor K_r increases as much as 58 per cent over the range of loading rates considered.

The factor $K_t - K_r$ decreases with increasing loading rate. This is an indication that the maximum normal stress theory of failure becomes more accurate as the loading rate is increased.

References

[1] Ely, R. E., *Description and Performance Data for a Pneumatically Operated Rapid-Rate Tensile Machine*, Ordnance Missile Laboratories Report No. 2R9P, January 16, 1956.

[2] *Metals Engineering, Design* (ASME Handbook), p. 110; McGraw-Hill Book Company, Inc., New York, 1953.

Errata—"Vibration of Clamped Parallelogrammic Isotropic Flat Plates"*

M. Hasegawa
Shimane University, Matsue, Japan
April 10, 1957

THE TERM $+ \partial w^4/\partial y^4$ should be added after $-4 \cos \alpha(\partial^4 w/\partial x \partial y^3)$ within the bracket in Eq. (1).

ρ should read p in Eq. (3).

ρ^2 should read p^2 in Eq. (6) and in the first line of Eqs. (11).

Errata—"Subsonic Oscillatory Control Surface Coefficients Computed by the Method of Reissner and Haskind"†

Henry E. Fettis
Mathematician, Aeronautical Research Laboratory, Wright Air Development Center, ARDC, Wright-Patterson AFB, Ohio
May 10, 1957

THE FOLLOWING two errors exist in Table 1:

(1) The value of $\omega^2 L_\beta$ for $\omega = .40$ should be

$$-.68350 + .31076\,i$$

(2) The value of $\omega^2 M_\beta$ for $\omega = .20$ should be

$$-.60826 - .049698\,i$$

* Readers' Forum, Journal of the Aeronautical Sciences, Vol. 24, No. 2, pp. 145, 146, February, 1957.

† Readers' Forum, Journal of the Aeronautical Sciences, Vol. 24, No. 5, pp. 378, 379, May, 1957.

Change of Address

Since the Post Office Department does not as a rule forward magazines to forwarding addresses, it is important that the Institute be notified of changes in address 30 days in advance of publishing date to ensure receipt of every issue of the JOURNAL and REVIEW.

Notices should be printed legibly and sent directly to:

Institute of the Aeronautical Sciences, Inc.
2 East 64th Street, New York 21, N.Y.